ANALYSIS OF CENTRAL METABOLIC PATHWAYS IN CULTURED MAMMALIAN CELLS

A DISSERTATION

SUBMITTED TO THE FACULTY OF THE GRADUATE SCHOOL OF

THE UNIVERSITY OF MINNESOTA

BY

ANDREW YONGKY

IN PARTIAL FULFILLMENT OF THE REQUIREMENTS

FOR THE DEGREE OF

DOCTOR OF PHILOSOPHY

ADVISER: PROFESSOR WEI-SHOU HU

October 2014

Acknowledgements

I wish to express my gratitude to my advisor Professor Wei-Shou Hu for his constant support and guidance throughout my graduate study. His patience and mentorship were invaluable not only to my academic but also to my personal development. It has been a great privilege to work with him and being part of such an amazing group.

I am very thankful to Professor Prodromos Daoutidis and Professor Kechun Zhang in the Department of Chemical Engineering and Materials Science, and Professor Kim Do-Hyung in the Department of Biochemistry, Molecular Biology and Biophysics for taking the time to serve on my thesis committee and for their precious advice.

I would like to thank Professor Prodromos Daoutidis, Professor Kim Do-Hyung, Professor George Karypis, Dr. Catherine Verfaillie and Dr. Nobuaki Kikyo for their constructive advice in my research.

I would like to thank all members of the Hu group: Bhanu Mulukutla, Nitya Jacob, Nandita Vishwanathan, Huong Le, Kathryn Johnson, Siguang Sui, Kartik Subramanian, Shikha Sharma, Jason Owens, Marlene Castro, Anushree Chatterjee, Yonsil Park, Anne Kantardjieff, Ravali Raju, Dong Seong Cho, David Chau, Arpan Bandyopadhyay, Tung Le, Liang Zhao, Haiyun Pei, Kyoungho Lee and Hsu-Yuan Fu for being wonderful colleagues and making the lab a great place to work in. A special thanks to Bhanu for being a great comrade; I always enjoyed all the fun and intellectual discussions we had.

I also thank all my friends who have made my time in Minneapolis very memorable: Aloysius Gunawan, Sophie Christian, Effendy Liejanto, Budi Antony, Tjahjono Tjandra, Yahya Cahyadi, Erik Winardi, Iswandi Jarto, Selin Tosun, Ken-Hsuan Liao, Chiang Hsu, Yu-hsuan Yang and Chun-chi Chang.

Above all, I would like to thank my parents and my sister, Jeanny, for their unconditional love and support. I am also indebted to my aunts, uncles, and cousins for their love and support. None of this would have been possible without them.

Dedication

This thesis is dedicated to my loving parents,

Antonius Yongky and Dora Gobeawan

Abstract

Recombinant therapeutic proteins have transformed the field of medicine since their advent more than twenty years ago, providing treatments for various refractory illnesses. Mammalian cells are the preferred hosts for the production of these therapeutics. However, a lack of understanding of the behavior of the cells results in numerous issues that affect the performance of process cultures including inefficient glucose metabolism and improper post-translational modification of the product proteins. With the advances in the knowledge of regulation of metabolism of mammalian cells and the availability of genomics and transcriptomics resources, systems biology approach combining kinetic model and "-omics" tools can now be used to address such issues. The work presented in this thesis employs such systems biology approach to better understand the metabolic behavior of the cells and devise strategies to enhance their performance in culture.

Cultured mammalian cells consume huge amount of glucose and convert most of it towards lactate. The accumulation of lactate in culture adversely affects cell growth and productivity. The reliance of these cells on anaerobic glycolysis is also observed in proliferating cells such as cancer cells and embryonic stem cells. In contrast, quiescent cells metabolize glucose at slower rate and glucose is mostly oxidized to carbon dioxide. In the first part of this thesis, we attempt to unravel the regulation of glucose metabolism in proliferating and non-proliferating cells using a mechanistic model of glycolysis. We show that multiple allosteric regulations of glycolysis enzymes can act in synergy to confer bistable behavior to glycolysis activity: at a given glucose concentration, glycolysis can operate at either a high flux state or a low flux state. In proliferating cells, the default state of the cells is to operate at high glycolysis flux. However, it is possible to modulate factors extrinsic and intrinsic to the cells in order to make them switch to low flux state.

In the late stages of fed-batch culture, mammalian cells have been observed to shift their metabolism from lactate production to lactate consumption. While it has been correlated with higher productivity, such metabolic shift is not a consistent occurrence as some

cultures continue to produce lactate. The metabolic model is used to explain the underlying mechanism behind the metabolic shift to lactate consumption in fed-batch culture. We show that the bistable behavior in glycolysis differs somewhat due to lactate inhibition and growth rate regulation on metabolism. As a result, the cells in culture may or may not shift their metabolism to consume lactate depending on the glucose, lactate and growth rate of the cells.

In continuous culture, a similar metabolic behavior has been observed. With the same operating conditions of dilution rate and feed glucose concentration, some continuous cultures reach steady state with high glycolysis flux, while others reach steady state with low glycolysis. The two steady states are marked by distinct steady state cell concentrations. Using a multi-scale reactor model that combines the intracellular metabolism and macroscopic cell growth, we show that multiple steady states exist in continuous culture. At high flux steady state the vast majority of glucose is converted to lactate, whereas at low flux steady state most of the glucose consumed is converted to biomass. The two types of steady states thus have different metabolic efficiency, conferring different cell concentrations.

In the final part of the thesis, RNA-seq and microarray are employed to survey the variability in CHO cell lines. We observe a wide range of transcript levels of glycolysis enzymes in CHO cell lines, potentially contributing to distinct metabolic characteristics in different cell lines. The extent of genetic variation in the protein coding regions of the growth signaling pathway genes in CHO cells are discussed.

Table of Contents

List of Tables

List of Figures

Chapter 1 Introduction

1.1 Mammalian Cell Culture

The advent of recombinant protein therapeutics has transformed the field of medicine by providing treatments for various refractory diseases such as cancers, multiple sclerosis and arthritis. Ever since then, the proteins being produced have been increasing in structural complexity and many require post-translational modifications for their activities and efficacies. Proper protein folding and complex glycosylation modifications, for example, are carried out in the endoplasmic reticulum and Golgi of mammalian cells. Because of their capability to carry out these functions, mammalian cells have become the preferred hosts for recombinant protein production.

A number of mammalian cells have been used for therapeutic protein production in the industry including Chinese hamster ovary (CHO) cells, baby hamster kidney (BHK) cells, myeloma (NS0, SP2/0), HeLa and Vero. In 2012, the total annual sales of biologics produced in mammalian cells surpassed US $63 billion in the United States and US $125 billion globally [1,2]. Among all the mammalian cells used for production, CHO cells are indisputably the major workhorse, accounting for the production of an estimated 60% of the therapeutic proteins.

Despite the importance of mammalian cells for protein production, a lack of understanding of their behavior in the cultivation process presents a huge challenge for developing robust process technologies. A typical process development is performed empirically and requires extensive optimization of parameters including nutrient levels, temperature and pH. These parameters, however, have limited control on the physiology of the cells. As a result, inefficient metabolism, low productivities, and undesired post translational modifications of the product proteins are still plaguing the process industry. To add further complication, the majority of mammalian cell lines are transformed cells that have been cultivated for a large number of generations and adapted to grow in

different culture modes. Accumulation of mutations in the genome and alteration in the gene expression of the cells can potentially influence their behavior in culture.

In this study, we employ mathematical models of energy metabolism of mammalian cells using systems biology approach to provide a holistic understanding of the cells' physiology. In addition, the availability of genomics and transcriptomics tools allows one to examine the genetic makeup of the cells and survey the global gene expression levels of the cells. We combine the modeling effort with the quantitative information gathered from these "-omics" tools to dissect the physiological function of the cells and conceive strategies for controlling their behavior and enhance their performance for protein production.

1.2 Scope of the Thesis

Mammalian cells used for protein production have inefficient metabolism. Under normal culture conditions, cells consume glucose at very high rate and a large proportion of the glucose consumed is converted towards lactate. Lactate produced by the cells is secreted outside and accumulates in the extracellular medium. The decrease in pH due to lactate accumulation in the medium is detrimental to both cell growth and productivity. Base is typically added to the culture to neutralize the pH. However, this results in increased culture osmolarity causing additional stress on the cells. Therefore, controlling the metabolism of the cells to reduce lactate production is critical for favorable process outcome.

Industrially, the predominant cultivation method is fed-batch process, wherein glucose is fed regularly to the medium to sustain cell growth until the accumulation of lactate to high levels adversely affects cell growth and viability. In the later stages of this fed-batch process, sometimes a metabolic shift from a high lactate production state to a state of lactate consumption occurs. In other cases of seemingly identical culture conditions, cells continue to produce lactate. Cultures that exhibit metabolic shift to lactate consumption have been correlated with increased viability and higher productivity [3,4]. However, such metabolic shift is not a consistent occurrence and its underlying mechanism is not

well understood. Identifying the mechanism for such metabolic shift and the means to elicit it will be of crucial importance.

Another cell cultivation method practiced in industry is continuous culture, wherein feed media is being added continuously while reactor content is withdrawn at equivalent flow rate, keeping the reactor volume constant. Under seemingly identical operating conditions of dilution rate and feed glucose concentration, some continuous cultures reach steady state with high glycolysis flux, while others reach steady state with low glycolysis. The two types of steady state have different metabolic efficiency. At high flux steady state the vast majority of glucose is converted to lactate, whereas at low flux steady state most of the glucose consumed is converted to biomass. Thus different steady states are marked by distinct steady state cell concentrations. Understanding the precise conditions that lead to steady state with low glycolysis flux and high cell concentration will be of great interest.

In this study, we use a mechanistic kinetic modeling approach to unravel the regulation of energy metabolism in mammalian cells. We show that the synergistic action of enzyme regulations gives rise to steady state multiplicity in glycolysis. Within a range of glucose concentrations, two metabolic states corresponding to high glycolysis flux and low glycolysis flux exist for a given glucose concentration. We then use the metabolic model to explain the mechanism behind the metabolic shift to lactate consumption in fed-batch culture. Further, we also explain the nature of multiple steady states in continuous culture using a multi-scale model that incorporates the intracellular metabolism and macroscopic cell growth in the reactor.

In the final part of this thesis, we explore the gene expression and genetic variations in CHO cell lines. Using genomics and transcriptomics tools, we assess the diversity in gene expression and the rate of mutation in CHO cell lines. Such variations at transcript and genomic levels potentially contribute to the diverse metabolic and growth behaviors of different CHO cell lines.

1.3 Thesis Organization

This thesis is organized into eight chapters. Chapter 2 reviews the current knowledge of regulation of the central metabolic pathways in mammalian cells. Chapter 3 presents a summary of the methodology employed in cell cultures and analyses. Chapter 4 focuses on the modeling effort to study the effect of the allosteric regulations on the activity of the glycolysis pathway in proliferating and non-proliferating cells. Chapter 5 examines the mechanism of metabolic shift to lactate consumption in the fed-batch cultures of mammalian cells. The crucial parameters for inducing metabolic shift in fed-batch cultures are discussed. Chapter 6 focuses on the construction of a multi-scale kinetic model and the analysis of multiple steady states in continuous culture of mammalian cells. The steady state multiplicity behavior is harnessed to contrive strategies to achieve higher cell concentration in continuous culture of hybridoma cells. Chapter 7 presents the use of genomic and transcriptomic tools to examine gene expression and genetic variations in a number of CHO cell lines. The impact of such variations on the metabolic behavior of the cell lines is discussed. Chapter 8 summarizes the findings of this study and provides suggestions for future directions.

Chapter 2 Regulation of Energy Metabolism in Mammalian Cells

2.1 Summary

Energy metabolism of mammalian cells profoundly affects the performance of the culture. Cultured mammalian cells used in the industry exhibit wasteful metabolism characterized by the high rates of glucose consumption and lactate production. The accumulation of lactate in the extracellular medium adversely affects cell growth and productivity of the culture. Engineering the metabolism of the cell to be more efficient has therefore been the major focus of cell line and process optimization efforts in the industry. Recent research advances have increased our understanding of the regulation of glucose metabolism in mammalian cells and its link to the control of cell growth and proliferation. This chapter discusses the current understanding in this area of crucial importance to cell culture processes.

2.2 Introduction

Cultured mammalian cells are the workhorses for the production of recombinant therapeutic proteins. The majority of the cells used for manufacturing are continuous cell lines which have been cultivated for a large number of generations and are often aneuploid. Under normal culture conditions, these cells consume large quantity of glucose and convert the majority of it to lactate which is secreted into the extracellular medium. The hypermetabolic nature of the cells and their over reliance on aerobic glycolysis is referred to as the Warburg effect, and was first used to describe the contrast the metabolism of cancer cells and normal tissues. In industrial cell culture, lactate accumulation in the medium can reach levels of more than 100 mM which adversely affects cell growth and viability as well as productivity of the culture. A better understanding of metabolic regulation will allow for a better control of the metabolic state of the cell, which would lead to an increase in productivity. In recent years, much

progress has been made in elucidating the regulation of cell metabolism. This chapter presents some of the main findings relevant for process enhancement.

2.3 Regulation of Enzyme Kinetics

A host of enzymes in the central metabolism pathways are under allosteric regulations by metabolic intermediates or by various post translation modifications. Such a regulation at the level of kinetics confers cells with an ability to modulate the flux in an acute manner to respond to the changing nutritional and energetic requirements of the cells. Furthermore, many enzymes exist as multiple isoforms (isozymes) which differ in their substrate affinities and the allosteric regulations they are subjected to. These isozymes are expressed in different proportions in different cells or tissues. Thus different cells exhibit different metabolic behaviors depending on the composition of isozymes being expressed.

The key rate-controlling enzymes in the glycolysis pathway include hexokinase (HK), phosphofructokinase (PFK), 6-phosphofructo-2-kinase/fructose-2,6-bisphosphatase (PFKFB) and pyruvate kinase (PK) among few others. As stated earlier, allosteric regulations of enzyme kinetics are specific to the isozyme expressed. For example, hexokinase isozymes HK1, 2 and 3 are inhibited by glucose 6-phosphate (G6P) whereas HK4 (also called as glucokinase) is devoid of the G6P inhibition (Figure 2.1). Further, HK inhibition by G6P (or trehalose 6-phosphate in yeast) has been shown to be required for reaching a metabolic steady state [5]. Relieving this inhibition has been shown to result in an imbalanced state where cells accumulate glycolytic metabolites affecting their growth negatively.

PFK is one of the flux controlling enzymes in the glycolysis pathway which is heavily regulated. In mammalian cells, PFK exists in three different isoforms: the liver isozyme (PFKL), the muscle isozyme (PFKM) and the platelet isozyme (PFKP). The classic modulators of the PFK include fructose 6-phosphate (F6P), fructose 2,6-bisphosphate (F26BP), fructose 1,6-bisphosphate (F16BP), adenosine monophosphate (AMP), adenosine triphosphate (ATP), citrate and lactate among few others (Figure 2.1). The

affinity of the enzyme PFK to these modulators is also isozyme dependent. For example, all three isoforms of PFK are activated by F6P and F26BP [6], but only PFKM and PFKL are activated by F16BP [7-9]. More recently, PFK kinetics has been shown to be regulated in a post-translational fashion. O-GlcNAcylation at the Ser^{529} site was shown to interfere with the binding of F26BP molecule to PFK and thus decreases the allosteric activation of the PFK enzyme by F26BP [10]. Such an inhibitory effect reduces the flux through the glycolysis pathway and diverts it toward the pentose phosphate pathway for supplying carbon for biosynthetic needs of the cells. Further, this regulation is isozyme dependent with PFKL and PFKP being more sensitive to O-GlcNAcylation.

PFKFB is a bifunctional enzyme whose kinase and bisphosphatase domains catalyze the formation and hydrolysis reaction of F26BP, respectively [11,12]. There are four mammalian PFKFB isozymes: PFKFB1, 2, 3 and 4. Isozymes of PFKFB differ in their relative ratio of kinase to phosphatase activities and thus give rise to different cellular F26BP concentrations [12]. F26BP is a very potent activator of the enzyme PFK. Thus, each isozyme of PFKFB has a distinct capacity in modulating PFK activity (and thereby glycolysis activity). The PFKFB3 isoform, which has the highest kinase to phosphatase ratio, is highly expressed in several tumor cells.

Pyruvate kinase is another rate controlling enzyme which is expressed as four different isozymes in mammalian systems: M1, M2, L and R isozymes. The L and R isoforms are spliced variants expressed by the same gene in liver and red blood cells, respectively. The M1 and M2 isoforms are spliced variants expressed by another gene. PKM2 is one of the most studied isozymes as it has been linked to rapid proliferation and nutrient sensing. The M2 isozyme is regulated at allosteric level by a number of intermediates, both from glycolysis and other metabolic pathways. F16BP is the most well-known allosteric activator of PKM2 (Figure 2.1). Recently, succinylaminoimidazolecarboxamideribose-5′-phosphate (SAICAR), an intermediate of *de novo* purine nucleotide biosynthetic pathway, was identified as another allosteric activator of PKM2 [13]. Under low glucose conditions (or starvation), SAICAR accumulates in the cells and induces PKM2 activity. Induction of PKM2 activity by SAICAR provides a way for the cells to maintain

glycolysis flux to be high for ATP synthesis under reduced glucose availability. Thus, SAICAR allows cells to fine-tune control of their metabolism under demanding conditions for energy production rather than diverting the flux towards the pentose phosphate pathway for *de novo* nucleotide biosynthesis [13]. PKM2 is also allosterically regulated by a number of amino acids including serine and phenylalanine. This allows PKM2 to operate as a nutrient sensor. Positive regulation by serine gives the enzyme the ability to operate as a rheostat for maintaining the intracellular level of serine. Under conditions of low serine, the activity of PKM2 drops resulting in a higher channeling of 3-phosphoglycerate (3PG) toward serine biosynthesis (Figure 2.1) [14]. Conversely, when intracellular level of serine increase, PKM2 is activated and 3PG is channeled toward pyruvate for lactate production or energy synthesis. In the case of essential amino acids such as phenylalanine, which acts as an allosteric inhibitor of PKM2, the regulation allows the cells to increase catabolic metabolism for ATP synthesis and repress cell proliferation under conditions of phenylalanine starvation [15].

Furthermore, PKM2 has also been reported to respond to other physiological factors such as the tyroid hormone T3 and reactive oxygen species (ROS). The T3 hormone, a pro-growth hormone, has been shown to trap the M2 isoform in the monomeric state and thereby restraining the enzyme in its low activity state [15]. Similarly, oxidative stress has been demonstrated to reduce the isozyme activity through oxidation of the Cys^{358} residue [16]. The reduction of PKM2 activity allows channeling of the glycolytic intermediates towards branching pathways to generate biosynthetic precursors such as NADPH and ribose nucleotides among others, required for cellular proliferation. The reducing agents generated are also used to trigger the antioxidant response when cells undergo oxidative stress.

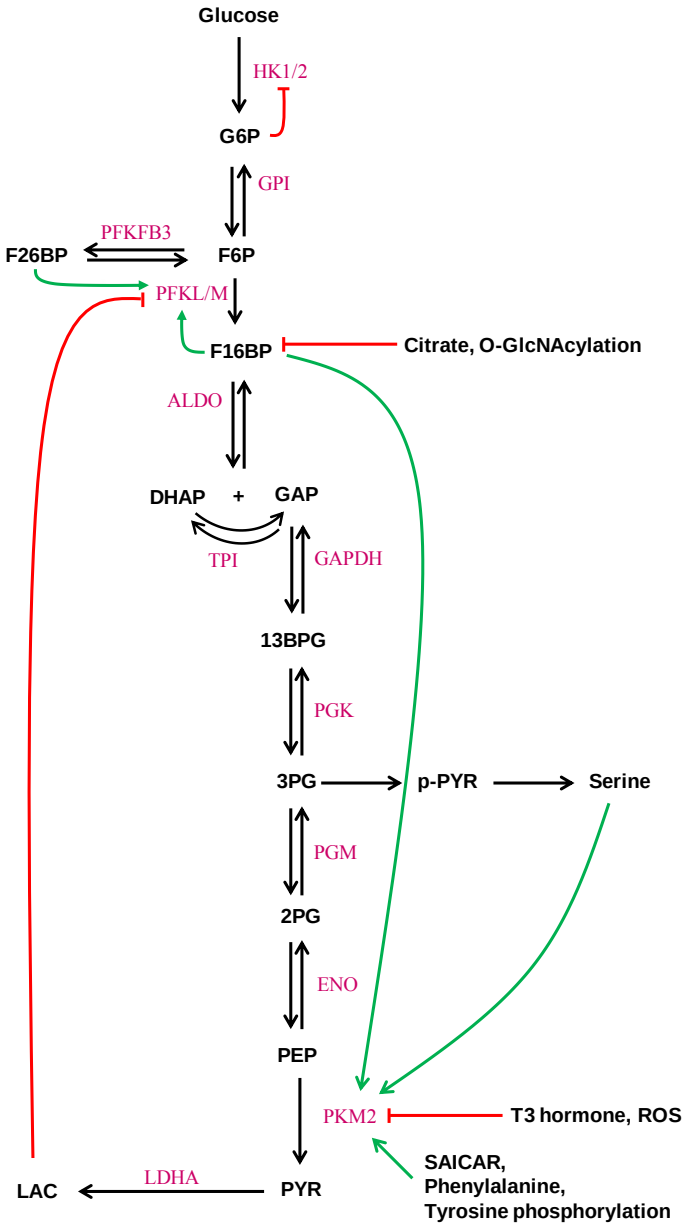

Figure 2.1: Regulation of glycolysis enzymes in proliferating cells. The rate-controlling enzymes of glycolysis HK, PFK and PK are heavily regulated by a host of enzyme activity modulators.

2.4 Regulation of Glucose Metabolism by Signaling Pathways and Growth Control Elements

Cells, in their native environments, adjust the rate at which they metabolize glucose and amino acids in response to external and internal signals. The external stimuli include metabolic hormones and growth factors, such as insulin, glucagon and epidermal growth factor, as well as cues from nutrient abundance or scarcity. An internal stimulus could be the energetic state of the cells or the growth conditions such as stress. At the core of the interface between energy metabolic pathways and those stimuli are signaling pathways that transduce the external cues to the internal regulators of energetic state and growth control elements that ultimately influence metabolic fluxes. When growth control goes awry, such as in cancer cells or continuous cell lines, a concomitant alteration in energy metabolism is observed, possibly through these coordinated regulations of growth and metabolism.

2.4.1 AKT1

AKT1 is a serine/threonine protein kinase that plays a key role in regulating a range of cellular processes such as glucose metabolism, apoptosis, cell growth and proliferation. Alterations that cause constitutive activation of AKT1, such as in cancer cells, result in dysregulation of these cellular functions. Activation of AKT1 is mediated by phosphoinositide 3-kinase (PI3K), a kinase downstream of the insulin receptor substrate (IRS) (Figure 2.2). The activated AKT1 stimulates glycolysis flux by increasing the transcription and plasma membrane localization of the glucose transporter, GLUT1 [17]. AKT1 also mediates the association of hexokinase 1 and 2 (HK1 and HK2) with outer mitochondrial membrane [18,19], providing direct access to ATP generated by mitochondria for increased activity of HK. In addition, activated AKT1 also increases the phosphorylation of PFKFB to shift its kinase/phosphatase ratio to increase the formation of F26BP [20-22], which in turn increases PFK activity and glycolysis flux. CHO and SP2/0 cells express high levels of AKT1, indicating the potential role it may play in

conferring high glycolytic nature of these cells. Interestingly, inhibition of AKT1 using LY294002 in SP2/0 cells caused a reduced phosphorylated (active) state of AKT1 and decreased glucose metabolism of the cells [23].

In addition, AKT1 also plays a role in coordinating glucose and lipid metabolism. Citrate generated in the mitochondrial TCA cycle is exported to the cytoplasm, where it is utilized for Acetyl CoA generation by the enzyme ATP-citrate lyase (ACL). ACL is directly phosphorylated and activated by AKT1 [24]. By increasing citrate utilization, AKT1 may help in driving the TCA cycle flux, in addition to providing precursors for lipid biosynthesis for new cell membrane generation.

AKT1 is also linked to positive regulation of cell survival and proliferation through inhibition of several pro-apoptotic proteins by regulating their transcription or phosphorylation. AKT1 can phosphorylate the Bcl-2-associated death promoter (BAD) protein on Ser^{136} which leads to an inhibition of cytochrome c release in response to apoptotic stimuli [25,26]. Furthermore, AKT1 promotes cell growth by activating the global growth regulator mechanistic target of rapamycin complex 1 (mTORC1).

2.4.2 mTORC1

The mechanistic target of rapamycin (mTOR) is a serine/threonine protein kinase that integrates various upstream signals including stress, growth factors and nutrients availability and relay this information to control multiple cellular processes including growth, proliferation, survival, and protein synthesis. mTOR forms two structurally distinct complexes: mTOR complex 1 (mTORC1) and 2 (mTORC2). mTORC1 consists of mTOR, regulatory-associated protein of mTOR (Raptor) and other core and non-core components. mTORC1 functions as a nutrient, energy and redox sensor and controls protein synthesis. The activity of mTORC1 is stimulated by growth factors, amino acids and oxidative stress. mTORC2 consists of mTOR, rapamycin-insensitive companion of mTOR (Rictor) and other components. mTORC2 acts as a regulator of the cytoskeleton. In this review, our focus is strictly on mTORC1 regulations.

Activation of mTORC1 requires both growth factors and amino acids availability. Insulin and other growth factors signal through the PI3K/AKT signaling pathway (Figure 2.2). Activation of AKT1 inhibits the activity of the heterodimer consisting of tuberous sclerosis 1 and 2 (TSC1 and 2). The TSC1/TSC2 complex is a negative regulator of mTORC1. Inhibition of the TSC1/TSC2 complex by AKT, therefore results in the activation mTORC1. mTORC1 also requires amino acids, particularly leucine, for its activation. Activation of mTORC1 by amino acids is mediated by the Rag-GTPases (Figure 2.2). Intracellular nutrients only basally activate mTORC1, but are essential for robust stimulation of mTORC1 by growth factors.

Global cellular protein synthesis is regulated by mTORC1 through direct phosphorylation of the eukaryotic translation initiation factor 4E-binding protein 1 (4EBP1) and the p70-S6 kinase 1 (S6K1). Phosphorylation of 4EBP1 releases the eukaryotic translation initiation factor 4E (eIF4E) allowing it to participate in the formation of the cap-dependent translation initiation complex. Activation of S6K1 by mTORC1 stimulates protein synthesis through the activation of the S6 ribosomal protein and allowing its recruitment to the pre-initiation complex. Through 4EBP1 and S6K1, mTORC1 signaling can globally enhance protein synthesis in the cells.

mTORC1 positively affects cellular metabolism and increases the flux of glycolysis. Activation of mTORC1 has been shown to globally upregulate the expression of the genes in the glycolysis, the lipid biosynthesis and the pentose phosphate pathways [27]. The action of mTORC1 is mediated by two major downstream effectors: the hypoxia-inducible factor 1-alpha (HIF1α) protein and the sterol regulatory element-binding proteins (SREBPs). mTORC1 enhances the translation of HIF1α mRNA through phosphorylation of 4EBP1 [27,28]. The increase in HIF1α protein level results in the induction of glucose transporters and many glycolytic enzymes and promotes a switch from mitochondrial oxidative metabolism to glycolysis (to be described in a later section). mTORC1 activation also dramatically increases the processing of SREBPs to their active forms through the action of S6K1 [27,29,30]. Activation of SREBPs induces

global expression of genes involved in the oxidative branch of pentose phosphate pathway and lipid biosynthesis.

2.4.3 AMPK

AMP-activated protein kinase (AMPK) is an enzyme that plays a key role in sensing the cellular energy level. An increase in the cellular AMP and a decrease in the cellular ATP levels such as during nutrient deprivation and hypoxia result in the activation of AMPK. Upon activation, AMPK inhibits anabolic ATP-consuming processes such as fatty acid and protein synthesis, and initiates catabolic ATP-producing processes including glucose catabolism and fatty acid oxidation [31,32]. Critical to this is the role of AMPK as an antagonist of mTORC1. When ATP levels are low, AMPK activates TSC2 and inactivates Raptor through phosphorylation, resulting in the suppression of mTORC1 activity (Figure 2.2) [33,34]. Suppression of mTORC1 activity by AMPK under low ATP levels thus results in the inhibition of anabolic processes including cell growth, protein synthesis and lipid synthesis.

AMPK also functions independently of mTORC1. AMPK promotes glucose catabolism under low cellular ATP level by inducing the expression of the glucose transporters GLUT1 and GLUT4 and stimulating their translocation to the plasma membrane [35,36]. AMPK has also been shown to directly phosphorylate multiple isoforms of the glycolysis enzyme PFKFB [37,38]. Phosphorylation of PFKFB serves as a conduit for AMPK as a cellular energy sensor to modulate glycolysis flux. In addition, AMPK is capable of inhibiting ATP-consuming processes including fatty acid and cholesterol synthesis by phosphorylating the enzymes acetyl-CoA carboxylase (ACC1) [39] and HMG-CoA reductase (HMGCR) [40].

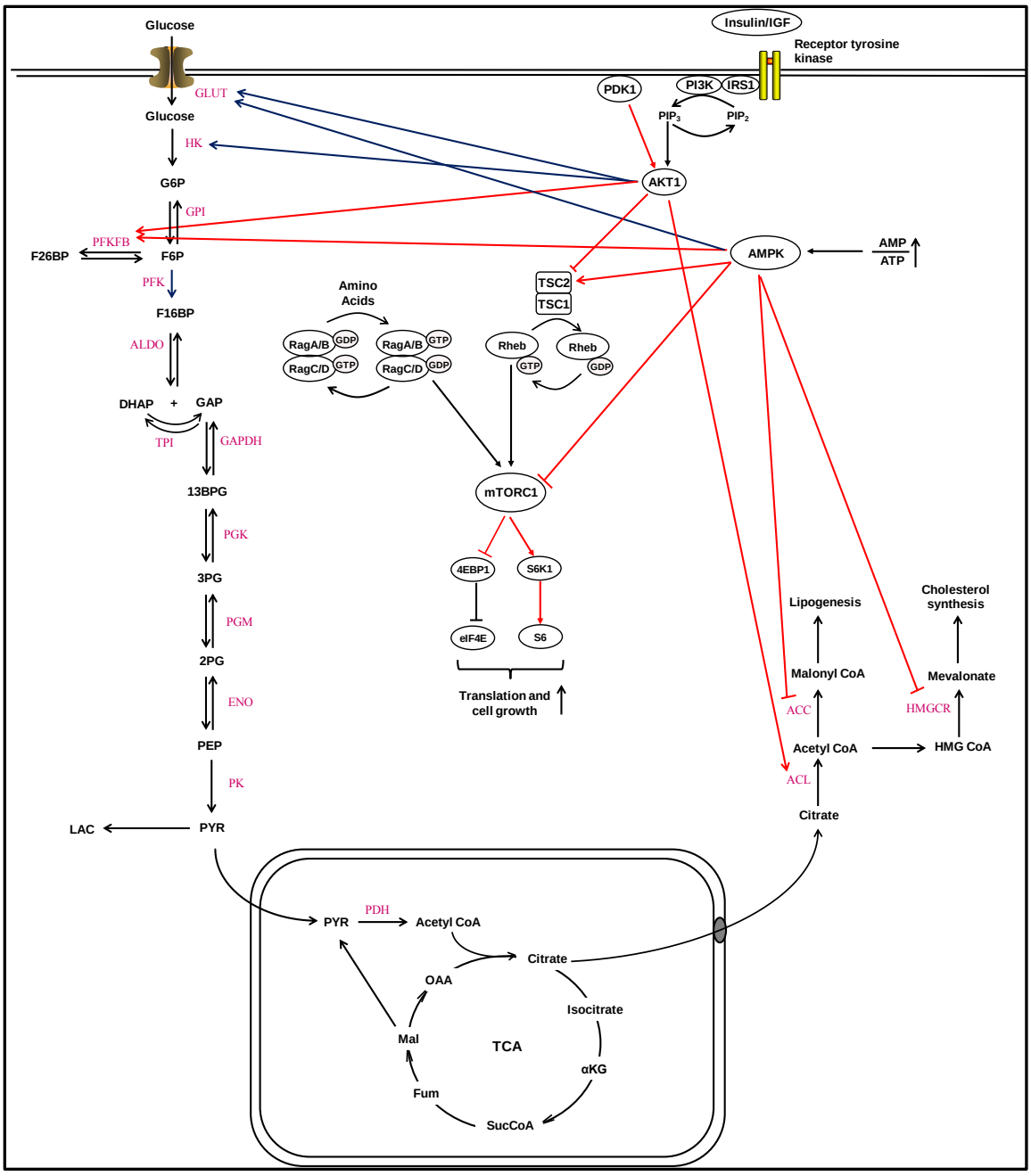

Figure 2.2: Regulatory roles of the PI3K/AKT/mTORC1 and AMPK signaling pathways in mammalian cells. The receptor tyrosine kinases are stimulated upon association with their ligands (insulin/IGF). The activated receptors recruit IRS1 and IRS2 (not shown), which cross-phosphorylate each other and recruit PI3K. Subsequently, PI3K is activated, which catalyzes the synthesis of phosphatidylinositol (3,4,5)-

triphosphate (PIP3) and recruits 3-phosphoinositide-dependent kinase 1 (PDK1) and AKT to the plasma membrane. Afterwards, PDK1 phosphorylates and activates AKT. Once active, AKT triggers pleiotropic effects, such as growth and protein translation. AKT phosphorylates TSC2 and inhibits its role as GTPase activating protein (GAP) for Rheb thereby increasing the levels of GTP-bound Rheb. Association of GTP-bound Rheb with mTORC1 stimulates its activity, which subsequently facilitates growth and protein translation through inhibition of 4EBP1 and activation of S6K1. AKT also stimulates glycolytic activity by increasing the transcription and membrane localization of GLUT1, increasing HK activity by mediating its association with outer mitochondrial membrane and increasing the activity of PFKFB. The figure also shows the regulatory roles of AMPK. AMPK is activated under the conditions of high levels of AMP and low levels of ATP such as during metabolic stresses by nutrients deprivation. Once activated, AMPK phosphorylates TSC2 to activate its GAP activity for Rheb thereby decreasing the levels of GTP-bound Rheb. AMPK also phosphorylates the Raptor component of mTORC1 resulting in the inhibition of its activity. Altogether, they result in negative regulation of mTORC1 activity, which reduces growth and protein translation. Similar to AKT, AMPK promotes glycolysis activity through induction and translocation of GLUT4 to cell membrane and phosphorylation of PFKFB to increase its activity. AMPK also phosphorylates the enzymes ACC1 and HMGCR to inhibit the synthesis of lipid and cholesterol.

2.4.4 HIF1α

The hypoxia-inducible factor (HIF) family consists of three members: HIF1, 2 and 3. HIF1 is ubiquitously expressed while HIF2 is expressed only in kidney, heart, lung and endothelial cells; HIF3 is poorly understood [41]. Each HIF is composed of a heterodimer of α and β subunits. HIF1β subunit is constitutively expressed in the cells while the level of HIF1α subunit is subject to cellular regulation. The protein level of HIF1α is regulated in oxygen dependent manner by prolyl hydroxylation. Under normal oxygen tension, HIF1α subunits are modified by prolyl hydroxylases (PHDs) which promotes their recognition by the von Hippel-Lindau (VHL) ligase resulting in the proteasomal degradation of HIF1α [42]. Under hypoxic conditions, where oxygen tensions are low, these PHDs are inhibited resulting in the stabilization of HIF1α protein level.

HIF1α promotes aerobic glycolysis through increased transcription of many glycolysis genes and inhibition of mitochondrial oxidation. The transcription of specific isozymes in glycolysis LDHA, PFKL and PKM2 among many others are upregulated upon hypoxia (Figure 2.3) [43-45]. In addition, HIF1α induces the transcription of pyruvate dehydrogenase kinase 1 (PDK1), which represses the pyruvate dehydrogenase complex (PDH), leading to decreased flux to mitochondria [46]. Altogether, these results in the inhibition of glucose flux from entering mitochondria and diverting it towards lactate production. While HIF1α is mostly active in hypoxic conditions, cancers with VHL deficiency exhibit constitutive activation and stabilization of HIF1α even in oxygenated environments.

Furthermore, the catabolic intermediates of glucose metabolism have also been shown to induce HIF1α stabilization in normoxic conditions. The intermediates mainly include the 2-oxo acids including pyruvate and oxaloacetate, among few others. The effect of pyruvate and oxaloacetate on HIF1α is attributed to the inactivation of the PHD enzymes. One hypothesis is that these metabolites render the state of the enzyme to be inactive by oxidizing a specific amino acid residue or by changing the oxidation state of the iron, a cosubstrate required for the hydroxylation reaction. This inhibition of the PHDs has been

shown to be reversible and can be relieved when treated either with amino acids, including cysteine and histidine, or ferrous (Fe(II)) ion. In addition to the glucose intermediates, accumulation of succinate or fumarate has been shown to induce HIF1α stabilization [47,48]. These compounds inhibit PHDs by interacting directly with the substrate binding site of the enzyme.

In fed-batch processes used for therapeutic protein production, typically the processes are designed such that the extracellular medium is replete of nutrients, including glucose and amino acids. However, depending on the feeding strategies employed and process parameters used, the nutrient levels in the medium can fluctuate across different processes. Such fluctuations can induce normoxic stabilization of HIF1α provided that the right nutrient conditions are met in the medium. Of late it has been observed in some fed-batch processes that lactate is produced late in culture after a period of lactate consumption or low lactate production. Such lactate production occurs upon increased feeding of nutrients. Hence, the normoxic stabilization of HIF1α could be one of the potential causes of upregulation of glycolysis and lactate production in the late stages of these fed-batch processes.

2.4.5 cMYC

The cMYC proto-oncogene is a transcription factor that can activate a large number of genes through binding to the enhancer box (E-box) sequences. Activation of cMYC in the presence of mitogenic factors including Wnt and epidermal growth factor (EGF) affects myriad of cellular processes including proliferation, metabolism and apoptosis. In many cancer cells, mutations in the cMYC gene result in its constitutive activation independent of growth factors presence or unregulated expression that leads to very high cMYC transcript levels.

cMYC has been shown to induce the expression of many glycolysis genes including LDHA, PFK, GLUT1, GPI, PGAM and ENO [49]. cMYC shares a large number of overlapping target genes with HIF1α due to the striking similarity in their binding motifs (Figure 2.3) [45,50,51]. The elevated expression of glycolysis genes in cells with

dysregulated cMYC or HIF1α further supports the notion of increased reliance on aerobic glycolysis in cancers. Induction of cMYC also results in the upregulation of the glutamine transporter ASCT2 and glutaminase (GLS), leading to increased consumption of glutamine in cancer cells [52].

2.4.6 p53

p53 is a major tumor suppressor gene that plays a crucial role in regulating cell cycle. It is activated upon stimulation by numerous stressors including DNA damage, osmotic shock, oxidative stress, and deregulated oncogene expression. p53 also affects glucose metabolism. Increased expression of p53 reduces the transcription of GLUT1 and GLUT4 [53]. In addition, p53 also downregulates the activity and cellular protein level of the enzyme phosphoglycerate mutase (PGAM) [54]. Many tumor cells with dysfunctional p53 display elevated levels of PGAM, resulting in lower level of its substrate 3-phosphoglycerate (3PG) and higher level of its reaction product 2-phosphoglycerate (2PG) (Figure 2.3) [55]. 3PG is an inhibitor of 6-phosphogluconate dehydrogenase (6PGD), the rate controlling enzyme in the pentose phosphate pathway. In addition, 2PG is an activator of 3-phosphoglycerate dehydrogenase (3PGDH), the first enzyme in the serine biosynthesis pathway. Accordingly, 6PGD and 3PGDH are stimulated in these tumors with elevated PGAM, resulting in the channeling of the glycolytic flux towards pentose phosphate pathway and serine biosynthesis [55].

Furthermore, p53 has been shown to induce the expression of the protein TP53-induced glycolysis and apoptosis regulator (TIGAR). TIGAR has a high functional homology with the phosphatase domain of the enzyme PFKFB, which catalyzes the hydrolysis of F26BP [56]. Thus induction of TIGAR by p53 results in a decrease in the level of F26BP and leads to subsequent reduction in the activity of PFK and glycolysis flux.

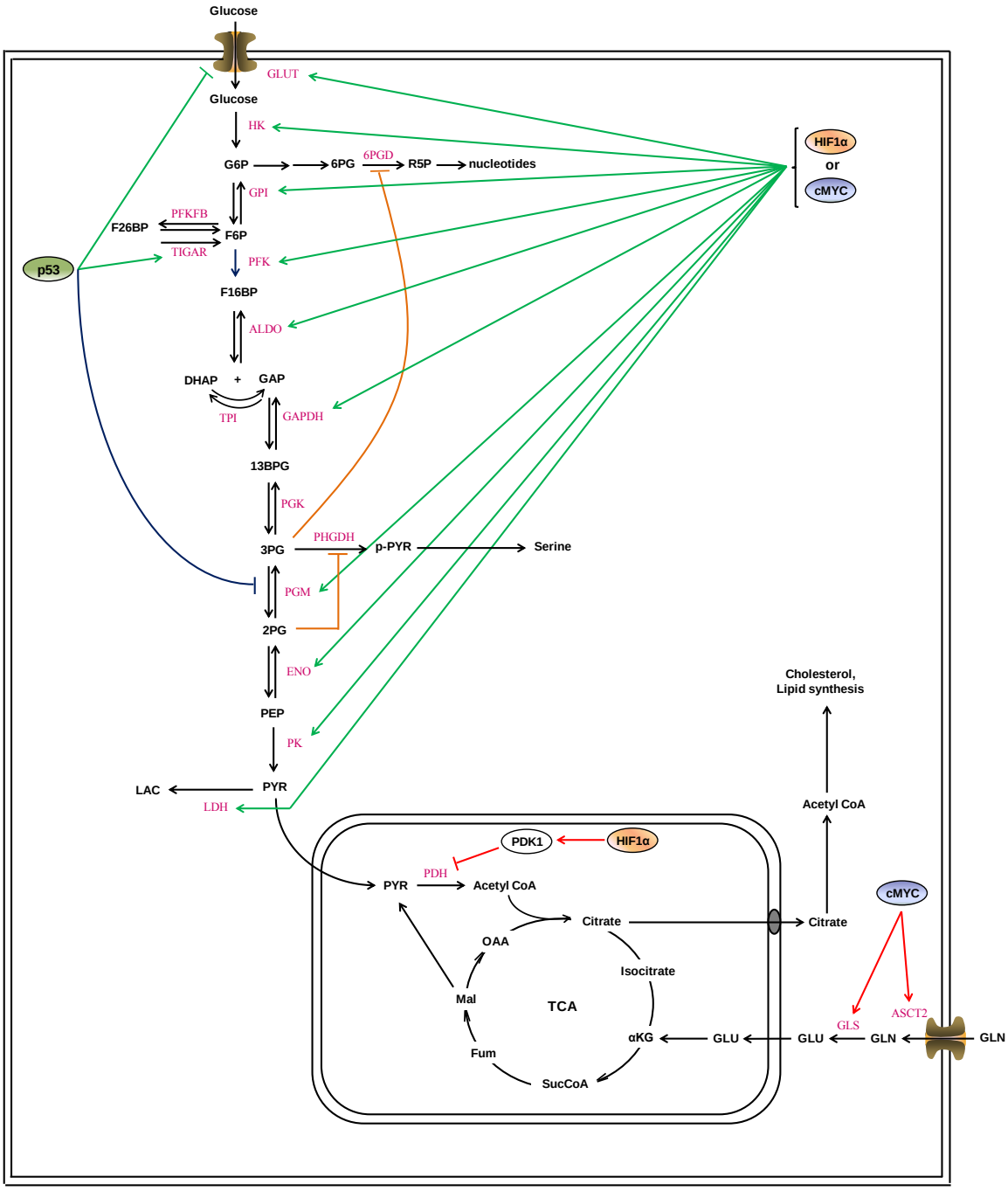

Figure 2.3: Regulatory roles of HIF1*α*, cMYC and p53 in mammalian cells. HIF1α protein level is stabilized under hypoxic conditions resulting in the induction of the expression of most glycolysis genes and PDK1. PDK1 subsequently phosphorylates PDH resulting in its inhibition which prevents glucose flux from entering the mitochondrial

TCA cycle. Also shown in the figure are the regulations by cMYC and p53. cMYC also induces a large number of glycolysis genes. The similarity in the binding motifs of cMYC and HIF1α results in a huge overlap of target genes. cMYC also strongly regulates glutaminolysis through the upregulation of the expression of GLS and ASCT2. Unlike HIF1α and cMYC, p53 decreases the activity of glycolysis by suppressing the transcription of GLUT1, by decreasing the F26BP through upregulation of TIGAR and by downregulating the protein levels of PGM.

Chapter 3 Materials and Methods

3.1 Mathematical Model of Central Metabolism Pathway

A kinetic metabolic model of energy metabolism of mammalian cells that encompasses glycolysis, pentose phosphate pathway (PPP), tricarboxylic acid (TCA) cycle, malate-aspartate shuttle and other inter-compartmental shuttles (between the cytosol and the mitochondria compartments) was constructed (Figure 3.1). The ordinary differential equation (ODE) model consists of mass balance equations for 40 reaction intermediates of the central metabolic pathways considered (Appendix Materials, Differential Equations section). The rate expressions for all enzymatic reactions were based on mechanistic derivation [57]. The rate expressions and the kinetic parameters along with their sources are listed in the Rate Equations section of the Appendix Materials. Many reactions are catalyzed by isozymes which differ not only in their rate constants but also in the type of the regulatory mechanisms they are subjected to. The allosteric regulations of these isozymes, specifically those of PFK, PFKFB and PK are considered in detail based on the Monod-Wyman-Changeaux method [58]. The levels of enzymes (or alternatively the V_{max}) were obtained from their corresponding transcript levels in cultured cells, assuming that the protein level is proportional to the transcript [23] and are listed in the Rate Equations section of the Appendix Materials.

In Chapter 4, the analyses focus on the allosteric regulations of glycolysis. A reduced model comprising of only the glycolysis pathway, the lactate production, and the pyruvate transport (Equations 1-13 in Appendix Materials, Differential Equations section) is therefore used in order to isolate the system.

In Chapter 5, we examine the shift in the metabolism of cultured mammalian cells from lactate production to lactate consumption. The complete model is therefore used since it is necessary to consider the uptake of lactate from the extracellular medium and its further oxidation in the TCA cycle (Figure 3.1, also see Equations 1-40 in Appendix Materials, Differential Equations section). The complete model also takes into account

the malate-aspartate shuttle pathway which transfers the reducing potential of cytosolic NADH into mitochondria. The malate-aspartate shuttle pathway thus plays a crucial role in maintaining the balance of NAD/NADH in the cytosolic compartment and is especially critical for the switch of metabolic state. In addition, lactate consumption phase occurs in the late stage of fed-batch cultures when the growth rate of the cells has slowed down significantly. The regulation of glycolysis flux by growth control is thus modeled by an activation of the kinase activity of the bifunctional enzyme PFKFB using an empirical formulation depicting an increasing kinase activity with increasing pAKT in a saturation type of kinetics (Equation S4 in Appendix Materials, Rate Equations section). A similar expression has been used previously to describe the effect of AKT on glycolysis [59,60].

In Chapter 6, we analyze the growth and metabolism of mammalian cells in the continuous culture. A multi-scale model is therefore constructed which incorporates the complete intracellular metabolic model described above and additional three mass balance equations describing cell growth, glucose and lactate concentrations in the bioreactor (Figure 3.2, also see Equations 1-44 in Appendix Materials, Differential Equations section). The rates of glucose consumption and lactate production are determined by the rates of intracellular metabolism of the cells (Equations 41 and 42 in Appendix Materials, Differential Equations section). The specific growth rate of the cells is assumed to follow Monod type kinetics with respect to glucose concentration and an inhibitory effect of lactate (Equation 44 in Appendix Materials, Differential Equations section) as described previously [61]. AKT activity is correlated to the growth rate of the cells. However, for the range of dilution rates considered in this study, growth rate is high and AKT is assumed to be fully active at all dilution rates.

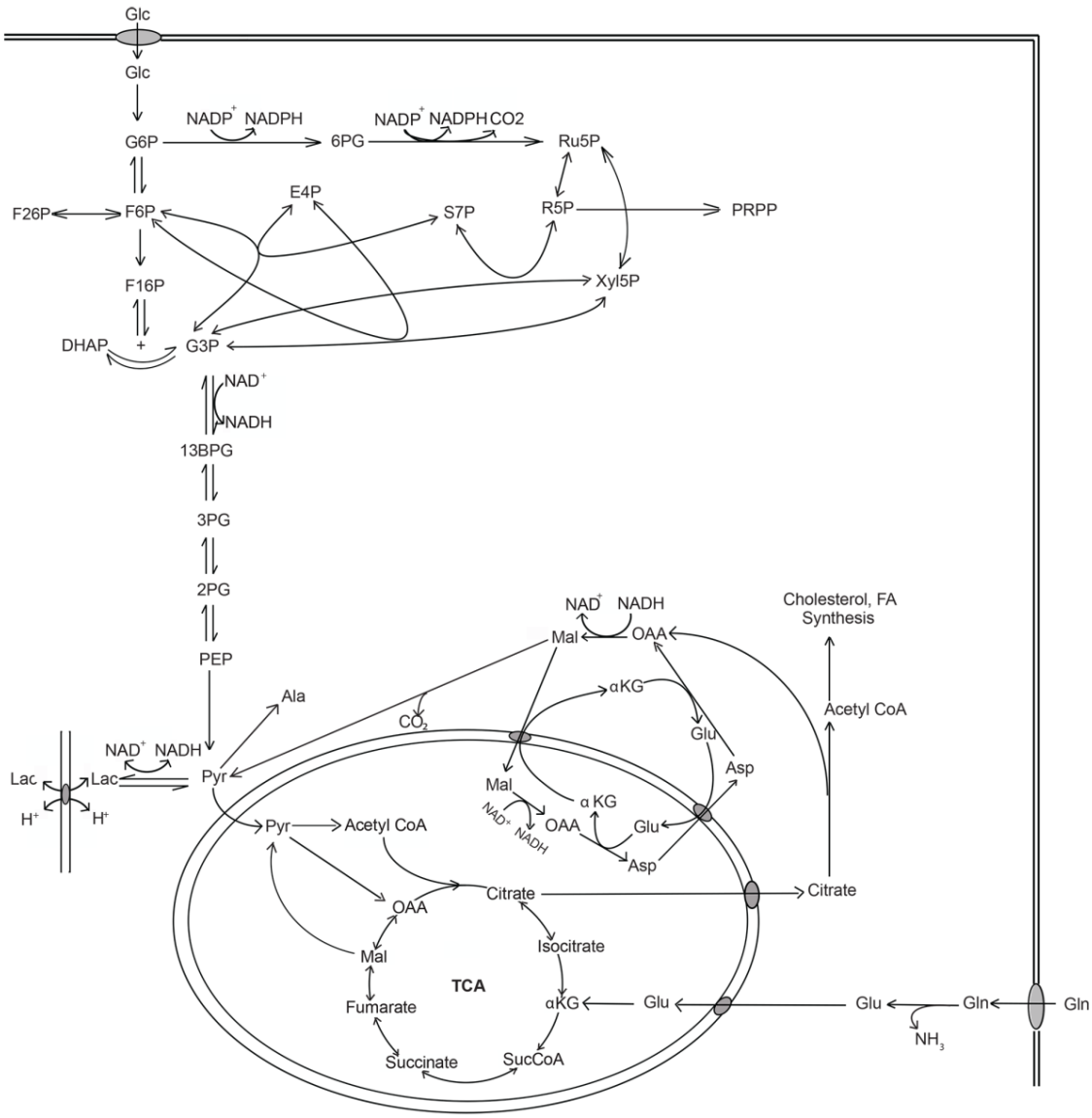

Figure 3.1: **Kinetic model of the central metabolic pathways.** The pathways include glycolysis, TCA cycle, pentose phosphate pathway (PPP) and the NAD/NADH shuttles between cytosol and mitochondria.

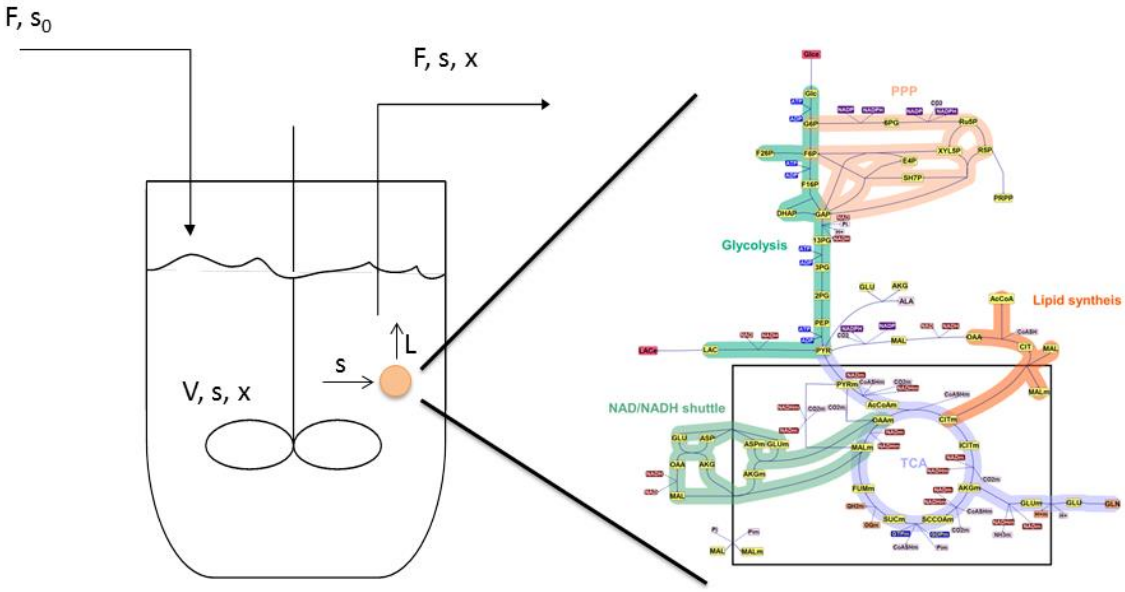

Figure 3.2: Schematic of the multi-scale reactor model. The model takes into account the intracellular metabolism of the cell and substrate utilization for macroscopic cell growth in the reactor. Notations: V, reactor volume; F, volumetric flowrate; s, glucose; L, lactate; x, cell concentration.

3.1.1 Steady State Solution

An algebraic model consisting of the steady state mass balance equations for the intermediates of all the reactions considered was derived from the ODE model. The algebraic model was used to find all the possible steady states and the corresponding eigenvalues. The inputs are the glucose concentration only for the reduced model; the glucose and lactate concentrations for the complete model; and the dilution rate and feed glucose concentration for the multi-scale model. In the simulations, intracellular concentrations of energy nucleotides (ATP, ADP, AMP) and metal ions influencing the kinetics of glycolytic enzymes (Mg^{2+}, K^{+}, Ca^{2+}) were set to be constant in order to insulate the behavior of the system from the effect of their concentration fluctuations. The fixed concentrations of these cofactors are tabulated in Appendix Table 1. The steady state solutions were obtained using the numerical solver *fsolve* in Matlab (Mathworks, Inc.). Positive and real-valued steady state solutions were calculated using initial guesses,

which were pseudorandom values drawn from the standard uniform distribution. Stability analysis was performed using eigenvalue analysis on each of the steady state solution obtained. In addition, all the intracellular concentrations at steady state were verified to ensure that they are within the same order of magnitude as the physiological range. For simulations using the complete model, the lactate export flux at steady state is generated. However, the concentration of lactate in the extracellular medium is dependent on the reactor volume, the cell concentration achieved and the duration of time that lactate is allowed to accumulate. We thus simulated the condition that extracellular lactate level is fixed independent of the lactate export flux.

3.1.2 Transient Simulation

Transient simulations of the complete model, which are discussed in Chapter 5, were performed using the ODE solver *ode15* in Matlab. The initial concentrations of extracellular glucose and lactate were 35 and 5 mM, respectively. The cell concentration was assumed to be constant at 2 $x10^7$ cells/mL throughout the duration of the simulation. pAKT activity was held constant at 0.17 in order to confine the simulations to the moment when the metabolic fate starts to diverge.

Transient simulations of the multi-scale model, which are discussed in Chapter 6, were performed using the ODE solver *ode15* in Matlab. The initial cell and lactate concentrations were $1.5x10^5$ cells/mL and 0 mM, respectively. For the batch culture simulation, the dilution rate was set to zero and the initial glucose concentration used was 15 mM. For the fed-batch culture, the dilution rate was set to zero and the extracellular glucose concentration was fixed at 0.5 mM by setting the right hand side of the differential equation for extracellular glucose (Equation 41 in Appendix Materials, Differential Equations section) to zero. Upon switching to continuous mode, the dilution rate was set at 0.033 h^{-1} and the feed glucose concentration was 7 mM. Changes in the extracellular concentrations of glucose, lactate and cell and the intracellular concentrations of all metabolites were followed.

3.1.3 Stability Analysis

For a system of ordinary differential equation $\frac{dx}{dt} = f(x)$, where $x \in R^n$ and $f : R^n \to R^n$, the Jacobian matrix, J is the $n \times n$ matrix defined by $J_{ij} = \partial f_i / \partial x_j$. The local stability of a steady state was investigated using the standard approach of calculating the eigenvalues of the Jacobian evaluated at the steady state. If all the eigenvalues have negative real part, the steady state is stable, if not it is unstable. The Jacobian matrix was calculated as part of the output of Matlab's *fsolve* function. The eigenvalues of the Jacobian matrix were evaluated using Matlab's *eig* function.

3.2 Single Nucleotide Variant Analysis

The pipeline for identification of single nucleotide variants in RNA-seq reads, which are discussed in Chapter 7, and the programs used are shown in Figure 3.3.

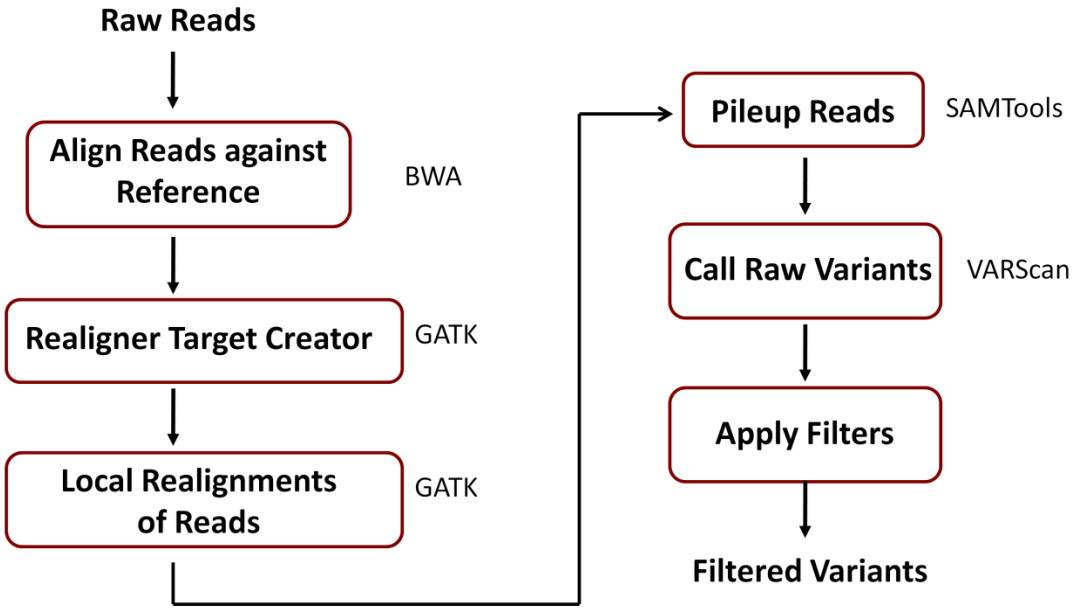

Figure 3.3: Workflow for single nucleotide variant detection.

3.2.1 Mapping and Local Realignment of Reads

RNA-seq reads were mapped to the reference transcriptome using the gap-enabled aligner BWA v.0.5.9 [62] with a maximum of 3 mismatches allowed. The resulting alignments were processed using SAMtools (v.0.1.18) [63].

BWA read alignments were refined by local realignment using GATK v. 1.5-20 [64]. A standard mapping algorithm takes each individual read and maps it to the reference. Such mapping is only optimal for each individual read, but may be sub-optimal when all of the reads are considered. The local realignment process takes into account all the reads that are locally mapped together (as opposed to individual read mapping) to correct for sub-optimal alignments that may introduce an erroneously called variant due to its close proximity to an insertion or a deletion (Figure 3.4).

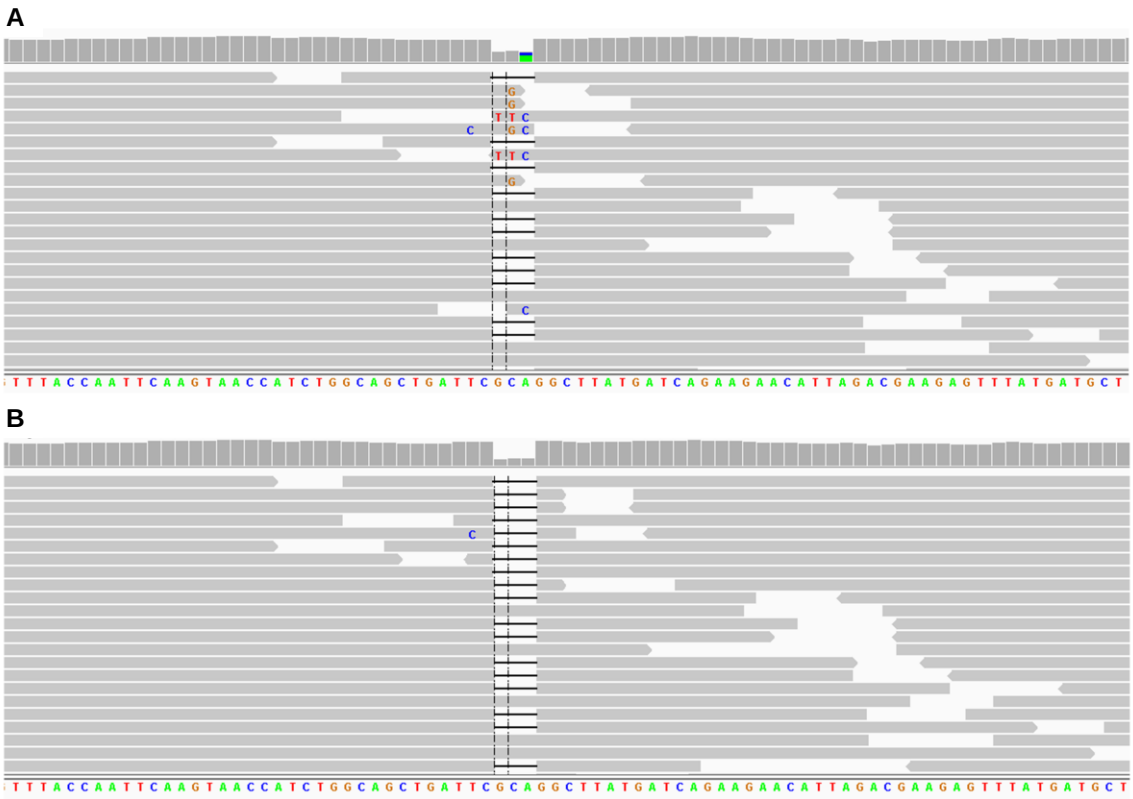

Figure 3.4: Variant call. (A) before and **(B)** after local realignment by GATK.

3.2.2 Transcript Level Quantification

All the mapped reads were then piled up on top of each other as illustrated in Figure 3.3. The number of reads mapping to a contig were summed up to generate count for each contig. The counts were then normalized across all the sample libraries to adjust for variability in sequencing depth using the upper quantile normalization method [65]. The upper quantile normalized values were further adjusted to account for variation in the contig length.

3.2.3 Identification of Single Nucleotide Variant

An initial single nucleotide variant (SNV) detection was made using Varscan v.2.3.4 [66] which employs the following heuristic approach: a minimum depth of 8 at the variant position; at least 3 reads at that position must support the variant call; and the variant call must constitute $\geq$ 1% of the total depth. Detected variants must have a base quality score $\geq$ 30 and a mapping quality score $\geq$ 20.

A Poisson model was employed to distinguish potentially real variants from random errors. In the Poisson model, the number of variant reads observed at a particular site is compared to the probability that all of those variant reads occurred due to random error (estimated at a maximum rate of 1% according to Illumina).The significance level at each variant site is quantified by the calculated *p*-value. Multiple hypothesis testing is performed by controlling the family-wise error rate (FWER) at a significance level α of 0.1 using the Bonferroni correction.

Systematic sequencing errors may also occur in RNA-seq as a result of ambiguity in base-calling. In particular, the spectra for the G and the T nucleotides are known to have significant overlap [67]. In addition, nucleotides in several specific sequence patterns, such as GGT, are prone to being misread. In the majority of cases, the problems will occur only in one strand of the reads, while the complementary reads will not be affected. Since the Illumina protocol used in this study involves sequencing both strands of the cDNA, such systematic error will manifest itself in the form of an incorrect base call in

only one specific direction of the reads. To eliminate this type of systematic error, variants that are supported by reads in only a single read direction are filtered out.

3.2.4 Phylogeny Analysis

SNVs that have sufficient depth of coverage in all libraries (depth $\geq$ 8 in all libraries) were used to construct a phylogeny tree using the DNA parsimony package in Mobyle [68].

3.2.5 Variant Verification by Sanger Sequencing

RNA was reverse transcribed using the Moloney Murine Leukemia Virus Reverse Transcriptase (M-MuLV RT) (New England Biolabs) with gene specific primers. cDNA was amplified with gene specific primers targeting the candidate variant-containing regions using the Phusion High-Fidelity DNA polymerase (New England Biolabs). PCR products were gel-purified using the QIAquick Gel Extraction kit (Qiagen), cloned into the TOPO-vector (Invitrogen), and transformed into One Shot TOP10 *E. coli* cells. Following transformation, the cells were spread on agar plates with 50 μg/mL kanamycin selection. The colonies were individually picked and expanded in LB broth containing 50 μg/mL kanamycin. The plasmids were purified using the Qiaprep Spin Miniprep kit (Qiagen) and subsequently, subjected to Sanger sequencing.

3.3 Cell Lines and Cell Culture

3.3.1 HeLa Cell Culture

The setup described here was used to perform the experiment demonstrating the existence of multiple steady states in the glycolysis of fast proliferating cells, and are discussed in detail in Chapter 4. HeLa cell line, originally obtained from ATCC (Manassas, VA) was a generous gift from Professor Kim Do-Hyung and has been reported previously [20]. HeLa cells were cultured in DMEM medium (Invitrogen, 11995-065) supplemented with 4% fetal bovine serum at 37 ^{o}C in 5% CO_2. 100 mL culture with 5 g/L of Cytodex 1 microcarriers (GE Healthcare, 17-0448-01) was carried out in a 250 mL spinner flask.

HeLa cells were inoculated at 2×10^5 cells/mL on Day 0. The procedure for microcarrier culture has been described previously [69]. On Day 5, cells on microcarriers were washed and re-suspended at 1×10^5 cells/mL in DMEM medium containing either 0.6 mM (LG) or 25 mM (HG) of glucose. The cell concentration was intentionally kept low such that the glucose concentration in the culture could be maintained at a relatively constant level without getting depleted. The two flasks were then maintained for a further 12 hours to allow the cells in LG condition to reach a low flux state and those in HG condition to reach a high flux state. Subsequently, the cells from each flask were washed twice with PBS and transferred to the wells of a 12-well plate containing 1 mL of medium with varying glucose concentration. Cells were inoculated at a high enough concentration (2×10^6 cells/mL) to allow measurable changes in the medium glucose concentration due to cellular glucose uptake. Supernatants were collected at time 0, 2, 4, and 6 hours which were then assessed for glucose and lactate levels using the Infinity Glucose reagent (Thermo Scientific, TR15421) and YSI 2700 SELECT industrial analyzer (YSI Inc.), respectively. Subsequently, using linear regression, specific rates of glucose uptake and lactate production were calculated from the glucose/lactate measurement data.

3.3.2 CHO Cell Culture

The setup described here was used to perform the experiments demonstrating the effect of initial lactate concentration and culture history on the metabolic state of CHO cells in fed-batch culture, and are discussed in detail in Chapter 5. Recombinant CHO cells producing an immunoglobulin were grown in shake flasks at 36.5 ^oC and 5% CO_2 environment. The medium and the culture conditions used have been previously reported [15,22]. Cells were inoculated at $6x10^5$ viable cells/mL. Starting on Day 3, the cultures were fed with feed medium equivalent to 1.8% of the initial culture volume. pH was measured daily using a blood gas analyzer and adjusted to 7.2 using 1.0 M sodium carbonate (Na_2CO_3). Samples were taken daily for measurements of cell density, viability, glucose and lactate concentrations using a Nova Bioprofile instrument. 500 g/L glucose solution was used to supplement the cultures with glucose as and when required to maintain the glucose levels above 1.5g/L.

3.3.3 MAK Cell Culture

The setup described here was used to perform the experiments demonstrating an approach to direct a continuous culture toward a steady state with high cell concentration and low metabolic flux, and are discussed in detail in Chapter 6. A mouse-mouse hybridoma cell line, MAK, and its defined, serum-free medium have been described before [70]. All experiments were performed in a 750 mL glass bioreactor with a working volume of 550 mL.

Fed-batch cultures were initiated using cells in the exponential growth phase at a concentration of $1.5x10^5$ cells/mL. The medium used was the same as that used for cell maintenance except for the initial glucose and glutamine concentrations which were at 0.55 mM and 0.17 mM, respectively. Oxygen Uptake Rate (OUR) was measured every five minutes and the cumulative oxygen consumption was calculated on-line. Using a previously established glucose and oxygen stoichiometric ratio [70], the amount of glucose consumed was calculated and the amount of feed medium required to maintain glucose at the set point was added. The culture was operated in batch mode until glucose concentration reached 0.28 mM as estimated by on-line calculation at which point concentrated nutrient feeding was initiated. The nutrient concentration in the feed was ten times higher than the maintenance medium, except for glucose which was at 66.7 mM. During the cultivation, glucose was measured off-line and if necessary the stoichiometric ratio used for estimating the on-line feeding rate to maintain the set point was adjusted.

Continuous cultures were initiated from either batch or fed-batch cultures. At the time point of switch, feed was added and culture fluid from the reactor was withdrawn at equal rate as dictated by the desired dilution rate. The feed for the continuous cultures had the same nutrient concentrations as that used for cell maintenance except for glucose (5.3 mM), glutamine (2.9 mM) and other amino acids (1.6x the concentration of maintenance medium).

Chapter 4 Bistability in Glycolysis as a Robust Biological Switch in Energy Metabolism

4.1 Summary

This chapter explores the effect of allosteric regulations on the behavior of glycolysis. The enzymes of glycolysis are tightly controlled by allosteric regulations by the intermediates upstream and downstream of the pathway. The literature is rife with in vitro studies assessing the effect of allosteric regulations on virtually all metabolic enzymes. However, such studies were performed often at single or few enzyme steps level. The holistic effect on the complete metabolic pathway level is not known. In this chapter, using a mathematical model based on reported mechanisms for the allosteric regulations of the enzymes, we show that the synergistic action of these regulations can confer glycolysis with novel, previously undiscovered behavior in mammalian cells. Two regulatory loops centering on the enzymes phosphofructokinase and pyruvate kinase each gives rise to multiple steady state behavior, segregating glucose metabolism into high flux and low flux states. The steady state multiplicity is observed only when specific combinations of isozymes are expressed. Distinct combination of isozymes in glycolysis gives different cell types the versatility in their responses to different energetic needs. Steady state multiplicity endows glycolysis with a robust switch to transit between the two flux states. Under physiological glucose levels, the glycolysis flux does not switch between the states easily without an external stimulus such as hormonal, signaling or oncogenic cues.

4.2 Introduction

Glycolysis is the conduit of glucose metabolism for generating energy and providing biosynthetic precursors for cellular materials. The flux of glycolysis in cancer cells is high compared to normal adult tissues and a vast amount of the glucose consumed is diverted towards lactate production; a phenomenon known as the Warburg effect [71]. This behavior is also typical of highly proliferative tissues such as fetal tissues and stem

cells [72,73]. In contrast, quiescent cells transport glucose at low rates and catabolize most glucose to carbon dioxide [74,75]. The Warburg effect was previously attributed to defective oxidative phosphorylation [71,76] until it was realized that the pathway was not impaired in most tumor cells (see review [77]).

The differences in glycolysis activity observed across various cell types are accomplished through different levels of regulation [78]. At one such level is the allosteric feed-back and feed-forward regulations exerted by the intermediate metabolites on its enzymes. Pivotal roles are played by three enzymes, (phosphofructokinase (PFK), pyruvate kinase (PK) and phosphofructokinase /fructose-2,6-bisphosphatase (PFKFB)) through their inhibition or activation by three reaction intermediates (fructose-1,6-bisphosphate (F16BP), fructose-2,6-bisphosphate (F26BP), and phosphoenolpyruvate (PEP)) in glycolysis. These enzymes have multiple isoforms (PFKL/M/P, PKM1/M2/L/R and PFKFB1-4) which are subjected to contrasting allosteric regulations [12,79,80]. Each isoform, therefore, affects the glycolytic activity in a distinct manner.

All three isoforms of PFK are activated by F6P and F26BP [6], but only PFKM and PFKL are activated by F16BP [7-9]. PFKFB is a bifunctional enzyme whose kinase and bisphosphatase domains catalyze the formation and hydrolysis reaction of F26BP, respectively [11,12]. Isozymes of PFKFB differ in their kinase and phosphatase activities as well as in their sensitivity to feedback inhibition by phosphoenolpyruvate (PEP) [81-83]. Thus, each isozyme of PFKFB has a profoundly distinct capacity in modulating PFK activity. Pyruvate kinase (PK) in mammalian systems is encoded by two genes that can produce two isoforms each. Except for the PKM1 isoform, the other three isoforms of PK, PKM2, PKL and PKR, are activated by F16BP to varying extents [80]. The sensitivity of the M2 isoform to such wide ranging modulators allows it to act, in-part, as the cell's nutrient sensing machinery [15]. Different tissues and cell types express different isoform combinations of these enzymes, thus giving rise to a suitable glycolytic flux behavior that caters to the biosynthetic and energetic needs of the cell type in question.

The expression of the isoforms of glycolytic enzymes and their regulation is tightly linked to the control of cell growth [84]. The make-up of the glycolytic isoforms in quiescent tissues strictly restrains its flux, thus restricting the provision of the carbon for growth and proliferation. There is increasing evidence that loss of the growth control as in the case of tumor formation caused by mutations in proto-oncogenes and tumor suppressors, is accompanied by alteration in the expression of specific glycolytic isozymes leading to metabolic reprogramming [85,86]. For example, HK2 is only expressed in limited number of adult tissues but is expressed at high levels in cancer cells. HK2 binds to the outer mitochondrial membrane and inhibits the release of cytochrome c to suppress apoptosis and promotes cell survival in cancer cells [19,87]. Analogously, the embryonic isoform of pyruvate kinase, PKM2, is found to be expressed in few adult tissues, but is known to be highly expressed across wide range of tumor cells. Interestingly, knockdown of PKM2 in cancer cells, such as the human lung cancer cell line H1299, and replacing it with PKM1 was demonstrated to result in a metabolic phenotype change involving decreased glucose uptake and increased oxidative phosphorylation [88]. Further, reprogramming of somatic cells to induced pluripotent stem cells (iPSCs) has also been shown to incur metabolic reprogramming; the change from a low glycolytic flux state of somatic cells to a high flux state of rapidly dividing iPSC cells is accompanied by a switch in the isozyme expression of HK and PFK enzymes [74].

The composition of isozymes in glycolysis, through these regulations, is therefore pivotal to the flux control and plays a key role in growth control and physiological balance. Over the last four decades, the kinetic behavior of isoforms of individual glycolytic enzymes has been examined in detail. However, a holistic understanding of the effect of different combinations of such isoforms on the flux behavior of the complete glycolysis pathway is yet to be attained. We have taken a systems biology approach to study the flux states of glycolysis pathway. Using a mathematical model that employs mechanistic rate equations for glycolysis enzymes, we demonstrate that glycolysis exhibits a classical multiple steady state behavior in terms of its flux with respect to the glucose

concentration. The multiplicity of steady states segregate cell metabolism into distinct states: high glycolytic flux states and low glycolytic flux states. Such bistable behavior is an output of complex allosteric regulations which in turn depend on the type of glycolytic isozymes expressed. We show that the presence of the muscle or the liver isozyme of PFK or/and the L, R or M2 isoform of PK is necessary for multistability in glycolytic flux. We substantiated the modeling insights with gene expression data from various tissues as well as experimental data from HeLa cells. Further, we discuss the factors that affect the bistable nature of the glycolysis such as the expression of different isozymes at different proportions.

Similar kinds of bistable behavior have been shown to act like a robust switch in many regulatory circuits including oocyte cell maturation [89], transition from quiescent to proliferative modes in mammalian cells [90], transition between multiple phospho-form stable states in multisite phosphorylation systems [91], among many others. The dissection of glycolytic flux as a bistable switch will provide new insights on the regulation of cell metabolism and possibly allow for a new perspective in identifying ways to modulate metabolic activities for therapeutic purposes.

4.3 Results

In the following sections we will first present the steady state behavior of the F6P-node, and then discuss the effect of the regulatory behavior of F6P-node on the glycolysis flux. This is followed by description and analysis of the effect of a second regulatory loop acting on the glycolysis pathway. Lastly, the combined effect of the two loops will be discussed.

4.3.1 Bistability in the F6P-node

PFK is a pivotal enzyme in glycolysis and exists in three distinct isoforms. The muscle (PFKM) and the liver (PFKL) isozymes are under allosteric feedback activation by F16BP to a varying extent [7,8,92], whereas the platelet isozyme (PFKP) is not [93]. It is well known that feedback activation can give rise to ultrasensitivity and even bistability.

To assess the effect of the allosteric regulation of F16BP on the PFK flux, we constructed a mechanistic model around the F6P-node encompassing the reactions catalyzed by the enzymes PFK and aldolase (ALDO) (Figure 4.1A, also see Materials and Methods, Mathematical Model of Central Metabolism Pathway section). The values of kinetic parameters for each enzyme were obtained from various literatures in which the values have been experimentally determined [6,8,94]. The simulated steady state behavior is thus only affected by the relative abundance levels of the two enzymes involved. The relative enzyme levels were obtained from their corresponding transcript levels in cultured cells and assuming that the protein level is proportional to the transcript [23].

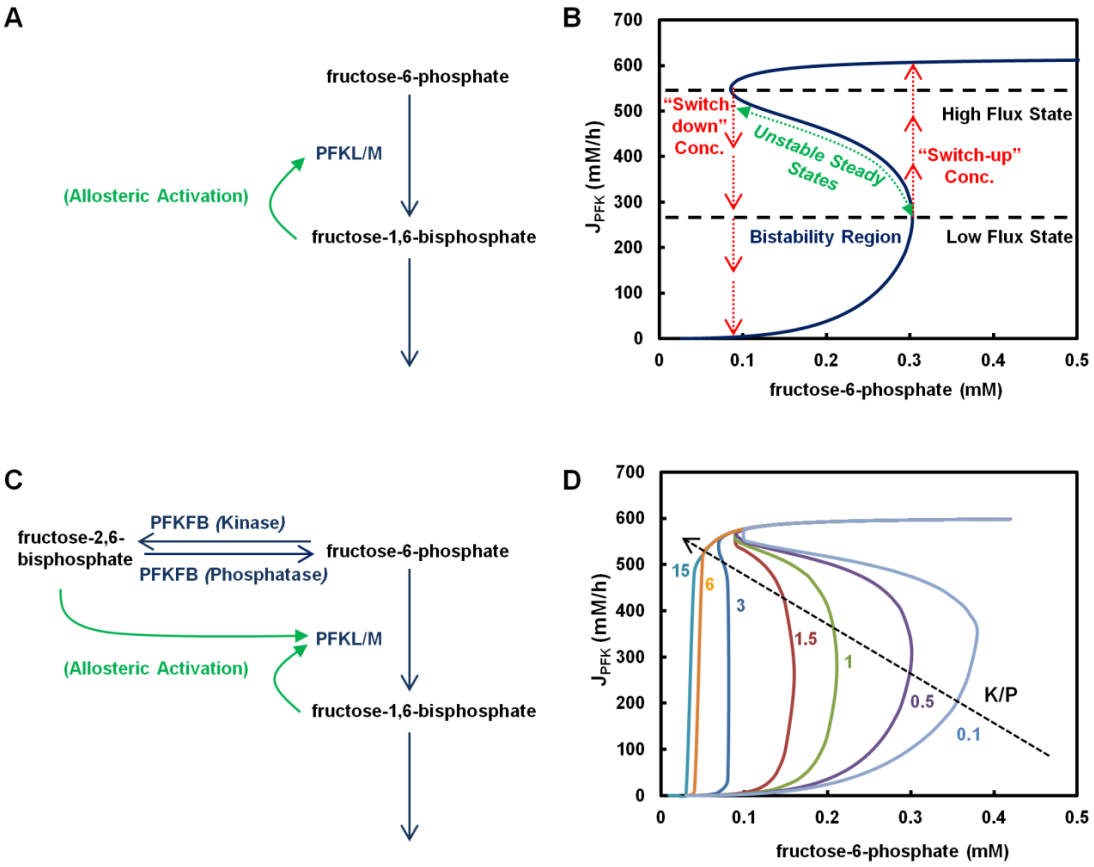

Figure 4.1: Multiplicity of steady states in the kinetics of fructose-6-phosphate node (F6P-node). **(A)** Feedback activation of phosphofructokinase (PFK) by fructose-1,6-bisphosphate (F16BP) **(B)** Bistability in the kinetics of PFK due to feedback regulation by F16BP. The simulation was performed using only two enzymes PFK and ALDO. F6P

was varied and the steady state PFK flux was solved algebraically. Activation of PFK by F16BP was set at $\boldsymbol{K_{PFK,fbp}}$ = 0.65 mM. **(C)** Allosteric regulations in the F6P-node. **(D)** Modulation of bistability span by kinase to phosphatase ratio (K/P) of PFKFB. The bifunctional enzyme PFKFB was integrated with PFK and ALDO to construct a three enzyme system. Simulations were performed at varying K/P value of PFKFB while keeping all other conditions the same as in **(B)**.

In the absence of feedback activation by F16BP, as is the case for PFKP, the steady state flux resembles a Michaelis-Menten type of kinetics (Appendix Figure 1). In contrast, the activation by F16BP on PFK as in the case of the isozyme PFKL (or PFKM) [6,8], causes the steady state flux of PFK at different F6P concentrations (Figure 4.1B) to bear the hallmark of bistability. In the region bound by F6P concentrations from 0.09 mM to 0.3 mM, three types of steady state can be seen, two of which are stable (low flux states and high flux states) and the ones in the middle are unstable. The physiological concentration of F6P in rat liver tissue has been reported to be ~0.1 mM [95]. Outside the region, only one steady state for a given F6P concentration is observed; below 0.09 mM the PFK steady state flux exists only in the low state, whereas above 0.3 mM it exists only at the high state. Eigenvalue analysis confirmed the stability of each steady state. It should be noted that the above specified concentration ranges for bistable behavior are subject to the model parameters (kinetic constants and enzyme levels) of the F6P-node.

In the bistable region, the flux can be either at a low or a high state depending on the previous state of the system. The in-between states are unstable in nature; these states are never realized experimentally. When the concentration of F6P is varied slowly, the PFK flux changes along the stable steady state lines. Starting at a low flux state, as the F6P concentration increases, the flux increases along the low flux steady state line until the F6P concentration reaches 0.3 mM ("switch-up" concentration, Figure 4.1B), and then the system undergoes a sharp transition to a high flux state. Further increase in F6P moves the system farther up along the high flux steady state line. Conversely, if the system is initially at a high flux state, as the F6P concentration decreases, the flux remains at the high state until the F6P concentration decreases to 0.09 mM ("switch-

down" concentration, Figure 4.1B) where it rapidly descends to the low state. Once the system is switched from the low flux state to the high flux state, or vice versa, it does not switch back to the original state by small fluctuations of F6P concentration at the switch-concentration. The system is thus marked by well separated high flux and low flux states, and very distinctive "switch-up" and "switch-down" F6P concentrations.

All three isozymes of PFK are activated by F26BP. The bi-functional enzyme PFKFB catalyzes both the formation and degradation of F26BP (Figure 4.1C). The steady state concentration of F26BP is thus not affected by the expression level of PFKFB but by the balance between the relative activities of the kinase (K) and the bisphosphatase (P) domains of PFKFB. Thus, the flux through PFK is indirectly influenced by the K to P activity ratio of PFKFB, also termed as the K/P ratio. We examined the regulation of the PFK flux by incorporating PFKFB into the model of the F6P-node. The experimentally determined values of kinetic parameters for PFKFB were also obtained from literature [96,97]. The K/P ratio of PFKFB alters the steady state behavior of PFK flux as shown in Figure 4.1D. Bistability is present for a wide range of K/P ratios. However, at a very high level of K/P ratios (>10), the bistable behavior disappears and the PFK flux exhibits a saturation type of kinetics. Thus, changes in the K/P ratio of the PFKFB result in the modulation of the steady state PFK flux.

Different isozymes of PFKFB have widely different K/P ratios [12], giving rise to different steady state behaviors of F6P-node. The brain isoform of PFKFB3 (with K/P ~ 700) will have a lower switch-up F6P concentration than the muscle isoform PFKFB1 (K/P ~ 0.4). In addition, hormonal or growth factor mediated regulations can modulate the K/P ratio of PFKFB isozymes (see review [11]). Such a regulation thus equips cells with a way to modulate the F6P-node steady state behavior acutely, without undergoing a switch in their isozyme composition (chronic effect).

4.3.2 Multiplicity of Steady States in Glycolysis

In the following discussions, we extend our analysis to the entire glycolysis pathway (Materials and Methods, Mathematical Model of Central Metabolism Pathways section).

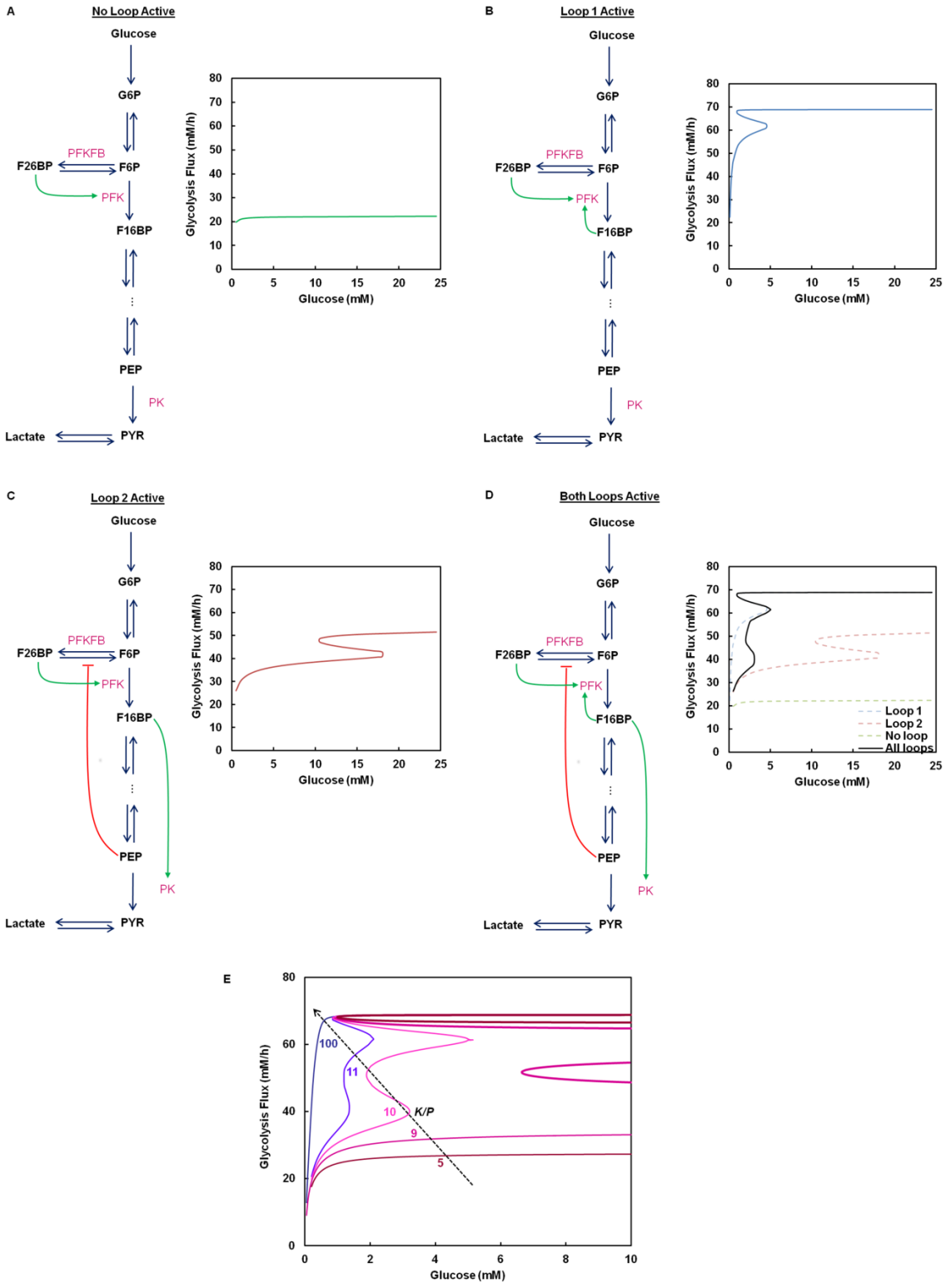
A
No Loop Active
Glucose
G6P
PFKFB
F26BP
F6P
PFK
F16BP
PEP
PK
Lactate
PYR
Glycolysis Flux (mM/h)
Glucose (mM)
B
Loop 1 Active
C
Loop 2 Active
D
Both Loops Active
Loop 1
Loop 2
No loop
All loops
E
100
11
10
K/P
9
5

Figure 4.2: Multiplicity of steady states in the glycolysis flux. (A) Steady state glycolysis flux with neither Loop 1 nor Loop 2 active. The isozyme set consisting of PFKP (no activation by F16BP) and PKM1 (no activation by F16BP) were used in the simulation. The steady state flux exhibits classical Michaelis-Menten kinetics. **(B)** Steady state glycolysis flux with only Loop 1 active. When only Loop 1 is active, the glycolysis flux exhibits bistability. The isozyme set PFKL ($K_{PFK,fbp}$ = 0.65 mM) and PKM1 were used in the simulation. **(C)** Steady state glycolysis flux with only Loop 2 active. When only Loop 2 is active, the glycolysis flux also exhibits bistability. The isozyme set PFKP and PKM2 ($K_{PK,fbp}$ = 0.04 mM) were used in the simulation. **(D)** Steady state glycolysis flux with both Loop 1 and Loop 2 active. The isozyme set PFKL and PKM2 were used in the simulation. When both Loop 1 and Loop 2 are active, multiplicity of steady states resembling superposition of **(B)** and **(C)** is observed. For **A-D** the K/P of PFKFB was set at 10. **(E)** The effect of modulation of the kinase to phosphatase ratio (K/P) of PFKFB on the multiplicity of steady states in glycolysis. In this simulation PFKL and PKM2 were used, while K/P was varied.

For the purpose of this study, we will be focusing on the regulations of PFK, PFKFB and PK. Feedback inhibition of HK by G6P and feed-forward activation of PFK by F26BP were considered and kept active in all the simulations discussed later. The known regulations for PFK, PFKFB and PK can be grouped into two regulatory loops: Loop 1 and Loop 2 (Figure 4.2). Loop 1 consists of the feedback activation of PFK by F16BP and activation of PFK by F26BP. Loop 2 entails three regulations consisting of the feed-forward activation of PK by F16BP, the feed-back inhibition of PFKFB by PEP and activation of PFK by F26BP. The three regulations in Loop 2, when active simultaneously, yield feedback activation effect on the activity of the glycolysis pathway.

The presence or absence of the allosteric regulations considered in Loop 1 and Loop 2 is determined by the isozymes that constitute the pathway. Loop 1 is operational with the muscle or liver isoforms of PFK (PFKM or PFKL), but not with the platelet isoform (PFKP) as the latter lacks the feedback activation by F16BP. Loop 2 is mainly seen with the expression of liver (PKL) or the red blood cell (PKR) or the M2 isoform of PK

(PKM2) which are strongly activated by F16BP, but not with the M1 isoform (PKM1). Depending on the make-up of the isozymes, the glycolysis pathway in a tissue or a cell may have allosteric regulations of Loop 1, Loop 2, both or neither. This is illustrated in the expression profile of glycolytic isozymes compiled from published RNAseq transcriptome data of developing human embryos [98], HeLa cells [99], mouse adult tissues and transformed cells [100] (Appendix Table 2 and Appendix Table 3).

We will show that the bistable behavior imparted by the allosteric regulation at F6P-node is extended to glycolysis pathways through Loop 1. Subsequently, we will also show that the allosteric regulation of Loop 2 also gives rise to bistability. However, Loop 2 encompasses a larger segment of glycolysis. Therefore the bistable behavior of Loop 2 will only be shown as glycolysis flux, rather than as an isolated node.

The glycolysis flux with neither Loop 1 nor Loop 2 regulation is shown in Figure 4.2A. This case reflects a combination of PFKP (thus Loop 1 inoperative) and PKM1 (Loop 2 inactive), such as in oocyte or zygote in which PFKP and PKM1 are the dominant isozymes expressed (Appendix Table 2). The simulation was performed by omitting both the terms corresponding to the F16BP feedback activation in the equation for PFK ($\boldsymbol{K_{PFK,fbp}}$) and the F16BP feed-forward activation in the equation for PK ($\boldsymbol{K_{PK,fbp}}$). In addition, the K/P ratio of PFKFB was set to 10. The simulated steady state glycolysis flux exhibits no bistability at any K/P ratio (Figure 4.2A and Appendix Figure 2); the steady state flux approaches its maximum level at a relatively low glucose concentration.

The case that only Loop 1 is active occurs when either PFKL or PFKM and PKM1 are the dominant isoforms expressed. Such a combination of isozymes is seen mainly in various sections of brain tissue including cerebellum, cortex and frontal lobe (Appendix Table 3). The simulation was performed by setting $\boldsymbol{K_{PFK,fbp}}$ = 0.65 mM (for PFKL [6,8] and omitting the F16BP feed-forward activation term in the rate equation for PK. The K/P ratio of PFKFB was set to 10. All the enzyme levels (including both PFK and PK) and all other kinetic constants were kept at the same values as in Figure 4.2A. As shown in Figure 4.2B, incorporation of Loop 1 (which is equivalent to introducing the F6P-node

to glycolysis), elevates the glycolysis flux to a much higher level and a region of bistability is seen.

Similarly, the effect of the Loop 2 alone is shown in Figure 4.2C. This is the case when PFKP is the dominating PFK isozyme with PKL, PKR or PKM2 as the PK isozyme. Large and small intestine express such a combination of isozymes (Appendix Table 3). The simulation was performed by omitting the F16BP feedback activation term in the equation for PFK and setting $\boldsymbol{K_{PK,fbp}}$ = 0.04 mM (for PKM2 [80]). The K/P ratio of PFKFB was set to 10. All the enzyme levels (including both PFK and PK) and all other kinetic constants were kept at the same values as in Figures 4.2A-B. In this case the extent of the maximal flux is somewhat lower than the case of Loop 1 alone. A bistable region is seen with both the switch-up and the switch-down concentrations of glucose shifted toward a higher level of glucose.

When both the loops are active, such as in case of hESCs, HeLa cells (Appendix Table 2) and mouse transformed cell lines (MEL and 10T1/2) (Appendix Table 3), the glycolysis flux has multi-stable behavior (Figure 4.2D). The simulation was performed by setting $\boldsymbol{K_{PFK,fbp}}$ = 0.65 mM (for PFKL) and $\boldsymbol{K_{PK,fbp}}$ = 0.04 mM (for PKM2). The K/P ratio of PFKFB was set to 10. All the enzyme levels (including both PFK and PK) and all other kinetic constants were kept at the same values as in Figures 4.2A-C. Three stable steady states and two unstable steady states can be seen for this case. The maximum flux is the same as that of Loop 1 alone while the multiple steady state region resembles the composite of the stability curves for Loop 1 and Loop 2 (Figures 4.2B and 4.2C).

The results show that the steady state glycolytic flux may be at a high flux or a low flux state depending on the presence or absence of the regulatory Loop 1 and Loop 2. Without Loop 1 and Loop 2 active, in the physiological range of glucose concentration (5-10 mM) glycolysis flux is at a low flux state (Figure 4.2A). With Loop 1 active alone, it will be at a high flux state (Figure 4.2B). To switch to a low flux state from a high flux state, the glucose concentration will need to decrease to a low level that is rarely seen physiologically; whereas if the initial flux is at a low state, as soon as the glucose level

reaches a physiological level of 5 mM the flux will switch to a high state. The steady state behavior with Loop 2 active alone is rather different from the case of Loop 1 active alone; the flux in the physiological glucose concentration range is at a low state with a switch up concentration at the high end edge of physiological concentration (Figure 4.2C). Even if the flux is initially at a high state, it will switch to a low state when glucose decreases to a physiological level below 10 mM.

With both Loop 1 and Loop 2 active, the flux is at a high state in the physiological range of glucose. Interestingly, from a high flux state the system can switch only to the low state, bypassing the intermediate stable steady states. The intermediate stable steady states can be reached only from a low flux state by increasing glucose concentration. The stability of those steady states was verified by eigenvalue analysis.

In both the loops described above, F26BP plays a regulatory role through its allosteric control over PFK. The level of F26BP can be modulated by the K/P ratio of PFKFB. We have shown above that modulation of K/P affects the bistability behavior in the F6P-node alone (Figure 4.1D). This effect of flux modulation through K/P is also translated to the entire glycolysis flux (Figure 4.2E). The simulations were performed using exactly the same conditions as those used in Figure 4.2D, except for the K/P value which was varied. The multiple steady state region shifts as K/P ratio of PFKFB changes. At higher values the multiple steady state region is lost and the flux behaves like typical saturation type of kinetics. Reducing K/P has the effect of shifting the multiple steady state region to higher concentration range of glucose. At very low levels of K/P the multiple steady state region moves outside of the normal physiological range of glucose (> 10 mM).

To evaluate the robustness of the multiple steady state behavior, sensitivity analysis on the multiplicity of steady states was performed by changing the levels of each enzyme (over a range of two orders of magnitude) while holding all the other kinetic parameter values constant. The results show that for all enzymes, the multiplicity of steady states can be seen to exist over a wide range of enzyme levels except for HK (Appendix Figure 3). It has been reported that such a tight control of HK, either at enzyme level or through

allosteric regulation, is required in order for the glycolysis flux to reach a steady state [5]. Changing the concentration of the enzyme in the ranges shown in Appendix Figure 3 maintains the presence of the bistable behavior but shifts the switch-up and the switch-down concentrations.

We further examined the sensitivity of the steady state behavior to a number of model parameters whose value was kept constant in this study, including the cellular redox state ([NAD]/NADH]), the ratio of mitochondrial pyruvate and lactate concentrations ($[PYR]_m$/[LAC]) and the ratio of mitochondrial pyruvate and alanine concentrations ($[PYR]_m$/[ALA]). For [NAD]/NADH], multiplicity of steady states was observed over a wide range of the ratio (0.5 to 700) (Appendix Figure 4A). At very low [NAD]/[NADH] ratios ($\leq$ 1), glycolytic flux has three steady states as compared to five steady states seen at higher [NAD]/NADH] ratios ($\geq$ 9). The data suggest that [NAD]/NADH] ratio has a marginal effect at very low values. The effects of $[PYR]_m$/[LAC] and $[PYR]_m$/[ALA] were probed by maintaining $[PYR]_m$ constant (at 0.1 mM) and varying either [LAC] or [ALA] (Appendix Figure 4B and Appendix Figure 4C). Multiplicity of steady states was observed across the range in which lactate and alanine were varied. No effect on the steady state flux profile was observed when lactate was varied. Whereas, at higher concentrations of alanine, the switch-up concentration moves closer to upper bounds of (or in some cases beyond) the typical range of physiological glucose concentrations.

4.3.3 Bistability in Cultured Cells

We employed HeLa cells to examine the bistability in glycolysis flux. HeLa cells initially grown on microcarriers in high glucose (HG) medium were split into two cultures with either low glucose (LG) (0.6 mM) or high glucose (HG) (25 mM) (see Materials and Methods, HeLa Cell Culture section). The cell concentration was kept low such that glucose would not be depleted in the LG condition due to the uptake by the cells. Cells were then allowed to reach steady states in LG and HG conditions, which were the low flux state (0.05 mmol/10^9 cells/h) and high flux state (0.31 mmol/10^9 cells/h), respectively. Cells from both these conditions were then re-suspended in medium

containing varying glucose concentrations and the specific rates of glucose consumption and lactate production were monitored.

When exposed to 25 mM glucose, cells showed high specific glucose consumption rate of ~ 0.31 mmol/10^9 cells/h regardless whether they were previously at a low flux or a high flux state (Figure 4.3A). When exposed to 0.6 mM glucose, cells from both HG and LG showed low specific glucose consumption rate of 0.05 mmol/10^9 cells/h. However, when exposed to intermediate glucose concentrations of 2 mM, 3 mM and 4.5 mM, contrasting specific rates were observed for the cells from HG and LG conditions. Cells that were previously cultured in HG maintained high specific glucose consumption rate (0.31 mmol/10^9 cells/h), whereas cells that were previously cultured in LG had low specific glucose consumption rate (0.05 mmol/10^9 cells/h). The flux in the intermediate glucose concentration range is thus dependent on the prior state or history of the cell. Since a high flux of glucose is accompanied by a high lactate flux and vice versa, the bistable behavior of glucose flux should be reflected in lactate flux. This is indeed seen when lactate efflux was measured (Figure 4.3B).

The experimental results thus show the characteristic of bistability in HeLa cell glucose metabolism: cells which were at a high flux state (previously in HG) have to experience glucose levels below the "switch-down" concentration to reach the low flux state while cells from a low flux state (previously in LG) have to experience glucose levels higher than the "switch-up" concentration to reach the high flux state.

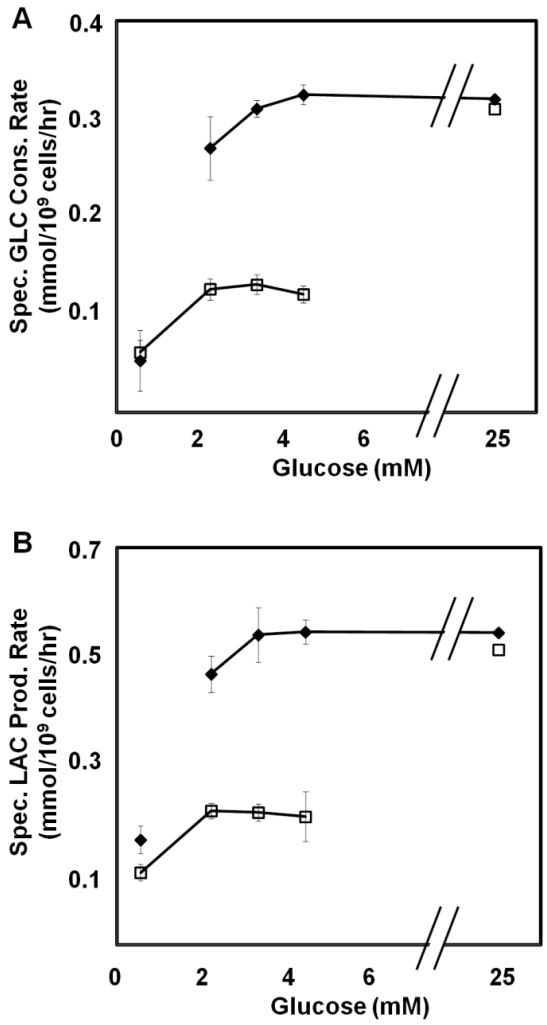

Figure 4.3: Bistability in cultured HeLa cells. Cells initially cultured in high glucose (♦) or low glucose (□) exhibit different rates of **(A)** specific glucose consumption and **(B)** specific lactate production when exposed to varying glucose concentrations.

4.3.4 Effect of Isozyme Composition on the Steady State Behavior

Many isoforms of the same enzyme are expressed at different levels in the same tissue cell. The presence of different isoforms with different allosteric regulations makes the steady state flux behavior deviate from that seen with a single isoform. We evaluated the effect of the isoform mixtures on the glycolytic flux. In each case, the total level of the

isoform mix for each enzymatic step was kept at the same level as the one used in the original model (with single isoform for each enzymatic step). The steady state behaviors of single PFK isoforms (PFKM, PFKL or PFKP) as well as mixed expression of these isoforms, in conjunction with PKM2 are shown in Appendix Figure 5. In all cases, the steady state behavior of the isoform mix takes the shape of that conferred by the mixture's dominant isoform. As shown in Figures 4.2A-D, the presence of only a single isoform in any active Loop precisely fixes the switch-up and the switch-down glucose concentrations. Interestingly, co-expression of the dominant isoform with smaller fractions of other isoforms allows for the movement of the switch-up and switch-down glucose concentrations within the physiological range, thus equipping cells with yet another way to control the span of the bistable region (Appendix Figure 5D-F).

4.4 Discussion

In this study we demonstrated that in the physiological range of glucose concentration the glycolysis flux exhibits multiple steady state behavior. The multiple steady states arise from the regulatory loops centering at PFK and PK. The presence of M/L isoforms PFK and the M2 isoform of PK, which are all subjected to activation by their respective effectors, give rise to steady state multiplicity.

The sets of isoforms, (PFKM/PFKL and PKM2) and (PFKP and PKM1), confer contrasting multiple steady state and the saturation type steady state behaviors to glycolysis flux, respectively (Figure 4.4). With the latter set of isozymes, the flux is at a low flux state under physiological glucose concentrations. In contrast, the bistable region conferred by the former set of isozymes can span the physiological concentration range of glucose. The model thus predicts that the flux will be at a high flux state under physiological conditions. Only upon a long period of exposure to a very low glucose concentration (< ~1 mM) will the glyolysis flux switch to a low flux state. A high flux state is also associated with a high lactate production as shown by the model simulation (Appendix Figure 6).

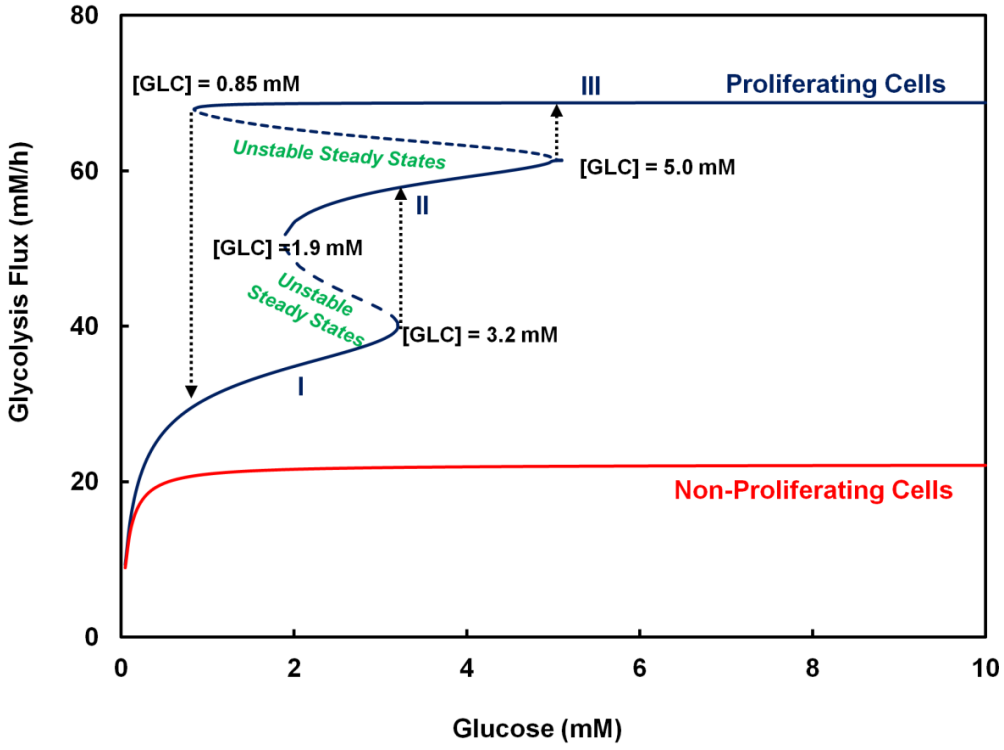

Figure 4.4: Glycolytic behaviors observed in mammalian cells. Two types of glycolytic steady state kinetics were observed. These include steady state behavior with no multiplicity of states or those with multiplicity of states. The type of glycolytic isozymes expressed forms the basis for presence or absence of multiplicity of states in glycolysis activity. In case of non-proliferating cell, isozyme combination comprising of PFKP, PKM1 and PFKFB with K/P = 0.5 was used whereas in case of proliferating cell, isozyme combination including PFKM, PKM2 and PFKFB with K/P =10 was employed.

In the bistable region, the stable steady state at which the glycolysis resides at a particular glucose concentration is dictated by the trajectory along which the system moves. Cells which are originally at a high flux state will remain at high flux state until the glucose concentration is reduced to a level below the switch-down concentration; whereas cells which are originally at a low flux state, will stay at low flux state until the glucose concentration is increased beyond the switch-up concentration. Using HeLa cells we

demonstrated this effect of cell's "history" in terms of the fluxes of both glucose consumption and lactate production (Figure 4.3).

Metabolic switch between low and high flux states to meet the changing bioenergetic demands caused by oncogenic or developmental events may be brought about by expression of a different set of isozymes (see review [72,73,77]). Mature oocyte and zygote exhibit the oxidative type of metabolism [72]. As zygote differentiates and reaches the late blastocyst state, the metabolic phenotype changes to predominantly glycolytic. Such a change in the metabolic phenotype from the oxidative state of quiescent oocyte and zygote to glycolytic state of the blastocyst is associated with changes in glycolytic isozymes from PKM1, PFKP and PFKFB2 to PKM2, PFKM/PFKL and PFKFB3/PFKFB4 isozymes (Appendix Table 2). The concurrent switch in the isozyme pattern and the flux behavior observed in the above scenario matches that presented by our model simulations (Figure 4.4).

It should be noted that most cells express a mixture of isoforms rather than a single one [101-106]. Such pattern is also observed in the tissues described above (oocyte, zygote and blastocyst), where other isoforms are also expressed in small fractions (Appendix Table 2). We evaluated the effect of mixed expression of multiple isoforms of PFK on the multiple steady state behavior. When different isoforms of PFK are expressed, the isoforms which exhibit bistable behavior, namely PFKL and PFKM, dominate over PFKP unless PFKP is present in a much larger proportion than the other isoforms (Appendix Figure 5). It is also worth noting that not all proliferating cells and quiescent cells have the same isozyme patterns. However, it has been reported that fast proliferating cells typically express PFKM/PFKL, PKM2 and PFKFB3 as the major isoforms; whereas quiescent cells favor PFKP, PKM1 and other isoforms of PFKFB as the dominating isoforms [88,107,108].

Metabolic shift may also come about by hormonal or signaling regulation, such as those that change the K/P ratio of PFKFB (Figure 4.2E). For example, the K/P ratio of PFKFB in hepatocytes can be quickly modulated by glucagon-triggered cAMP signaling [12].

Furthermore, a number of factors that affect the allosteric state of PKM2 isozyme, including serine, SAICAR and phenylalanine, can influence the transition between the two metabolic states [13-15,109].

PFKFB affects the activity of PFK through its reaction product F26BP. Different isoforms of PFKFB have different K/P ratios that give rise to different steady state behavior of glycolysis (Figure 4.2E). An isoform with a high K/P ratio yields a higher level of F26BP at steady state, exerts a stronger activation of PFK and moves the switch-up glucose concentration to lower levels. With hormonal actions that change the K/P of PFKFB, the steady state behavior of glycolysis can be altered quickly without resorting to changes in the isoform expression.

The bistable behavior in glycolysis confers robustness to the response of glycolysis to changes in glucose concentration; within the physiological range of glucose concentration a change in the flux state is not readily realized unless via a regulatory action, differentiation or oncogenic event. In recent years there has been increasing interest in developing treatment strategies of suppressing hyperactive cellular metabolism to control cancer cell growth or diabetes development. The glycolysis flux behavior revealed in this study may be exploited to negatively manipulate the metabolism of tumor cells by rendering Loop 1 or Loop 2 inoperative. Decreasing the activation of PFK by F16BP can make Loop 1 less active. Tumor cells typically express PKM2 as the dominant pyruvate kinase isozyme. Disrupting the allosteric regulations of PKM2 activity, such as by administering SAICAR [13], will make Loop 2 inactive. Further, suppressing the K/P ratio of PFKFB3 through expression of TIGAR [56] or by the use of small molecule modulators such as 3-(3-pyridinyl)-1-(4-pyridinyl)-2-propen-1-one (3PO) can make Loop 2 inoperative [21]. A mechanistic understanding of the regulation of glycolytic flux will have a positive impact on the advances of these metabolism-based therapeutic treatments.

Chapter 5 Regulatory Mechanism for Metabolic Shift to Lactate Consumption in Cultured Mammalian Cells

5.1 Summary

In the industrial bioprocesses for therapeutic protein production, glucose is fed regularly to the medium to sustain cell growth until the accumulation of lactate to high levels adversely affects cell growth and viability. In such fed-batch processes, glucose and lactate concentrations in the culture reach levels that are far beyond the physiological ranges. In the later stages of those cultures, sometimes a metabolic shift from a metabolic state of high glycolysis flux and high lactate production to a state of low glycolysis flux and lactate consumption is observed. While in other cases of very similar culture conditions with the same cell line and medium, cells continue to produce lactate. The occurrence of the metabolic shift to lactate consumption has been correlated to the productivity of the process. However, the cause that triggers lactate consumption is yet to be identified. We have previously shown that the glycolysis of proliferating cells can exhibit bistability with well-segregated high flux and low flux states. The cells can only transit from a high flux state to a low flux state when glucose is at very low levels. However, metabolic shift to lactate consumption observed in industrial fed-batch cultures often occurs when glucose is still available at high levels. In this chapter, using the complete mathematical model we demonstrate that inhibition by high lactate concentration coupled with AKT regulation on glycolysis enzymes can profoundly influence the bistable behavior resulting in a complex steady-state topology. The transition from the high flux to the low flux state can only occur in certain regions of the steady state topology determined by the glucose, lactate and AKT. Consequently, the metabolic fate of the cells depends on the culture trajectory encountering the regions that allow such metabolic state switch.

5.2 Introduction

Glucose metabolism plays a central role in supplying cellular needs of energy and precursors for many cellular materials. Cancer cells have elevated glucose consumption and glycolytic flux in ways similar to the response of tissues to growth promoting signals [71]. Cellular glucose metabolism is subjected to vast interacting regulations exerted at various levels [78,86,110]. The regulatory effectors and control action on the enzyme kinetics differ for different isozymes catalyzing the same reaction step. Cells in different tissues and even cells at different disease or development stage, may express different isozymes to meet their cellular needs [72,74]. Additionally, through signaling pathways, glycolysis activity is tied to growth control [78,110].

The high rates of glucose consumption and lactate production seen in cancer cells are also observed in other fast proliferating cells such as the cultured mammalian cell lines. In the past two decades, fed-batch cultures have become extensively used in cell culture bioprocessing. In such cultures, concentrated feed medium is fed intermittently to the culture to make up for the consumed nutrients. The volume of the reactor increases through the culture duration. The total amount of glucose added and the resulting glucose concentration in the culture are far higher than the range commonly seen in typical culture media. Lactate accumulation seen in culture also greatly exceeds the physiological levels. The accumulation of lactate in culture has long been recognized as an inhibitory factor for cell growth and recombinant protein production [70,111]. The viability of the cells in the culture eventually drops and the culture is terminated.

Cells in the later stages of their growth in a fed-batch culture sometimes switch their metabolism from lactate production to consuming lactate [23]. However, such metabolic shift is elusive; under seemingly similar conditions, some cultures switch their metabolism and consume lactate while others continue to produce lactate. The metabolic shift to lactate consumption has been shown to positively correlate to higher productivity [3,4]. Thus, a better understanding of the lactate consumption phenomena will help contrive strategies for robust control of cell metabolism and higher protein yields.

We have previously demonstrated that the combination of isoforms of glycolytic enzymes commonly seen in many rapidly growing cells give rise to bistable behavior in glycolysis activity [112]. Under physiological glucose concentrations, the steady state glycolysis flux may be at a high state or a low state. Although cells may switch their metabolism between the two flux states, the switching concentrations are outside the physiological range. This is consistent with the experimental observation that a shift from a high flux state to a low flux state was accomplished only by controlling glucose concentration at very low levels [70,111,112] .

We hypothesize that the switch of metabolism in fed-batch culture is a reflection of the bistable behavior described above. The glucose and lactate concentrations in contemporary fed-batch processes often reach levels beyond 50 mM and 100 mM, respectively [3,4]. Such non-physiological conditions may elicit dynamic responses unseen in vivo. In particular the inhibitory effect of lactate on PFK that is relatively minor in most tissues in vivo may become prominent due to its high level of accumulation.

In this work we extend our modeling explorations to the previously unexplored space of glucose and lactate concentrations that are non-physiological and yet important in biopharmaceutical manufacturing. Since lactate consumption occurs through its conversion to pyruvate and oxidation in the tricarboxylic acid (TCA) cycle, we extended our model to include the TCA cycle and the malate-aspartate shuttles (Figure 3.1 in Materials and Methods). Metabolic shift in cultured cells largely occurs after the rapid growth period is over. The link between metabolism and growth control has been a subject of intense research in the past decade.

AKT is a serine/threonine kinase that plays a key role in multiple cellular processes including cell proliferation and glucose metabolism (for reviews, see [78,86,110]). AKT exists in an active/phosphorylated form and an inactive/unphosphorylated form. The AKT signaling cascade has been shown to activate the transcription of GLUT1 [17] and mediates the association of hexokinase 1 and 2 (HK1 and HK2) with outer mitochondrial

membrane [18,19]. In addition, the phosphorylated form of AKT (pAKT) can increase the phosphorylation of PFKFB to shift its kinase/phosphatase ratio to increase the formation of fructose 2,6-bisphosphate levels [20-22], which in turn increases PFK activity and glycolysis flux. A decrease in the growth rate of the cells observed during the course of the culture is accompanied by the decrease in the pAKT activity [23]. Thus, in the extended model the effect of cell growth rate on glycolysis flux is dealt with by a dependence of kinase activity of the bifunctional enzyme PFKFB activities on pAKT. We report herein that our extended model for cell metabolism reveals multiplicity of steady states of glycolysis activity, the topology of which is modulated by three culture parameters including glucose, lactate and growth rate. Such an understanding of the metabolic flux topology can help control the metabolic state and enhance process robustness.

5.3 Results

5.3.1 Bistability in Glucose Flux in Energy Metabolism

In our previous study we have demonstrated that a combination of isozymes confers glycolysis flux with multiplicity of steady states. We showed that the presence of multiple steady states is the result of the regulatory action of two allosteric feedback loops [112]. Survey of transcriptome data of various CHO cell lines revealed that CHO cells typically express the same set of isozymes that confers glycolysis flux with the hallmarks of bistable behavior (Appendix Figure 7). The glycolysis flux behavior of CHO cells was simulated using the metabolic model that incorporates the muscle isozyme of phosphofructokinase (PFKM), the M2 isozyme of pyruvate kinase (PKM2) and the brain isozyme of 6-phosphofructo-2-kinase/2,6-bisphosphatase (PFKFB3), which are the respective dominating isozymes observed to be expressed CHO cells. The allosteric regulations which are active in CHO cells are shown in Figure 5.1A. The multiplicity of steady states of glycolysis flux is seen in CHO cells (Figure 5.1B).

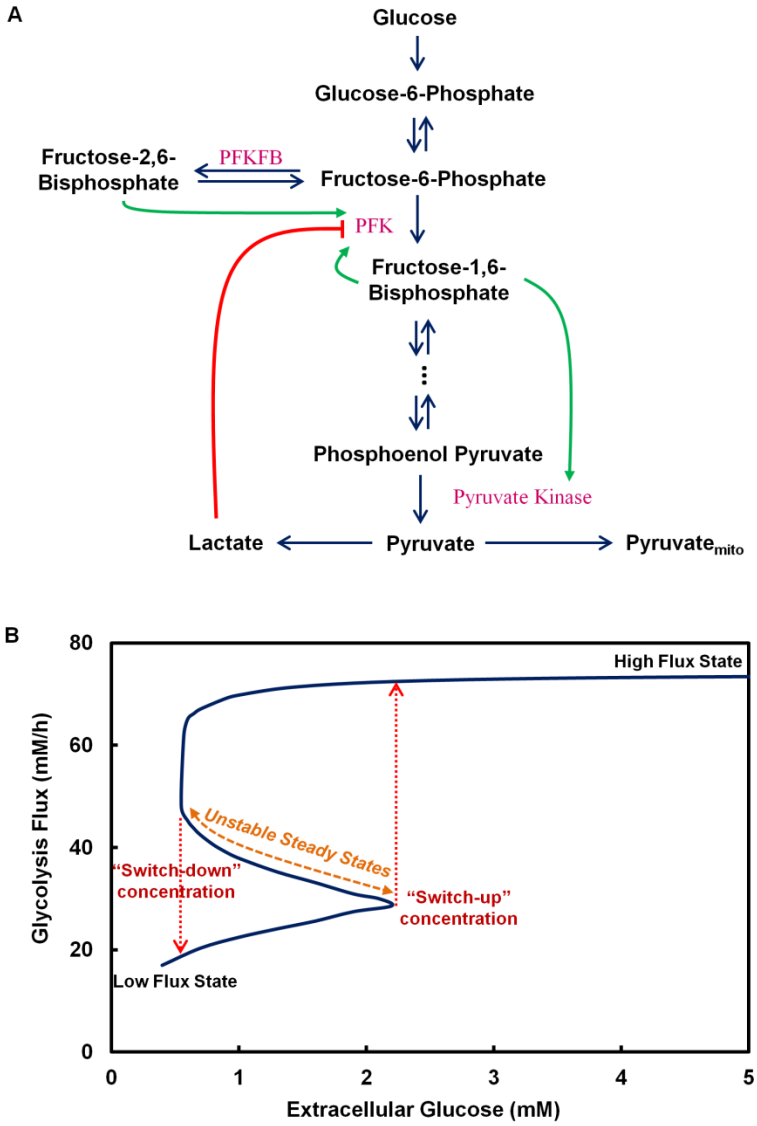

Figure 5.1: **Multiplicity of steady states in glycolytic activity of CHO cells. (A)** Isozymes of glycolysis are subjected to multiple allosteric regulations **(B)** Bistability in glycolysis flux

In the glucose concentration range of ~0.5 mM to ~2.2 mM, three types of steady states in glycolysis flux are seen: two are stable which represent the high and the low flux states, and the in-between steady states are the unstable states. The stability of each steady state was confirmed by eigenvalue analysis. Outside this region, only one steady

state is observed for a given glucose concentration; below 0.5 mM, glycolysis has only the low flux state, whereas above 2.2 mM, only the high flux state exists. In the high glycolysis flux state, glucose is consumed rapidly and lactate is produced at a high rate (Figure 5.1B). In the low glycolysis flux region, glucose consumption rate is low. The behavior of lactate in the low flux region varies somewhat; it is produced at a slow rate in the bistable region, but is consumed at a low rate as glucose concentration decreases further.

In the bistable region, glycolysis can operate at either a high or a low state depending on the previous state of the system. The middle steady states being unstable cannot be realized experimentally. When the glucose concentration changes, the glycolysis flux changes along the stable steady state lines. Starting from a high glucose concentration (thus the high flux state), as glucose concentration decreases the flux remains at the high state until the concentration decreases to 0.5 mM ("switch-down" concentration, Figure 5.1B), where it decreases abruptly to a low state. Further decrease in glucose causes the system to travel farther down along the low flux steady state line. Once the system reaches a low state, it does not switch back to the high flux state at the "switch-down" concentration by a small perturbation (increase) in glucose level. In order to return to the high flux state, the system must now travel along a distinct trajectory. From a low flux state, glucose concentration must increase above 2.2 mM ("switch-up" concentration, Figure 5.1B), before it sharply transits to a high flux state. Further increase in glucose causes the system to travel farther up along the high flux steady state line. The system is thus marked by well separated high flux and low flux states and very distinct "switch-up" and "switch-down" glucose concentrations.

Sensitivity analysis on the multiplicity of steady states was performed by varying the level of each enzyme over the range of two orders of magnitude while holding all the other kinetic parameter values constant. Exhaustive simulation for evaluation of steady state behavior on all possible enzyme level combinations is clearly not feasible. The results of the sensitivity analysis show that multiple steady states can be seen over a wide

range of enzyme levels for many enzymes except for HK and pyruvate dehydrogenase (PDHC) (Appendix Table 4).

Altogether, these results indicate the potential for two systems to be at the same extracellular glucose concentration inside the bistable region, while showing different flux behaviors depending on their histories.

5.3.2 Effect of Lactate Concentration on Bistability

Lactate exerts an inhibitory effect on glycolysis flux through its feedback regulation on PFK (Fig 5.1A) [113,114]. The steady state behavior shown in Figure 5.1B was obtained at a constant extracellular lactate concentration of 0.4 mM. In fed-batch cultures, lactate may accumulate to high levels that greatly exceed the physiological range [4]. We thus examined the effect of a wide range of lactate concentrations on the glycolysis flux. The results are presented in a three-dimensional plot with the flux plotted against glucose and lactate concentrations (Figure 5.2). The resulting plot shows a high and a low surfaces representing high and low fluxes, respectively. The surfaces are colored in red, blue and yellow. The top (red) surface represents the plane of high flux steady states. The bottom (blue) surface represents the plane of low flux steady states and the yellow region represents the plane of unstable steady states. A slice of the plot at a fixed lactate concentration of 0.4 mM along the glucose axis yields the curve shown in Figure 5.1B. On this constant lactate plane the "switch-up" and "switch-down" points can be seen. With increasing levels of lactate, the "switch-up" glucose concentration shifts to higher glucose levels. At very high lactate concentrations (> 40 mM), the "switch-up" concentration will move to extremely high glucose concentrations that are not seen even in culture as they would represent near lethal high osmolality to cells. Even in this region of very high lactate, switching down from high state to low state is feasible if glucose concentration falls to very low levels.

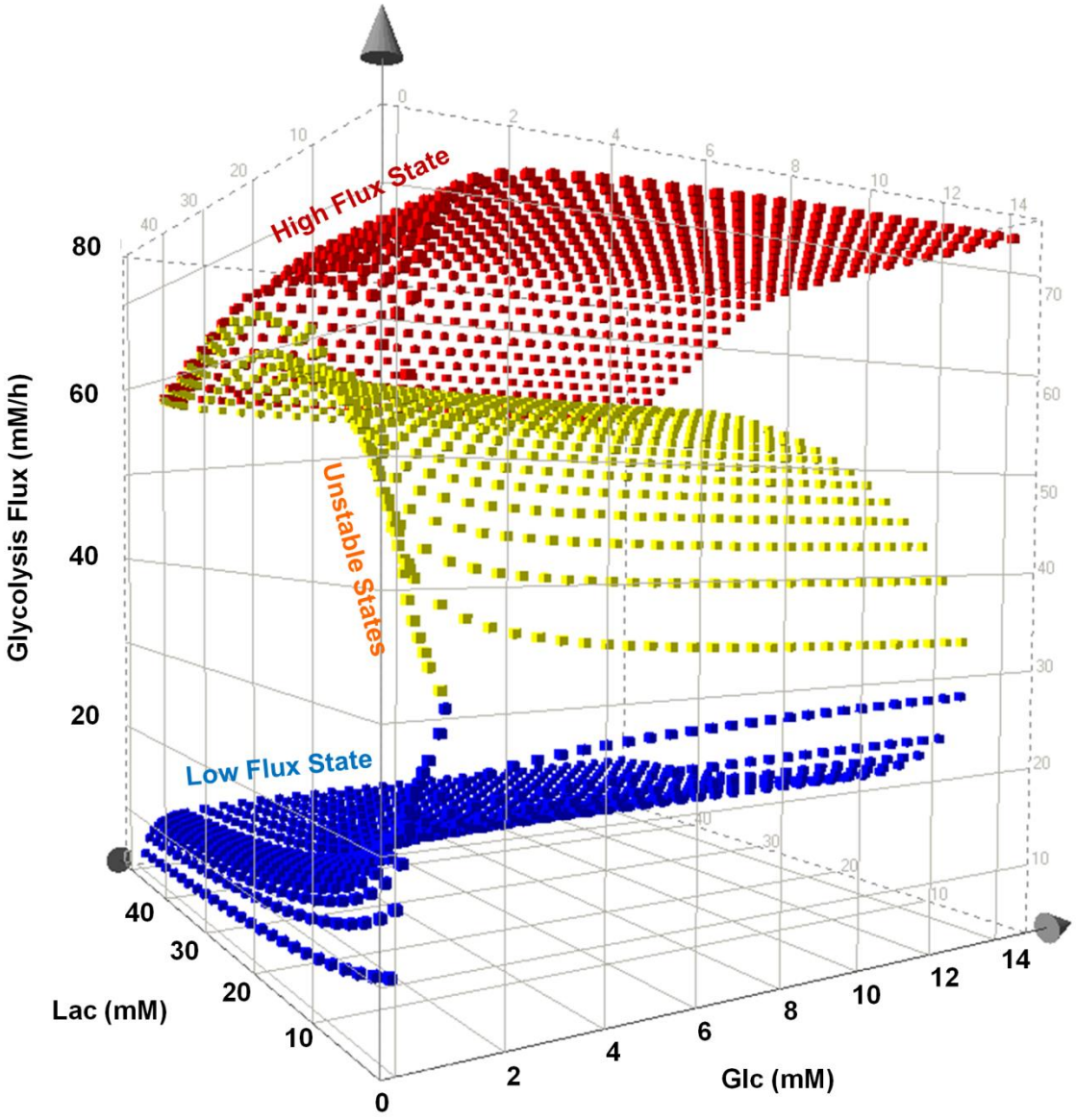

Figure 5.2: **Effect of lactate on bistability.** Effect of lactate on the multiplicity of states in glycolysis is probed by model simulation at various combinations of lactate (0-50 mM) and glucose (0-15 mM) concentrations typically seen in cell culture processes. The bistable behavior in glycolysis imparts more complex dynamics as lactate concentration is varied.

5.3.3 Effect of AKT on Bistability

The AKT signaling pathway regulates growth and proliferation, and stimulates the activity of glycolysis [78,110]. The AKT signaling cascade induces the transcription of the glucose transporter GLUT1 and mediates the association of HK1 with outer mitochondrial membrane (Figure 5.3). The active form pAKT can also phosphorylate the enzyme PFKFB to enhance its kinase activity [20,21] resulting in an increase of F26BP production and thus increasing the flux of glycolysis. In fed-batch cultures, cells grow to a maximum concentration after which they cease to proliferate. As the growth rate of the cells slows down, simultaneous reduction in the pAKT level has been observed in the late stage of fed-batch cultures [23], causing glycolysis activity to also decrease. Among the three enzymes regulated by AKT, PFKFB is stimulated at its activity level whereas the other two (GLUT1 and HK1) are regulated at the transcriptional or spatial level. For stability behavior our focus is on the system in which enzyme levels are kept constant and uniformly distributed inside the cells. Our investigation on the effect of growth on glycolysis flux thus focused on the regulation of AKT on PFKFB.

The regulation of glycolysis flux by growth control is modeled by an activation of the kinase activity of the bifunctional enzyme PFKFB using an empirical formulation depicting an increasing kinase activity with increasing pAKT in a saturation type of kinetics (Eq. S4 in Appendix Materials, Rate Equations section). A similar expression has been used previously to describe the effect of AKT on glycolysis [59,60].

Four discrete values of pAKT activity were examined and the steady-state behavior of glycolysis flux at various glucose and lactate concentrations are shown in Figure 5.4. At a high pAKT activity (pAKT = 1, Figure 5.4A), a shift from the high flux plane to the low flux plane can occur only at very low glucose concentrations (~1 mM) for the entire lactate concentration range examined. However, with lower pAKT activities, a section of the top plane recedes towards higher glucose concentration such that a metabolic shift from the high flux plane to the low flux plane is possible at higher glucose concentrations

(Figure 5.4B-D). The section of the top plane that regresses is confined to a small range of lactate concentration (~15-40 mM).

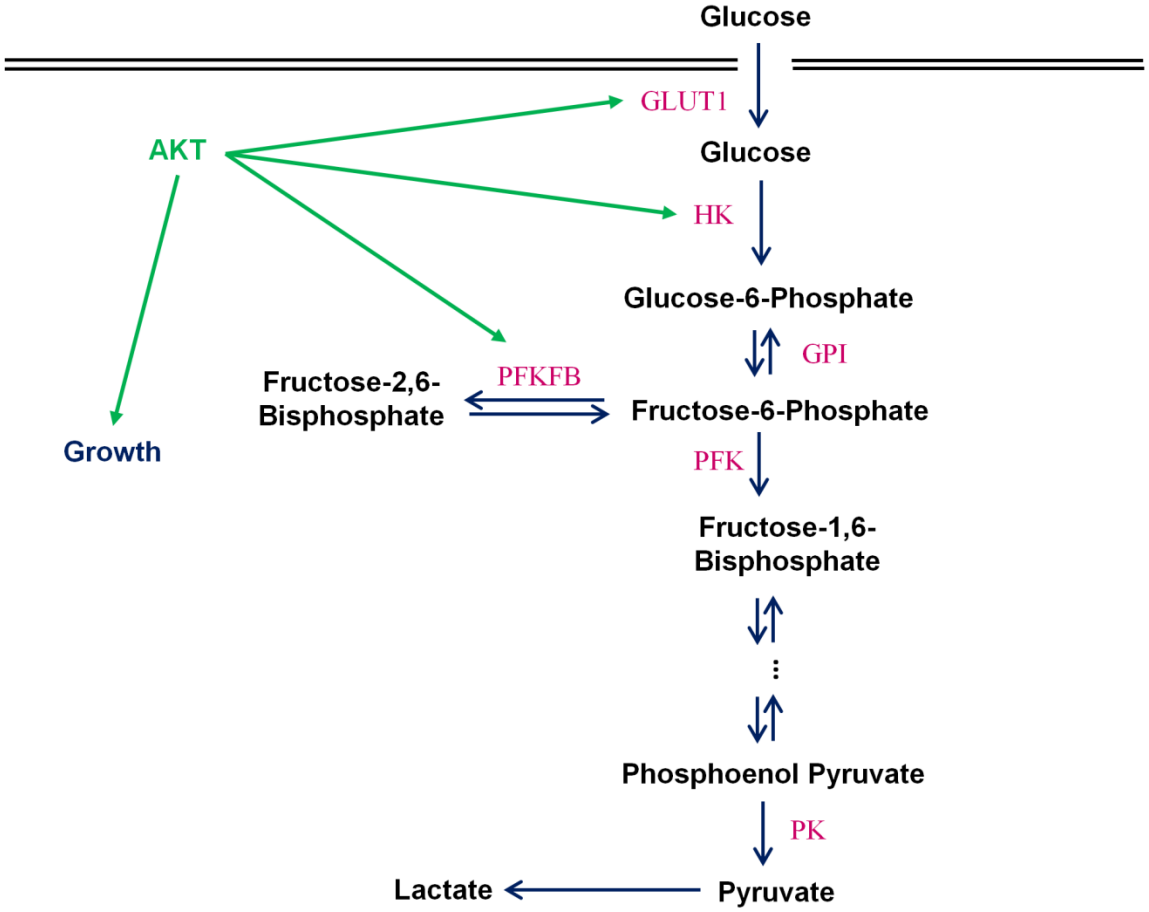

Figure 5.3: Regulations of AKT on glycolysis. The metabolic control of the cells is tightly linked to growth control through signaling pathways such as AKT. The AKT signaling cascade has been shown to activate the transcription of GLUT1 and mediates the association of HK with outer mitochondrial membrane to provide direct access to ATP as a driving force for high rate of glycolysis. In addition, AKT can phosphorylate PFKFB to shift its kinase/phosphatase ratio to increase the formation of fructose 2,6-bisphosphate levels which in turn increases PFK activity and glycolysis flux.

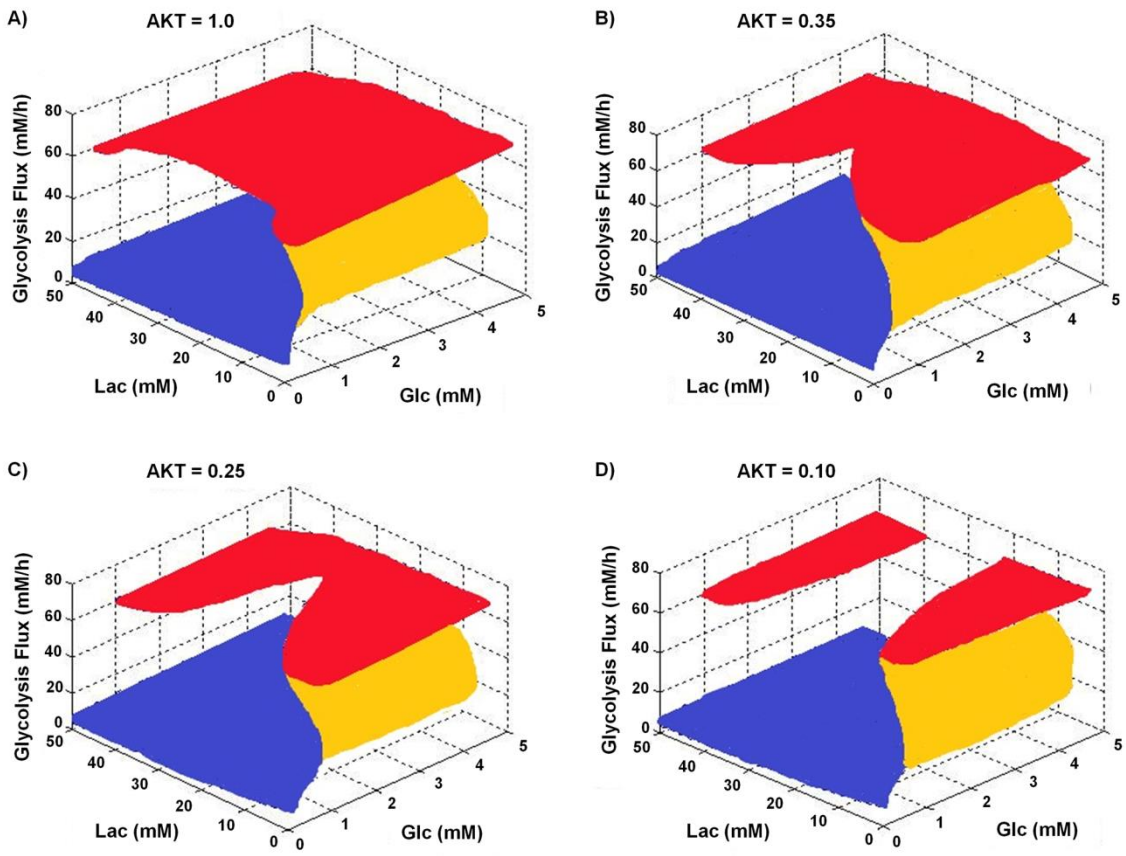

Figure 5.4: Effect of AKT on the bistability in glycolysis activity. The red and blue surfaces are stable steady states representing the high and the low glycolytic flux states, respectively. Yellow surfaces are unstable steady states.

5.3.4 Trajectory of the Metabolic Shift

In a fed-batch culture glucose is added intermittently to sustain its concentration within a range. Lactate is produced at a high specific rate in the growth phase, but its production rate is subject to variation when the growth rate decreases in the late stage of cell cultivation. In some cases the culture continues to consume glucose and produces lactate at high rates during the period when cell growth has ceased; while in other cases glucose consumption rate on a per cell basis becomes small and lactate production diminishes, or lactate is even consumed [4]. The phenomenon thus suggests that the two types of cultures differ in their trajectories while progressing on the high flux plane.

We performed a set of transient simulations to demonstrate different scenarios where cultures may have different metabolic fates. Cells are initially at a position on the high flux plane of high pAKT activity in growth stage and move along a path with decreasing glucose concentration (due to glucose consumption) and increasing lactate concentration (due to lactate production). As the growth rate decreases in the later stages of the cell culture, the culture behavior is depicted by a line (line AB in Figure 5.5) in a surface plot resembling Figure 5.4C. In the first case the path encounters the receded section of the high flux plane leading to a switch down from the high flux plane to the low flux plane (line BC in Figure 5.5). In the other case, while moving along the path, glucose concentration is increased due to glucose feeding in fed-batch culture (line BF, Figure 5.5). The feeding causes the path to shift and eventually leads to a trajectory that does not encounter the receded plane thus confining the cells to the high flux plane. In the first case, upon switching to a low flux state, an addition of the same amount of glucose to the culture (line CD, Figure 5.5) will not cause the culture to switch back to a high flux state. Such a difference in the timing of glucose feeding is not uncommon in industrial manufacturing, as observed in the archived manufacturing data [3,4] and in laboratory practices. Even cultures under the same conditions are not exact replicas. Feeding of nutrient and glucose to a fed-batch culture is either prescribed as fixed time point or responding to a range of the controlled variable. A small difference in the timing of glucose feeding may cause cultures with very similar metabolic behavior to diverge to different outcomes.

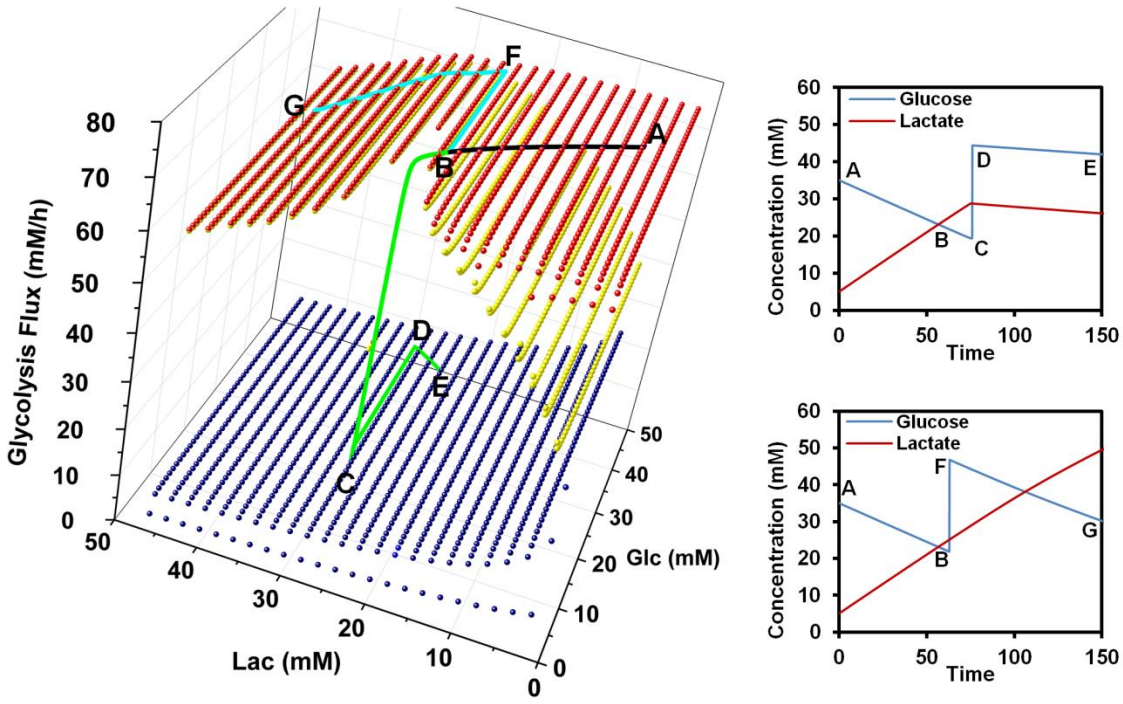

Figure 5.5: Transient simulations of cultures with and without metabolic shift. Cells at exponential stage are initially cultured in high glucose and low lactate concentrations and exhibit high growth rate/AKT activity. (A-B) As the culture progresses, AKT activity decreases, glucose is consumed and lactate accumulates in the culture such that the trajectory follows the curve A-B in the top plane. (B-C) After certain time, the culture encounters a section of the top plane that regresses at slow growth phase. Such culture with slightly later glucose feeding time shows a metabolic shift. The cells have sufficient time to enter the regressed region and shift their metabolism from the high flux state to the low flux state. (C-D-E) After addition of glucose, cells remain at the low flux state and consume lactate. (B-F) Culture with early glucose feeding time shows no metabolic shift behavior. Simulation shows that with early glucose feed the cells are able to avoid the regressed region of the top plane and continue their trajectory along the top plane, consuming huge amount of glucose and producing large amount of lactate (F-G).

5.3.5 Experimental Evidence of the Effect of Lactate

A recombinant CHO cell line was grown in four fed-batch cultures with initial sodium lactate concentrations of 0, 10, 30 and 50 mM (Figure 5.6A, also see the CHO Cell Culture section of the Materials and Methods). Osmolarity at inoculation was adjusted to 340 mOsm/kg in all four conditions, using appropriate amounts of sodium chloride. In the culture without any initial lactate supplementation (0 mM), a metabolic shift to lactate consumption was seen after cell concentration peaked at $8x10^6$ cells/mL (Figure 5.6C). During the period of lactate consumption, glucose consumption is at a low flux state. A similar shift of metabolism was observed in the culture with 10 mM initial lactate supplementation. In contrast, the cultures initially at higher lactate levels of 30 and 50 mM did not shift to lactate consumption (Figure 5.6A).

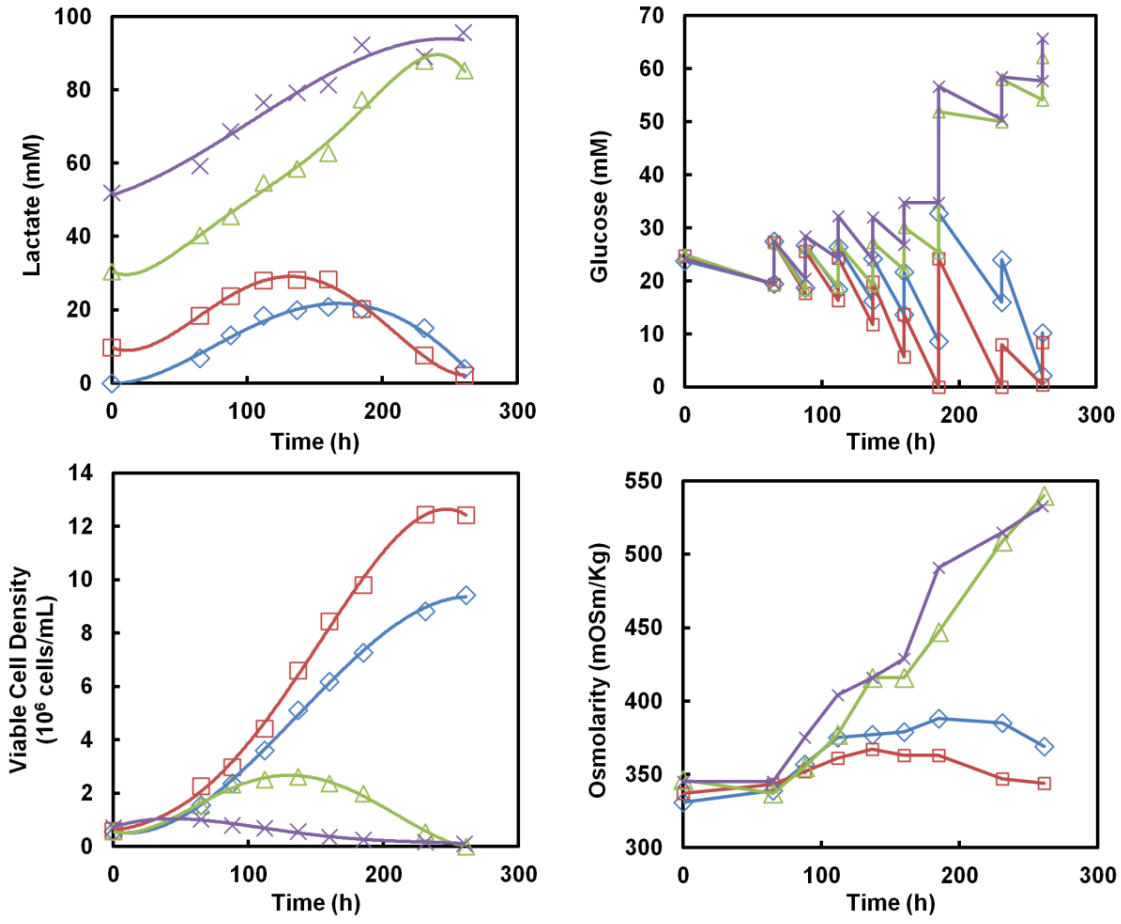

Figure 5.6: Effect of lactate on the metabolic fate of cell culture. Four fed-batch cultures of a recombinant CHO cell line were started with various amounts of initial lactate supplementation. The metabolic fate of a culture depends on the initial lactate concentration. **(A)** Lactate **(B)** Glucose **(C)** Viable cell concentration **(D)** Osmolarity

Admittedly lactate concentration also exerted a significant effect of growth rate, thus the difference in the metabolism of the four cultures may not be solely attributable to lactate concentration. Nevertheless, the results are consistent with the model prediction shown in Figure 5.4 that a switch from the high flux state to the low flux state while glucose level is moderately high occurs only within a certain range of extracellular lactate concentrations. At higher levels of lactate than the "switch-permissible" range, as in the cases of 30 and 50 mM, cells cannot switch to low flux state; whereas at lower levels of lactate the switch to low flux state, as indicated by lactate consumption, is observed.

5.3.6 Experimental Evidence of the Effect of History on Metabolic Shift

Cells were next cultivated in two fed-batch cultures supplemented with 30 mM of sodium lactate as described above. The two cultures were under identical treatment until in late exponential growth stage, when one of them received glucose feeding to maintain a high level of glucose (Figure 5.7A, open diamonds). For the other culture, glucose was allowed to decrease to a low level and was maintained at low levels for a period of time by intermittent glucose spiking (Figure 5.7A, open squares). In the first culture, glucose continued to be consumed at a high rate and lactate continued to accumulate until even after viable cell concentration decreased. The results for the first culture are the same as shown in Figure 5.6 where at high levels of lactate, a switch to a low glycolytic flux (or alternatively lactate consumption state) at moderately high level of glucose is not possible. This is in contrast to the second culture. By allowing glucose concentration to decrease to a very low level, metabolism switched to a low flux state as predicted in Figure 5.4. Upon switching to a low flux state with lactate consumption, the glucose level in the second culture was increased to high levels again at 230h. In this case glucose consumption continued to be low, a clear indication that once a low flux state is achieved

cell metabolism can be maintained at a low flux state even with an increase in glucose concentration, unless the glucose concentration is increased to a level beyond the switch-up concentration.

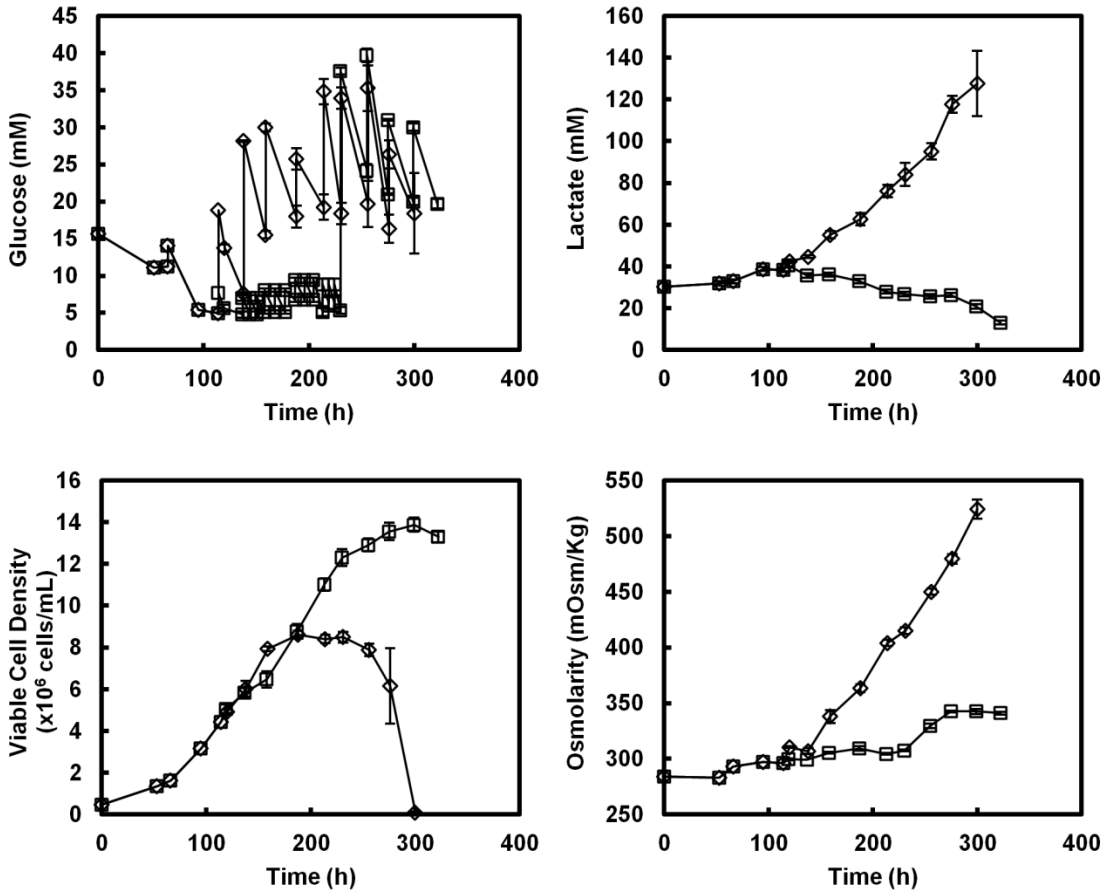

Figure 5.7: Memory of metabolic state. Two fed-batch cultures of a recombinant CHO cell line were run with different feeding strategy. (◊) Glucose was maintained at high levels. The culture continued to produce lactate. (□) Glucose was maintained at a low concentration for a period of time by intermittent glucose feeding. The cells shifted their metabolism to lactate consumption. Lactate continued to be consumed even after glucose was restored to a high concentration.

5.4 Discussion

Using a mechanistic model we have shown previously that with the combination of isozymes typically seen in proliferating cells the glycolysis flux exhibits classical steady state multiplicity [112]. In the bistable region, high flux and low flux steady states coexist; at the edges of bistable region, the metabolism may shift-up or shift-down to a different flux state when glucose concentration is changed from the bistable region into regions in which only one steady state is possible. The glucose concentration for shift-down from a high flux state to a low flux state is notably low and outside the physiological range. The model prediction of low "switch-down" glucose concentration is consistent with experimental observations reported in fed-batch cultures [70,111,115]. Using an on-line control system to deliver glucose and to control glucose concentration at low levels, the high glucose consumption rate and lactate production rate in hybridoma cells were switched to low levels. It was notable that in those studies the glucose concentration was controlled at very low levels in order for the switch to occur, akin to the model prediction.

Lactate may also be consumed in the late stages of fed-batch culture when the cell concentration is high and the growth rate is decreasing [23]. In those cultures, cells switch from a lactate production state during the exponential growth to a lactate consumption state when the growth rate diminishes. The switch occurs only when glucose flux is low. A prominent difference between the contemporary metabolic switch in the late stages of fed-batch culture and the earlier reports of metabolic shift through controlled glucose feeding is the glucose level at the point of metabolic switch. While in the early studies it was necessary to control glucose at very low levels, in later stage fed-batch cultures the glucose concentration can be high at the time of switching.

In recent times much progress has been made in advancing our understanding of the interplay between energy metabolism and growth control and oncological transformation. Of particular relevance to cell culture bioprocessing is the influence of lactate levels and growth control on glycolysis. We incorporated the inhibitory effects of lactate and

regulatory role of growth (through AKT) in our mechanistic model of energy metabolism.

Model simulation demonstrated that increasing lactate concentration increases the shift-down glucose concentration, allowing the switch to low flux state at a higher level of glucose as seen in the late stage of culture. However, at a low AKT activation level, the effect of lactate is not monotonic (Figure 5.4). At low levels of lactate an increase of its concentration increases the "switch-down" glucose concentration, but beyond a point the trend is reversed; further increase of lactate concentration actually decreases the "switch-down" glucose concentration. There is thus a window of lactate concentrations within which the "switch-down" glucose concentration is highest; at lactate concentrations higher or lower than that, the "switch-down" glucose concentration decreases again. This rather complex steady state behavior in response to lactate level is the result of the balance of two factors at play, the suppression effect on flux by lactate and the stimulatory effect on flux by F16BP. As the growth rate decreases, the window widens and the "switch-down" glucose concentration becomes higher.

In fed-batch cultures, even under seemingly identical culture conditions, the physiological trajectory of the culture may not be identical. The different metabolic outcomes seen in industrial biomanufacturing processes might be the outcome of subtle differences in their operation. Using our model we demonstrated a scenario in which difference in the timing of glucose addition results in two different metabolic states (Figure 5.5). The experimental data presented in this study provide further evidence to support our model prediction.

The steady state profile of glycolysis flux is affected by the isozymes that are expressed in the cell. Most cells and tissues express a mixture of different isoforms of the same enzyme, although one isoform is often the dominant type. Different producing cell lines often have varying composition of isozymes in glycolysis. Furthermore, the relative abundance levels of different enzymes are also somewhat different. In our previous study we have shown that the expression of mixture of isozymes alters the switch-up and shift-

down glucose concentrations [112]. It is likely that different cell lines will have somewhat different dynamic behaviors of glucose metabolism.

Recently there has been increasing interest in employing continuous culture or continuous culture with cell recycle (perfusion culture) for cell cultivation. The rationale is that continuous processes minimize equipment down time and increase overall productivity. Since multiplicity of metabolic states occurs under some conditions, it is likely that those distinctive metabolic states will also lead to different steady states of the culture: at a high flux state, the vast majority of glucose is converted to lactate, hence a low cell concentration; conversely at a low flux state, little glucose is diverted to lactate, and a high cell concentration is achieved. Published experimental results of continuous culture did suggest that difference in metabolism gave rise to different cell concentrations [61,116,117].

The mechanistic metabolic model presented above has provided insights into the possible cause of the somewhat erratic behavior of metabolic shift to a low flux and lactate consumption state often seen in cell culture bioprocessing. The experimental evidence supports the notion that the steady state multiplicity is at play, and may possibly be the root cause of this behavior. With a better understanding of the mechanistic cause of the lack of consistency of metabolic shift in culture, one can begin to explore the feasibility of controlling the metabolism and ensuring metabolic shift through external medium components such as enzyme inhibitors or through cell engineering.

Chapter 6 Multiplicity of Steady States with Distinct Cell Concentration in Continuous Culture of Mammalian Cells

6.1 Summary

In some cases of industrial bioprocessing, continuous mode of operation, wherein feed media is being added continuously while reactor content is withdrawn at equivalent flow rate, is used. The continuous removal of the reactor content is especially suitable for cases where the product is unstable such as Factor VIII. In addition, continuous culture offers great advantages including increased productivity, consistent product quality and longer culture duration. Accumulation of lactate produced by the cells, however, inhibits cells from growing to high concentration. Even when cell retention devices are employed such as in perfusion cultures, operation at high dilution rate is required to purge lactate from the reactor and sustain long culture duration. Under certain conditions, multiplicity of steady state in continuous culture has been observed. At seemingly identical dilution rate and feed glucose concentration, some continuous cultures reach steady state with high glycolysis flux and high lactate production, while others reach steady state with low glycolysis flux and low lactate production. The two kinds of steady states have different metabolic efficiency and thus exhibit distinct steady state cell concentrations. Understanding the precise conditions that lead to those steady states is therefore critical to achieve the desired cell density and productivity. We have previously demonstrated that cultured mammalian cells exhibit bistable behavior in glycolysis with distinct high flux and low flux states. In this study, we establish a multi-scale model taking into account the intracellular metabolism and macroscopic cell growth in the reactor. Using the model, we show that steady state multiplicity exists in a range of dilution rates in continuous culture as a result of the bistable behavior in glycolysis. The actual steady state reached is dependent on the trajectory followed by the culture.

6.2 Introduction

Mammalian cells are the predominant host cells for the production of therapeutic recombinant proteins. In the past two decades, fed-batch cultures, wherein feed containing nutrients including glucose and amino acids are regularly added to the culture to replenish the nutrients consumed to sustain a longer cell growth and production period, has become the prevailing form of process. The product accumulates to very high concentration in the reactor and is harvested at the end of the fed-batch culture. Another culture mode is continuous culture, wherein feed media is being added continuously while reactor content is withdrawn at equivalent flow rate simultaneously, keeping the reactor volume constant. The product is extracted from this efflux continuously. While continuous process has been explored as a process technology and for kinetic studies of cell growth and metabolism [118-127], its industrial applications are mostly in the case that the product is labile or is produced at a rather low concentration, such as Factor VIII and Protein C.

A simple continuous culture is limited in its productivity because of the large amount of metabolites, including lactate and ammonia that accumulate in the culture from the catabolism of glucose and amino acids. The accumulation of those metabolites has adverse effects on cell growth [128,129] and productivity [130-132]. Such accumulation is detrimental for continuous cultures, as steady growth must be sustained for long culture duration. Typically the dilution rate that is needed to purge out the metabolites and to sustain cell growth is higher than the specific growth rate. As a consequence, a cell recycle stream is often employed to return a concentrated cell stream to the reactor and to avoid a wash-out of the culture [133-135]. This mode of operation, called perfusion culture, mitigates the accumulation of inhibitory metabolites and provides an environment favorable to the cells to grow to a much higher density compared to a simple continuous culture.

A key factor for the successful implementation of a perfusion culture is the robustness of the cell separation device that takes the exhaust stream from the reactor and returns a

concentrated cell stream to the reactor. Various technologies such as spin filters [136,137], centrifuges [138,139], gravitational settlers [140,141], hollow-fiber separators [142,143], acoustic separators [133,144,145], microfiltration [146-148] and alternating tangential flow filters [149,150] among others have been employed in perfusion culture. In recent years the cell separation technologies have been refined to become more robust and the protein content of the medium employed in cell culture has been reduced to alleviate equipment fouling problems. Some industrial perfusion cultures are now practiced for as long as six months.

The successful practice of perfusion culture for many products has spurred a renewed interest in continuous processes for biologics manufacturing. Continuous cell culture processes allow a very high cell concentration to be sustained in the reactor for an extended period. The increased productivity allows a small manufacturing facility to be used. Continuous cell culture processes also offer the advantage of a steady state operation and possibly allow for a better control of the cells' physiological state, thereby enhancing our ability to control product quality.

However, the growth and metabolic behavior of mammalian cells differ significantly from those of most microbial cells. While the growth of microorganisms can often be adequately described by a Monod growth model and be shown experimentally to have a unique stable steady state under a set of nutrient conditions and at a fixed dilution rate, the complex metabolism of cultured mammalian cells is known to utilize nutrients differently under different physiological states. Such capability was demonstrated in metabolic shift of glucose catabolism in many types of cultured cells [70,131]. Under those different metabolic states, the proportion of carbon source diverted to lactate changed from a very high value of over 90% of glucose being converted to lactate to less than 10%. Given the same input of carbon sources, the metabolic shift resulted in a higher proportion of carbon being directed toward cell mass. This rationale led to the attempts of altering cell metabolism to low lactate production by controlling glucose levels in a fed-batch culture prior to the initiation of continuous culture [116,117]. The culture reached a steady state with a higher cell concentration compared to the culture

started from batch mode without alteration in cell metabolism. Because the feed and the operating dilution rate are the same, these results suggest the existence of steady state multiplicity. Similar demonstrations of steady state multiplicity in continuous culture were reported in other studies [151,152]. Such steady state multiplicity was observed merely through conjecture based on metabolic observation and was only explored in a narrow range of dilution rate, as the true cause of multiplicity and the range of conditions that multiplicity exist are not known.

We have previously shown that, with the combination of isozymes expressed in mammalian cell lines, the glycolysis flux exhibits multiple steady state behavior [153]. The glycolysis flux increases with increasing extracellular glucose concentration as in most metabolic pathways, but in a range of glucose concentrations multiple steady states exist for a given glucose concentration. Because of allosteric inhibition of the enzyme phosphofructokinase (PFK) by lactate, the bistable behavior differs somewhat at different lactate levels (see Chapter 5 of this thesis). In the bistable region, the glycolysis flux (i.e. the specific glucose consumption rate of the cell) may be at either a high flux state or a low flux state. At a high flux state, glucose is consumed rapidly and lactate is produced at a high rate. At a low flux state, glucose consumption rate is low and lactate is either produced at a slow rate or even consumed. In the late growth phase of a fed-batch culture, the culture can move into a region in the steady state space where it can transit from a high flux state to a low flux state (see Chapter 5 of this thesis). The metabolic model thus provides a mechanistic foundation for the metabolic shift seen in fed-batch cultures as well as in continuous cultures.

In this study, we extend our exploration to continuous culture systems by constructing a multi-scale reactor model that incorporated the intracellular metabolism of the cells and the macroscopic evolutions of cell growth, glucose and lactate in the reactor. Through model simulations, we show that multiplicity of steady states is present in a range of dilution rates in continuous culture as a result of the bistable behavior in glycolysis, and that different metabolic states are marked by distinct steady state cell concentrations. In

addition, the path followed by the culture dictates the actual steady state reached. Strategies to guide the culture towards a desired steady state are discussed.

6.3 Results

6.3.1 Multiplicity of Steady States in Continuous Culture

The multi-scale model encompassing intracellular metabolism and macroscopic evolutions of cell growth and glucose and lactate concentrations in the reactor (Figure 3.2 in Materials and Methods) was used to first find the steady state reached in continuous culture. The steady state concentrations of cells, glucose and lactate as well as the flux (i.e. specific consumption rate) of glucose and lactate at different dilution rates are shown in Figure 6.1. The glucose concentration in the feed was fixed at 5 mM (Figures 6.1A-C). The figures depict classical bistable behavior where two stable metabolic steady states exist in the dilution rate ranging from 0.029 to 0.039 h^{-1}. The middle steady states are unstable ones which can never be realized in the culture. The glucose flux and lactate flux data in the bistable region indicate that a set of stable steady states corresponds to high flux state and the other set correspond to low flux state. At high flux states, glucose is mostly converted towards lactate as indicated by the ratio of lactate flux and glucose flux into glycolysis (J_L/J_G) which is in the range of 1.45-1.6 mol/mol. In contrast, the low flux states have (J_L/J_G) < 0.8 mol/mol. In addition, the high flux states have lower cell concentrations and higher lactate levels, while the low flux states have higher cell concentrations and lower lactate levels. Thus, glucose is more efficiently metabolized to support cell proliferation at low flux states. Outside of the bistable region, only one steady state exists for a given dilution rate: at dilution rate <0.029 h^{-1} only the low metabolic flux state (high cell concentration) exists whereas at dilution rate > 0.039 h^{-1} only the high metabolic flux state (low cell concentration) exists.

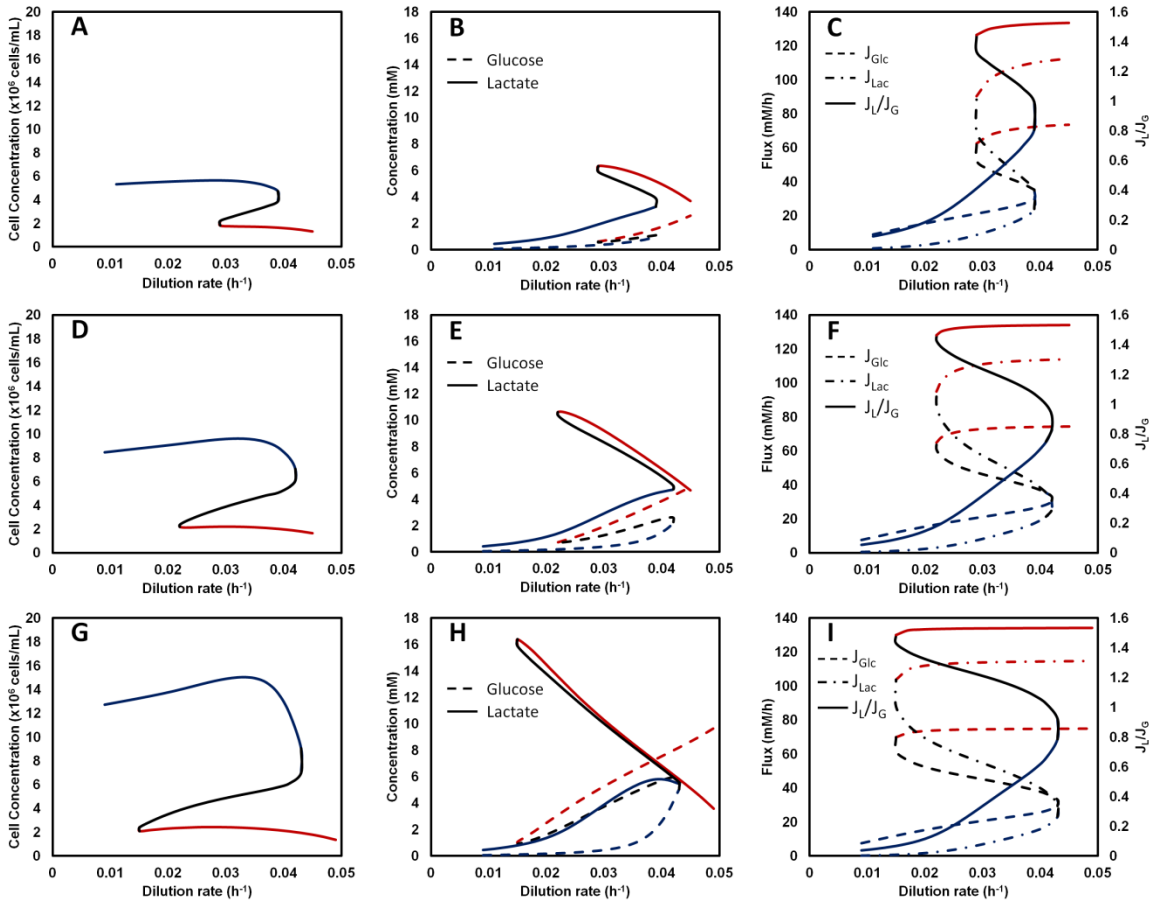

Figure 6.1: Multiple steady states in continuous culture. Bistability is observed in the profiles of cell concentration **(A,D,G)**, extracellular concentrations of glucose and lactate **(B,E,H)**, rates of glucose consumption and lactate production and the ratio of the two rates **(C,F,I)**. Feed glucose concentration was 5 mM **(A-C)**, 8 mM **(D-F)** and 12 mM **(G-I)**, respectively. The steady states corresponding to low metabolic flux are in blue, while those corresponding to high metabolic flux are in red. The unstable steady states are in black. Note that the steady states with low metabolic flux confer high cell concentration and vice versa.

The effect of increasing the feed glucose concentration on the steady state behavior was then investigated by varying the feed glucose concentrations from 5 mM to 8 mM (Figures 6.1D-F) and 12 mM (Figures 6.1G-I), respectively. At a low flux steady state increasing feed glucose concentration gives rise to a higher steady state cell

concentrations as well as somewhat elevated residual glucose and lactate concentrations (comparing Figures 6.1B,E,H), although the extent of cell concentration increase diminishes somewhat at the high dilution rate region at a feed glucose concentration of 12 mM. This is due to the higher levels of residual glucose concentration (thus lower amounts of glucose taken up by cells) at those steady states. In contrast, increasing feed glucose concentration at high flux states does not increase the cell concentration substantially, rather the residual lactate concentration increases significantly. At the low feed glucose concentration of 5 mM, the high flux state extends only to a dilution rate of 0.029 h^{-1}, below that only the low flux state is observed. Whereas at higher feed glucose concentrations the high flux metabolic steady states reach into lower dilution rate range.

6.3.2 Effect of Feed Lactate on Steady State

Consumption of lactate typically occurs in the late stage of fed-batch cultures. It happens when the glycolysis flux is low [23]. In continuous culture, while steady states with low lactate production rate are possible under normal feed condition as shown in Figure 6.1, steady states with lactate consumption do not occur unless lactate is present in the feed.

The steady state profiles of continuous cultures with a feed glucose concentration of 5 mM and lactate supplemented at 2 mM and 5 mM are shown in Figure 6.2. In both cases, lactate consumption only occurs at dilution rate < 0.021 h^{-1}. In this range of dilution rate in which lactate consumption is observed, cell concentration is hardly affected compared to the case of no lactate supplementation (comparing with Figure 6.1A). In the lactate consumption state a significant residual lactate concentration is present in order to drive lactate uptake by cells. At higher concentrations of lactate supplemented in the feed, the maximum achievable cell concentrations are reduced due to lactate inhibition on growth (data not shown).

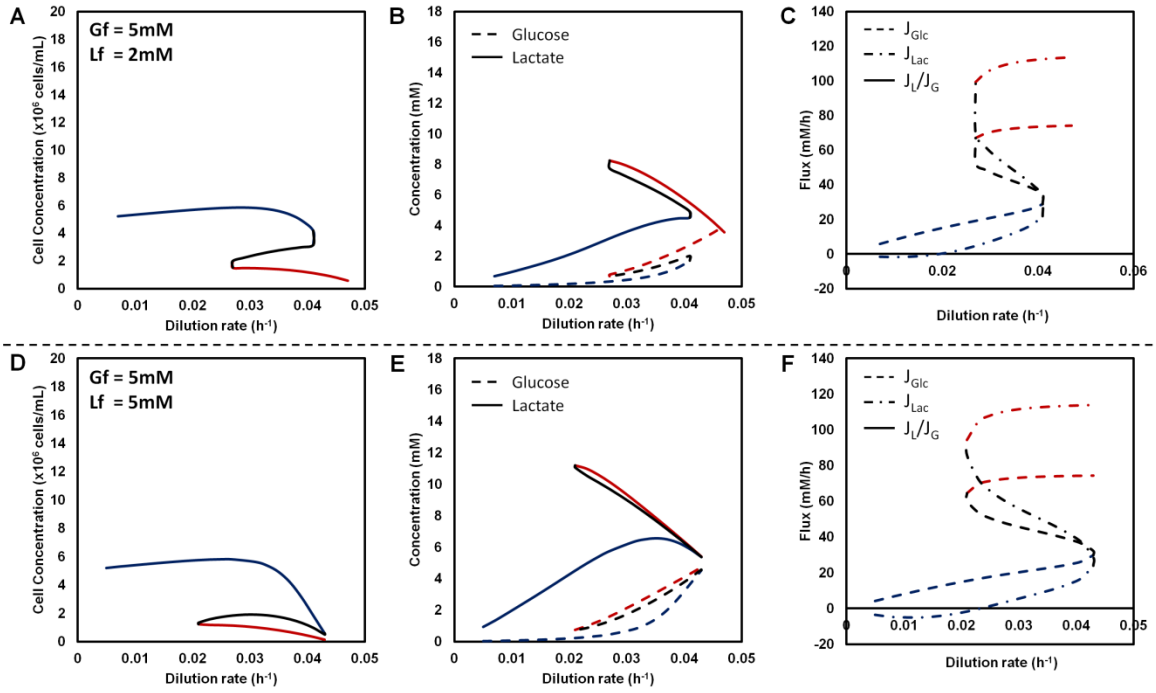

Figure 6.2: Effect of feed lactate on the bistable behavior in continuous culture. Lactate concentration in the feed was 2 mM **(A-C)** and 5 mM **(D-F)**, respectively. Lactate is consumed only at dilution rate <0.021 h^{-1}.

6.3.3 Trajectory to Steady State in Continuous Culture

We next ask the question of how to direct a continuous culture to a different steady state in the bistable region. The key is to "guide" the cells to the desired flux state before the culture reaches steady state. For increasing the productivity, the desired steady state is the low flux state with a higher cell concentration compared to the high flux state. In a batch culture of mammalian cells the default steady state is always the high flux state as cells in culture, without intervention, always consume glucose at a high rate and convert a large portion of glucose to lactate. To "guide" the system toward a low flux steady state in continuous culture, one strategy is to first culture them in fed-batch with glucose maintained at low concentration. Such strategy allows the culture to move to a region in which only the low flux state exists (Appendix Figure 8). Once the metabolic state is at a low flux state one can switch the culture to a continuous mode.

This scenario is illustrated by two simulated cultures: in one case a batch culture is switched to a continuous mode without guiding cells to a low flux state (Figure 6.3A-B); in the other a low glucose concentration is imposed in fed-batch culture to first guide cells to a low flux state (Figure 6.3C-D). The initial conditions used are $1.5x10^5$ cells/mL and 0 mM lactate in both cases. Upon switching to continuous mode, the dilution rate is 0.033 h^{-1} and feed glucose concentration is 7 mM in both.

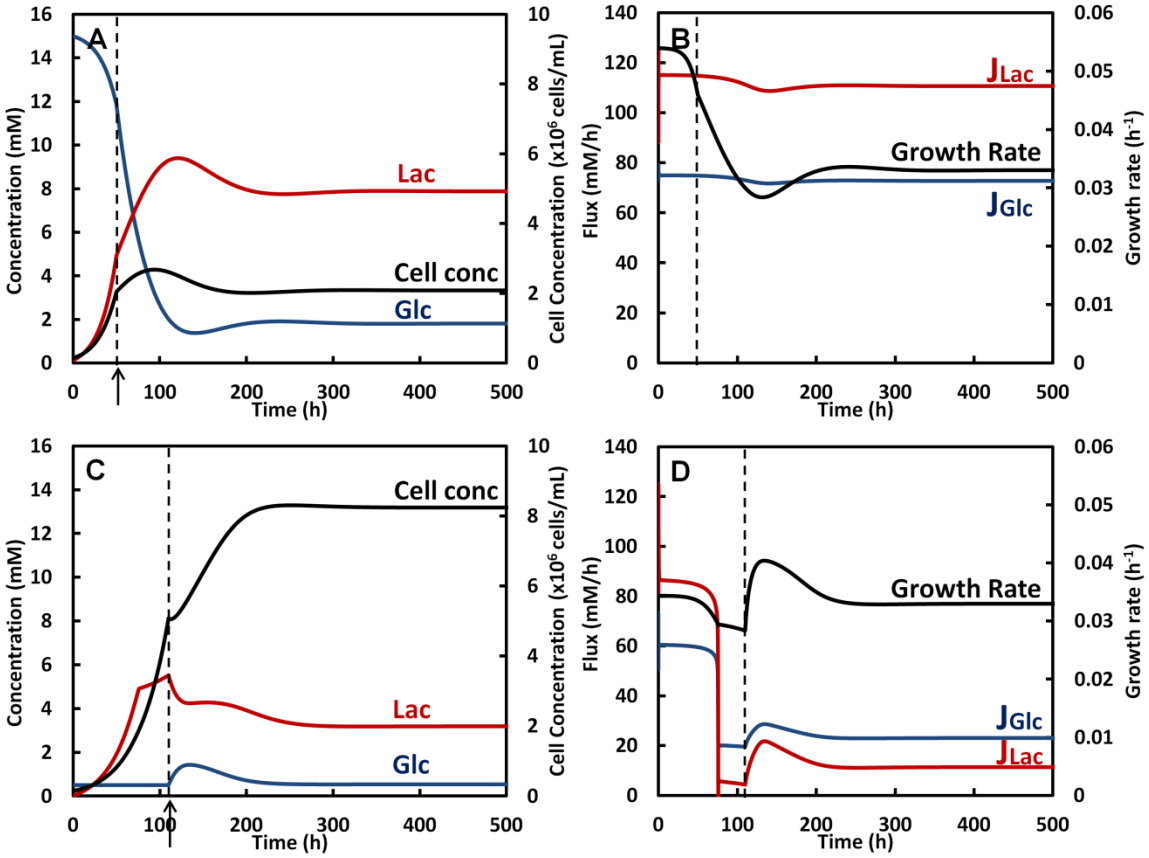

Figure 6.3: Transient simulations of continuous culture that reaches steady states with distinct cell concentration. (A-B) Culture started from batch mode exhibits high metabolic flux and remains at high flux state upon initiation of continuous culture. Such culture reaches steady state with high metabolic flux and lower cell concentration. **(C-D)** Culture started from fed-batch with glucose maintained at low level exhibits a metabolic shift to low flux state. Upon initiation of continuous mode, the culture remains at low flux state and reaches steady state with higher cell concentration. Arrow (↑) indicates the

time at which continuous mode is initiated. In the continuous mode, dilution rate and feed glucose concentration were fixed at 0.033 hr^{-1} and 7 mM, respectively.

The batch culture is initiated with a glucose concentration of 15 mM. It consumes glucose and produces lactate at very high rates and reached 11.8 mM and 4.9 mM of glucose and lactate respectively at 50 h (Figures 6.3A-B). The ratio of glucose to lactate conversion (J_L/J_G) is 1.55 mol/mol, indicating that the culture operates at high metabolic flux state. At this time, with a cell concentration of $1.3x10^6$ cells/mL, the culture is switched to a continuous mode. The culture continues at a high flux state (J_L/J_G is 1.53 mol/mol) to reach a steady state with a relatively low cell concentration of $2.1x10^6$ cells/mL.

For the fed-batch culture, glucose concentration is maintained at 0.5 mM. Over time the culture undergoes metabolic shift to a low flux state. After 110 h (Figures 6.3C-D) J_L/J_G was 0.22 mol/mol indicating low metabolic state. Cell concentration reaches $5.1x10^6$ cells/mL. At this point, the culture is switched to continuous mode, where it continues at a low flux state as indicated by the low J_L/J_G. Glucose and lactate concentrations settled down to 0.54 mM and 3.2 mM, respectively, and the cells continued to grow before reaching a final steady state concentration of $8.2x10^6$ cells/mL.

6.3.4 Directing Continuous Culture to Steady State with Low Glycolysis Flux

Continuous cultures of MAK hybridoma cells were initiated either from batch or fed-batch mode (also see the MAK Cell Culture section of the Materials and Methods). A typical continuous culture, started from a batch culture, is shown in Figure 6.4 (solid squares). Cells were inoculated at a concentration of $1.5x10^5$ cells/mL using a medium identical to that used for cell maintenance except that the initial glucose concentration was 3 mM. After 45 hours, the cell concentration increased to $8x10^5$ cells/mL while lactate accumulated to 3.9 mM. J_L/J_G is 1.44 mol/mol, which is in the range typically seen in batch cultures. At this point, the culture was switched to continuous mode.

Dilution rate of 0.033 h^{-1} and feed medium as described in the MAK Cell Culture section of the Materials and Methods were used. Steady state, as judged from the cell, glucose and lactate concentrations, was reached at approximately 200 h. The viable cell concentration at steady state was $3.6x10^6$ cells/mL, whereas glucose and lactate concentrations were 0.23 mM and 2.7 mM, respectively. J_L/J_G is approximately 1.30 mol/mol at steady state.

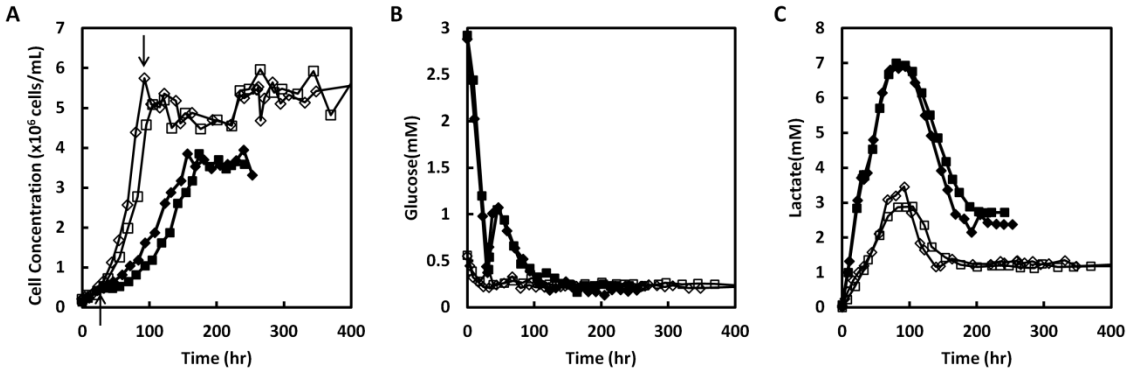

Figure 6.4: Directing continuous culture to steady state with low glycolysis flux by glucose control. Continuous cultures were started either from batch cultures (■ and ♦) or fed-batch cultures with glucose maintained at 0.3 mM (□ and ◊). Cultures initiated from batch mode reached steady states with lower cell concentrations while those started from fed-batch mode reached steady states with higher cell concentrations. Arrow (↑) indicates the time at which continuous mode is initiated.

Cultures were also started from fed-batch mode. Cells were inoculated at a concentration of $1.5x10^5$ cells/mL using a medium identical to that used for maintenance except that the initial glucose concentration was 0.55 mM. Enriched medium with fortified nutrient concentrations was fed according to a strategy previously described [70] to maintain residual glucose concentration near a set point of 0.28 mM. Cell concentration increased steadily to $5x10^6$ cells/mL for 90 hr. During this time period, lactate accumulated to 2.8 mM (Figure 6.4). At this point, J_L/J_G was 0.13 mol/mol, indicating a shift in metabolism towards low lactate production. The culture was then switched to continuous mode at dilution rate of 0.033 hr^{-1} and feed medium as described in the Materials and Methods

was used. Steady state was reached at approximately 250 hr. The steady state viable cell concentration was $5.4x10^6$ cells/mL, while glucose and lactate concentrations were 0.21 mM and 1.2 mM, respectively. J_L/J_G is approximately 0.12 mol/mol at steady state.

Consistent with the model prediction, these results show that guiding the metabolic state of the cells prior to initiation of the continuous culture can determine the actual steady state reached at identical operating conditions.

6.4 Discussion

We constructed a multi-scale model combining intracellular metabolic pathways with the macroscopic cell concentration in a continuous bioreactor. The steady state multiplicity predicted by the mechanistic metabolism model is manifested in the continuous bioreactor. In the bistable region, for a given dilution rate, the culture can exist at either a high flux steady state or a low flux steady state. The two kinds of steady states have different metabolic efficiency. At a high flux state the vast majority of glucose is converted to lactate, whereas at a low flux state more glucose consumed is converted to biomass. Thus different steady states are marked by distinct steady state cell concentrations. With the feed glucose concentration used in the simulation, multiple steady states are observed only in a range of dilution rates. Outside of the bistable region, in the high dilution rate region only the high flux states are present whereas in the low dilution rate region only the low flux states exist. It is notable that the model predicts that in the range of lactate production rate to glucose consumption rate ratio (J_L/J_G) between 0.8-1.45 no stable steady state exists. The experimental data in literature are in close agreement to this finding [126,127].

In the bistable region, which steady state (high flux state or low flux state) a culture will reside in is dependent on the history of the culture. One can thus influence the steady state to be reached by controlling the cell's metabolic state before steady state is reached. Since the "default" state of cells in culture under typical culture conditions is a high flux state, at issue is thus "guiding" the cells to a low flux state before steady state is reached. This was illustrated by two approaches: one by eliciting a metabolic shift to a low flux

state in fed-batch culture via controlling glucose at low levels (Figure 6.3), and the other by operating at a low dilution rate region in which only the low flux steady state exists before gradually increasing the dilution rate to the bistable region (Figure 6.5). Indeed these two approaches were used to reach a low flux steady state in two experimental studies [117,151].

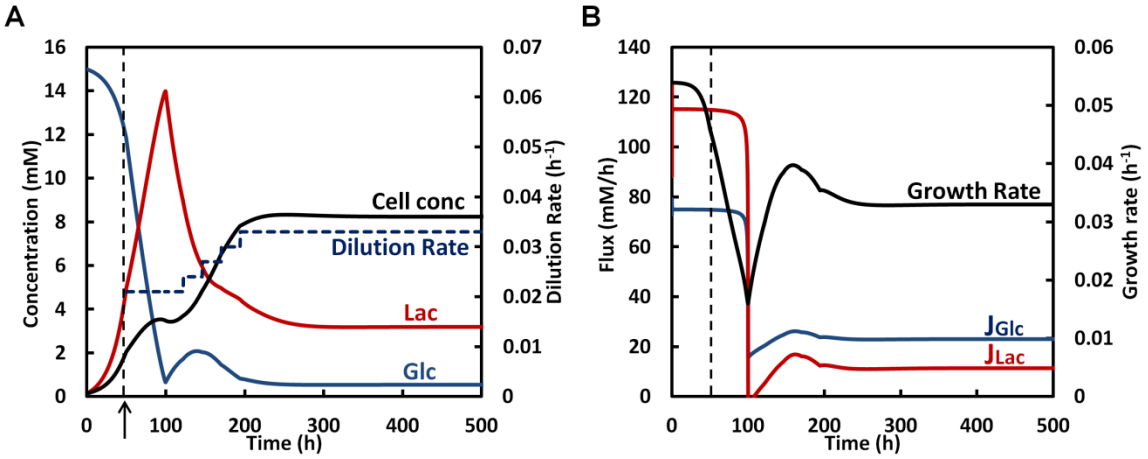

Figure 6.5: Directing continuous culture to steady state with a low glycolysis flux by controlling dilution rate. Culture was started in batch mode and exhibits high metabolic flux. The culture is then switched to continuous mode with dilution rate of 0.021 h^{-1} and feed glucose concentration of 7 mM. By operating at a low dilution rate, the culture reaches a steady state with low metabolic flux. Incrementally increasing the dilution rate to a final rate of 0.033 h^{-1} allows the culture to remain at low flux and reaches a final steady state with higher cell concentration (compared to Figure 6.3A). Arrow (↑) indicates the time at which continuous mode is initiated.

The bistable behavior observed in continuous culture is reminiscent of that observed in fed-batch cultures. Cells in the later stage of fed-batch cultures can switch their metabolism from high rate of lactate production to lactate consumption. Metabolic shift to lactate consumption in fed-batch cultures has been shown to be correlated with a higher productivity [3,4]. In continuous culture, steady state with lactate consumption does not exist without lactate supplementation in the feed. Addition of lactate to the feed

medium of a continuous culture may not be used in practice, but the result does show its feasibility as a steady state operation.

There has been a resurgence of interest in using continuous culture for recombinant therapeutic protein production [154]. With the patent expiration of older generation of therapeutics, follow-on biologics, also called biosimilars, are entering the market creating a wave of generic drugs. The prospect of producing biosimilars in different regions in the world has provided incentives for constructing regional manufacturing facilities. Many new facilities will aim to be smaller and more flexible in terms of the product they produce while sustaining a high throughput similar to the facility designed for fed-batch manufacturing. Continuous processes are well suited to such purposes.

Furthermore continuous processes offer the possibility of steady state operation in which the metabolic state of cells is kept relatively constant as opposed to constantly changing nature in fed-batch cultures. Increasingly biopharmaceutical production is focusing on controlling product quality in addition to the productivity. The glycosylation pattern of the product protein is a key product attribute that process engineers strive to control and is reported to be affected by many environmental factors that fluctuate in typical fed-batch cultures [155-158]. Steady state operation of continuous cultures may minimize such culture variations and provides greater control of product quality.

The multi-scale model presented demonstrates that multiple steady states exist under some culture conditions. Since those different steady states represent different metabolic states, they may also elicit different glycosylation patterns or other product quality attributes with some being the preferred. In view of such possibilities, controlling the culture condition to ensure it follows the trajectory to reach the desired steady state is thus critical. The model we established should provide mechanistic understanding to prescribe such trajectories to enhance process performance.

Chapter 7 Diversity of the Chinese Hamster Ovary Cell Line Transcriptomes

7.1 Summary

The metabolic behavior of mammalian cells in culture depends not only on the external cues such as glucose and growth factors availabilities but also on the intrinsic attributes of the cells including gene expression and genetic variations. Different cell lines may express different isoforms of metabolic enzymes in different proportions. Furthermore, their cultivation for a large number of generations may lead to accumulation of mutations in their genomes. These variations can potentially influence their behavior in culture. In this chapter, we unveil the transcript level and genetic diversities among different Chinese hamster ovary (CHO) cell lines using transcriptomics tools including RNA-seq and microarray. We find that CHO cells have the preference for glycolysis isozymes that confer high glycolytic flux, similar to proliferating cells such as cancers and embryonic stem cells. Among different CHO cell lines, the variability of transcript levels of glycolysis enzymes is high suggesting its crucial role in determining the metabolic characteristics of the cells. Using RNA-seq, we find that the number of sequence variants and the corresponding mutation rate in CHO cells does not appear to be alarmingly high, implying mutations in the gene coding regions may not be key to cell line variability. The knowledge of the variability in CHO cells will serve as tremendous resource in devising strategies to counter the variability in cell line development.

7.2 Introduction

Cultured mammalian cells are widely used for the production of recombinant therapeutic proteins. Because of their economic importance, much effort has been devoted to enhancing our understanding of the physiology of those cell lines. In recent years, global survey of the transcriptome using microarrays has been increasingly employed to better understand a number of producing cell lines and production processes [159-162]. With the rapid advances in sequencing technology, especially direct

sequencing of transcripts, or RNA-seq, the repertoire of CHO transcriptome data has been expanding [163-166]. These resources will usher the research in cell culture bioprocessing into a post-genomic era, increasingly using systems approaches and integrating data from various -omics based global surveys (reviewed in [167,168]).

The use of genomics and transcriptomics tools holds great potential to advance the understanding of cellular behavior. It is well known that different production cell lines display different characteristics. These differences are not only in productivity but also in their growth rate, metabolic behavior and even in the post translational modification patterns of the product protein. Such cell line dependent characteristics are possibly linked to the variation in gene expression profile. For example, mammalian cells can express multiple isoforms of the same metabolic enzyme which catalyze the same reaction but have different kinetic properties and are subjected to contrasting regulations. The expression of these distinct glycolysis isozymes in different proportions may account for the different metabolic behaviors observed in different cell lines. An integrated transcriptome-based systems biology approach can be employed to provide insights into cell line selection for specific gene expression. In this study, we survey the transcript expression data of the genes in CHO cell lines using microarray. We highlight the characteristic isoform expression of CHO cells and the variability among different CHO cell lines. The effect of the variation on the metabolic characteristics will be discussed.

Another possible source of variability is genomic variation, especially in the gene coding regions. Cell lines have a propensity to accumulate single nucleotide mutations and copy number differences over the course of continual culture since their isolation almost six decades ago [169,170]. Accumulation of mutations in the genome can potentially dictate their behavior in culture. However, the fraction of the population harboring such mutations may remain low unless it offers some growth advantage or recurs repeatedly. A majority of such mutations in recombinant cell lines has gone unnoticed because few cell lines have been sequenced to adequate depth to detect such low-frequency mutations. Even with high-throughput genome sequencing, the depth of coverage employed is rarely more than 100. RNA-seq, on the other hand, sequences the transcripts of abundant genes

to much greater depth, sometimes to tens of thousands of reads per base. The high depth of RNA-seq data enables the detection of large number of low frequency single nucleotide variants in cultured cell lines with a high degree of confidence. We thus also analyzed the single nucleotide variants in the cell lines for which RNA-seq data are available.

7.3 Results

7.3.1 Analysis of Transcript Levels of Glycolysis Genes in CHO Cell Lines

We quantified of the expression levels of genes in fourteen CHO cell lines using microarray (Appendix Table 5). The use of these diverse samples was intended to give a representative view of the range of transcript expression level for genes that are relevant for bioprocessing. The transcript levels of glycolysis enzymes in fourteen CHO cell lines are shown in Figure 7.1.

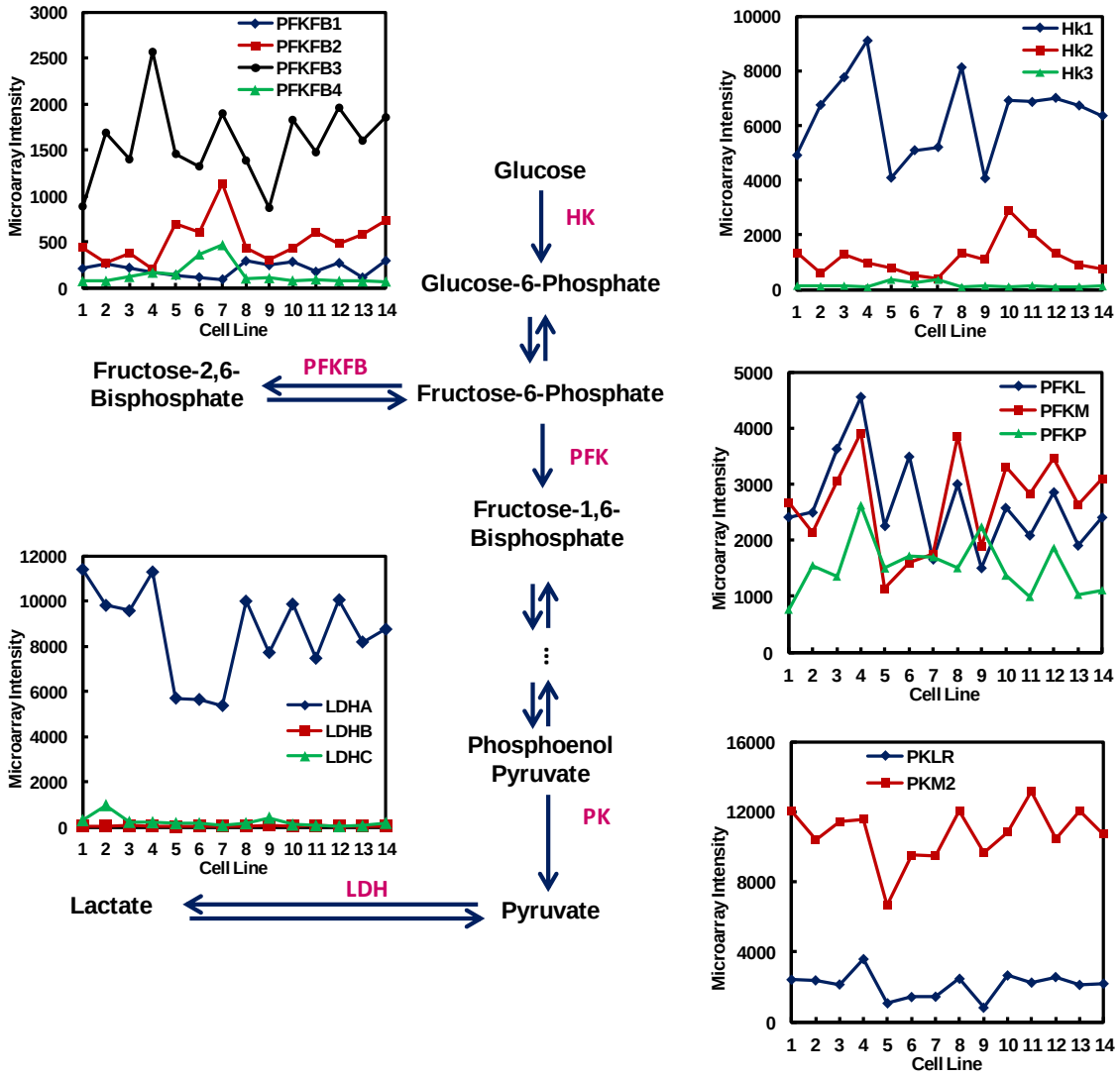

Figure 7.1: Gene expression levels of several glycolysis isozymes from microarray data of 14 CHO cell lines. The identity of the cell lines are given in Appendix Table 5.

The hexokinase isozymes HK1 and HK2, are highly expressed in CHO cell lines. Both HK1 and HK2 have strong affinity to glucose (low K_m) and can physically bind to the outer membrane of mitochondria (reviewed in [79]), giving them direct access to ATP generated by mitochondria for increased rate of glycolysis.

CHO cell lines express predominantly the liver (PFKL) and the muscle (PFKM) forms of phosphofructokinase (PFK). Both PFKL and PFKM are subjected to activation by

fructose-1,6-bisphosphate (F16BP), however, this interaction is absent for PFKP. They thus confer a high glycolytic rate as a result of F16BP activation.

PFKFB3 is the dominant isoform of 6-phosphofructo-2-kinase/fructose-2,6-bisphosphatase (PFKFB) expressed in CHO cell lines. The balance between the activities of the kinase (K) and the bisphosphatase (P) domains of PFKFB controls the steady state concentration of fructose-2,6-bisphosphate (F26BP) [11,12]. F26BP is a very potent activator of the glycolysis enzyme PFK. The flux through glycolysis is, therefore, influenced by the K/P activity ratio of PFKFB. Isozymes of PFKFB differ in their K/P ratio [81-83]. The K/P ratio of PFKFB3 (~ 700) is the highest among all PFKFB isozymes, conferring very strong activation to the flux of glycolysis.

CHO cell lines express PKM2 as the dominant pyruvate kinase isoform. PKM1 and PKM2 are alternatively spliced transcripts encoded by the Pkm gene, with a difference in 23 amino acids from one alternatively spliced exon. PKM2, but not PKM1, is activated by F16BP. PKM2 is under the regulation by many allosteric modulators which is crucial for controlling the flux of glycolysis for ATP production and the channeling of the flux for biosynthetic needs of the cell. PKM1 is expressed in the majority of adult tissues, whereas PKM2 is restricted to embryonic tissues and transformed cells.

The LDHA isozyme of lactate dehydrogenase isozyme is very highly expressed in CHO cell lines. Lactate dehydrogenase is a tetrameric enzyme that catalyzes the reversible conversion of pyruvate to lactate. LDHB and LDHC, which are found in heart and spermatozoa, respectively, convert lactate to pyruvate that is further oxidized. In contrast, LDHA, which is also predominantly expressed in skeletal muscle, kinetically favors the reverse conversion of pyruvate to lactate. Many cancers also express LDHA at higher levels compared to normal tissues [171].

All CHO cell lines express the same dominant isoforms but at different levels. They also express different proportions of isoforms of a given enzyme, including those which play major regulatory roles. PFKFB2 and PFKFB3 vary by 4-fold and 3-fold, respectively. Mulukutla *et al.* [153] showed that the level of PFKFB enzymes determine the response

rate of cells to changes in glucose concentration cells. Similarly, PFKL and PFKM, each vary by 3-fold among CHO cell lines. Such variation in the isozyme composition of PFK can affect the metabolic profile of cells (Appendix Figure 5) [153]. Other enzymes in glycolysis also show some degree of variations (Figure 7.2). The diversity in metabolic characteristics of CHO cells under identical culture conditions and/or treatments [172] may potentially be the result of such intrinsic variation in gene expression.

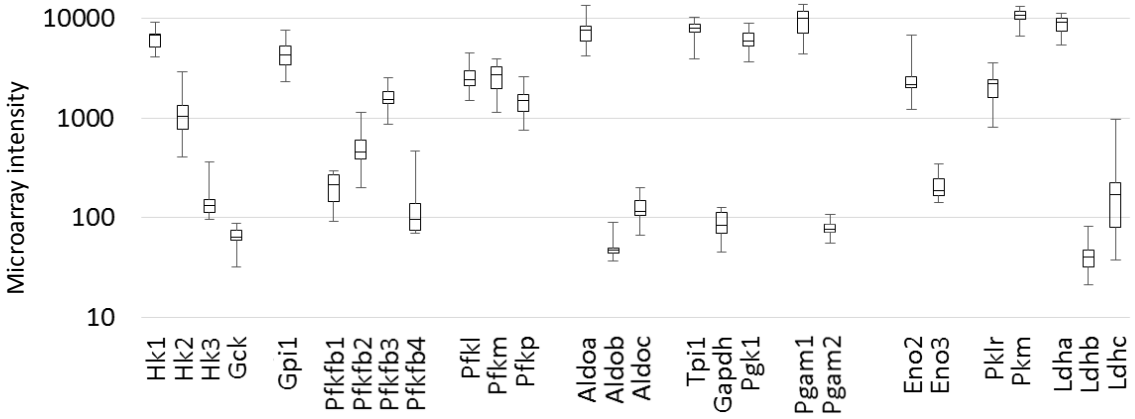

Figure 7.2: Variation in glycolysis gene expression levels from 14 CHO cell lines.

7.3.2 Sequence Variation in CHO Cell Lines

In addition to the variation in the transcript level, genomic variation can confer distinct characteristics in mammalian cells. Typical mammalian diploid genomes harbor two copies of the same genes. While many genes are homozygous, some are heterozygous and have differences in the alleles. Cultured cells derived from a mammal retain those heterozygote sequences, and accumulate additional somatic mutations, including the single nucleotide mutations in their genomes. These heterozygous mutations are carried over when the gene is transcribed into RNA. The great sequencing depth provided by RNA-seq, especially for abundant transcripts, houses a trove of information on single nucleotide variants (SNVs). In RNA-seq, a SNV is characterized by a fraction of the reads with one base call and another fraction with a different base call at the same location (Appendix Figure 9). We identified these SNVs in the transcriptome of five

CHO cell lines and in tissue samples from RNA-seq data (Appendix Table 6). On an average, each cell line possesses approximately 4,000 SNVs which correspond to a rate of $1.6x10^{-4}$/bp (Figure 7.3A). This rate is substantially lower in liver and brain.

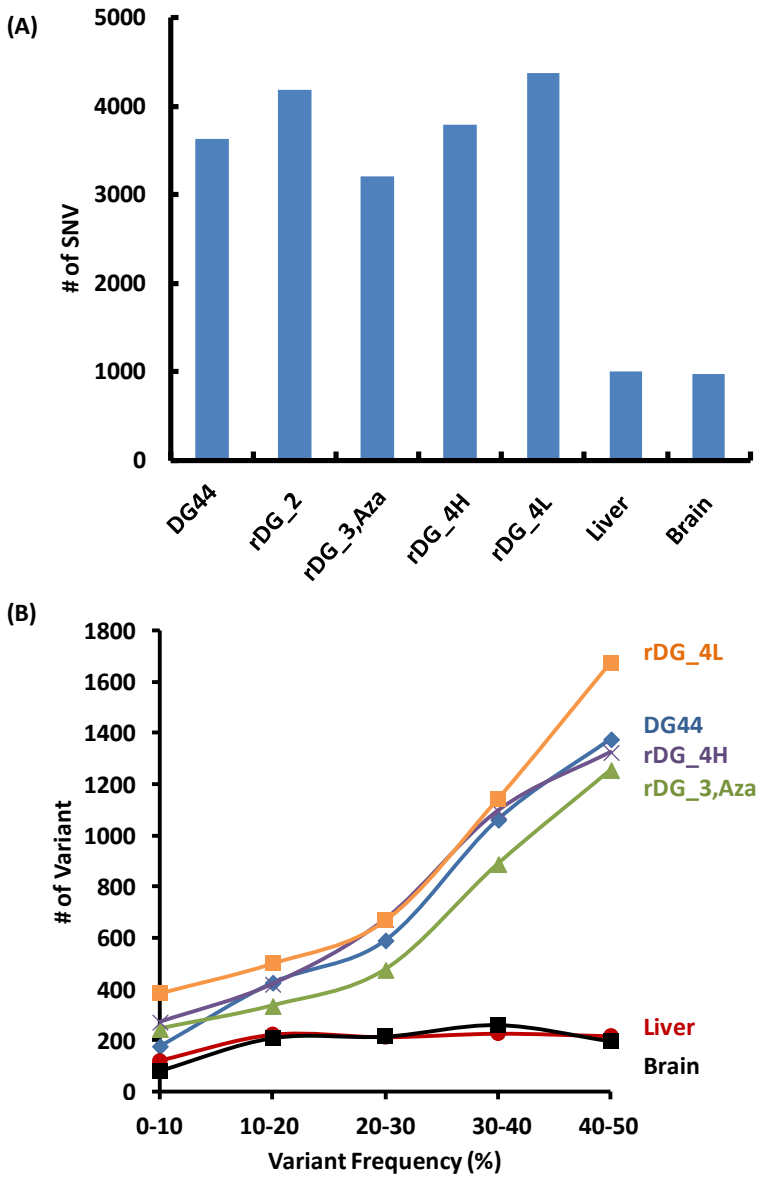

Figure 7.3: Single nucleotide variants in the transcripts of five CHO cell lines and two Chinese hamster tissues. (A) Number of variants identified and **(B)** Distribution of variants according to the fraction of variant call at each location. The identity of the cell lines are given in Appendix Table 6.

These sequence variants occur at different frequencies. In a diploid cell or tissue, a variant that arises from heterozygocity will constitute close to 50% of all base calls at that particular location. Since CHO cell lines are aneuploid, it is possible that even a variant caused by heterozygocity may be present close to 30% or 25% depending on the number of that genomic segment in the genome. The recombinant cell lines used in the study have undergone single cell cloning at the time they were first derived. They have since been in culture for a large number of cell generations. A variant resulting from a mutation after single cell cloning will most likely occur in only a small portion of cells unless that mutation confers an advantage under some growth conditions to overtake the population. To analyze the source of the variants, we plotted the count of variants and the percentage of the variant call at each variant location for the five cell lines as well as the liver and brain tissues (Figure 7.3B). A majority of the variants in cell lines were present at 40-50% of all reads at that position, suggesting a strong possibility that they arose from heterozygocity of the tissue of their origin or from the mutation that occurred prior to the last single cell cloning. This is in contrast with the variants in tissues for which there is no strong presence of variants at 40-50%, possibly as a consequence of extensive inbreeding that leads to homozygocity from genetic drift.

Comparisons were performed to identify sites with distinct nucleotide sequences between pairs of closely related cell lines. Each comparison indicates the presence of ~500 – 1,200 such sites (Appendix Figure 10). Twenty one sites with distinct nucleotide sequence between DG44 and rDG_2 were selected to be examined at the cDNA and genomic DNA level using Sanger sequencing method. In both cDNA and gDNA (Appendix Figure 11), 17 sites (71%) were confirmed while four others were false positive.

7.3.3 Mutations in Growth Signaling Pathways

We examined the sequences of the genes in the PI3K/AKT, mTOR, p53, cMYC and MAPK pathways for mutations that are present in all CHO cell lines compared to Chinese hamster tissues. A total of 61 potential sites were spread across 22 genes, 42 of

which are located in the protein coding regions. Five of them cause amino acid changes in Pdpk1, Trp53, Map3k10, Mapk8ip3 and Taok2 (Table 7.1).

Table 7.1: Potential mutations in the growth signaling pathways of CHO cell lines.

Gene	Nucleotide Position	Feature	Amino acid change	Base call in tissues	Base call in cell lines
Trp53	783	Exon	Thr -> Lys	C	A
Pdpk1	1669	Exon	His -> Gln	C	A
Map3k10	864	Exon	Glu -> Gln	G	C
Mapk8ip3	1537	Exon	Ile -> Val	A	G
Taok2	1739	Exon	Arg -> Arg/Leu	G	G/T

Their positions relative to functional domains in those proteins are shown in Fig. S7. Except for those in Mapk8ip3, the mutations identified in Trp53, Pdpk1, Map3k10 and Taok2 are located in the function-related protein domain (Appendix Figure 12A-E). Many mutations in those genes have been reported in human cancer. A few mutations in human cancer that are located in close proximities/correspond to those in CHO cell lines are shown in Appendix Figure 12F-J. Except for Taok2, the other four mutations were homozygous in all cell lines. These same mutations were also observed at genome level in CHO K1 [173] and rDG_2 (unpublished data) cell lines compared to the Chinese hamster genome [174]. These mutations probably occurred very early in the establishment of CHO cell line.

7.3.4 Variant in Product Gene Not Detected

Protein sequence variants in the product may be caused by mutations in the product gene [175,176]. The presence of such variants, even at small levels, causes grave concern. The great depth of coverage of product transcript in high producing cells allows for the detection of low levels of SNVs at a high confidence level. Three high confidence variants in the IgG transcripts in rDG_2 (coverage depth > 20,000) were detected at a low frequency (< 4.5 %). All are located in the heavy chain of IgG. Sanger sequencing was performed on both cDNA and gDNA to verify the presence of variants. None of 103

cDNA and 110 gDNA *E. coli* clones sequenced revealed any variants (Appendix Table 7). These variants, if indeed present, must be present only at very low levels.

7.3.3 Clustering of Cell Lines by Single Nucleotide Variants

The SNVs identified in all the cell lines were used to construct the phylogeny tree. The phylogeny tree generated from the SNV data grouped the cell lines derived from the same parent together (Figure 7.4). When a mutation first occurs, it is most likely to occur in one cell initially, and the vast majority of cells in the population retain the parental base unless the mutant cell somehow increases its representation in the population. The variant markers of distinct nucleotides at the same location are thus signatures of parental lineage. It is interesting to see that the nucleotide variants accurately trace the lineage of cell lines.

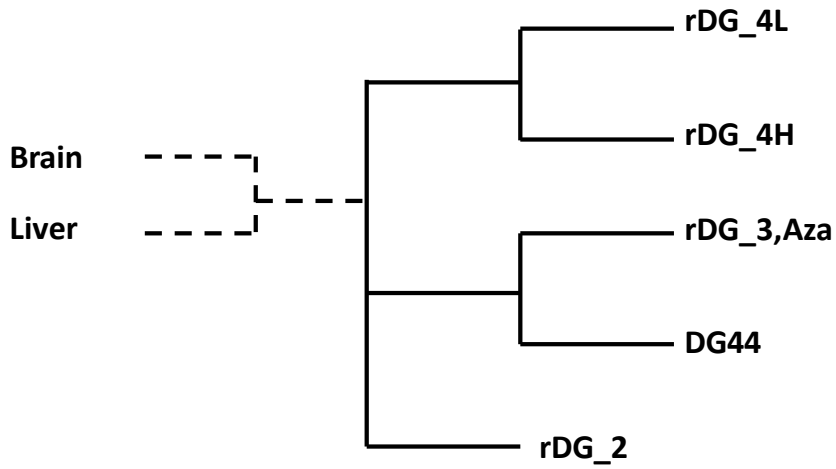

Figure 7.4: Lineage tracing of various CHO cell lines through sequence variant profiles identified using RNA-seq.

7.4 Discussion

In this study, vast microarray data from our previous studies were collected to provide a reference for transcriptome analysis. The transcript levels of genes in the central glycolysis pathway were compiled from fourteen CHO cell lines to allow for a handy

reference of “typical” expression levels and identity of isozymes involved. The composition of the enzymes in this pathway greatly influences cellular metabolism.

The glycolytic isozyme profile of CHO cells was very similar to that reported for proliferating cells such as cancer or embryonic cells. Overall, the variability of gene expression level in glycolysis was high. PKM2 isoform of PK, the pivotal isozyme that gives fast growing cells their high flux glycolysis characteristics, was expressed at a very high level and varied across a wide range among different cell lines. The enzyme PFKFB, which plays an important role in regulating glycolysis flux, also showed variable expression among cell lines. How the knowledge of the expression profiles of PKM2 and PFKFB can be leveraged to exert better control of metabolic behavior, awaits further exploration.

We took advantage of the very high level of IgG transcripts in the high producing cells and its great depth in RNA-seq to search for possible sequence variants at very low levels. Three SNVs identified in RNA-seq were either present at very low frequency that was not detected in our verification sequencing or false positives possibly caused by errors in reverse transcription or sequencing.

The recombinant cell lines used in the study have undergone single cell cloning during cell line development. Upon single cell cloning, the mutations accumulated by the cloned cell will be present at 50% (for a heterozygous diploid cell) or at 100% for homozygous mutation. Excluding very low level variants, we estimated that about 4,000 sequence variants have accumulated in the transcripts analyzed in most cell lines. Most of those variants were present at or near 50% (Figure 7.3B). These SNVs include heterozygous base pairs originated from the animal from which CHO cells were first derived [169,170] or from the mutation accumulated prior to the last single cell cloning. The SNVs accumulated in producing cell lines at a lower frequency are likely to represent mutations accumulated after single cell cloning. The number is in the range of a few hundreds. Since those cell lines all have been passaged extensively (>> 60 generations), the mutation rate does not appear to be alarmingly high. This is also consistent with the fact

that no detectable mutation was seen in the IgG product transcript. In contrast to the cell line data, SNVs in the liver and brain of Chinese hamster were relatively evenly distributed over different frequencies. Since the animal we used to isolate liver and brain tissue were inbred animals for the past five decades, it is not surprising that little heterozygocity remains due to genetic drift in inbred animals.

The accumulated experiences in cultivating numerous recombinant CHO cell lines have given us insights into their variability in growth, metabolism, and nutritional needs. The variability also affects the consistency of product quality produced in different clones. Understanding the cause of the variability and devising means to counter the variability will be a major step forward in cell line development. We reckon that the mutation frequency in the transcribed region in CHO cells is not alarmingly high, implying mutations in those regions may not be influential to cell line variability. It is possible that mutations in the intergenic regions and other epigenetic events play more significant roles in the variability of gene expression and the diversity of the behavior of CHO cells in culture. The transcriptome data can provide us with a range of expression levels that we can utilize to begin epigenetic exploration and to apply systems analysis to better model cellular processes for enhancing process robustness and product consistency.

Chapter 8 Concluding Remarks and Future Directions

Energy metabolism of mammalian cells profoundly affects the performance of cell culture processes. Reducing the production of lactate is desirable for sustained viability and increased productivity of the cells in culture. The lack of understanding of the metabolism of the cells and ways to control it has led to inefficient processes. This thesis presents a systems biology approach that provides insights into cell physiology and its behavior in culture. Such knowledge can be used to control process culture for more consistent behavior.

We showed using a mathematical model that bistability is at the heart of the glucose metabolism of proliferating cells including cultured mammalian cells. Such bistable behavior is the root cause of phenomena of metabolic shift to lactate consumption in fed-batch culture and multiplicity of steady state in continuous culture. In fed-batch culture, inhibition of glycolysis by lactate accumulation and by growth rate affects the topology of steady state glycolysis flux. Using the model, strategies to direct the culture to desired metabolic fate were explored. Metabolic shift to lactate consumption in fed-batch culture can be robustly induced by controlling glucose at low levels, by suppressing growth rate of the cells, or by modulating lactate concentration in the culture. In continuous culture, the bistability in energy metabolism leads to distinct achievable steady state cell concentrations. The steady state with higher cell concentration can be reached by directing cells to low glycolysis flux by first cultivating the cells in fed-batch with glucose maintained at a low level. Alternatively, one can initially operate the continuous culture at low dilution rate before incrementally increasing it to higher dilution rate. Exploration of the model for further novel strategies to robustly control cell metabolism awaits.

CHO cells exhibit a wide range of variability in gene expression of metabolic genes. Using such information, one can begin to use the model to predict the steady state or transient behavior of different CHO cell lines in culture. The insights obtained will be valuable for screening cell lines that can robustly shift metabolism to low glycolysis flux

or for selecting targets for cell line engineering. This can possibly be achieved by switching the isozymes of phosphofructokinase to platelet type or the isozyme of pyruvate kinase to M1. Alternatively one can overexpress the kinase-deficient PFKFB enzyme. Finally, one can consider altering the expression or modulating the activity of growth control genes that affect glucose metabolism such as mTOR, AMPK, and HIF1α.

One of the biggest challenges in the process cell culture is to achieve proper and consistent glycosylation of the product which greatly affects its efficacy. It is known that glucose metabolism affects the glycosylation pattern of the product. Glucose 6-phosphate and fructose 6-phosphate are channeled from glycolysis to the nucleotide sugar biosynthesis pathways. The synthesized nucleotide sugar precursors are then transported to the golgi apparatus and participate in the glycosylation process. The metabolic model presented here can therefore be expanded to include the glycosylation pathway. The resulting model will be very useful for systematically studying the effect of perturbation in glucose metabolism and its intermediates on the glycoform profile. Importantly, the model can serve as a guide for future engineering of glycoproteins.

Chapter 9 References

1. Aggarwal RS (2014) What's fueling the biotech engine-2012 to 2013. Nat Biotechnol 32: 32-39.
2. Kantardjieff A, Zhou W (2014) Mammalian cell cultures for biologics manufacturing. Adv Biochem Eng Biotechnol 139: 1-9.
3. Charaniya S, Le H, Rangwala H, Mills K, Johnson K, et al. (2010) Mining manufacturing data for discovery of high productivity process characteristics. J Biotechnol 147: 186-197.
4. Le H, Kabbur S, Pollastrini L, Sun Z, Mills K, et al. (2012) Multivariate analysis of cell culture bioprocess data--lactate consumption as process indicator. J Biotechnol 162: 210-223.
5. van Heerden JH, Wortel MT, Bruggeman FJ, Heijnen JJ, Bollen YJ, et al. (2014) Lost in transition: start-up of glycolysis yields subpopulations of nongrowing cells. Science 343: 1245114.
6. Vora S, Oskam R, Staal GE (1985) Isoenzymes of phosphofructokinase in the rat. Demonstration of the three non-identical subunits by biochemical, immunochemical and kinetic studies. Biochem J 229: 333-341.
7. Van Schaftingen E, Jett MF, Hue L, Hers HG (1981) Control of liver 6-phosphofructokinase by fructose 2,6-bisphosphate and other effectors. Proc Natl Acad Sci U S A 78: 3483-3486.
8. Reinhart GD, Lardy HA (1980) Rat liver phosphofructokinase: kinetic activity under near-physiological conditions. Biochemistry 19: 1477-1484.
9. Yaney GC, Schultz V, Cunningham BA, Dunaway GA, Corkey BE, et al. (1995) Phosphofructokinase isozymes in pancreatic islets and clonal beta-cells (INS-1). Diabetes 44: 1285-1289.
10. Yi W, Clark PM, Mason DE, Keenan MC, Hill C, et al. (2012) Phosphofructokinase 1 glycosylation regulates cell growth and metabolism. Science 337: 975-980.
11. Schulze A, Ros S (2013) Balancing glycolytic flux: the role of 6-phosphofructo-2-kinase/fructose 2,6-bisphosphatases in cancer metabolism. Cancer and Metabolism 1: 10.
12. Okar DA, Manzano A, Navarro-Sabate A, Riera L, Bartrons R, et al. (2001) PFK-2/FBPase-2: maker and breaker of the essential biofactor fructose-2,6-bisphosphate. Trends Biochem Sci 26: 30-35.
13. Keller KE, Tan IS, Lee YS (2012) SAICAR stimulates pyruvate kinase isoform M2 and promotes cancer cell survival in glucose-limited conditions. Science 338: 1069-1072.
14. Chaneton B, Hillmann P, Zheng L, Martin AC, Maddocks OD, et al. (2012) Serine is a natural ligand and allosteric activator of pyruvate kinase M2. Nature 491: 458-462.
15. Morgan HP, O'Reilly FJ, Wear MA, O'Neill JR, Fothergill-Gilmore LA, et al. (2013) M2 pyruvate kinase provides a mechanism for nutrient sensing and regulation of cell proliferation. Proc Natl Acad Sci U S A 110: 5881-5886.

16. Anastasiou D, Poulogiannis G, Asara JM, Boxer MB, Jiang JK, et al. (2011) Inhibition of pyruvate kinase M2 by reactive oxygen species contributes to cellular antioxidant responses. Science 334: 1278-1283.
17. Barthel A, Okino ST, Liao J, Nakatani K, Li J, et al. (1999) Regulation of GLUT1 gene transcription by the serine/threonine kinase Akt1. J Biol Chem 274: 20281-20286.
18. Robey RB, Hay N (2006) Mitochondrial hexokinases, novel mediators of the antiapoptotic effects of growth factors and Akt. Oncogene 25: 4683-4696.
19. Majewski N, Nogueira V, Bhaskar P, Coy PE, Skeen JE, et al. (2004) Hexokinase-mitochondria interaction mediated by Akt is required to inhibit apoptosis in the presence or absence of Bax and Bak. Mol Cell 16: 819-830.
20. Bandhakavi S, Kim YM, Ro SH, Xie H, Onsongo G, et al. (2010) Quantitative nuclear proteomics identifies mTOR regulation of DNA damage response. Mol Cell Proteomics 9: 403-414.
21. Clem B, Telang S, Clem A, Yalcin A, Meier J, et al. (2008) Small-molecule inhibition of 6-phosphofructo-2-kinase activity suppresses glycolytic flux and tumor growth. Mol Cancer Ther 7: 110-120.
22. Gagnon M, Hiller G, Luan YT, Kittredge A, DeFelice J, et al. (2011) High-end pH-controlled delivery of glucose effectively suppresses lactate accumulation in CHO fed-batch cultures. Biotechnol Bioeng 108: 1328-1337.
23. Mulukutla BC, Gramer M, Hu WS (2012) On metabolic shift to lactate consumption in fed-batch culture of mammalian cells. Metab Eng 14: 138-149.
24. Berwick DC, Hers I, Heesom KJ, Moule SK, Tavare JM (2002) The identification of ATP-citrate lyase as a protein kinase B (Akt) substrate in primary adipocytes. J Biol Chem 277: 33895-33900.
25. del Peso L, Gonzalez-Garcia M, Page C, Herrera R, Nunez G (1997) Interleukin-3-induced phosphorylation of BAD through the protein kinase Akt. Science 278: 687-689.
26. Dijkers PF, Birkenkamp KU, Lam EW, Thomas NS, Lammers JW, et al. (2002) FKHR-L1 can act as a critical effector of cell death induced by cytokine withdrawal: protein kinase B-enhanced cell survival through maintenance of mitochondrial integrity. J Cell Biol 156: 531-542.
27. Duvel K, Yecies JL, Menon S, Raman P, Lipovsky AI, et al. (2010) Activation of a metabolic gene regulatory network downstream of mTOR complex 1. Mol Cell 39: 171-183.
28. Wouters BG, Koritzinsky M (2008) Hypoxia signalling through mTOR and the unfolded protein response in cancer. Nat Rev Cancer 8: 851-864.
29. Porstmann T, Santos CR, Griffiths B, Cully M, Wu M, et al. (2008) SREBP activity is regulated by mTORC1 and contributes to Akt-dependent cell growth. Cell Metab 8: 224-236.
30. Wang BT, Ducker GS, Barczak AJ, Barbeau R, Erle DJ, et al. (2011) The mammalian target of rapamycin regulates cholesterol biosynthetic gene expression and exhibits a rapamycin-resistant transcriptional profile. Proc Natl Acad Sci U S A 108: 15201-15206.

31. Carling D (2004) The AMP-activated protein kinase cascade--a unifying system for energy control. Trends Biochem Sci 29: 18-24.
32. Yuan HX, Xiong Y, Guan KL (2013) Nutrient sensing, metabolism, and cell growth control. Mol Cell 49: 379-387.
33. Inoki K, Zhu T, Guan KL (2003) TSC2 mediates cellular energy response to control cell growth and survival. Cell 115: 577-590.
34. Gwinn DM, Shackelford DB, Egan DF, Mihaylova MM, Mery A, et al. (2008) AMPK phosphorylation of raptor mediates a metabolic checkpoint. Mol Cell 30: 214-226.
35. Barnes K, Ingram JC, Porras OH, Barros LF, Hudson ER, et al. (2002) Activation of GLUT1 by metabolic and osmotic stress: potential involvement of AMP-activated protein kinase (AMPK). J Cell Sci 115: 2433-2442.
36. Kurth-Kraczek EJ, Hirshman MF, Goodyear LJ, Winder WW (1999) 5' AMP-activated protein kinase activation causes GLUT4 translocation in skeletal muscle. Diabetes 48: 1667-1671.
37. Marsin AS, Bertrand L, Rider MH, Deprez J, Beauloye C, et al. (2000) Phosphorylation and activation of heart PFK-2 by AMPK has a role in the stimulation of glycolysis during ischaemia. Curr Biol 10: 1247-1255.
38. Marsin AS, Bouzin C, Bertrand L, Hue L (2002) The stimulation of glycolysis by hypoxia in activated monocytes is mediated by AMP-activated protein kinase and inducible 6-phosphofructo-2-kinase. J Biol Chem 277: 30778-30783.
39. Munday MR, Carling D, Hardie DG (1988) Negative interactions between phosphorylation of acetyl-CoA carboxylase by the cyclic AMP-dependent and AMP-activated protein kinases. FEBS Lett 235: 144-148.
40. Carling D, Zammit VA, Hardie DG (1987) A common bicyclic protein kinase cascade inactivates the regulatory enzymes of fatty acid and cholesterol biosynthesis. FEBS Lett 223: 217-222.
41. Gordan JD, Simon MC (2007) Hypoxia-inducible factors: central regulators of the tumor phenotype. Curr Opin Genet Dev 17: 71-77.
42. Brahimi-Horn MC, Chiche J, Pouyssegur J (2007) Hypoxia signalling controls metabolic demand. Curr Opin Cell Biol 19: 223-229.
43. Semenza GL, Jiang BH, Leung SW, Passantino R, Concordet JP, et al. (1996) Hypoxia response elements in the aldolase A, enolase 1, and lactate dehydrogenase A gene promoters contain essential binding sites for hypoxia-inducible factor 1. J Biol Chem 271: 32529-32537.
44. Semenza GL, Roth PH, Fang HM, Wang GL (1994) Transcriptional regulation of genes encoding glycolytic enzymes by hypoxia-inducible factor 1. J Biol Chem 269: 23757-23763.
45. Gordan JD, Thompson CB, Simon MC (2007) HIF and c-Myc: sibling rivals for control of cancer cell metabolism and proliferation. Cancer Cell 12: 108-113.
46. Kim JW, Tchernyshyov I, Semenza GL, Dang CV (2006) HIF-1-mediated expression of pyruvate dehydrogenase kinase: a metabolic switch required for cellular adaptation to hypoxia. Cell Metab 3: 177-185.

47. Koivunen P, Hirsila M, Remes AM, Hassinen IE, Kivirikko KI, et al. (2007) Inhibition of hypoxia-inducible factor (HIF) hydroxylases by citric acid cycle intermediates: possible links between cell metabolism and stabilization of HIF. J Biol Chem 282: 4524-4532.
48. Selak MA, Armour SM, MacKenzie ED, Boulahbel H, Watson DG, et al. (2005) Succinate links TCA cycle dysfunction to oncogenesis by inhibiting HIF-alpha prolyl hydroxylase. Cancer Cell 7: 77-85.
49. Kim JW, Zeller KI, Wang Y, Jegga AG, Aronow BJ, et al. (2004) Evaluation of myc E-box phylogenetic footprints in glycolytic genes by chromatin immunoprecipitation assays. Mol Cell Biol 24: 5923-5936.
50. Dang CV, Kim JW, Gao P, Yustein J (2008) The interplay between MYC and HIF in cancer. Nat Rev Cancer 8: 51-56.
51. Sloan EJ, Ayer DE (2010) Myc, mondo, and metabolism. Genes Cancer 1: 587-596.
52. Wise DR, DeBerardinis RJ, Mancuso A, Sayed N, Zhang XY, et al. (2008) Myc regulates a transcriptional program that stimulates mitochondrial glutaminolysis and leads to glutamine addiction. Proc Natl Acad Sci U S A 105: 18782-18787.
53. Schwartzenberg-Bar-Yoseph F, Armoni M, Karnieli E (2004) The tumor suppressor p53 down-regulates glucose transporters GLUT1 and GLUT4 gene expression. Cancer Res 64: 2627-2633.
54. Kondoh H, Lleonart ME, Gil J, Wang J, Degan P, et al. (2005) Glycolytic enzymes can modulate cellular life span. Cancer Res 65: 177-185.
55. Hitosugi T, Zhou L, Elf S, Fan J, Kang HB, et al. (2012) Phosphoglycerate mutase 1 coordinates glycolysis and biosynthesis to promote tumor growth. Cancer Cell 22: 585-600.
56. Bensaad K, Tsuruta A, Selak MA, Vidal MN, Nakano K, et al. (2006) TIGAR, a p53-inducible regulator of glycolysis and apoptosis. Cell 126: 107-120.
57. Segel IH (1975) Enzyme kinetics : behavior and analysis of rapid equilibrium and steady state enzyme systems. New York: Wiley.
58. Monod J, Wyman J, Changeux JP (1965) On the Nature of Allosteric Transitions: a Plausible Model. J Mol Biol 12: 88-118.
59. Mosca E, Barcella M, Alfieri R, Bevilacqua A, Canti G, et al. (2012) Systems biology of the metabolic network regulated by the Akt pathway. Biotechnol Adv 30: 131-141.
60. Mosca E, Alfieri R, Maj C, Bevilacqua A, Canti G, et al. (2012) Computational modeling of the metabolic States regulated by the kinase akt. Front Physiol 3: 418.
61. Gambhir A, Zhang C, Europa A, Hu WS (1999) Analysis of the use of fortified medium in continuous culture of mammalian cells. Cytotechnology 31: 243-254.
62. Li H, Durbin R (2009) Fast and accurate short read alignment with Burrowsâ€“Wheeler transform. Bioinformatics 25: 1754-1760.
63. Li H, Handsaker B, Wysoker A, Fennell T, Ruan J, et al. (2009) The Sequence Alignment/Map format and SAMtools. Bioinformatics 25: 2078-2079.

64. McKenna A, Hanna M, Banks E, Sivachenko A, Cibulskis K, et al. (2010) The Genome Analysis Toolkit: a MapReduce framework for analyzing next-generation DNA sequencing data. Genome Res 20: 1297-1303.
65. Bullard JH, Purdom E, Hansen KD, Dudoit S (2010) Evaluation of statistical methods for normalization and differential expression in mRNA-Seq experiments. BMC Bioinformatics 11: 94.
66. Koboldt DC, Zhang Q, Larson DE, Shen D, McLellan MD, et al. (2012) VarScan 2: somatic mutation and copy number alteration discovery in cancer by exome sequencing. Genome Res 22: 568-576.
67. Meacham F, Boffelli D, Dhahbi J, Martin DI, Singer M, et al. (2011) Identification and correction of systematic error in high-throughput sequence data. BMC Bioinformatics 12: 451.
68. Neron B, Menager H, Maufrais C, Joly N, Maupetit J, et al. (2009) Mobyle: a new full web bioinformatics framework. Bioinformatics 25: 3005-3011.
69. Park Y, Subramanian K, Verfaillie CM, Hu WS (2010) Expansion and hepatic differentiation of rat multipotent adult progenitor cells in microcarrier suspension culture. J Biotechnol 150: 131-139.
70. Zhou W, Rehm J, Hu WS (1995) High viable cell concentration fed-batch cultures of hybridoma cells through on-line nutrient feeding. Biotechnol Bioeng 46: 579-587.
71. Warburg O (1956) On the origin of cancer cells. Science 123: 309-314.
72. Folmes CD, Dzeja PP, Nelson TJ, Terzic A (2012) Metabolic plasticity in stem cell homeostasis and differentiation. Cell Stem Cell 11: 596-606.
73. Zhang J, Nuebel E, Daley GQ, Koehler CM, Teitell MA (2012) Metabolic regulation in pluripotent stem cells during reprogramming and self-renewal. Cell Stem Cell 11: 589-595.
74. Folmes CD, Nelson TJ, Martinez-Fernandez A, Arrell DK, Lindor JZ, et al. (2011) Somatic oxidative bioenergetics transitions into pluripotency-dependent glycolysis to facilitate nuclear reprogramming. Cell Metab 14: 264-271.
75. Locasale JW, Cantley LC (2011) Metabolic flux and the regulation of mammalian cell growth. Cell Metab 14: 443-451.
76. Koppenol WH, Bounds PL, Dang CV (2011) Otto Warburg's contributions to current concepts of cancer metabolism. Nat Rev Cancer 11: 325-337.
77. Vander Heiden MG, Cantley LC, Thompson CB (2009) Understanding the Warburg effect: the metabolic requirements of cell proliferation. Science 324: 1029-1033.
78. Mulukutla BC, Khan S, Lange A, Hu WS (2010) Glucose metabolism in mammalian cell culture: new insights for tweaking vintage pathways. Trends Biotechnol 28: 476-484.
79. Wilson JE (2003) Isozymes of mammalian hexokinase: structure, subcellular localization and metabolic function. J Exp Biol 206: 2049-2057.
80. Yamada K, Noguchi T (1999) Nutrient and hormonal regulation of pyruvate kinase gene expression. Biochem J 337 (Pt 1): 1-11.
81. Kretschmer M, Hofmann E (1984) Inhibition of rat liver phosphofructokinase-2 by phosphoenolpyruvate and ADP. Biochem Biophys Res Commun 124: 793-796.

82. Tominaga N, Tsujikawa T, Minami Y, Wu RF, Watanabe F, et al. (1997) Effect of replacement of the amino and the carboxyl termini of rat testis fructose 6-phosphate, 2-kinase:fructose 2,6-bisphosphatase with those of the liver and heart isozymes. Arch Biochem Biophys 347: 275-281.
83. Manes NP, El-Maghrabi MR (2005) The kinase activity of human brain 6-phosphofructo-2-kinase/fructose-2,6-bisphosphatase is regulated via inhibition by phosphoenolpyruvate. Arch Biochem Biophys 438: 125-136.
84. Ward PS, Thompson CB (2012) Metabolic reprogramming: a cancer hallmark even warburg did not anticipate. Cancer Cell 21: 297-308.
85. Kroemer G, Pouyssegur J (2008) Tumor cell metabolism: cancer's Achilles' heel. Cancer Cell 13: 472-482.
86. Levine AJ, Puzio-Kuter AM (2010) The control of the metabolic switch in cancers by oncogenes and tumor suppressor genes. Science 330: 1340-1344.
87. Gottlob K, Majewski N, Kennedy S, Kandel E, Robey RB, et al. (2001) Inhibition of early apoptotic events by Akt/PKB is dependent on the first committed step of glycolysis and mitochondrial hexokinase. Genes Dev 15: 1406-1418.
88. Christofk HR, Vander Heiden MG, Harris MH, Ramanathan A, Gerszten RE, et al. (2008) The M2 splice isoform of pyruvate kinase is important for cancer metabolism and tumour growth. Nature 452: 230-233.
89. Xiong W, Ferrell JE, Jr. (2003) A positive-feedback-based bistable 'memory module' that governs a cell fate decision. Nature 426: 460-465.
90. Yao G, Lee TJ, Mori S, Nevins JR, You L (2008) A bistable Rb-E2F switch underlies the restriction point. Nat Cell Biol 10: 476-482.
91. Thomson M, Gunawardena J (2009) Unlimited multistability in multisite phosphorylation systems. Nature 460: 274-277.
92. Tornheim K, Lowenstein JM (1976) Control of phosphofructokinase from rat skeletal muscle. Effects of fructose diphosphate, AMP, ATP, and citrate. J Biol Chem 251: 7322-7328.
93. Bosca L, Aragon JJ, Sols A (1982) Specific activation by fructose 2,6-bisphosphate and inhibition by P-enolpyruvate of ascites tumor phosphofructokinase. Biochem Biophys Res Commun 106: 486-491.
94. Mulquiney PJ, Kuchel PW (1999) Model of 2,3-bisphosphoglycerate metabolism in the human erythrocyte based on detailed enzyme kinetic equations: equations and parameter refinement. Biochem J 342 Pt 3: 581-596.
95. Albe KR, Butler MH, Wright BE (1990) Cellular concentrations of enzymes and their substrates. J Theor Biol 143: 163-195.
96. Kitajima S, Sakakibara R, Uyeda K (1984) Kinetic studies of fructose 6-phosphate,2-kinase and fructose 2,6-bisphosphatase. J Biol Chem 259: 6896-6903.
97. Kretschmer M, Schellenberger W, Hofmann E (1985) Quasi-stationary concentrations of fructose-2,6-bisphosphate in the phosphofructokinase-2/fructose-2,6-bisphosphatase cycle. Biochem Biophys Res Commun 131: 899-904.
98. Yan L, Yang M, Guo H, Yang L, Wu J, et al. (2013) Single-cell RNA-Seq profiling of human preimplantation embryos and embryonic stem cells. Nat Struct Mol Biol 20: 1131-1139.

99. Cabili MN, Trapnell C, Goff L, Koziol M, Tazon-Vega B, et al. (2011) Integrative annotation of human large intergenic noncoding RNAs reveals global properties and specific subclasses. Genes Dev 25: 1915-1927.
100. Mouse EC, Stamatoyannopoulos JA, Snyder M, Hardison R, Ren B, et al. (2012) An encyclopedia of mouse DNA elements (Mouse ENCODE). Genome Biol 13: 418.
101. Clower CV, Chatterjee D, Wang Z, Cantley LC, Vander Heiden MG, et al. (2010) The alternative splicing repressors hnRNP A1/A2 and PTB influence pyruvate kinase isoform expression and cell metabolism. Proc Natl Acad Sci U S A 107: 1894-1899.
102. David CJ, Chen M, Assanah M, Canoll P, Manley JL (2010) HnRNP proteins controlled by c-Myc deregulate pyruvate kinase mRNA splicing in cancer. Nature 463: 364-368.
103. Zancan P, Sola-Penna M, Furtado CM, Da Silva D (2010) Differential expression of phosphofructokinase-1 isoforms correlates with the glycolytic efficiency of breast cancer cells. Mol Genet Metab 100: 372-378.
104. Moreno-Sanchez R, Marin-Hernandez A, Gallardo-Perez JC, Quezada H, Encalada R, et al. (2012) Phosphofructokinase type 1 kinetics, isoform expression, and gene polymorphisms in cancer cells. J Cell Biochem 113: 1692-1703.
105. Kurata N, Matsushima T, Sugimura T (1972) Multiple forms of phosphofructokinase in rat tissues and rat tumors. Biochem Biophys Res Commun 48: 473-479.
106. Desai S, Ding M, Wang B, Lu Z, Zhao Q, et al. (2013) Tissue-specific isoform switch and DNA hypomethylation of the pyruvate kinase PKM gene in human cancers. Oncotarget URL: http://www.impactjournals.com/oncotarget/index.php?journal=oncotarget&page=article&op=view&path%5B%5D=1159.
107. Marin-Hernandez A, Gallardo-Perez JC, Ralph SJ, Rodriguez-Enriquez S, Moreno-Sanchez R (2009) HIF-1alpha modulates energy metabolism in cancer cells by inducing over-expression of specific glycolytic isoforms. Mini Rev Med Chem 9: 1084-1101.
108. Chesney J (2006) 6-phosphofructo-2-kinase/fructose-2,6-bisphosphatase and tumor cell glycolysis. Curr Opin Clin Nutr Metab Care 9: 535-539.
109. Gui DY, Lewis CA, Vander Heiden MG (2013) Allosteric regulation of PKM2 allows cellular adaptation to different physiological states. Sci Signal 6: pe7.
110. Cairns RA, Harris IS, Mak TW (2011) Regulation of cancer cell metabolism. Nat Rev Cancer 11: 85-95.
111. Zhou W, Rehm J, Europa A, Hu WS (1997) Alteration of mammalian cell metabolism by dynamic nutrient feeding. Cytotechnology 24: 99-108.
112. Mulukutla BC, Yongky A, Doutidis P, Hu WS (2014) Bistability in glycolysis pathway as a physiological switch in energy metabolism. PLoS One Accepted.
113. Leite TC, Coelho RG, Da Silva D, Coelho WS, Marinho-Carvalho MM, et al. (2011) Lactate downregulates the glycolytic enzymes hexokinase and phosphofructokinase in diverse tissues from mice. FEBS Lett 585: 92-98.

114. Costa Leite T, Da Silva D, Guimaraes Coelho R, Zancan P, Sola-Penna M (2007) Lactate favours the dissociation of skeletal muscle 6-phosphofructo-1-kinase tetramers down-regulating the enzyme and muscle glycolysis. Biochem J 408: 123-130.
115. Gambhir A, Europa AF, Hu WS (1999) Alteration of cellular metabolism by consecutive fed-batch cultures of mammalian cells. J Biosci Bioeng 87: 805-810.
116. Europa AF, Gambhir A, Fu PC, Hu WS (2000) Multiple steady states with distinct cellular metabolism in continuous culture of mammalian cells. Biotechnol Bioeng 67: 25-34.
117. Gambhir A, Korke R, Lee J, Fu PC, Europa A, et al. (2003) Analysis of cellular metabolism of hybridoma cells at distinct physiological states. J Biosci Bioeng 95: 317-327.
118. Hiller GW, Aeschlimann AD, Clark DS, Blanch HW (1991) A kinetic analysis of hybridoma growth and metabolism in continuous suspension culture on serum-free medium. Biotechnol Bioeng 38: 733-741.
119. Kurokawa HO, T.; Kamihira, M.; Park, Y.S.; Iijima, S.; Kobayashi, T. (1993) Kinetic Study of Hybridoma Metabolism and Antibody Production in Continuous Culture Using Serum-Free Medium. Journal of Fermentation and Bioengineering 76: 128-133.
120. Miller WM, Blanch HW, Wilke CR (1988) A kinetic analysis of hybridoma growth and metabolism in batch and continuous suspension culture: effect of nutrient concentration, dilution rate, and pH. Biotechnol Bioeng 32: 947-965.
121. Miller WM, Wilke CR, Blanch HW (1987) Effects of dissolved oxygen concentration on hybridoma growth and metabolism in continuous culture. J Cell Physiol 132: 524-530.
122. Miller WM, Wilke CR, Blanch HW (1989) The transient responses of hybridoma cells to nutrient additions in continuous culture: II. Glutamine pulse and step changes. Biotechnol Bioeng 33: 487-499.
123. Miller WM, Wilke CR, Blanch HW (1989) Transient responses of hybridoma cells to nutrient additions in continuous culture: I. Glucose pulse and step changes. Biotechnol Bioeng 33: 477-486.
124. Miller WMW, C.R.; Blanch, H.W. (1988) Transient responses of hybridoma cells to lactate and ammonia pulse and step changes in continuous culture. Bioprocess Engineering 3: 113-122.
125. Miller WMW, C.R.; Blanch, H.W. (1988) Transient responses of hybridoma metabolism to changes in the oxygen supply rate in continuous culture. Bioprocess Engineering 3: 103-111.
126. Frame KK, Hu WS (1991) Kinetic study of hybridoma cell growth in continuous culture: II. Behavior of producers and comparison to nonproducers. Biotechnol Bioeng 38: 1020-1028.
127. Frame KK, Hu WS (1991) Kinetic study of hybridoma cell growth in continuous culture. I. A model for non-producing cells. Biotechnol Bioeng 37: 55-64.
128. Hu WS, Dodge TC, Frame KK, Himes VB (1987) Effect of glucose on the cultivation of mammalian cells. Dev Biol Stand 66: 279-290.

129. Omasa T, Higashiyama K, Shioya S, Suga K (1992) Effects of lactate concentration on hybridoma culture in lactate-controlled fed-batch operation. Biotechnol Bioeng 39: 556-564.
130. Doyle C, Butler M (1990) The effect of pH on the toxicity of ammonia to a murine hybridoma. J Biotechnol 15: 91-100.
131. Glacken MW, Fleischaker RJ, Sinskey AJ (1986) Reduction of waste product excretion via nutrient control: Possible strategies for maximizing product and cell yields on serum in cultures of mammalian cells. Biotechnol Bioeng 28: 1376-1389.
132. Ozturk SS, Riley MR, Palsson BO (1992) Effects of ammonia and lactate on hybridoma growth, metabolism, and antibody production. Biotechnol Bioeng 39: 418-431.
133. Ryll T, Dutina G, Reyes A, Gunson J, Krummen L, et al. (2000) Performance of small-scale CHO perfusion cultures using an acoustic cell filtration device for cell retention: characterization of separation efficiency and impact of perfusion on product quality. Biotechnol Bioeng 69: 440-449.
134. Tang YJ, Ohashi R, Hamel JF (2007) Perfusion culture of hybridoma cells for hyperproduction of IgG(2a) monoclonal antibody in a wave bioreactor-perfusion culture system. Biotechnol Prog 23: 255-264.
135. Mercille S, Johnson M, Lanthier S, Kamen AA, Massie B (2000) Understanding factors that limit the productivity of suspension-based perfusion cultures operated at high medium renewal rates. Biotechnol Bioeng 67: 435-450.
136. Deo YM, Mahadevan MD, Fuchs R (1996) Practical considerations in operation and scale-up of spin-filter based bioreactors for monoclonal antibody production. Biotechnol Prog 12: 57-64.
137. Yabannavar VM, Singh V, Connelly NV (1992) Mammalian cell retention in a spinfilter perfusion bioreactor. Biotechnol Bioeng 40: 925-933.
138. Takamatsu H, Hamamoto K, Ishimaru K, Yokoyama S, Tokashiki M (1996) Large-scale perfusion culture process for suspended mammalian cells that uses a centrifuge with multiple settling zones. Appl Microbiol Biotechnol 45: 454-457.
139. Tokashiki M, Arai T, Hamamoto K, Ishimaru K (1990) High density culture of hybridoma cells using a perfusion culture vessel with an external centrifuge. Cytotechnology 3: 239-244.
140. Arai T, Yokoyama S, Tokashiki M (1993) 50 L scale perfusion culture of hybridoma cells by gravitational settling for cell separation. Dordnecht: Kluwer Academic Publisher.
141. Tokashiki M, Takamatsu H (1993) Perfusion culture apparatus for suspended mammalian cells. Cytotechnology 13: 149-159.
142. Castillo FJ, Mullen LJ, Thrift JC, Grant BC (1992) Perfusion cultures of hybridoma cells for monoclonal antibody production. Ann N Y Acad Sci 665: 72-80.
143. Kyung YS, Peshwa MV, Gryte DM, Hu WS (1994) High density culture of mammalian cells with dynamic perfusion based on on-line oxygen uptake rate measurements. Cytotechnology 14: 183-190.

144. Doblhoff-Dier O, Gaida T, Katinger H, Burger W, Groschl M, et al. (1994) A novel ultrasonic resonance field device for the retention of animal cells. Biotechnol Prog 10: 428-432.
145. Trampler F, Sonderhoff SA, Pui PW, Kilburn DG, Piret JM (1994) Acoustic cell filter for high density perfusion culture of hybridoma cells. Biotechnology (N Y) 12: 281-284.
146. Kawahara H, Mitsuda S, Kumazawa E, Takeshita Y (1994) High-density culture of FM-3A cells using a bioreactor with an external tangential-flow filtration device. Cytotechnology 14: 61-66.
147. de la Broise D, Noiseux M, Massie B, Lemieux R (1992) Hybridoma perfusion systems: a comparison study. Biotechnol Bioeng 40: 25-32.
148. de la Broise D, Noiseux M, Lemieux R, Massie B (1991) Long-term perfusion culture of hybridoma: a "grow or die" cell cycle system. Biotechnol Bioeng 38: 781-787.
149. Clincke MF, Molleryd C, Zhang Y, Lindskog E, Walsh K, et al. (2013) Very high density of CHO cells in perfusion by ATF or TFF in WAVE bioreactor. Part I. Effect of the cell density on the process. Biotechnol Prog 29: 754-767.
150. Genzel Y, Vogel T, Buck J, Behrendt I, Ramirez DV, et al. (2014) High cell density cultivations by alternating tangential flow (ATF) perfusion for influenza A virus production using suspension cells. Vaccine 32: 2770-2781.
151. Follstad BD, Balcarcel RR, Stephanopoulos G, Wang DI (1999) Metabolic flux analysis of hybridoma continuous culture steady state multiplicity. Biotechnol Bioeng 63: 675-683.
152. Altamirano C, Illanes A, Casablancas A, Gamez X, Cairo JJ, et al. (2001) Analysis of CHO cells metabolic redistribution in a glutamate-based defined medium in continuous culture. Biotechnol Prog 17: 1032-1041.
153. Mulukutla BC, Yongky A, Daoutidis P, Hu WS (2014) Bistability in glycolysis pathway as a physiological switch in energy metabolism. PLoS One 9: e98756.
154. Bonham-Carter J, Shevitz J (2011) A Brief History of Perfusion Biomanufacturing. BioProcess International 9: 24-30.
155. Borys MC, Linzer DI, Papoutsakis ET (1994) Ammonia affects the glycosylation patterns of recombinant mouse placental lactogen-I by chinese hamster ovary cells in a pH-dependent manner. Biotechnol Bioeng 43: 505-514.
156. Butler M (2006) Optimisation of the cellular metabolism of glycosylation for recombinant proteins produced by Mammalian cell systems. Cytotechnology 50: 57-76.
157. Hayter PM, Curling EM, Gould ML, Baines AJ, Jenkins N, et al. (1993) The effect of the dilution rate on CHO cell physiology and recombinant interferon-gamma production in glucose-limited chemostat culture. Biotechnol Bioeng 42: 1077-1085.
158. Muthing J, Kemminer SE, Conradt HS, Sagi D, Nimtz M, et al. (2003) Effects of buffering conditions and culture pH on production rates and glycosylation of clinical phase I anti-melanoma mouse IgG3 monoclonal antibody R24. Biotechnol Bioeng 83: 321-334.

159. Korke R, Gatti Mde L, Lau AL, Lim JW, Seow TK, et al. (2004) Large scale gene expression profiling of metabolic shift of mammalian cells in culture. J Biotechnol 107: 1-17.
160. Seth G, Philp RJ, Lau A, Jiun KY, Yap M, et al. (2007) Molecular portrait of high productivity in recombinant NS0 cells. Biotechnol Bioeng 97: 933-951.
161. Baik JY, Lee MS, An SR, Yoon SK, Joo EJ, et al. (2006) Initial transcriptome and proteome analyses of low culture temperature-induced expression in CHO cells producing erythropoietin. Biotechnol Bioeng 93: 361-371.
162. Yee JC, de Leon Gatti M, Philp RJ, Yap M, Hu WS (2008) Genomic and proteomic exploration of CHO and hybridoma cells under sodium butyrate treatment. Biotechnol Bioeng 99: 1186-1204.
163. Rupp O, Becker J, Brinkrolf K, Timmermann C, Borth N, et al. (2014) Construction of a Public CHO Cell Line Transcript Database Using Versatile Bioinformatics Analysis Pipelines. PLoS One 9: e85568.
164. Becker J, Hackl M, Rupp O, Jakobi T, Schneider J, et al. (2011) Unraveling the Chinese hamster ovary cell line transcriptome by next-generation sequencing. J Biotechnol 156: 227-235.
165. Birzele F, Schaub J, Rust W, Clemens C, Baum P, et al. (2010) Into the unknown: expression profiling without genome sequence information in CHO by next generation sequencing. Nucleic Acids Res 38: 3999-4010.
166. Johnson KC, Yongky A, Vishwanathan N, Jacob NM, Jayapal KP, et al. (2013) Exploring the transcriptome space of a recombinant BHK cell line through next generation sequencing. Biotechnol Bioeng.
167. Farrell A, McLoughlin N, Milne JJ, Marison IW, Bones J (2014) Application of multi-omics techniques for bioprocess design and optimization in chinese hamster ovary cells. J Proteome Res 13: 3144-3159.
168. Kildegaard HF, Baycin-Hizal D, Lewis NE, Betenbaugh MJ (2013) The emerging CHO systems biology era: harnessing the 'omics revolution for biotechnology. Curr Opin Biotechnol 24: 1102-1107.
169. Tijo JH, Puck TT (1958) Genetics of Somatic Mammalian Cells II. Chromosomal Constitution of Cells in Tissue Culture. Journal of Experimental Medicine: 259-271.
170. Puck TT, Cieciura SJ, Robinson A (1958) Genetics of Somatic Mammalian Cell III. Long-Term Cultivation of Euploid Cells from Human and Animal Subjects. Journal of Experimental Medicine: 945-959.
171. Goldman RD, Kaplan NO, Hall TC (1964) Lactic Dehydrogenase in Human Neoplastic Tissues. Cancer Res 24: 389-399.
172. Luo J, Vijayasankaran N, Autsen J, Santuray R, Hudson T, et al. (2012) Comparative metabolite analysis to understand lactate metabolism shift in Chinese hamster ovary cell culture process. Biotechnol Bioeng 109: 146-156.
173. Xu X, Nagarajan H, Lewis NE, Pan S, Cai Z, et al. (2011) The genomic sequence of the Chinese hamster ovary (CHO)-K1 cell line. Nat Biotechnol 29: 735-741.

174. Lewis NE, Liu X, Li Y, Nagarajan H, Yerganian G, et al. (2013) Genomic landscapes of Chinese hamster ovary cell lines as revealed by the Cricetulus griseus draft genome. Nat Biotechnol 31: 759-765.
175. Guo D, Gao A, Michels DA, Feeney L, Eng M, et al. (2010) Mechanisms of unintended amino acid sequence changes in recombinant monoclonal antibodies expressed in Chinese Hamster Ovary (CHO) cells. Biotechnol Bioeng 107: 163-171.
176. Harris RJ, Murnane AA, Utter SL, Wagner KL, Cox ET, et al. (1993) Assessing genetic heterogeneity in production cell lines: detection by peptide mapping of a low level Tyr to Gln sequence variant in a recombinant antibody. Biotechnology (N Y) 11: 1293-1297.
177. Fornaini G, Magnani M, Fazi A, Accorsi A, Stocchi V, et al. (1985) Regulatory properties of human erythrocyte hexokinase during cell ageing. Arch Biochem Biophys 239: 352-358.
178. Gerber G, Preissler H, Heinrich R, Rapoport SM (1974) Hexokinase of human erythrocytes. Purification, kinetic model and its application to the conditions in the cell. Eur J Biochem 45: 39-52.
179. Magnani M, Stocchi V, Ninfali P, Dacha M, Fornaini G (1980) Action of oxidized and reduced glutathione on rabbit red blood cell hexokinase. Biochim Biophys Acta 615: 113-120.
180. Rijksen G, Jansen G, Kraaijenhagen RJ, Van der Vlist MJ, Vlug AM, et al. (1981) Separation and characterization of hexokinase I subtypes from human erythrocytes. Biochim Biophys Acta 659: 292-301.
181. Rijksen G, Staal GE (1977) Regulation of human erythrocyte hexokinase. The influence of glycolytic intermediates and inorganic phosphate. Biochim Biophys Acta 485: 75-86.
182. Gracy RW, Tilley BE (1975) Phosphoglucose isomerase of human erythrocytes and cardiac tissue. Methods Enzymol 41: 392-400.
183. Kahana SE, Lowry OH, Schulz DW, Passonneau JV, Crawford EJ (1960) The kinetics of phosphoglucoisomerase. J Biol Chem 235: 2178-2184.
184. Tilley BE, Gracy RW, Welch SG (1974) A point mutation increasing the stability of human phosphoglucose isomerase. J Biol Chem 249: 4751-4759.
185. Dunaway GA, Kasten TP, Sebo T, Trapp R (1988) Analysis of the phosphofructokinase subunits and isoenzymes in human tissues. Biochem J 251: 677-683.
186. Hanson RL, Rudolph FB, Lardy HA (1973) Rabbit muscle phosphofructokinase. The kinetic mechanism of action and the equilibrium constant. J Biol Chem 248: 7852-7859.
187. Merry S, Britton HG (1985) The mechanism of rabbit muscle phosphofructokinase at pH8. Biochem J 226: 13-28.
188. Otto M, Heinrich R, Jacobasch G, Rapoport S (1977) A mathematical model for the influence of anionic effectors on the phosphofructokinase from rat erythrocytes. Eur J Biochem 74: 413-420.

189. Otto M, Heinrich R, Kuhn B, Jacobasch G (1974) A mathematical model for the influence of fructose 6-phosphate, ATP, potassium, ammonium and magnesium on the phosphofructokinase from rat erythrocytes. Eur J Biochem 49: 169-178.
190. Beutler E (1971) 2,3-diphosphoglycerate affects enzymes of glucose metabolism in red blood cells. Nat New Biol 232: 20-21.
191. Beutler E (1984) Red Cell Metabolism: A Manual of Biochemical Methods. New York: Grune and Stratton.
192. Mehler AH (1963) Kinetic properties of native and carboxy-peptidase-altered rabbit muscle aldolase. J Biol Chem 238: 100-104.
193. Mehler AH, Bloom B (1963) Interaction between rabbit muscle aldolase and dihydroxyacetone phosphate. J Biol Chem 238: 105-107.
194. Penhoet EE, Kochman M, Rutter WJ (1969) Ioslation of fructose diphosphate aldolases A, B, and C. Biochemistry 8: 4391-4395.
195. Penhoet EE, Kochman M, Rutter WJ (1969) Molecular and catalytic properties of aldolase C. Biochemistry 8: 4396-4402.
196. Rose IA, O'Connell EL, Mehler AH (1965) Mechanism of the Aldolase Reaction. J Biol Chem 240: 1758-1765.
197. Srivastava SK, Beutler E (1972) The effect of normal red cell constituents on the activities of red cell enzymes. Arch Biochem Biophys 148: 249-255.
198. Strapazon E, Steck TL (1977) Interaction of the aldolase and the membrane of human erythrocytes. Biochemistry 16: 2966-2971.
199. Yeltman DR, Harris BG (1977) Purification and characterization of aldolase from human erythrocytes. Biochim Biophys Acta 484: 188-198.
200. Gracy RW (1975) Triosephosphate isomerase from human erythrocytes. Methods Enzymol 41: 442-447.
201. Sawyer TH, Tilley BE, Gracy RW (1972) Studies on human triosephosphate isomerase. II. Nature of the electrophoretic multiplicity in erythrocytes. J Biol Chem 247: 6499-6505.
202. Schneider AS, Valentine WN, Hattori M, Heins HL, Jr. (1965) Hereditary Hemolytic Anemia with Triosephosphate Isomerase Deficiency. N Engl J Med 272: 229-235.
203. Cori CF, Velick SF, Cori GT (1950) The combination of diphosphopyridine nucleotide with glyceraldehyde phosphate dehydrogenase. Biochim Biophys Acta 4: 160-169.
204. Furfine CS, Velick SF (1965) The Acyl-Enzyme Intermediate and the Kinetic Mechanism of the Glyceraldehyde 3-Phosphate Dehydrogenase Reaction. J Biol Chem 240: 844-855.
205. Heinz F, Freimuller B (1982) Glyceraldehyde-3-phosphate dehydrogenase from human tissues. Methods Enzymol 89 Pt D: 301-305.
206. Wang CS, Alaupovic P (1980) Glyceraldehyde-3-phosphate dehydrogenase from human erythrocyte membranes. Kinetic mechanism and competitive substrate inhibition by glyceraldehyde 3-phosphate. Arch Biochem Biophys 205: 136-145.
207. Ali M, Brownstone YS (1976) A study of phosphoglycerate kinase in human erythrocytes. II. Kinetic properties. Biochim Biophys Acta 445: 89-103.

208. Krietsch WK, Bucher T (1970) 3-phosphoglycerate kinase from rabbit sceletal muscle and yeast. Eur J Biochem 17: 568-580.
209. Lee CS, O'Sullivan WJ (1975) Properties and mechanism of human erythrocyte phosphoglycerate kinase. J Biol Chem 250: 1275-1281.
210. Yoshida A, Watanabe S (1972) Human phosphoglycerate kinase. I. Crystallization and characterization of normal enzyme. J Biol Chem 247: 440-445.
211. Mulquiney PJ, Bubb WA, Kuchel PW (1999) Model of 2,3-bisphosphoglycerate metabolism in the human erythrocyte based on detailed enzyme kinetic equations: in vivo kinetic characterization of 2,3-bisphosphoglycerate synthase/phosphatase using 13C and 31P NMR. Biochem J 342 Pt 3: 567-580.
212. Mulquiney PJ, Kuchel PW (1999) Model of 2,3-bisphosphoglycerate metabolism in the human erythrocyte based on detailed enzyme kinetic equations: computer simulation and metabolic control analysis. Biochem J 342 Pt 3: 597-604.
213. Garfinkel L, Garfinkel D (1985) Magnesium regulation of the glycolytic pathway and the enzymes involved. Magnesium 4: 60-72.
214. Rider CC, Taylor CB (1974) Enolase isoenzymes in rat tissues. Electrophoretic, chromatographic, immunological and kinetic properties. Biochim Biophys Acta 365: 285-300.
215. Wold F, Ballou CE (1957) Studies on the enzyme enolase. I. Equilibrium studies. J Biol Chem 227: 301-312.
216. Holzhutter HG, Jacobasch G, Bisdorff A (1985) Mathematical modelling of metabolic pathways affected by an enzyme deficiency. A mathematical model of glycolysis in normal and pyruvate-kinase-deficient red blood cells. Eur J Biochem 149: 101-111.
217. Kahn A, Marie J (1982) Pyruvate kinases from human erythrocytes and liver. Methods Enzymol 90 Pt E: 131-140.
218. Koster JF, Slee RG, Staal GE, van Berkel TJ (1972) The influence of glucose I,6-diphosphate on the enzymatic activity of pyruvate kinase. Biochim Biophys Acta 258: 763-768.
219. Mc QJ, Utter MF (1959) Equilibrium and kinetic studies of the pyruvic kinase reaction. J Biol Chem 234: 2151-2157.
220. Rozengurt E, Jimenez de Asua L, Carminatti H (1969) Some kinetic properties of liver pyruvate kinase (type L). II. Effect of pH on its allosteric behavior. J Biol Chem 244: 3142-3147.
221. Borgmann U, Moon TW, Laidler KJ (1974) Molecular kinetics of beef heart lactate dehydrogenase. Biochemistry 13: 5152-5158.
222. Wang CS (1977) Inhibition of human erythrocyte lactate dehydrogenase by high concentrations of pyruvate. Evidence for the competitive substrate inhibition. Eur J Biochem 78: 569-574.
223. Zewe V, Fromm HJ (1965) Kinetic Studies of Rabbit Muscle Lactate Dehydrogenase. Ii. Mechanism of the Reaction. Biochemistry 4: 782-792.
224. Kanji MI, Toews ML, Carper WR (1976) A kinetic study of glucose-6-phosphate dehydrogenase. J Biol Chem 251: 2258-2262.

225. Thorburn DR, Kuchel PW (1985) Regulation of the human-erythrocyte hexose-monophosphate shunt under conditions of oxidative stress. A study using NMR spectroscopy, a kinetic isotope effect, a reconstituted system and computer simulation. Eur J Biochem 150: 371-386.
226. Kirkman HN, Wilson WG, Clemons EH (1980) Regulation of glucose-6-phosphate dehydrogenase. I. Intact red cells. J Lab Clin Med 95: 877-887.
227. Glaser L, Brown DH (1955) Purification and properties of d-glucose-6-phosphate dehydrogenase. J Biol Chem 216: 67-79.
228. Villet RH, Dalziel K (1972) Studies of 6-phosphogluconate dehydrogenase from sheep liver. 2. Kinetics of the oxidative-decarboxylation reaction, coenzyme binding and analyses for metals. Eur J Biochem 27: 251-258.
229. Pearse BM, Rosemeyer MA (1974) Human 6-phosphogluconate dehydrogenase. Purification of the erythrocyte enzyme and the influence of ions and NADPH on its activity. Eur J Biochem 42: 213-223.
230. Villet RH, Dalziel K (1969) The nature of the carbon dioxide substrate and equilibrium constant of the 6-phosphogluconate dehydrogenase reaction. Biochem J 115: 633-638.
231. McIntyre LM, Thorburn DR, Bubb WA, Kuchel PW (1989) Comparison of computer simulations of the F-type and L-type non-oxidative hexose monophosphate shunts with 31P-NMR experimental data from human erythrocytes. Eur J Biochem 180: 399-420.
232. Casazza JP, Veech RL (1986) The interdependence of glycolytic and pentose cycle intermediates in ad libitum fed rats. J Biol Chem 261: 690-698.
233. Wood T (1979) Purification and properties of D-ribulose-5-phosphate 3-epimerase from calf liver. Biochim Biophys Acta 570: 352-362.
234. Horecker BL, Hurwitz J (1956) The purification of phosphoketopentoepimerase from Lactobacillus pentosus and the preparation of xylulose 5-phosphate. J Biol Chem 223: 993-1008.
235. Urivetzky M, Tsuboi KK (1963) Enzymes of the Human Erythrocyte. V. Pentose Phosphate Isomerase, Purification and Properties. Arch Biochem Biophys 103: 1-8.
236. Kiely ME, Stuart AL, Wood T (1973) Partial purification and kinetic properties of ribose-5-phosphate ketol-isomerase and ribulose-5-phosphate 3-epimerase from various sources. Biochim Biophys Acta 293: 534-541.
237. Joshi A, Palsson BO (1990) Metabolic dynamics in the human red cell. Part III--Metabolic reaction rates. J Theor Biol 142: 41-68.
238. Warnock LG, Prudhomme CR (1982) The isolation and preliminary characterization of apotransketolase from human erythrocytes. Biochem Biophys Res Commun 106: 719-723.
239. Venkataraman R, Racker E (1961) Mechanism of action of transaldolase. II. The substrate-enzyme intermediate. J Biol Chem 236: 1883-1886.
240. Horecker BL, Smyrniotis PZ (1955) Purification and properties of yeast transaldolase. J Biol Chem 212: 811-825.

241. Kuhn E, Brand K (1972) Purification and properties of transaldolase from bovine mammary gland. Biochemistry 11: 1767-1772.
242. Datta AG, Racker E (1961) Mechanism of action of transketolase. I. Properties of the crystalline yeast enzyme. J Biol Chem 236: 617-623.
243. Mannervik B (1973) A branching reaction mechanism of glutathione reductase. Biochem Biophys Res Commun 53: 1151-1158.
244. Worthington DJ, Rosemeyer MA (1976) Glutathione reductase from human erythrocytes. Catalytic properties and aggregation. Eur J Biochem 67: 231-238.
245. Scott EM, Duncan IW, Ekstrand V (1963) Purification and Properties of Glutathione Reductase of Human Erythrocytes. J Biol Chem 238: 3928-3933.
246. Wu F, Yang F, Vinnakota KC, Beard DA (2007) Computer modeling of mitochondrial tricarboxylic acid cycle, oxidative phosphorylation, metabolite transport, and electrophysiology. J Biol Chem 282: 24525-24537.
247. Kohn MC, Achs MJ, Garfinkel D (1979) Computer simulation of metabolism in pyruvate-perfused rat heart. III. Pyruvate dehydrogenase. Am J Physiol 237: R167-173.
248. Tsai CS, Burgett MW, Reed LJ (1973) Alpha-keto acid dehydrogenase complexes. XX. A kinetic study of the pyruvate dehydrogenase complex from bovine kidney. J Biol Chem 248: 8348-8352.
249. Kohn MC, Achs MJ, Garfinkel D (1979) Computer simulation of metabolism in pyruvate-perfused rat heart. II. Krebs cycle. Am J Physiol 237: R159-166.
250. Kohn MC, Garfinkel D (1983) Computer simulation of metabolism in palmitate-perfused rat heart. II. Behavior of complete model. Ann Biomed Eng 11: 511-531.
251. Shepherd D, Garland PB (1969) The kinetic properties of citrate synthase from rat liver mitochondria. Biochem J 114: 597-610.
252. Smith CM, Williamson JR (1971) Inhibition of citrate synthase by succinyl-CoA and other metabolites. FEBS Lett 18: 35-38.
253. Thomson JF, Nance SL, Bush KJ, Szczepanik PA (1966) Isotope and solvent effects of deuterium on aconitase. Arch Biochem Biophys 117: 65-74.
254. Denton RM, Richards DA, Chin JG (1978) Calcium ions and the regulation of NAD+-linked isocitrate dehydrogenase from the mitochondria of rat heart and other tissues. Biochem J 176: 899-906.
255. Plaut GW, Cheung CP, Suhadolnik RJ, Aogaichi T (1979) Cosubstrate and allosteric modifier activities of structural analogues of NAD and ADP for NAD-specific isocitrate dehydrogenase from bovine heart. Biochemistry 18: 3430-3438.
256. Williamson JR, Safer B, LaNoue KF, Smith CM, Walajtys E (1973) Mitochondrial-cytosolic interactions in cardiac tissue: role of the malate-aspartate cycle in the removal of glycolytic NADH from the cytosol. Symp Soc Exp Biol 27: 241-281.
257. Smith CM, Bryla J, Williamson JR (1974) Regulation of mitochondrial alpha-ketoglutarate metabolism by product inhibition at alpha-ketoglutarate dehydrogenase. J Biol Chem 249: 1497-1505.
258. Cha S, Parks RE, Jr. (1964) Succinic Thiokinase. Ii. Kinetic Studies: Initial Velocity, Product Inhibition, and Effect of Arsenate. J Biol Chem 239: 1968-1977.

259. Barman TE (1969) Enzyme Handbook. New York: Springer-Verlag.
260. Gutman M (1977) Regulation of mitochondrial succinate dehydrogenase by substrate type activators. Biochemistry 16: 3067-3072.
261. Hatefi Y, Stiggall DL (1976) Metal-containing flavoprotein dehydrogenases. In: Boyer PD, editor. The Enzymes. New York: Academic Press. pp. 175-297.
262. Brant DA, Barnett LB, Alberty RA (1963) The temperature dependence of the steady state kinetic parameters of the fumarase reaction. J Am Chem Soc 85: 2204-2209.
263. Penner PE, Cohen LH (1969) Effects of adenosine triphosphate and magnesium ions on the fumarase reaction. J Biol Chem 244: 1070-1075.
264. Kimball DF, Peterson L, McLoughlin DJ, Wolfe RG (1979) Malate dehydrogenase. Kinetic studies with meso-tartrate and 2-keto-3-hydroxysuccinate, comparison of the mitochondrial and supernatant pig heart enzymes. Arch Biochem Biophys 195: 66-73.
265. Oza NB, Shore JD (1973) The effects of adenine nucleotides on NADH binding to mitochondrial malate dehydrogenase. Arch Biochem Biophys 154: 360-365.
266. Henson CP, Cleland WW (1964) Kinetic Studies of Glutamic Oxaloacetic Transaminase Isozymes. Biochemistry 3: 338-345.
267. Crow KE, Braggins TJ, Batt RD, Hardman MJ (1982) Rat liver cytosolic malate dehydrogenase: purification, kinetic properties, role in control of free cytosolic NADH concentration. Analysis of control of ethanol metabolism using computer simulation. J Biol Chem 257: 14217-14225.
268. Indiveri C, Dierks T, Kramer R, Palmieri F (1991) Reaction mechanism of the reconstituted oxoglutarate carrier from bovine heart mitochondria. Eur J Biochem 198: 339-347.
269. Dierks T, Riemer E, Kramer R (1988) Reaction mechanism of the reconstituted aspartate/glutamate carrier from bovine heart mitochondria. Biochim Biophys Acta 943: 231-244.
270. Uldry M, Thorens B (2004) The SLC2 family of facilitated hexose and polyol transporters. Pflugers Arch 447: 480-489.
271. Haser WG, Shapiro RA, Curthoys NP (1985) Comparison of the phosphate-dependent glutaminase obtained from rat brain and kidney. Biochem J 229: 399-408.
272. Rife JE, Cleland WW (1980) Kinetic mechanism of glutamate dehydrogenase. Biochemistry 19: 2321-2328.
273. Frieden C (1959) Glutamic dehydrogenase. III. The order of substrate addition in the enzymatic reaction. J Biol Chem 234: 2891-2896.
274. Houston B, Nimmo HG (1985) Effects of phosphorylation on the kinetic properties of rat liver ATP-citrate lyase. Biochim Biophys Acta 844: 233-239.
275. Plowman DM, Cleland WW (1967) Purification and kinetic studies of the citrate cleavage enzyme. J Biol Chem 242: 4239-4247.
276. Ranganathan NS, Srere PA, Linn TC (1980) Comparison of phospho- and dephospho-ATP citrate lyase. Arch Biochem Biophys 204: 52-58.

277. Houston B, Nimmo HG (1984) Purification and some kinetic properties of rat liver ATP citrate lyase. Biochem J 224: 437-443.
278. Teller JK, Fahien LA, Davis JW (1992) Kinetics and regulation of hepatoma mitochondrial NAD(P) malic enzyme. J Biol Chem 267: 10423-10432.
279. Hsu RY, Lardy HA, Cleland WW (1967) Pigeon liver malic enzyme. V. Kinetic studies. J Biol Chem 242: 5315-5322.
280. Bulos B, Handler P (1965) Kinetics of Beef Heart Glutamic-Alanine Transaminase. J Biol Chem 240: 3283-3294.
281. Jitrapakdee S, Walker ME, Wallace JC (1999) Functional expression, purification, and characterization of recombinant human pyruvate carboxylase. Biochem Biophys Res Commun 266: 512-517.
282. Halestrap AP, Meredith D (2004) The SLC16 gene family-from monocarboxylate transporters (MCTs) to aromatic amino acid transporters and beyond. Pflugers Arch 447: 619-628.
283. Juel C, Halestrap AP (1999) Lactate transport in skeletal muscle - role and regulation of the monocarboxylate transporter. J Physiol 517 (Pt 3): 633-642.

Chapter 10 Appendix

10.1 Appendix Figures

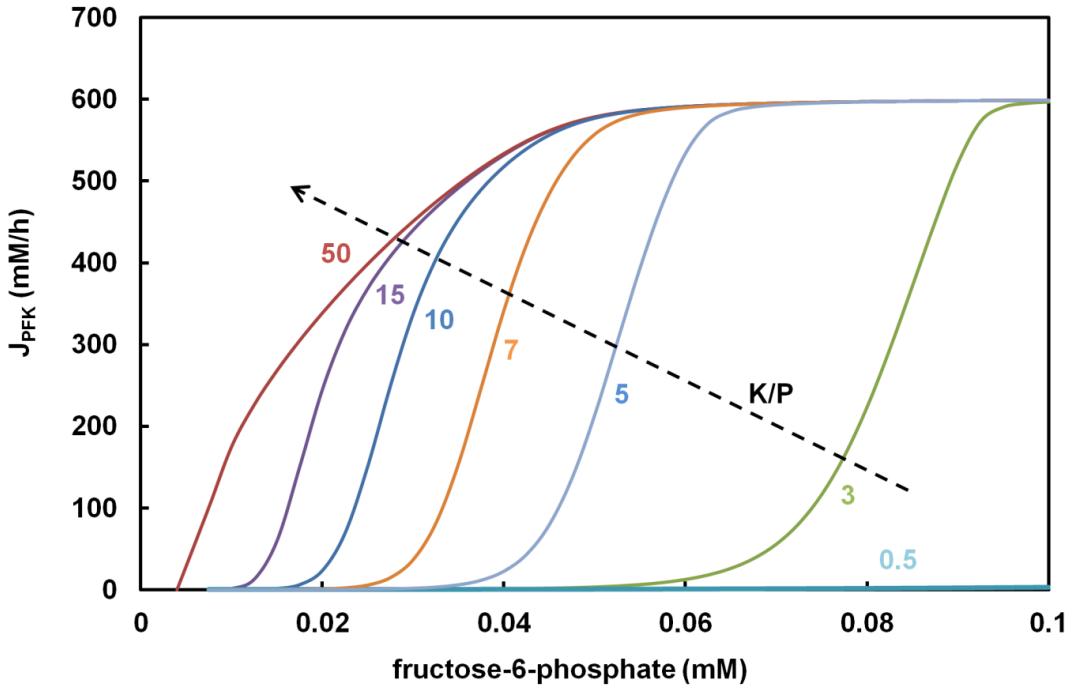

Appendix Figure 1: Steady state behavior of F6P-node with PFKP as the sole PFK isozyme expressed. F6P-node was simulated using PFKP as the sole PFK isozyme, at different K/P ratios (range: 0.5-50). In all the cases, the steady state flux of the system (J_{PFK}) followed the Michaelis-Menten type of kinetics. No multiplicity of states was observed in the range of K/P simulated.

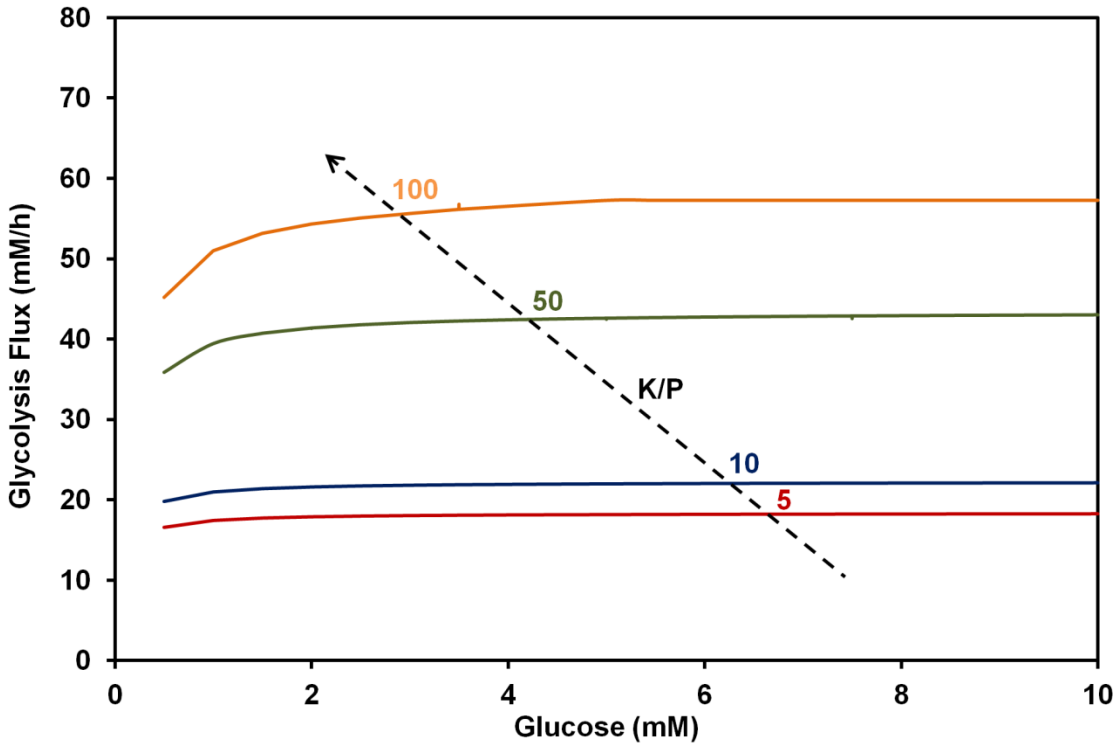

Appendix Figure 2: Steady state behavior of the glycolysis flux with no loop active and with PFKP as the sole PFK isozyme expressed. The steady state glycolysis flux was simulated using PFKP as the sole PFK isozyme, at different K/P ratios (range: 5-100). In all the cases, the steady state flux followed the Michaelis-Menten type of kinetics. No multiplicity of states was observed in the range of K/P simulated.

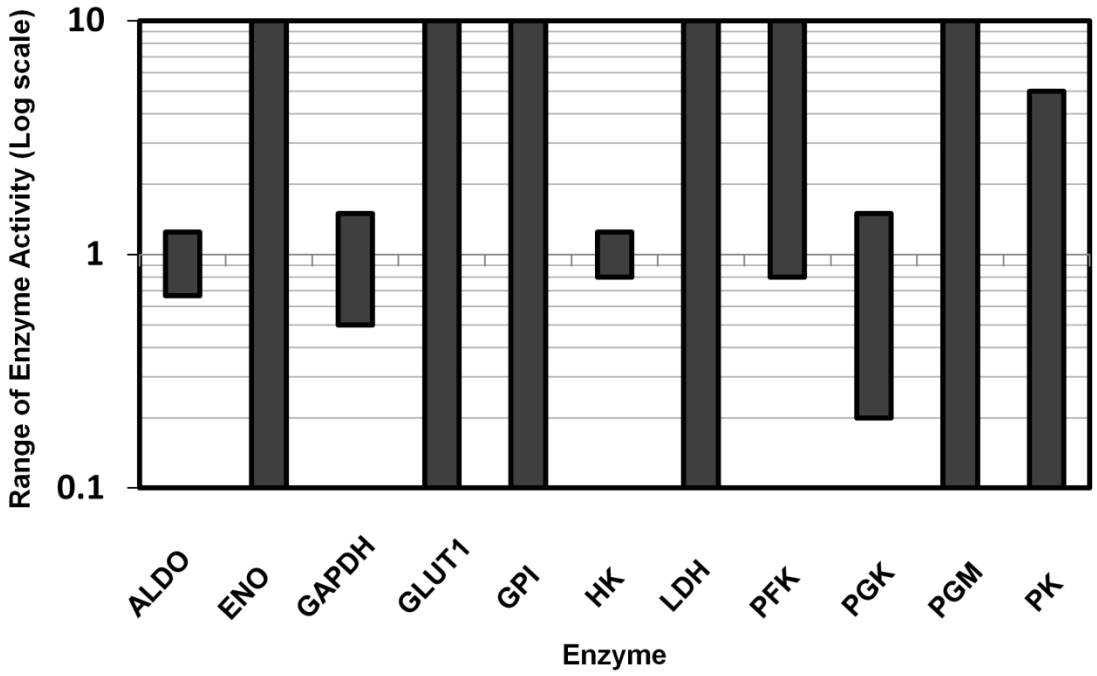

Appendix Figure 3: Bounds of enzyme activity within which bistability in glycolysis is observed. Sensitivity analysis was performed on the glycolytic enzyme activity levels. Each enzyme level was varied individually while holding all other parameters constant. The values shown are normalized to the concentration of enzyme used in the original simulation (shown in Figure 4.2D). The range of enzyme activities in which bistability was observed for each enzyme are plotted. The majority of enzymes have a large range of enzyme activity in which bistable behavior is observed for complete glycolysis. Only few enzymes including HK, ALDO and GAPDH have small enzyme activity range for bistable behavior.

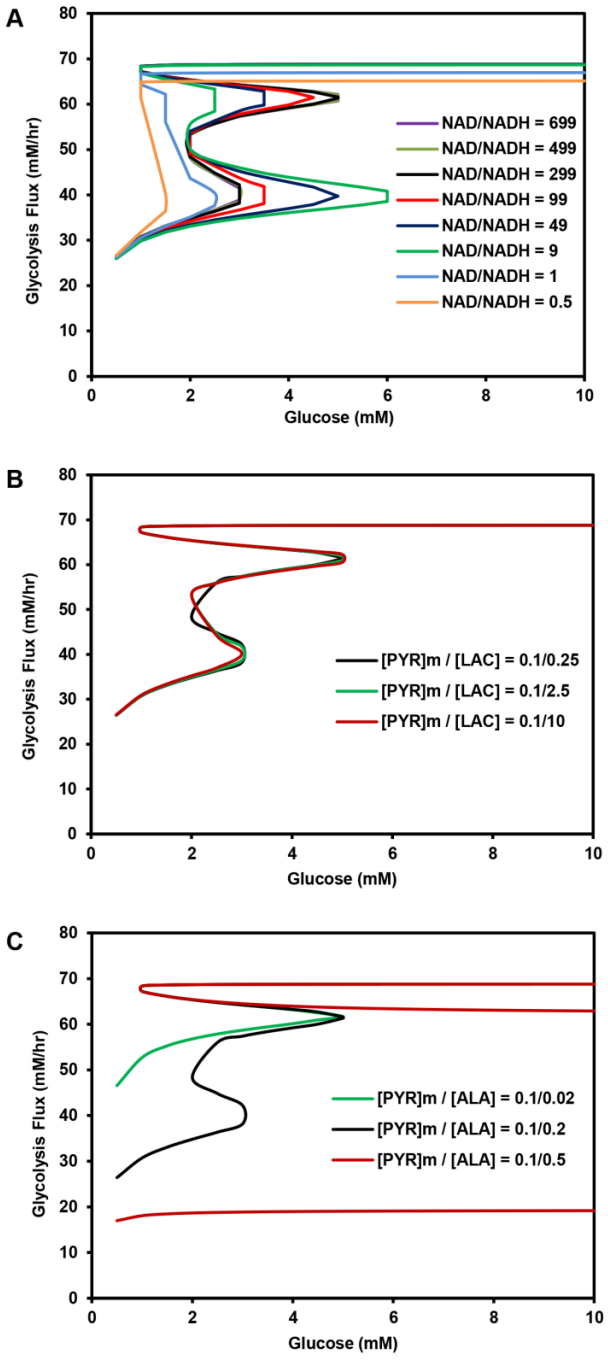

Appendix Figure 4: Sensitivity of the steady state behavior of glycolysis to the perturbations in: (A) NAD/NADH ratio **(B)** $[Pyruvate]_m$/[Lactate] ratio and **(C)** $[Pyruvate]_m$/[Alanine] ratio.

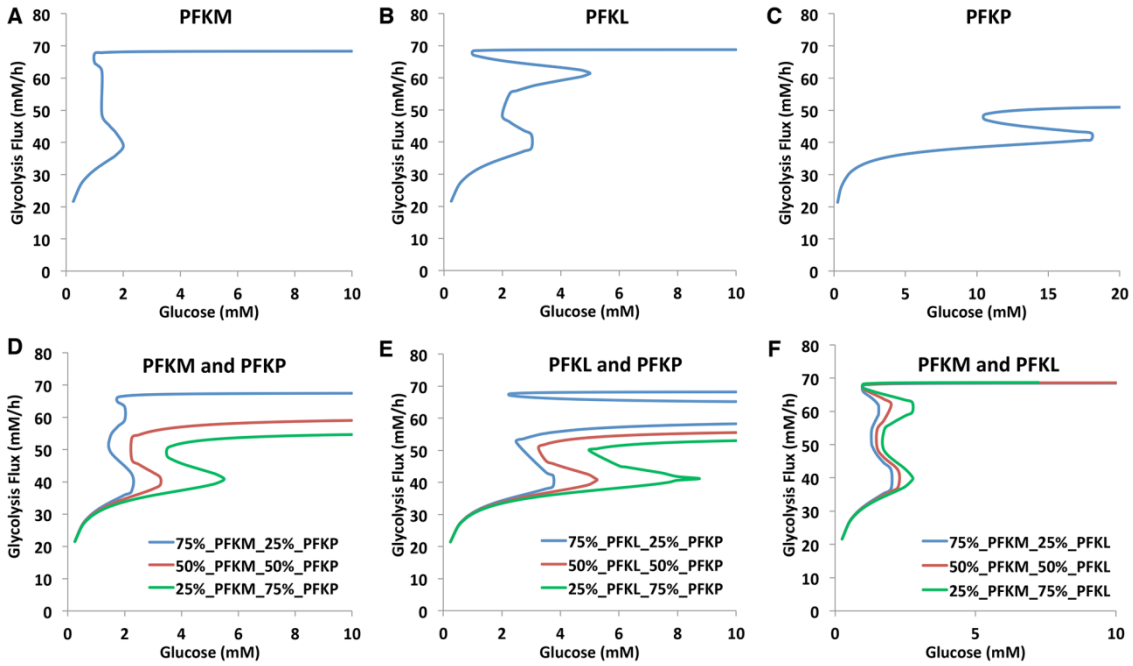

Appendix Figure 5: Effect of single or mixtures of PFK isozymes on the bistability in glycolysis. (A) Single PFKM isozyme **(B)** Single PFKL isozyme **(C)** Single PFKP isozyme **(D)** Mixtures of varying levels of PFKM and PFKP. **(E)** Mixtures of varying levels of PFKL and PFKP. **(F)** Mixtures of varying levels of PFKM and PFKL.

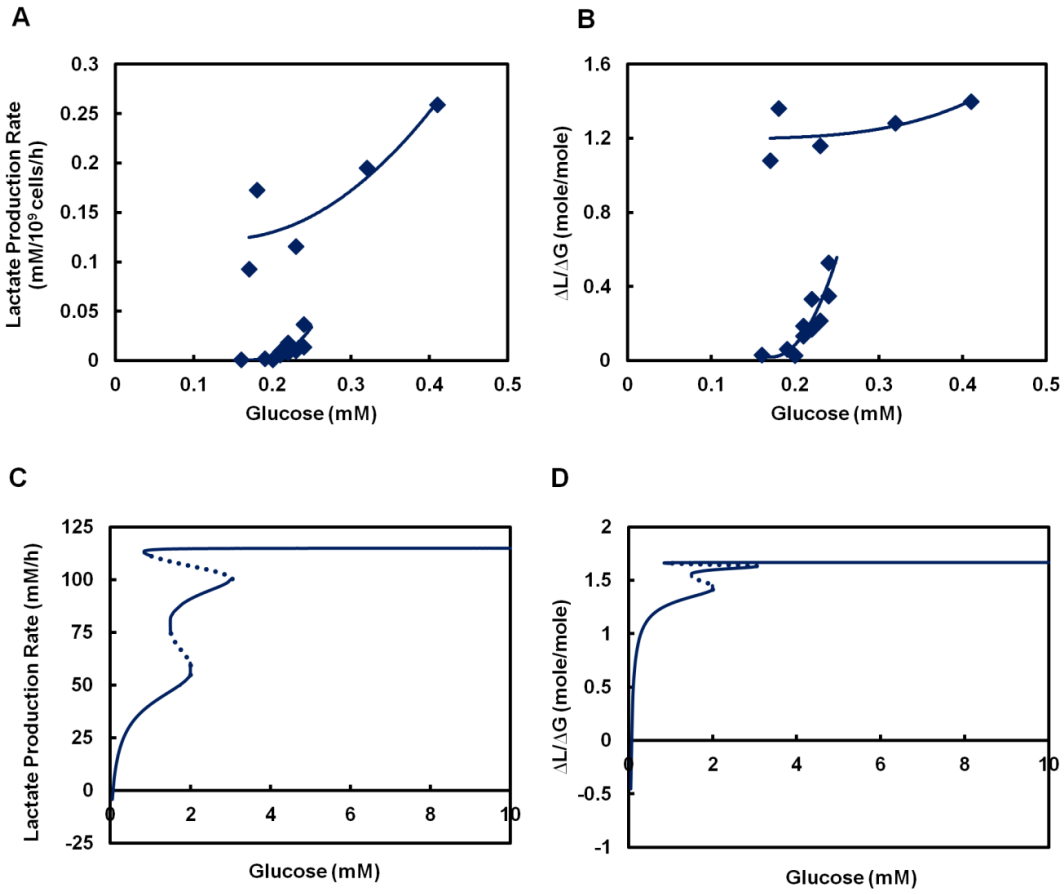

Appendix Figure 6: Experimental data of glycolysis rate at varying glucose concentration. Data from continuous culture of mouse hybridoma cells (reference [117] of the Supplementary Information) were used to plot the metabolic rates as a function of glucose concentration (**A**). The continuous culture data were from a total of 14 runs and reported data were all from steady states with a dilution rate (or growth rate) in the range of 0.30 to 0.33 h^{-1}. (**B**) The ratio of lactate production (analogous to LDH rate) to glucose consumption (analogous to glycolysis rate) is shown as ΔL/ΔG. A sharp transition from high flux state to a low flux state can be seen (0.24 mM glucose). The overlapping region of high flux and low flux state resembles that of bistability (0.17-0.24 mM). The ΔL/ΔG plot is consistent with that postulated in Warburg effect. (**C**-**D**) Simulation results corresponding to the glycolysis activity and ΔL/ΔG shown in (**A**-**B**).

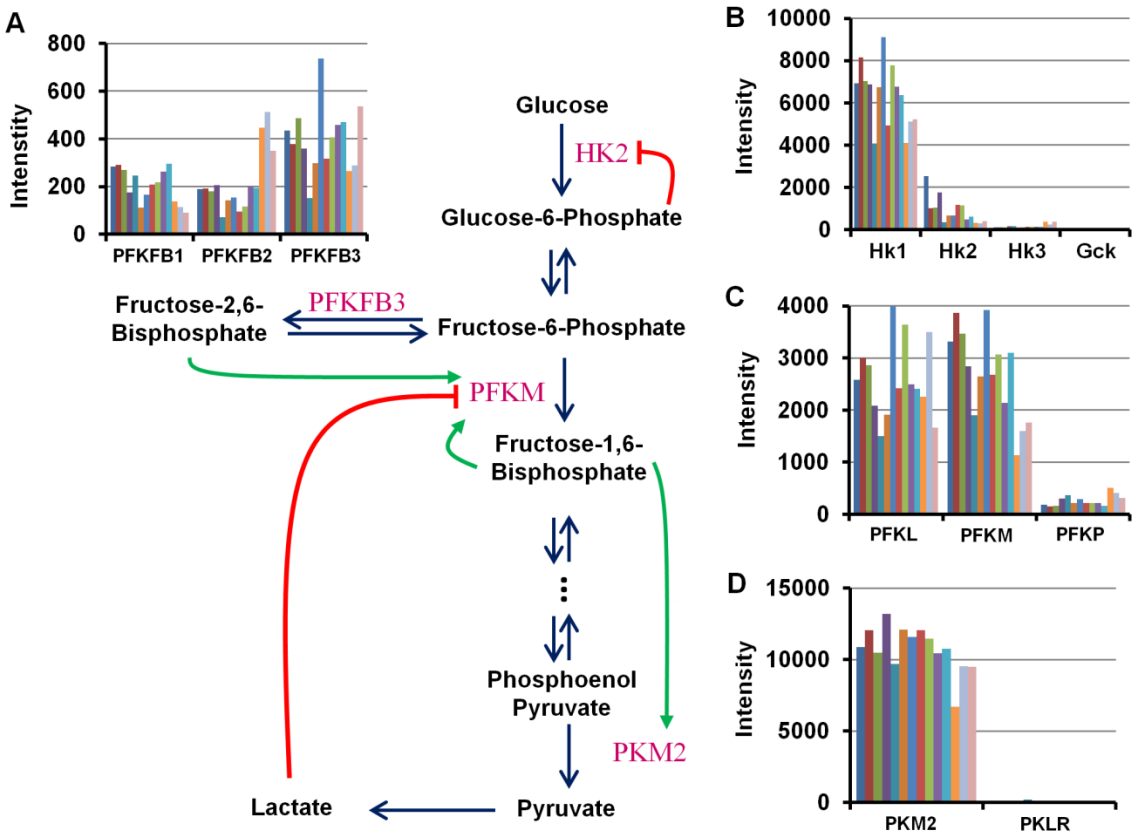

Appendix Figure 7: Expression levels of glycolytic isozymes across different types of CHO cells. Transcript levels of isozymes of **(A)** PFKFB, **(B)** HK, **(C)** PFK and **(D)** PK were probed using CHO microarrays.

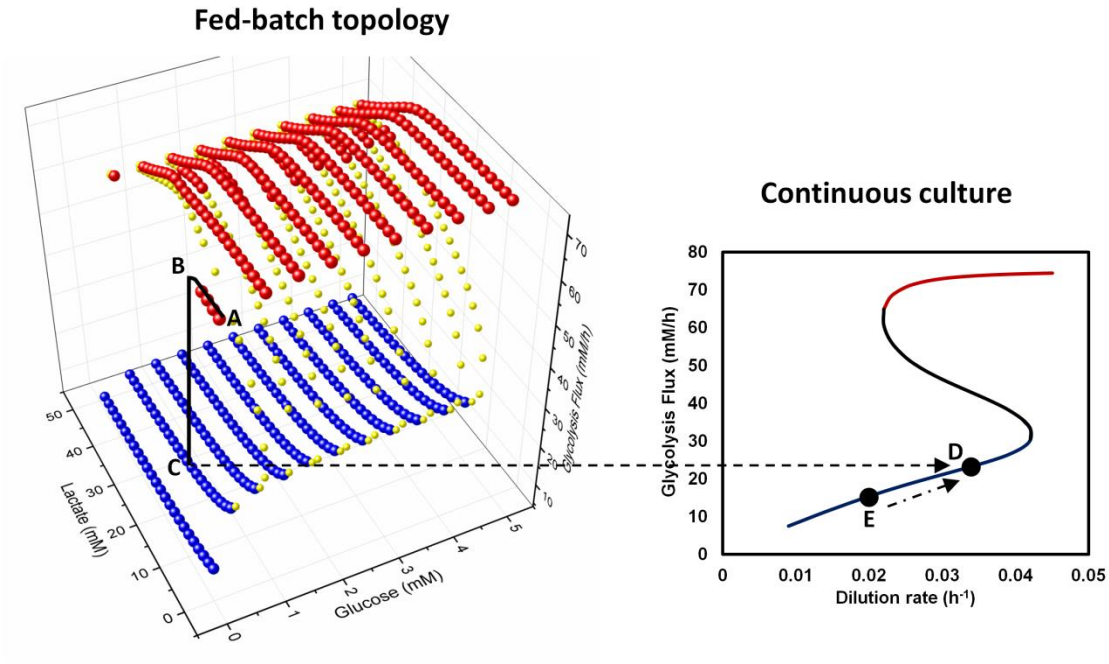

Appendix Figure 8: Strategies for guiding continuous culture to steady state with a low glycolysis flux. Two strategies for directing a continuous culture to low flux state are depicted. **(A-D)** Cells cultured in fed-batch with glucose maintained at 0.5 mM undergo a metabolic shift to low flux state. Once a low flux state is reached, the culture can be switched to continuous mode with a dilution rate located in the bistable region (0.033 h^{-1} in this example). The continuous culture will remain at low flux state and reaches steady state with a low metabolic flux and higher cell concentration. **(E-D)** Without controlling glucose at a low level, the continuous culture will reach steady state with low glycolysis flux only when it is operated at a low dilution rate ($\leq$0.021 h^{-1}). In the low dilution rate region, the only existing steady states are those with low glycolysis flux. The dilution rate can then be incrementally increased to a final dilution rate that is located in the bistable region (0.033 h^{-1} in this example). The culture will remain at low flux state and settles to steady state with a low flux and higher cell concentration.

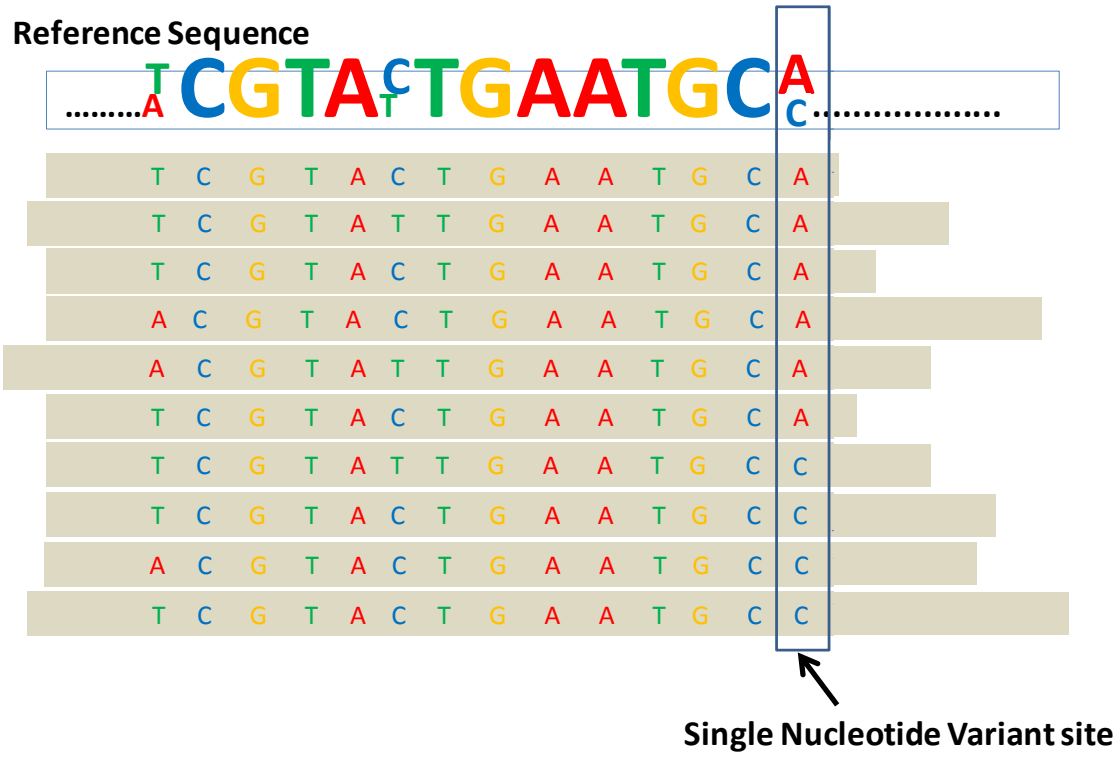

Appendix Figure 9: Schematic of single nucleotide variants in RNA Seq.

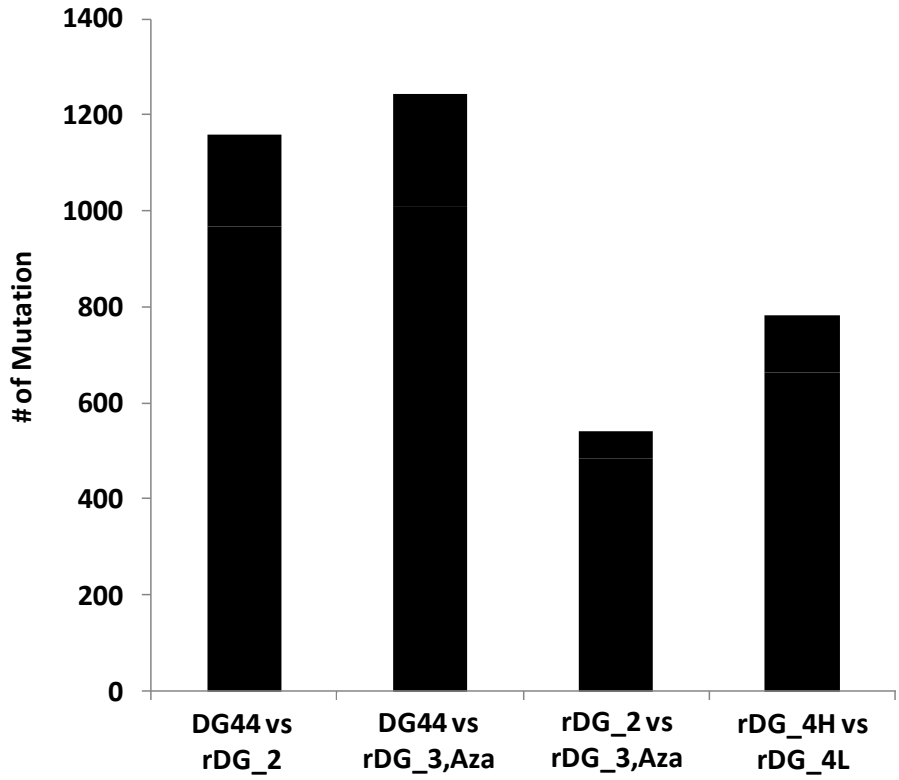

Appendix Figure 10: Number of mutations among CHO cell line pairs.

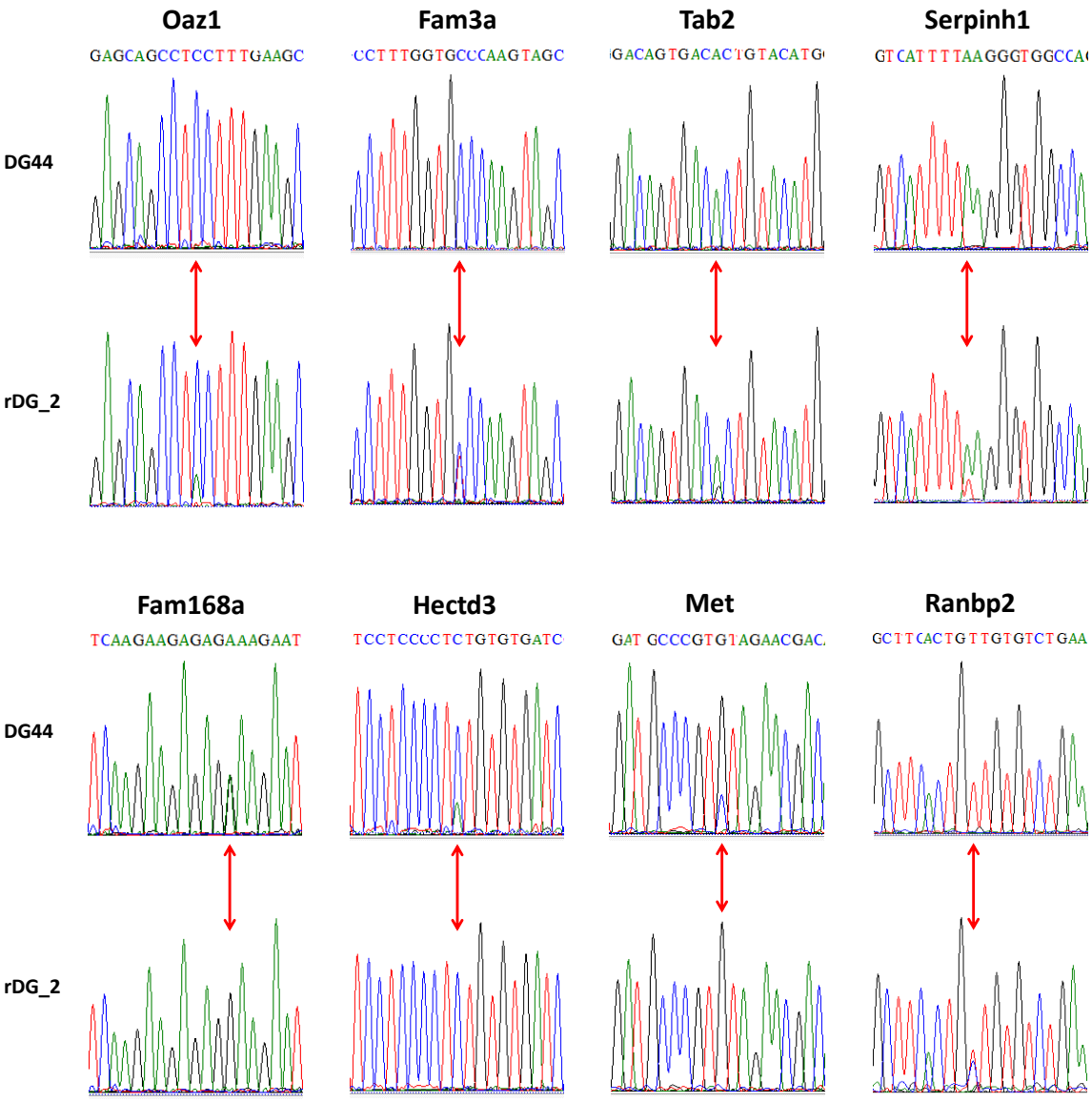

Appendix Figure 11: Chromatograms of confirmed mutations in various genes between DG44 and rDG_2.

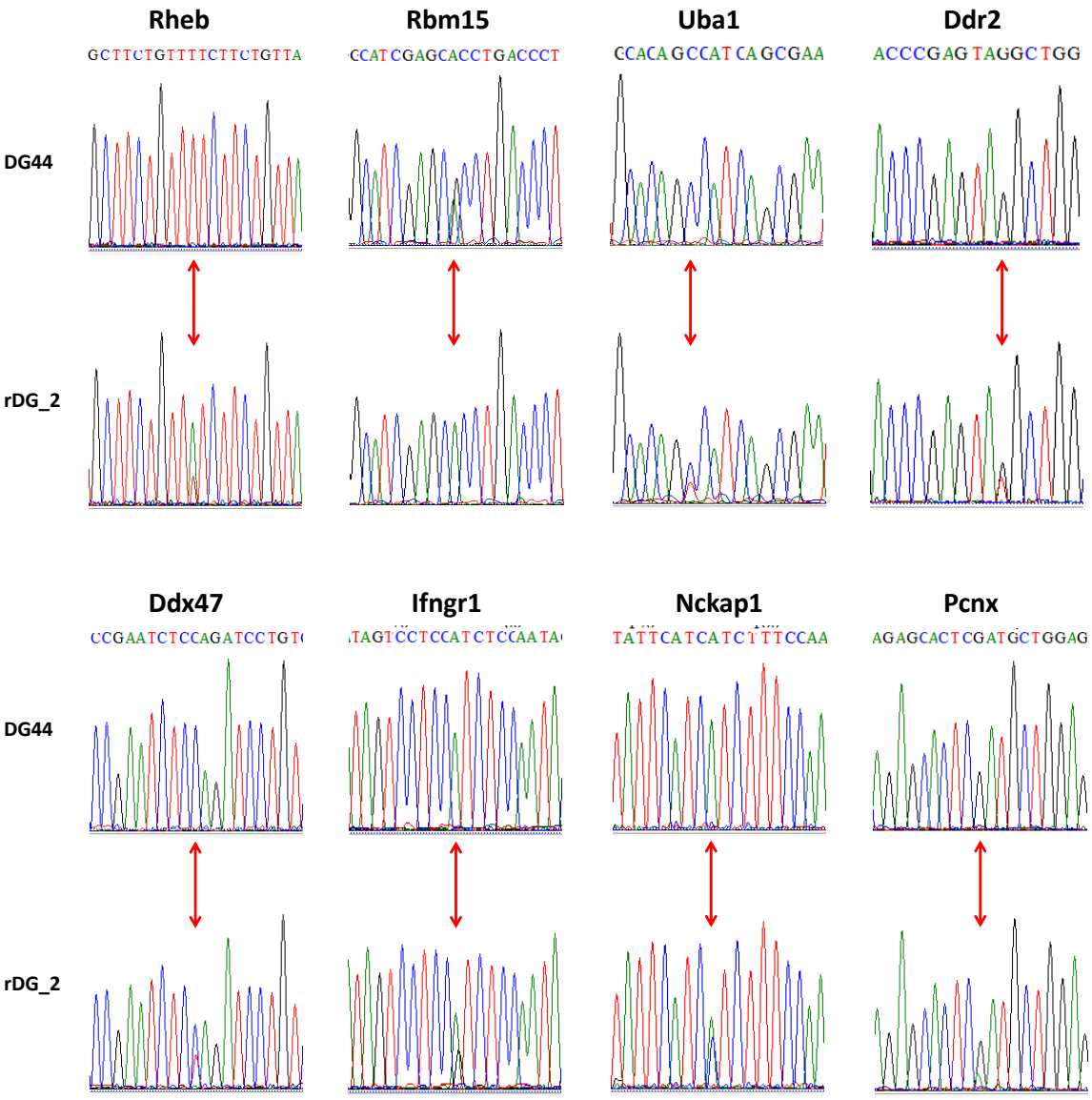

Appendix Figure 11 (continued)

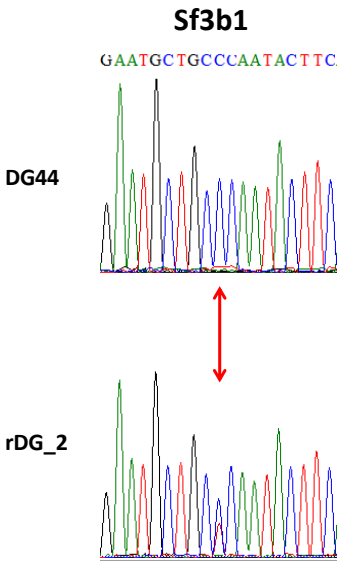

Appendix Figure 11 (continued)

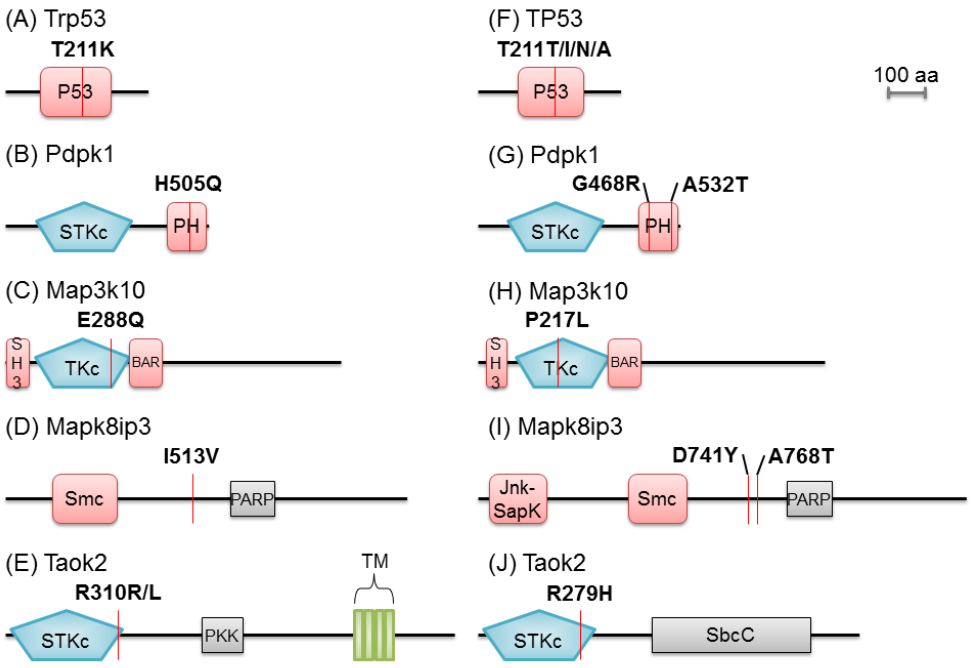

Appendix Figure 12: Protein domain annotation and mutation loci of Trp53, Pdpk1, Map3k10, Mapk8ip3 and Taok2 in Chinese hamster (A-E) and human (F-J).

Prediction of the protein domain was based on the NCBI conserved domain search using SMART protein domain analysis sever. The amino acid sequence is shown as a black horizontal line to the scale of protein length. The length corresponding to 100-amino acid is indicated. The protein domains are annotated as rectangle or pentagon with its corresponding function. The mutations are annotated with red vertical lines. The corresponding protein alignment location of mutations in Chinese hamster cell line is shown with blue vertical line in the human counterpart. P53, P53 DNA-binding domain; STKc, catalytic domain of the protein serine/threonine kinase; PH, Pleckstrin homology-like domain; SH3, Src Homology 3 domain of Mixed Lineage Kinases 1, 2, and 3; TKc, catalytic domain of protein tyrosine kinases; BAR, the Bin/Amphiphysin/Rvs domain; Smc, structural maintenance of chromosomes protein domain; PARP, procyclic acidic repetitive protein; JNK/SAPK, Jun amino-terminal kinase/stress-activated protein kinase domain; PKK, polo kinase kinase domain; TM, transmembrane domain; SbcC, domain related in ATPase involved in DNA repair.

10.2 Appendix Tables

Appendix Table 1: Fixed parameter values in the metabolic model

Parameter Symbol	Parameter Description	Value	Units
Ccadp	Cytosolic ADP concentration	0.54	mM
Cmadp	Mitochondrial ADP concentration	0.1	mM
Ccatp	Cytosolic ATP concentration	0.31	mM
Cmatp	Mitochondrial ATP concentration	0.1	mM
Ccamp	Cytosolic AMP concentration	0.03	mM
Cmamp	Mitochondrial AMP concentration	0.1	mM
Cmgtp	Mitochondrial GTP concentration	0.1	mM
Cmgdp	Mitochondrial GDP concentration	0.1	mM
pHm	Mitochondrial pH	8	
pHi	Intracellular pH	7.3	
Mg	Cytosolic magnesium concentration	0.7	mM
MgADP	Cytosolic MgADP concentration	0.46	mM
MgATP	Cytosolic MgATP concentration	2.69	mM
Ncd	Total cytosolic NAD concentration	0.32	mM
Ndp	Total cytosolic NADP concentration	0.065	mM
Ccpi	Cytosolic phosphate concentration	2.5	mM
Cmpi	Mitochondrial phosphate concentration	2.5	mM

Cc23p2g	Cytosolic 2,3-bisphosphoglycerate concentration	3.1	mM
Ccg16p	Cytosolic glucose 1,6-bisphosphate concentration	0.1	mM
Ccala	Cytosolic alanine concentration	1	mM
Cmcoq	Mitochondrial oxidized ubiquinol concentration	1.08	mM
Cmqh2	Mitochondrial reduced ubiquinol concentration	0.27	mM
Ccco2	Cytosolic CO_2 concentration	1.2	mM
Cmco2	Mitochondrial CO_2 concentration	21.4	mM
Cccoash	Cytosolic Coenzyme A concentration	0.02	mM
Ccaccoa	Cytosolic Acetyl-Coenzyme A concentration	0.001	mM
Cmcoash	Mitochondrial Coenzyme A concentration	0.04	mM
Cmnad	Mitochondrial NAD concentration	2.87	mM
Cmnadh	Mitochondrial NADH concentration	0.1	mM

Appendix Table 2: Composition of the transcript levels of several glycolysis isozymes at various stages of human embryonic development and cell lines.

Enzyme	Isozyme	Oocyte	Zygote	2cell	4cell	8cell	Morula	Blastocyst	hESC p10	HeLa
Hexokinase (HK)	%HK1	0	0	0	6	10	19	15	80	69
	%HK2	100	100	100	94	87	76	84	18	31
	%HK3	0	0	0	0	0	0	0	0	0
	%GCK	0	0	0	0	3	5	1	2	0
6-Phosphofructo-2-kinase/fructose-2,6-bisphosphatase (PFKFB)	%PFKFB1	9	2	0	0	0	0	0	6	0
	%PFKFB2	65	57	78	69	11	22	7	20	57
	%PFKFB3	9	7	7	9	87	65	0	12	17
	%PFKFB4	16	34	15	22	2	13	93	62	27
Phosphofructo kinase (PFK)	%PFKL	1	4	5	2	4	10	51	20	14
	%PFKM	9	5	6	4	17	42	9	50	52
	%PFKP	90	91	89	94	78	48	39	30	34
Pyruvate kinase (PK)	%PKL	0	0	0	0	0	0	0	0	0
	%PKR	0	0	0	0	0	0	0	0	0
	%PKM1	67	64	63	50	17	12	4	6	11
	%PKM2	33	36	37	50	83	88	96	94	89

Appendix Table 3: Composition of transcript levels of glycolysis isozymes in various mouse organs and cell lines.

	Bladder	Cerebellum	Cortex	Frontal Lobe	Colon	Heart	Large Intestine	Lung	Small Intestine	Spleen	Testis	Thymus	MEL	10T1/2
%PKM1	60	89	87	84	11	92	12	21	6	8	75	94	22	13
%PKM2	40	11	13	16	86	8	73	79	78	90	25	6	67	87
%PKL	0	0	0	0	2	0	14	0	15	1	0	0	5	0
%PKR	0	0	0	0	1	0	1	0	1	1	0	0	5	0
%PFKL	21	12	20	22	70	12	22	46	33	62	8	43	40	68
%PFKM	32	69	59	54	6	85	7	32	7	12	56	29	43	28
%PFKP	47	19	21	24	24	4	71	22	61	26	36	28	17	4
%PFKFB1	7	2	3	3	4	31	4	4	1	5	5	9	6	24
%PFKFB2	21	25	30	37	11	40	6	12	4	5	12	8	34	2
%PFKFB3	46	48	34	33	11	21	17	40	15	52	27	68	39	2
%PFKFB4	25	26	33	28	74	9	73	44	80	38	55	16	21	73

Appendix Table 4: Bounds of enzyme activity within which bistability is observed.

Enzyme	Lower bound	Upper bound
Glycolysis		
HK	0.4	2
GPI	< 0.1	> 10
PFK	0.4	> 10
ALDO	0.2	> 10
TPI	< 0.1	> 10
GAPDH	0.2	> 10
PGK	< 0.1	> 10
PGM	< 0.1	> 10
ENO	< 0.1	> 10
PK	< 0.1	> 10
LDH	< 0.1	> 10
Pentose Phosphate Pathway		
G6PD	< 0.1	> 10
6PGD	< 0.1	> 10
EPI	< 0.1	> 10
RPI	< 0.1	> 10
TK1	< 0.1	> 10
TK2	< 0.1	> 10
TA	< 0.1	> 10
TCA Cycle		
PDHC	0.5	2
CS	< 0.1	> 10
ACON	< 0.1	> 10
IDH	< 0.1	> 10
AKGD	< 0.1	> 10
SCOAS	0.4	> 10
SDH	< 0.1	> 10
FUM	< 0.1	> 10
MDH2	< 0.1	> 10
Malate-Aspartate Shuttle Cycle		
MDH1	< 0.1	> 10
GOT1	< 0.1	> 10
GOT2	< 0.1	> 10
AKGMAL	< 0.1	> 10
ASPGLU	< 0.1	> 10
Transporters		
GLUT1	< 0.1	> 10
PYRH	< 0.1	> 10

GLUH	< 0.1	> 10
CITMAL	< 0.1	> 10
MALPi	< 0.1	> 10
Other reactions		
PC	< 0.1	> 10
CMALIC	< 0.1	> 10
MMALIC	< 0.1	> 10
GPT1	< 0.1	> 10
GLS	< 0.1	> 10
GDH	< 0.1	> 10
CLY	< 0.1	> 10

Appendix Table 5: Summary of fourteen CHO cell lines used for microarray gene expression analysis.

Cell Line	*ID*	*Description (mRNA Source)*
1	CHO-K1	Parental CHO-K1
2	DG44	Parental DG44 • Exponential growth phase, adherent culture • Serum containing medium
3	DXB11	Parental DXB11
4	rDG_1	Recombinant DG44 (IgG TNF-alpha fusion protein producer) • Exponential growth phase, suspension culture • Serum free medium
5	rDG_2	Recombinant DG44 (IgG) • Exponential growth phase, suspension culture • Serum free medium
6	rDG_2, Late	Recombinant DG44 (IgG) • Late phase, suspension culture • Serum free medium
7	rDG_2, NaBu	Recombinant DG44 (IgG) • Late phase, 2mM butyrate for 24 hr • Serum free medium
8	rDX_1	DXB11-derived recombinant IgG producer 1
9	rDX_1M	DXB11-derived recombinant IgG producer 1 • 20 nM MTX treatment
10	rDX_2	DXB11-derived recombinant DHFR
11	rDX_2M	DXB11-derived recombinant DHFR • 20 nM MTX treatment
12	rDX_3	DXB11-derived recombinant IgG producer 3
13	rDX_3M	DXB11-derived recombinant IgG producer 3 • 20 nM MTX treatment
14	rDX_4	DXB11-derived recombinant IgG TNF-alpha fusion protein producer

Appendix Table 6: Summary of five CHO cell lines and two Chinese hamster tissues used for single nucleotide variant analysis.

ID	*Description (mRNA Source)*	*Total Output*
DG44	Parental DG44 • Exponential growth phase, adherent culture • Serum containing medium	3.32 Gbp
rDG_2	Recombinant DG44 (IgG) • Exponential growth phase, suspension culture • Serum free medium	2.57 Gbp
rDG_3,Aza	Recombinant DG44 (IgG)- High Producer • Exponential growth phase, suspension culture • Serum free medium • 5-azacytidine treatment	4.47 Gbp
rDG_4H	Recombinant DG44 (EPO) • Exponential growth phase, suspension culture • Serum free medium	3.94 Gbp
rDG_4L	Recombinant DG44 (EPO) • Exponential growth phase, suspension culture • Serum free medium	4.29 Gbp
Brain	Chinese Hamster Brain Tissue Brain mRNA from one late adolescent virgin female hamster	4.25 Gbp
Liver	Chinese Hamster Liver Tissue Liver mRNA from one late adolescent virgin female hamster	6.59 Gbp

Appendix Table 7: No variants are observed in r-IgG heavy chain upon Sanger sequencing. cDNA or gDNA of r-IgG heavy chain was cloned into TOPO-vector and transformed into *E. coli*. *E. coli* clones on agar plates were picked and plasmids were purified and subjected to Sanger sequencing.

Transcript	**Nucleotide Position**	**Base Change**	**RNA-seq (#Variant Reads/ #Consensus Reads)**	**cDNA Sanger (#Variant Clones/ #Total Clones)**	**gDNA Sanger (#Variant Clones/ #Total Clones)**
Heavy Chain	708	A → C	1,461/44,814	0/103	0/110
Heavy Chain	785	T → G	2,237/46,909	0/103	0/110
Heavy Chain	905	A → G	1,343/73,924	0/103	0/110

10.3 Appendix Materials

10.3.1 Rate Equations

Glycolysis

Hexokinase (HK): The rate equation for HK was taken from Mulquiney et al. [94]. The kinetic constants which correspond to those of the isozyme HK2 were adopted from previous literature [177-181]. The rate equation employs the partial rapid equilibrium random bi bi mechanism with the assumption that all the steps in the mechanism, except for the reactive-ternary complexes, are fast reactions. The inhibitions by *g6p*, glucose-1,6-phosphate (*g16bp*), 2,3-bisphosphoglycerate (*2,3bpg*) and glutathione (*gsh*) were modeled as mixed type of inhibition affecting both the activity (V_{max}) as well as the affinity (K_M) of the enzyme for glucose.

Eq. S1:

$$r_{HK} = \left(V_{mf}^{HK} \frac{C_{MgATP}^{c} C_{glc}^{c}}{K_{MgATP}^{HK} K_{glc}^{HK}} - V_{mr}^{HK} \frac{C_{MgADP}^{c} C_{g6p}^{c}}{K_{i,MgADP}^{HK} K_{g6p}^{HK}} \right) \frac{1}{N_{HK}}$$

$$N_{HK} = \left(1 + \frac{C_{MgATP}^{c}}{K_{i,MgATP}^{HK}} + \frac{C_{g6p}^{c}}{K_{i,g6p}^{HK}} + \frac{C_{glc}^{c}}{K_{glc}^{HK}} + \frac{C_{MgATP}^{c} C_{glc}^{c}}{K_{MgATP}^{HK} K_{glc}^{HK}} + \frac{C_{MgADP}^{c}}{K_{i,MgADP}^{HK}} + \frac{C_{MgADP}^{c} C_{g6P}^{c}}{K_{i,MgADP}^{HK} K_{g6P}^{HK}} + \frac{C_{glc}^{c} C_{g6P}^{c}}{K_{glc}^{HK} K_{g6P}^{HK}} + \frac{C_{glc}^{c} C_{g16bp}^{c}}{K_{glc}^{HK} K_{i,g16bp}^{HK}} + \frac{C_{glc}^{c} C_{2,3bpg}^{c}}{K_{glc}^{HK} K_{i,2,3bpg}^{HK}} + \frac{C_{glc}^{c} C_{gsh}^{c}}{K_{glc}^{HK} K_{i,gsh}^{HK}} \right)$$

$V_{mf}^{HK} = 9.59 * 10^{2}\ mM\ h^{-1}$
$V_{mr}^{HK} = 6.18\ mM\ h^{-1}$
$K_{MgATP}^{HK} = 1.0\ mM$
$K_{glc}^{HK} = 0.1\ mM$
$K_{i,MgADP}^{HK} = 1.0\ mM$
$K_{g6p}^{HK} = 0.47 mM$
$K_{i,g6p}^{"HK} = 2 * 10^{-2} mM$
$K_{i,g16bp}^{HK} = 3 * 10^{-2} mM$
$K_{i,gsh}^{HK} = 3.0\ mM$

Glucose Phosphate Isomerase (GPI): The rate equation for GPI was taken from Mulquiney et al. [94]. The kinetic constants were adopted from previous literature [182-184]. The rate equation employs the steady state uni uni reaction kinetics.

Eq. S2:

$$r_{GPI} = \frac{V_{mf}^{GPI}\frac{C_{g6p}^{c}}{K_{f}^{GPI}} - V_{mr}^{GPI}\frac{C_{f6p}^{c}}{K_{r}^{GPI}}}{1 + \frac{C_{g6p}^{c}}{K_{f}^{GPI}} + \frac{C_{f6p}^{c}}{K_{r}^{GPI}}}$$

$V_{mf}^{GPI} = 2.4*10^{3} mM\ h^{-1}$
$V_{mr}^{GPI} = 2.0*10^{3} mM\ h^{-1}$
$K_{f}^{GPI} = 9.6*10^{-1} mM$
$K_{r}^{GPI} = 1.23*10^{-1} mM$

Phosphofructokinase (PFK): The rate equation for PFK was taken from Mulquiney et al. [94]. The kinetic constants were adopted from previous literature [185-189]. The rate kinetics was based on the two state allosteric model using ordered bi bi mechanism. The two state model considers that the enzyme can exist in the active or the non-active state as determined by the levels of the activity modulators. These include activators (*f16bp, f26bp, g16bp,* AMP etc) and inhibitors (ATP, Mg etc). These activity modulators are isozyme specific. For example, *f16bp* only stimulates PFKM and PFKL. The fraction of enzyme in the active state is represented by the nonlinear term N_{PFK} which is a function of the levels of the activity modulators. L_{PFK} represents the equilibrium constant between the two states of the enzyme in the absence of any substrates. The initial velocity expression for the enzyme fraction in the active state was modeled as partial rapid equilibrium random bi bi steady state equation similar to the HK kinetics.

Eq. S3:

$$r_{PFK} = \frac{\frac{V_f^{PFK} C_{MgATP}^c C_{f6p}^c}{K_{f6p}^{PFK} K_{MgATP}^{PFK}} - \frac{V_r^{PFK} C_{MgADP}^c C_{f16bp}^c}{K_{f16bp}^{PFK} K_{MgADP}^{PFK}}}{\left(\left(1+\frac{C_{f6p}^c}{K_{f6p}^{PFK}}\right)\left(1+\frac{C_{MgATP}^c}{K_{MgATP}^{PFK}}\right)+\left(1+\frac{C_{f16bp}^c}{K_{f16bp}^{PFK}}\right)\left(1+\frac{C_{MgADP}^c}{K_{MgADP}^{PFK}}\right)-1\right)} \frac{1}{N_{PFK}}$$

$$N_{PFK} = 1 + \frac{L_{PFK}\left(1+\frac{C_{ATP}^c}{K_{ATP}^{PFK}}\right)^4\left(1+\frac{C_{Mg}^c}{K_{Mg}^{PFK}}\right)^4\left(1+\frac{C_{2,3bpg}^c}{K_{2,3bpg}^{PFK}}\right)^4\left(1+\frac{C_{Lac}^c}{K_{Lac}^{PFK}}\right)^4}{\left(1+\frac{C_{f6p}^c}{K_{f6p}^{PFK}}+\frac{C_{f16bp}^c}{K_{f16bp}^{PFK}}\right)^4\left(1+\frac{C_{AMP}^c}{K_{AMP}^{PFK}}\right)^4\left(1+\frac{C_{g16bp}^c}{K_{g16bp}^{PFK}}\right)^4\left(1+\frac{C_{Pi}^c}{K_{Pi}^{PFK}}\right)^4\left(1+\frac{C_{f26bp}^c}{K_{f26bp}^{PFK}}\right)^4}$$

$V_f^{PFK} = 2.63*10^2\ mM^{-1}h^{-1}$
$V_r^{PFK} = 11.53\ mM^{-1}h^{-1}$
$K_{f6p}^{PFK} = 6*10^{-2}\ mM$
$K_{MgATP}^{PFK} = 6.8*10^{-2}\ mM$
$K_{MgADP}^{PFK} = 0.54\ mM$
$K_{ATP}^{PFK} = 0.1\ mM$
$K_{AMP}^{PFK} = 0.3\ mM$
$K_{Mg}^{PFK} = 0.2\ mM$
$K_{Pi}^{PFK} = 30\ mM$
$K_{f16bp}^{PFK} = 0.3\ mM$
$K_{f26bp}^{PFK} = 5.5*10^{-3} mM$
$K_{g16bp}^{PFK} = 0.1\ mM$
$K_{23bpg}^{PFK} = 0.5\ mM$
$L_{PFK} = 2*10^{-3}$
$K_{Lac}^{PFK} = 30\ mM$

<u>6-Phosphofructo-2-Kinase/Fructose-2,6-Bisphosphatase</u> (PFKFB): The rate equation for PFKFB and the kinetic constants were taken from previously reported studies [96,97]. PFKFB is a bi-functional enzyme with kinase and bisphosphatase activities, each localized to either terminals of the enzyme and are independent of each other's activity. The kinase domain catalyzes the synthesis of fructose-2,6-bisphosphate (*f26bp*) from fructose-6-phoshate (*f6p*) and the bisphosphatase domain mediates the hydrolysis of *f26bp* to *f6p*. The reaction kinetics for the kinase domain (r_{PFK2}) follows the ordered bi bi steady state kinetics, with phosphoenolpyurvate (*pep*) inhibition of the kinase domain modeled as non-competitive inhibition. The bisphosphatase reaction kinetics ($r_{F2,6BPase}$) was modeled as simple Michaelis-Menten kinetics with non-competitive product

inhibition by *f6p*. Isozymes of PFKFB vary in their kinase to bisphosphatase activity (K/P) [12]. The effect of isozyme (or K/P) was modeled by changing the Vmax of r_{PFK2} and holding $r_{F2,6BPase}$ constant.

Eq. S4:

$$r_{PFK2} = \frac{V_{f,PFK2}\left(C^c_{ATP}C^c_{f6p} - \frac{C^c_{ADP}C^c_{f26bp}}{K_{eq,PFK2}}\right)\left(0.2 + \frac{0.8}{1+\frac{K_{AKT}}{pAKT}}\right)}{\left(K^{PFK2}_{i,ATP}K^{PFK2}_{m,f6p} + K^{PFK2}_{m,f6p}C^c_{ATP} + K^{PFK2}_{m,ATP}C^c_{f6p} + \frac{K^{PFK2}_{m,ADP}C^c_{f26bp}}{K_{eq,PFK2}} + C^c_{ATP}C^c_{f6p} + \frac{K^{PFK2}_{m,f26bp}C^c_{ADP}}{K_{eq,PFK2}} + \frac{K^{PFK2}_{m,ADP}C^c_{ATP}C^c_{f26bp}}{K_{eq,PFK2}K^{PFK2}_{i,ATP}} + \frac{C^c_{ADP}C^c_{f26bp}}{K_{eq,PFK2}} + \frac{K^{PFK2}_{m,ATP}C^c_{ADP}C^c_{f6p}}{K^{PFK2}_{i,ADP}} + \frac{C^c_{ATP}C^c_{f6p}C^c_{f26bp}}{K^{PFK2}_{i,f26bp}} + \frac{C^c_{ADP}C^c_{f6p}C^c_{f26bp}}{K_{eq,PFK2}K^{PFK2}_{i,f6p}}\right)\left(1+\frac{C^c_{pep}}{K^{PFK2}_{i,pep}}\right)}$$

$V_{f,PFK2} = 300\ mM\ h^{-1}$
$K^{PFK2}_{m,ATP} = 0.15\ mM$
$K^{PFK2}_{m,f6p} = 0.032\ mM$
$K^{PFK2}_{m,f26bp} = 0.008\ mM$
$K^{PFK2}_{m,ADP} = 0.062\ mM$
$K^{PFK2}_{i,ATP} = 0.15\ mM$
$K^{PFK2}_{i,f6p} = 0.001\ mM$
$K^{PFK2}_{i,f26bp} = 0.02\ mM$
$K^{PFK2}_{i,ADP} = 0.23\ mM$
$K^{PFK2}_{i,pep} = 0.013\ mM$
$K^{PFK2}_{eq} = 16$
$K_{AKT} = 0.5$

$$r_{F2,6BPase} = \frac{V_{F2,6BPase}C^c_{f26bp}}{\left(1+\frac{C^c_{f6p}}{K^{F2,6BPase}_{i,f6p}}\right)\left(K^{F2,6BPase}_{m,f26bp} + C^c_{f26bp}\right)}$$

$V_{F2,6BPase} = 13.86\ mM^{-1}h^{-1}$
$K^{F2,6BPase}_{m,f26bp} = 10^{-3}\ mM$
$K^{F2,6BPase}_{i,f6p} = 25*10^{-3}\ mM$

<u>Aldolase</u> (ALDO): The rate equation for ALDO was taken from Mulquiney et al. [94]. The kinetic constants were adopted or estimated from previous literature [190-199]. The reaction kinetics of ALDO follows the ordered uni bi steady state kinetics. Inhibition due to *2,3bpg* as described in the original expression was retained in this study. However, since *2,3bpg* is not a reaction intermediate considered in the model, its concentration was held constant for the purpose of this study.

Eq. S5:

$$r_{ALD} = \frac{\frac{V_{mf}^{ALD} C_{f16bp}^{c}}{K_{f16bp}^{ALD}} - \frac{V_{mr}^{ALD} C_{gap}^{c} C_{dhap}^{c}}{K_{gap}^{ALD} K_{i,dhap}^{ALD}}}{\left(1 + \frac{C_{2,3bpg}^{c}}{K_{i,2,3bpg}^{ALD}} + \frac{C_{f16bp}^{c}}{K_{f16bp}^{ALD}} + \frac{K_{dhap}^{ALD} C_{gap}^{c}}{K_{gap}^{ALD} K_{i,dhap}^{ALD}}\left(1 + \frac{C_{2,3bpg}^{c}}{K_{i,2,3bpg}^{ALD}}\right) + \frac{C_{dhap}^{c}}{K_{i,dhap}^{ALD}} + \frac{K_{dhap}^{ALD} C_{F1,6P}^{c} C_{gap}^{c}}{K_{i,f16bp}^{ALD} K_{gap}^{ALD} K_{i,dhap}^{ALD}} + \frac{C_{dhap}^{c} C_{gap}^{c}}{K_{gap}^{ALD} K_{i,dhap}^{ALD}}\right)}$$

$V_{mf}^{ALD} = 1.33*10^{2}\, mM\ h^{-1}$
$V_{mr}^{ALD} = 4.57*10^{2}\, mM\ h^{-1}$
$K_{f16bp}^{ALD} = 5*10^{-2}\, mM$
$K_{i,f16bp}^{ALD} = 1.98*10^{-2}\, mM$
$K_{dhap}^{ALD} = 3.5*10^{-2}\, mM$
$K_{i,dhap}^{ALD} = 1.1*10^{-2}\, mM$
$K_{gap}^{ALD} = 0.189 mM$
$K_{i,2,3bpg}^{ALD} = 1.5 mM$

Triose Phosphate Isomerase (TPI): The rate equation for TPI was taken from Mulquiney et al. [94]. The kinetic constants were adopted from previous literature [191,200-202]. The rate kinetics of TPI follows a simple steady state uni uni reaction kinetics.

Eq. S6:

$$r_{TPI} = \frac{V_{mf}^{TPI} \frac{C_{dhap}^{c}}{K_{f}^{TPI}} - V_{mr}^{TPI} \frac{C_{gap}^{c}}{K_{r}^{TPI}}}{1 + \frac{C_{dhap}^{c}}{K_{f}^{TPI}} + \frac{C_{gap}^{c}}{K_{r}^{TPI}}}$$

$V_{mf}^{TPI} = 5.10*10^{2}\, mM\ h^{-1}$
$V_{mr}^{TPI} = 2.76*10^{3}\, mM\ h^{-1}$
$K_{f}^{TPI} = 1.62*10^{-1}\, mM$
$K_{r}^{TPI} = 4.30*10^{-1}\, mM$

Glyceraldehyde 3-Phosphate Dehydrogenase (GAPDH): The rate equation for GAPDH was taken from Mulquiney et al. [94]. The kinetic constants were adopted from previous literature [203-206]. The rate kinetics of GAPDH follows the ter ter (bi uni uni bi ping pong) steady state kinetics.

Eq. S7:

$$r_{GAPD} = \frac{V_{mf}^{GAPD}\frac{C_{NAD^+}^{c}C_{Pi}^{c}C_{gap}^{c}}{K_{NAD^+}^{GAPD}K_{i,Pi}^{GAPD}K_{i,gap}^{GAPD}} - V_{mr}^{GAPD}\frac{C_{1,3bpg}^{c}C_{NADH}^{c}C_{H^+}^{c}}{K_{i,1,3bpg}^{GAPD}K_{NADH}^{GAPD}}}{\begin{aligned}&\frac{C_{gap}^{c}}{K_{i,gap}^{GAPD}}\left(1+\frac{C_{gap}^{c}}{K_{i,gap}^{'GAPD}}\right)+\frac{C_{1,3bpg}^{c}}{K_{i,1,3bpg}^{GAPD}}\left(1+\frac{C_{gap}^{c}}{K_{i,GAP}^{'GAPD}}\right)+\frac{K_{1,3bpg}^{GAPD}C_{NADH}^{c}C_{H^+}^{c}}{K_{i,1,3bpg}^{GAPD}K_{NADH}^{GAPD}}+\frac{K_{gap}^{GAPD}C_{NAD^+}^{c}C_{Pi}^{c}}{K_{NAD^+}^{GAPD}K_{i,Pi}^{GAPD}K_{i,gap}^{GAPD}}\\&+\frac{C_{NAD^+}^{c}C_{gap}^{c}}{K_{i,NAD^+}^{GAPD}K_{i,gap}^{GAPD}}+\frac{C_{Pi}^{c}C_{gap}^{c}}{K_{i,Pi}^{GAPD}K_{i,gap}^{GAPD}}\left(1+\frac{C_{gap}^{c}}{K_{i,gap}^{'GAPD}}\right)+\frac{C_{NAD^+}^{c}C_{1,3bpg}^{c}}{K_{i,NAD^+}^{GAPD}K_{i,1,3bpg}^{GAPD}}+\frac{K_{1,3bpg}^{GAPD}C_{Pi}^{c}C_{NADH}^{c}C_{H^+}^{c}}{K_{i,Pi}^{GAPD}K_{i,1,3bpg}^{GAPD}K_{NADH}^{GAPD}}\\&+\frac{C_{gap}^{c}C_{NADH}^{c}C_{H^+}^{c}}{K_{i,gap}^{GAPD}K_{i,NADH}^{GAPD}}+\frac{C_{1,3bpg}^{c}C_{NADH}^{c}C_{H^+}^{c}}{K_{i,1,3bpg}^{GAPD}K_{NADH}^{GAPD}}+\frac{C_{NAD^+}^{c}C_{Pi}^{c}C_{gap}^{c}}{K_{NAD^+}^{GAPD}K_{i,Pi}^{GAPD}K_{i,gap}^{GAPD}}+\frac{K_{gap}^{GAPD}C_{NAD^+}^{c}C_{Pi}^{c}C_{1,3bpg}^{c}}{K_{i,gap}^{GAPD}K_{NAD^+}^{GAPD}K_{i,Pi}^{GAPD}K_{i,1,3bpg}^{'GAPD}}\\&+\frac{C_{Pi}^{c}C_{gap}^{c}C_{NADH}^{c}C_{H^+}^{c}}{K_{i,Pi}^{GAPD}K_{i,gap}^{GAPD}K_{i,NADH}^{GAPD}}+\frac{C_{Pi}^{c}C_{1,3bpg}^{c}C_{NADH}^{c}C_{H^+}^{c}}{K_{i,1,3bpg}^{GAPD}K_{NADH}^{GAPD}K_{i,Pi}^{GAPD}K_{i,1,3bpg}^{'GAPD}}\end{aligned}}$$

$V_{mf}^{GAPD} = 5.317*10^{3}\,mMh^{-1}$ $K_{gap}^{GAPD} = 0.095mM$

$V_{mr}^{GAPD} = 3.919*10^{3}\,mMh^{-1}$ $K_{i,gap}^{GAPD} = 1.59*10^{-16}\,mM$

$K_{NAD^+}^{GAPD} = 0.045mM$ $K_{i,gap}^{'GAPD} = 0.031mM$

$K_{i,NAD^+}^{GAPD} = 0.045mM$ $K_{1,3bpg}^{GAPD} = 0.000671mM$

$K_{Pi}^{GAPD} = 2.5mM$ $K_{i,1,3bpg}^{GAPD} = 1.52*10^{-18}\,mM$

$K_{i,Pi}^{GAPD} = 2.5mM$ $K_{i,1,3bpg}^{'GAPD} = 0.001mM$

$K_{NADH}^{GAPD} = 0.0033mM$ $K_{eq}^{GAPD} = 1.9*10^{-8}$

$K_{i,NADH}^{GAPD} = 0.01mM$

Phosphoglycerate Kinase (PGK): The rate equation for PGK was taken from Mulquiney et al. [94]. The kinetic constants were adopted from previous literature [207-210]. The rate kinetics of PGK follows the partial rapid equilibrium random bi bi steady state kinetics.

Eq. S8:

$$r_{PGK} = \frac{V_{mf}^{PGK}\frac{C_{1,3bpg}^{c}C_{MgADP}^{c}}{K_{i,MgADP}^{PGK}K_{1,3bpg}^{PGK}} - V_{mr}^{PGK}\frac{C_{3pg}^{c}C_{MgATP}^{c}}{K_{i,MgATP}^{PGK}K_{3pg}^{PGK}}}{1+\frac{C_{1,3bpg}^{c}}{K_{i,1,3bpg}^{PGK}}+\frac{C_{MgADP}^{c}}{K_{i,MgADP}^{PGK}}+\frac{C_{1,3bpg}^{c}C_{MgADP}^{c}}{K_{i,MgADP}^{PGK}K_{1,3bpg}^{PGK}}+\frac{C_{3pg}^{c}}{K_{i,3pg}^{PGK}}+\frac{C_{MgATP}^{c}}{K_{i,MgATP}^{PGK}}+\frac{C_{3pg}^{c}C_{MgATP}^{c}}{K_{i,MgATP}^{PGK}K_{3pg}^{PGK}}}$$

$V_{mf}^{PGK} = 5.96*10^{4} mM/h$
$V_{mr}^{PGK} = 2.39*10^{4} mM/h$
$K_{MgADP}^{PGK} = 0.1mM$
$K_{i,MgADP}^{PGK} = 0.08mM$
$K_{1,3bpg}^{PGK} = 0.002mM$
$K_{i,1,3bpg}^{PGK} = 1.6mM$
$K_{MgATP}^{PGK} = 1mM$
$K_{i,MgATP}^{PGK} = 0.186mM$
$K_{3pg}^{PGK} = 1.1mM$
$K_{i,3pg}^{PGK} = 0.205mM$
$K_{eq}^{PGK} = 3.2*10^{3}$

Phosphoglycerate Mutase (PGM): The rate equation for PGM was taken from Mulquiney et al. [94]. The kinetic constants were adopted from previous literature [211,212]. The rate kinetics of PGM follows the uni uni steady state kinetics.

Eq. S9:

$$r_{PGAM} = \frac{V_{mf}^{PGAM}\frac{C_{3pg}^{c}}{K_{3pg}^{PGAM}} - V_{mr}^{PGAM}\frac{C_{2pg}^{c}}{K_{2pg}^{PGAM}}}{1+\frac{C_{3pg}^{c}}{K_{3pg}^{PGAM}}+\frac{C_{2pg}^{c}}{K_{2pg}^{PGAM}}}$$

$V_{mf}^{PGAM} = 4.894*10^{5} mM\ h^{-1}$
$V_{mr}^{PGAM} = 4.395*10^{5} mM\ h^{-1}$
$K_{3pg}^{PGAM} = 0.168mM$
$K_{2pg}^{PGAM} = 0.0256mM$
$K_{eq}^{PGAM} = 0.17$

Enolase (ENO): The rate equation for ENO was taken from Mulquiney et al. [94]. The kinetic constants were adopted from previous literature [213-215]. The rate kinetics of ENO follows the partial rapid equilibrium random bi bi steady state kinetics.

Eq. S10:

$$r_{ENO} = \frac{V_{mf}^{ENO}\frac{C_{2\,pg}^{c}C_{Mg^{2+}}^{c}}{K_{i,Mg^{2+}}^{ENO}K_{2\,pg}^{ENO}} - V_{mr}^{ENO}\frac{C_{pep}^{c}C_{Mg^{2+}}^{c}}{K_{i,Mg^{2+}}^{ENO}K_{pep}^{ENO}}}{1+\frac{C_{2\,pg}^{c}}{K_{i,2\,pg}^{ENO}}+\frac{C_{Mg^{2+}}^{c}}{K_{i,Mg^{2+}}^{ENO}}+\frac{C_{2\,pg}^{c}C_{Mg^{2+}}^{c}}{K_{i,Mg^{2+}}^{ENO}K_{2\,pg}^{ENO}}+\frac{C_{pep}^{c}}{K_{i,pep}^{ENO}}+\frac{C_{Mg^{2+}}^{c}}{K_{i,Mg^{2+}}^{ENO}}+\frac{C_{pep}^{c}C_{Mg^{2+}}^{c}}{K_{i,Mg^{2+}}^{ENO}K_{pep}^{ENO}}}$$

$$V_{mf}^{ENO} = 2.106*10^{4} mM\ h^{-1}$$
$$V_{mr}^{ENO} = 5.542*10^{3} mM\ h^{-1}$$
$$K_{i,Mg^{2+}}^{ENO} = K_{Mg^{2+}}^{ENO} = 0.14 mM$$
$$K_{pep}^{ENO} = K_{PEP}^{ENO} = 0.11 mM$$
$$K_{2\,pg}^{ENO} = K_{2PG}^{ENO} = .046 mM$$
$$K_{eq}^{ENO} = 3.0$$

Pyruvate Kinase (PK): The rate equation for PK was taken from Mulquiney et al. [94]. The kinetic constants were adopted from previous literature [95,216-220]. Like PFK, the rate kinetics of PK was based on the two state allosteric model using the ordered bi bi mechanism. The two state model considers that the enzyme can exist in active or non-active state determined by the levels of the activity modulators. These include activators (*f16bp, pep, pyr* etc) and inhibitors (ATP, *ala* etc). The fraction of the enzyme in the active state is represented by the nonlinear term N_{PK} which is a function of levels of activity modulators. L_{PK} represents the equilibrium constant between enzymes at the two states in the absence of any substrates. The initial velocity expression for the enzyme fraction in the active state is modeled as partial rapid equilibrium random bi bi steady state equation.

Eq. S11:

$$r_{PK} = \left(\frac{V_{mf}^{PK} \frac{C_{pep}^{c}}{K_{pep}^{PK}} \frac{C_{MgADP}^{c}}{K_{MgADP}^{PK}} - V_{mr}^{PK} \frac{C_{pyr}^{c}}{K_{pyr}^{PK}} \frac{C_{MgATP}^{c}}{K_{MgATP}^{PK}}}{\left(1+\frac{C_{pep}^{c}}{K_{pep}^{PK}}\right)\left(1+\frac{C_{MgADP}^{c}}{K_{MgADP}^{PK}}\right)+\left(1+\frac{C_{pyr}^{c}}{K_{pyr}^{PK}}\right)\left(1+\frac{C_{MgATP}^{c}}{K_{MgATP}^{PK}}\right)-1} \right) \frac{1}{N_{PK}}$$

$$N_{PK} = 1 + L_{PK} \frac{\left(1+\frac{C_{ATP}^{c}}{K_{ATP}^{PK}}\right)^{4}\left(1+\frac{C_{ala}^{c}}{K_{ala}^{PK}}\right)^{4}}{\left(1+\frac{C_{pep}^{c}}{K_{pep}^{PK}}+\frac{C_{pyr}^{c}}{K_{pyr}^{PK}}\right)^{4}\left(1+\frac{C_{f16bp}^{c}}{K_{f16bp}^{PK}}+\frac{C_{g16bp}^{c}}{K_{g16bp}^{PK}}\right)^{4}}$$

$V_{mf}^{PK} = 2.02*10^{3} mM\ h^{-1}$
$V_{mf}^{PK} = 4.75 mM\ h^{-1}$
$K_{pep}^{PK} = 2.25*10^{-1} mM$
$K_{MgADP}^{PK} = 4.74*10^{-1} mM$
$K_{MgATP}^{PK} = 3\ mM$
$K_{ATP}^{PK} = 3.39\ mM$
$K_{pyr}^{PK} = 4\ mM$
$K_{f16bp}^{PK} = 5.0*10^{-3} mM$
$K_{g16bp}^{PK} = 0.1\ mM$
$L_{PK} = 0.398$
$K_{ala}^{PK} = 0.02\ mM$

<u>Lactate Dehydrogenase</u> (LDH): The rate equation for LDH and the kinetic constants were adopted from previous literature [94,221-223]. The kinetics of LDH was modeled as ordered bi bi steady state kinetics, with substrate inhibition by pyruvate.

Eq. S12:

$$r_{LDH} = \frac{V_{mf}^{LDH} \frac{C_{NADH}^{c} C_{pyr}^{c}}{K_{i,NADH}^{LDH} K_{pyr}^{LDH}} - V_{mr}^{LDH} \frac{C_{NAD}^{c} C_{lac}^{c}}{K_{i,NAD}^{LDH} K_{lac}^{LDH}}}{\left(1+\frac{K_{NADH}^{LDH} C_{pyr}^{c}}{K_{i,NADH}^{LDH} K_{pyr}^{LDH}}+\frac{K_{NAD}^{LDH} C_{lac}^{c}}{K_{i,NAD}^{LDH} K_{lac}^{LDH}}\right)\left(1+\frac{C_{pyr}^{c}}{K_{i,pyr}^{"LDH}}\right)+\frac{C_{NADH}^{c}}{K_{i,NADH}^{LDH}}+\frac{C_{NAD}^{c}}{K_{i,NAD}^{LDH}}} + \frac{C_{NADH}^{c} C_{pyr}^{c}}{K_{i,NADH}^{LDH} K_{pyr}^{LDH}} + \frac{K_{NAD}^{LDH} C_{NADH}^{c} C_{lac}^{c}}{K_{i,NAD}^{LDH} K_{i,NADH}^{LDH} K_{lac}^{LDH}} + \frac{K_{NADH}^{LDH} C_{NAD}^{c} C_{pyr}^{c}}{K_{i,NAD}^{LDH} K_{i,NADH}^{LDH} K_{pyr}^{LDH}} + \frac{C_{NAD}^{c} C_{lac}^{c}}{K_{i,NAD}^{LDH} K_{lac}^{LDH}} + \frac{C_{NADH}^{c} C_{pyr}^{c} C_{lac}^{c}}{K_{i,NADH}^{LDH} K_{pyr}^{LDH} K_{i,lac}^{LDH}} + \frac{C_{NAD}^{c} C_{pyr}^{c} C_{lac}^{c}}{K_{i,NAD}^{LDH} K_{i,pyr}^{LDH} K_{lac}^{LDH}}$$

$V_{mf}^{LDH} = 8.66*10^{2} mM\ h^{-1}$
$V_{mr}^{LDH} = 2.17*10^{2} mM\ h^{-1}$
$K_{pyr}^{LDH} = 0.2\ mM$
$K_{i,pyr}^{LDH} = 0.228\ mM$
$K_{NAD}^{LDH} = 0.107\ mM$
$K_{i,NAD}^{LDH} = 0.503\ mM$
$K_{lac}^{LDH} = 10.1\ mM$
$K_{i,lac}^{LDH} = 30\ mM$
$K_{i,NADH}^{LDH} = 2.45*10^{-3}\ mM$
$K_{NADH}^{LDH} = 8.44*10^{-3}\ mM$
$K_{i,pyr}^{"LDH} = 0.101\ mM$

Pentose Phosphate Pathway

Glucose 6-phosphate Dehydrogenase (G6PD)

G6PD is part of oxidative pentose phosphate pathway. Kinetics of G6PD was modeled as ordered bi bi steady state kinetics [224]. The rate equation for G6PD was taken from [225]. The kinetic constants were adopted from previous literature [226,227].

Eq. S13:

$$r_{G6PD}=\frac{V_{mf}^{G6PD}C_{NADP}^{c}C_{g6p}^{c}-V_{mr}^{G6PD}C_{6pg}^{c}C_{NADPH}^{c}}{D_{G6PD}}$$

$$V_{mf}^{G6PD}=4.39*10^{20}\,mM^{-1}h^{-1}$$

$$V_{mr}^{G6PD}=7.48*10^{19}\,mM^{-1}h^{-1}$$

$$D_{G6PD}=1.45*10^{15}+2.04*10^{20}C_{NADPH}^{c}+1.83*10^{20}C_{NADP}^{c}+$$
$$C_{g6p}^{c}\left(4.29*10^{19}+6.01*10^{24}C_{NADPH}^{c}+6.84*10^{24}C_{NADP}^{c}\right)+$$
$$C_{6pg}^{c}\left(5.74*10^{17}+5.01*10^{24}C_{NADPH}^{c}+7.26*10^{22}C_{NADP}^{c}+C_{g6p}^{c}\left(1.10*10^{29}C_{NADPH}^{c}+8.65*10^{27}C_{NADP}^{c}\right)\right)$$

6-Phosphogluconate Dehydrogenase (6PGD):

6PGD is part of oxidative pentose phosphate pathway. Kinetics of 6PGD was modeled as ordered sequential bi ter steady state kinetics [228]. The rate equation for 6PGD was taken from [225]. The kinetic constants were adopted from previous literature [229,230].

Eq. S14:

$$r_{6PGD}=\frac{V_{mf}^{6PGD}C_{NADP}^{c}C_{6pg}^{c}-V_{mr}^{6PGD}C_{ru5p}^{c}C_{NADPH}^{c}CO_{2}}{D_{6PGD}}$$

$$V_{mf}^{6PGD}=1.83*10^{19}\,mM^{-1}h^{-1}$$

$$V_{mr}^{6PGD}=9.0*10^{19}\,mM^{-2}h^{-1}$$

$$D_{6PGD}=5.38*10^{15}+7.86*10^{19}C_{NADPH}^{c}+6.97*10^{18}C_{NADP}^{c}+$$
$$C_{ru5p}^{c}\left(1.04*10^{18}+3.99*10^{23}C_{NADPH}^{c}+3.03*10^{21}C_{NADP}^{c}\right)+$$
$$C_{6pg}^{c}\left(7.26*10^{18}+2.40*10^{23}C_{NADPH}^{c}+4.46*10^{23}C_{NADP}^{c}+C_{ru5p}^{c}\left(2.63*10^{27}C_{NADPH}^{c}+3.19*10^{27}C_{NADP}^{c}\right)\right)$$

Ribulose Phosphate Epimerase (RPE)

RPE is part of non-oxidative pentose phosphate pathway. Kinetics of RPE was modeled as steady state uni uni mechanism. The kinetic constants were adopted from previous literature [231-234].

Eq. S15:

$$r_{RPE} = \frac{V_{mf}^{RPE}\frac{C_{ru5p}^{c}}{K_{f}^{RPE}} - V_{mr}^{RPE}\frac{C_{xyl5p}^{c}}{K_{r}^{RPE}}}{1+\frac{C_{ru5p}^{c}}{K_{f}^{RPE}}+\frac{C_{xyl5p}^{c}}{K_{r}^{RPE}}}$$

$$V_{mf}^{RPE} = 4.642*10^{4}\,mM\ h^{-1}$$
$$V_{mr}^{RPE} = 6.667*10^{4}\,mM\ h^{-1}$$
$$K_{f}^{RPE} = 1.90*10^{-1}\,mM$$
$$K_{r}^{RPE} = 5.00*10^{-1}\,mM$$

Ribose Phosphate Isomerase (RPI)

RPI is part of non-oxidative pentose phosphate pathway. Kinetics of RPI was modeled as steady state uni uni mechanism. The kinetic constants were adopted from previous literature [231,232,235,236].

Eq. S16:

$$r_{RPI} = \frac{V_{mf}^{RPI}\frac{C_{ru5p}^{c}}{K_{f}^{RPI}} - V_{mr}^{RPI}\frac{C_{r5p}^{c}}{K_{r}^{RPI}}}{1+\frac{C_{ru5p}^{c}}{K_{f}^{RPI}}+\frac{C_{r5p}^{c}}{K_{r}^{RPI}}}$$

$$V_{mf}^{RPI} = 2.56*10^{4}\,mM\ h^{-1}$$
$$V_{mr}^{RPI} = 1.09*10^{4}\,mM\ h^{-1}$$
$$K_{f}^{RPI} = 7.80*10^{-1}\,mM$$
$$K_{r}^{RPI} = 2.20\ mM$$

Phosphoribosylpyrophosphate Synthetase (PRPPS)

PRPPS channels ribose-5-phosphate (*r5p*) towards nucleotide synthesis. The rate is relatively small portion of total PPP flux. Kinetics of PRPPS was modeled as rapid

equilibrium random bi reactant system. The kinetic constants were adopted from previous literature [237].

Eq. S17:

$$r_{PRPPS} = V_m^{PRPPS} \frac{C^c_{MgATP} C^c_{r5p}}{\left(K^{PRPPS}_{MgATP} + C^c_{MgATP}\right)\left(K^{PRPPS}_{r5p} + C^c_{r5p}\right)}$$

$$V_m^{PRPPS} = 25.3\ mM\ h^{-1}$$
$$K^{PRPPS}_{MgATP} = 0.01\ mM$$
$$K^{PRPPS}_{r5p} = 0.57\ mM$$

<u>Transketolase1</u> (TK1)

TK1 is part of non-oxidative pentose phosphate pathway. Kinetics of TK1 was modeled as steady state bi bi ping pong mechanism. The kinetic constants were adopted from previous literature [231,232,238].

Eq. S18:

$$r_{TK1} = \frac{V^{TK1}_{mf} C^c_{xyl5p} C^c_{r5p} - V^{TK1}_{mr} C^c_{s7p} C^c_{gap}}{D_{TK1}}$$

$$D_{TK1} = 2.63*10^{16} C^c_{s7p} + C^c_{r5p}\left(4.40*10^{16} + 4.92*10^{16} C^c_{s7p}\right) + 5.96*10^{16} C^c_{gap} + 6.94*10^{16} C^c_{s7p} C^c_{gap} + C^c_{xyl5P}\left(7.35*10^{16} + 2.44*10^{17} C^c_{r5p} + 3.38*10^{17} C^c_{gap}\right)$$

$$V^{TK1}_{mf} = 5.3210^{18}\ mM^{-1} h^{-1}$$
$$V^{TK1}_{mr} = 2.58*10^{18}\ mM^{-1} h^{-1}$$

<u>Transaldolase</u> (TA)

TA is part of non-oxidative pentose phosphate pathway. Kinetics of TA was modeled as steady state bi bi ping pong mechanism. The rate equation for TA was taken from [231]. The kinetic constants were adopted from previous literature [232,239-241].

Eq. S19:

$$r_{TA}=\frac{V_{mf}^{TA}C_{s7p}^{c}C_{gap}^{c}-V_{mr}^{TA}C_{f6p}^{c}C_{e4p}^{c}}{D_{TA}}$$

$$D_{TA}=3.4*10^{16}C_{s7p}^{c}+2.38*10^{16}C_{gap}^{c}+1.64*10^{17}C_{e4p}^{c}+2.72*10^{15}C_{f6p}^{c}+4.41*10^{17}C_{s7p}^{c}C_{gap}^{c}+7.83*10^{16}C_{e4p}^{c}C_{F6P}^{c}+2.21*10^{16}C_{gap}^{c}C_{f6p}^{c}+2.1*10^{18}C_{s7p}^{c}C_{e4p}^{c}$$

$$V_{mf}^{TA}=1.36*10^{20}\,mM^{-1}h^{-1}$$

$$V_{mr}^{TA}=7.53*10^{19}\,mM^{-1}h^{-1}$$

<u>Transketolase2</u> (TK2)

TK2 is part of non-oxidative pentose phosphate pathway. Kinetics of TK2 was modeled as steady state bi bi ping pong mechanism. The kinetic constants were adopted from previous literature [231,232,238,242].

Eq. S20:

$$r_{TK2}=\frac{V_{mf}^{TK2}C_{xyl5p}^{c}C_{e4p}^{c}-V_{mr}^{TK2}C_{f6p}^{c}C_{gap}^{c}}{D_{TK2}}$$

$$D_{TK2}=\left(3.01*10^{17}C_{e4p}^{c}+5.96*10^{16}C_{gap}^{c}+C_{f6p}^{c}\left(1.25*10^{16}+1.60*10^{17}C_{e4p}^{c}+3.31*10^{16}C_{gap}^{c}\right)\right)+C_{xyl5p}^{c}\left(7.35*10^{16}+1.67*10^{18}C_{e4p}^{c}+3.38*10^{17}C_{gap}^{c}\right)$$

$$V_{mf}^{TK2}=3.64*10^{19}\,mM^{-1}h^{-1}$$

$$V_{mr}^{TK2}=1.23*10^{18}\,mM^{-1}h^{-1}$$

<u>Glutathione Peroxidase</u> (GPX)

GPX oxidizes the reduced form of glutathione (*gsh*) into glutathione disulfide (*gssg*) while hydrogen peroxide (H_2O_2) is reduced into water. Thus this reaction plays an important role in preventing cells from oxidative stress. The kinetics of GPX was modeled as first order reaction kinetics.

Eq. S21:

$$r_{GPX}=V_{f}^{GPX}C_{gsh}^{c}$$

$$V_{f}^{GPX}=1.56*10^{4}\,mM^{-1}h^{-1}$$

Glutathione Reductase (GSSGR)

The enzyme GSSGR converts *gssg* back into *gsh* while NADPH produced in the pentose phosphate pathway is oxidized into NADP. The kinetics of GSSGR was modeled as ordered sequential steady state kinetics [243]. The rate equation for GSSGR was taken from [225]. The kinetic constants were adopted from previous literature [244,245].

Eq. S22:

$$r_{GSSGR}=\frac{V_{mf}^{GSSGR}C_{NADPH}^{c}C_{gssg}^{c}-V_{mr}^{GSSGR}C_{gsh}^{c}C_{NADP}^{c}}{D_{GSSGR}}$$

$$V_{mf}^{GSSGR}=5.5*10^{44}\,mM^{-1}h^{-1}$$

$$V_{mr}^{GSSGR}=1.05*10^{40}\,mM^{-1}h^{-1}$$

$$D_{GSSGR}=1.73*10^{40}+2.88*10^{42}C_{NADPH}^{c}+3.43*10^{41}C_{gssg}^{c}+7.77*10^{35}C_{gsh}^{c}+2.47*10^{41}C_{NADP}^{c}$$
$$+4.02*10^{43}C_{NADPH}^{c}C_{gssg}^{c}+1.3*10^{38}C_{NADPH}^{c}C_{gsh}^{c}+4.90*10^{42}C_{gssg}^{c}C_{NADP}^{c}+5.55*10^{36}C_{gsh}^{c}C_{gsh}^{c}$$
$$+1.11*10^{37}C_{gsh}^{c}C_{NADP}^{c}+1.24*10^{40}C_{gsh}^{c}C_{NADP}^{c}+3.26*10^{39}C_{NADPH}^{c}C_{gssg}^{c}C_{gsh}^{c}$$
$$+2.08*10^{41}C_{NADPH}^{c}C_{gssg}^{c}C_{gsh}^{c}+9.25*10^{38}C_{NADPH}^{c}C_{gsh}^{c}C_{gsh}^{c}+2.45*10^{41}C_{gssg}^{c}C_{gsh}^{c}C_{NADP}^{c}$$
$$+1.78*10^{39}C_{gsh}^{c}C_{gsh}^{c}C_{NADP}^{c}+2.32*10^{40}C_{NADPH}^{c}C_{gssg}^{c}C_{gsh}^{c}C_{gsh}^{c}+2.74*10^{40}C_{gssg}^{c}C_{gsh}^{c}C_{NADP}^{c}C_{gsh}^{c}$$

TCA Cycle

Pyruvate Dehydrogenase (PDH)

The rate equation for PDH was taken from [246]. The kinetics of PDH was modeled as hexa uni ping pong mechanism.The kinetic constants were adopted from previous literature [247,248].

Eq. S23:

$$r_{PDH} = \frac{V_{f,PDH}\left(C^m_{pyr}C^m_{CoASH}C^m_{NAD^+} - \frac{C^m_{AcCoA}C^m_{NADH}C^m_{CO_2}}{K_{eq,PDH}}\right)}{K^{PDH}_{NAD^+}\alpha_{PDH,i2}C^m_{pyr}C^m_{CoASH} + K^{PHD}_{CoASH}\alpha_{PDH,i1}C^m_{pyr}C^m_{NAD^+} + K^{PDH}_{pyr}C^m_{CoASH}C^m_{NAD^+} + C^m_{pyr}C^m_{CoASH}C^m_{NAD^+}}$$

$$\alpha_{PDH,i1} = \left(1 + \frac{C^m_{AcCoA}}{K^c_{i,AcCoA}}\right)$$

$$\alpha_{PDH,i2} = \left(1 + \frac{C^m_{NADH}}{K^{PDH}_{i,NADH}}\right)$$

$V_{f,PDH} = 189.7 mMh^{-1}$
$K_{eq,PDH} = 1.2*10^4$
$K^{PDH}_{pyr} = 38.8*10^{-3} mM$
$K^{PDH}_{CoASH} = 9.9*10^{-3} mM$
$K^{PDH}_{NAD^+} = 60.7*10^{-3} mM$
$K^{PDH}_{i,AcCoA} = 40.0*10^{-3} mM$
$K^{PDH}_{i,NADH} = 40.2*10^{-3} mM$

<u>Citrate Synthase</u> (CS)

The rate equation for CS was taken from [246]. The kinetic constants were adopted from previous literature [249-252]. The kinetics of CS was modeled as ordered bi bi mechanism.

Eq. S24:

$$r_{CS} = \frac{V_{f,CS}\left(C^m_{OAA}C^m_{AcCoA} - \frac{C^m_{CoASH}C^m_{cit}}{K_{eq,CS}}\right)}{K^{CS}_{i,OAA}K^{CS}_{i,AcCoA}\alpha_{CS,i1} + K^{CS}_{OAA}\alpha_{CS,i1}C^m_{AcCoA} + K^{CS}_{AcCoA}\alpha_{CS,i2}C^m_{OAA} + C^m_{OAA}C^m_{AcCoA}}$$

$$\alpha_{CS,i1} = \left(1 + \frac{C^m_{cit}/P_{cit}}{K^{CS}_{i,cit}}\right)$$

$$\alpha_{CS,i2} = \left(1 + \frac{C^m_{ATP}/P_{ATP}}{K^{CS}_{i,ATP}} + \frac{C^m_{ADP}/P_{ADP}}{K^{CS}_{i,ADP}} + \frac{C^m_{AMP}/P_{AMP}}{K^{CS}_{i,AMP}} + \frac{C^m_{CoASH}}{K^{CS}_{i,CoASH}} + \frac{C^m_{scoa}}{K^{CS}_{i,scoA}}\right)$$

$V_{f,CS} = 1804\ mMh^{-1}$
$K^0_{eq,CS} = 6.22*10^{12}$
$K^{CS}_{OAA} = 4*10^{-3} mM$
$K^{CS}_{AcCoA} = 1.4*10^{-3} mM$
$K^{CS}_{i,OAA} = 3.33*10^{-3} mM$
$K^{CS}_{i,cit} = 1600*10^{-3} mM$
$K^{CS}_{i,ATP} = 900*10^{-3} mM$
$K^{CS}_{i,ADP} = 1800*10^{-3} mM$
$K^{CS}_{i,AMP} = 6000*10^{-3} mM$
$K^{CS}_{i,CoASH} = 67*10^{-3} mM$
$K^{CS}_{i,scoa} = 140*10^{-3} mM$

Aconitase (ACON)

The rate equation for ACON was taken from [246]. The kinetics of ACON employs the steady state uni uni reaction kinetics. The kinetic constants were adopted from previous literature [249,250,253].

Eq. S25:

$$r_{ACON} = \frac{V_{f,ACON}\left(C^m_{cit} - \frac{C^m_{icit}}{K_{eq,ACON}}\right)}{K^{ACON}_{cit} + C^m_{cit} + \frac{K^{ACON}_{cit} C^m_{icit}}{K^{ACON}_{icit}}}$$

$V_{f,ACON} = 1*10^5 mMh^{-1}$
$K_{eq,ACON} = 2.7*10^{-2}$
$K^{ACON}_{cit} = 1161*10^{-3} mM$
$K^{ACON}_{icit} = 434*10^{-3} mM$

Isocitrate Dehydrogenase (IDH)

The rate equation for IDH was taken from [246]. The kinetics of IDH was modeled as ordered bi ter mechanism. The kinetic constants were adopted from previous literature [249,250,254,255].

Eq. S26:

$$r_{IDH} = \frac{V_{f,IDH}\left(1 - \frac{1}{K_{eq,IDH}}\frac{C^m_{akg} C^m_{NADH} C^m_{CO_2}}{C^m_{NAD^+} C^m_{icit}}\right)}{1 + \left(\frac{K^{IDH}_{m,icit}}{C^m_{icit}}\right)^{n_H} \alpha_{IDH,i1} + \frac{K^{IDH}_{m,NAD^+}}{C^m_{NAD^+}}\left(1 + \left(\frac{K^{IDH}_{i,icit}}{C^m_{icit}}\right)^{n_H} \alpha_{IDH,i1} + \frac{C^m_{NADH}}{K^{IDH}_{i,NADH}} \alpha_{IDH,i1}\right)}$$

$$\alpha_{IDH,i1} = \left(1 + \frac{K^{IDH}_{a,ADP} P_{ADP}}{C^m_{ADP} P_{fADP}}\left(1 + \frac{C^m_{ATP} P_{fATP}}{K^{IDH}_{i,ATP} P_{ATP}}\right)\right)$$

$V_{f,AKG} = 2.75*10^4 mMh^{-1}$
$K_{eq,IDH} = 30.5$
$K^{IDH}_{m,NAD^+} = 74*10^{-3} mM$
$K^{IDH}_{m,icit} = 183*10^{-3} mM$
$K^{IDH}_{a,ADP} = 50*10^{-3} mM$
$K^{IDH}_{i,ATP} = 91*10^{-3} mM$
$K^{IDH}_{i,icit} = 23.8*10^{-3} mM$
$K^{IDH}_{i,NADH} = 29*10^{-3} mM$
$n_H = 3$

α-Ketoglutarate Dehydrogenase (AKGD)

The rate equation for AKGD was taken from [246]. The kinetics of AKGD was modeled as hexa uni ping pong ter ter mechanism. The kinetic constants were adopted from previous literature [249,250,256,257].

Eq. S27:

$$r_{AKGD} = \frac{V_{f,AKGD}\left(1-\frac{1}{K_{eq,AKGD}}\frac{C^m_{SCoA}C^m_{NADH}C^m_{CO_2}}{C^m_{akg}C^m_{CoASH}C^m_{NAD^+}}\right)}{1+\left(\frac{K^{AKGD}_{m,akg}}{C^m_{akg}}\right)\alpha_{AKGD,i1}+\frac{K^{AKGD}_{m,CoASH}}{C^m_{CoASH}}\left(1+\frac{C^m_{SCoA}}{K^{AKGD}_{i,SCoA}}\right)+\frac{K^{AKGD}_{m,NAD^+}}{C^m_{NAD^+}}\left(1+\frac{C^m_{NADH}}{K^{AKGD}_{i,NADH}}\right)}$$

$$\alpha_{AKGD,i1} = \left(1+\frac{K^{AKGD}_{a,ADP}P_{ADP}}{C^m_{ADP}P_{fADP}}\left(1+\frac{C^m_{ATP}P_{fATP}}{K^{AKGD}_{i,ATP}P_{ATP}}\right)\right)$$

$V_{f,AKGD} = 2495\ mMh^{-1}$
$K_{eq,AKGD} = 1.66*10^{8}$
$K^{AKGD}_{m,akg} = 120*10^{-3}mM$
$K^{AKGD}_{m,CoaSH} = 55*10^{-3}mM$
$K^{AKGD}_{m,NAD^+} = 21*10^{-3}mM$
$K^{AKGD}_{a,ADP} = 100*10^{-3}mM$
$K^{AKGD}_{i,ATP} = 50*10^{-3}mM$
$K^{AKGD}_{i,SCoA} = 6.9*10^{-3}mM$
$K^{AKGD}_{i,NADH} = 0.60*10^{-3}mM$

Succinyl-CoA Synthetase (SCOAS)

The rate equation for SCOAS was taken from [246]. The kinetics of SCOAS follows the ordered ter ter mechanism. The kinetic constants were adopted from previous literature [249,250,258].

Eq. S28:

$$r_{SCoAS} = \frac{V_{f,SCoAS}\left(C^m_{GDP}C^m_{SCoA}C^m_{Pi} - \frac{C^m_{CoASH}C^m_{suc}C^m_{GTP}}{K_{eq,SCoAS}}\right)}{K^{SCoAS}_{i,GDP}K^{SCoAS}_{i,SCoA}K^{SCoAS}_{m,Pi} + K^{SCoAS}_{i,SCoA}K^{SCoAS}_{m,Pi}C^m_{GDP} + K^{SCoAS}_{i,GDP}K^{SCoAS}_{m,SCoA}C^m_{Pi} + K^{SCoAS}_{m,Pi}C^m_{GDP}C^m_{SCoA} + K^{SCoAS}_{m,SCoA}C^m_{GDP}C^m_{Pi}}$$

$$K^{SCoAS}_{m,GDP}C^m_{SCoA}C^m_{Pi} + C^m_{GDP}C^m_{SCoA}C^m_{Pi} + \left(\frac{K^{SCoAS}_{i,GDP}K^{SCoAS}_{i,SCoA}K^{SCoAS}_{m,Pi}}{K^{SCoAS}_{i,suc}K^{SCoAS}_{i,GTP}K^{SCoAS}_{m,CoASH}}\right)\left(K^{SCoAS}_{i,GTP}K^{SCoAS}_{m,suc}C^m_{CoASH} + K^{SCoAS}_{i,suc}K^{SCoAS}_{m,CoASH}C^m_{GTP} + \right.$$

$$K^{SCoAS}_{m,GTP}C^m_{CoASH}C^m_{suc} + K^{SCoAS}_{m,suc}C^m_{CoASH}C^m_{GTP} + K^{SCoAS}_{m,CoASH}C^m_{suc}C^m_{GTP} + C^m_{CoASH}C^m_{suc}C^m_{GTP} + \frac{K^{SCoAS}_{m,suc}K^{SCoAS}_{i,GTP}C^m_{GDP}C^m_{SCoA}C^m_{suc}}{K^{SCoAS}_{i,GDP}K^{SCoAS}_{i,SCoA}}$$

$$+ \frac{K^{SCoAS}_{m,GTP}C^m_{GDP}C^m_{CoASH}C^m_{suc}}{K^{SCoAS}_{i,GDP}} + \frac{K^{SCoAS}_{i,GTP}K^{SCoAS}_{m,suc}C^m_{GDP}C^m_{SCoA}C^m_{Pi}C^m_{CoASH}}{K^{SCoAS}_{i,GDP}K^{SCoAS}_{i,SCoA}K^{SCoAS}_{i,Pi}} + \frac{K^{SCoAS}_{m,suc}K^{SCoAS}_{i,GTP}C^m_{GDP}C^m_{CoASH}}{K^{SCoAS}_{i,GDP}}$$

$$\left. + \frac{K^{SCoAS}_{i,CoASH}K^{SCoAS}_{m,GTP}C^m_{GDP}C^m_{SCoA}C^m_{Pi}C^m_{suc}}{K^{SCoAS}_{i,GDP}K^{SCoAS}_{i,SCoA}K^{SCoAS}_{i,Pi}} + \frac{K^{SCoAS}_{m,GTP}C^m_{GDP}C^m_{SCoA}C^m_{CoASH}C^m_{suc}}{K^{SCoAS}_{i,GDP}K^{SCoAS}_{i,SCoA}} + \frac{K^{SCoAS}_{m,GTP}C^m_{GDP}C^m_{SCoA}C^m_{Pi}C^m_{CoASH}C^m_{suc}}{K^{SCoAS}_{i,GDP}K^{SCoAS}_{i,SCoA}K^{SCoAS}_{i,Pi}}\right)$$

$$+ \frac{K^{SCoAS}_{i,GDP}K^{SCoAS}_{m,SCoA}C^m_{Pi}C^m_{suc}C^m_{GTP}}{K^{SCoAS}_{i,suc}K^{SCoAS}_{i,GTP}} + \frac{K^{SCoAS}_{m,GDP}K^{SCoAS}_{i,Pi}C^m_{SCoA}C^m_{CoASH}C^m_{suc}C^m_{GTP}}{K^{SCoAS}_{i,CoASH}K^{SCoAS}_{i,suc}K^{SCoAS}_{i,GTP}} + \frac{K^{SCoAS}_{i,GDP}K^{SCoAS}_{m,SCoA}C^m_{Pi}C^m_{CoASH}C^m_{suc}C^m_{GTP}}{K^{SCoAS}_{i,CoASH}K^{SCoAS}_{i,suc}K^{SCoAS}_{i,GTP}} +$$

$$+ \frac{K^{SCoAS}_{m,GDP}C^m_{SCoA}C^m_{Pi}C^m_{GTP}}{K^{SCoAS}_{i,GTP}} + \frac{K^{SCoAS}_{i,GDP}K^{SCoAS}_{m,SCoA}C^m_{Pi}C^m_{GTP}}{K^{SCoAS}_{i,GTP}} + \frac{K^{SCoAS}_{m,GDP}C^m_{SCoA}C^m_{Pi}C^m_{suc}C^m_{GTP}}{K^{SCoAS}_{i,suc}K^{SCoAS}_{i,GTP}} + \frac{K^{SCoAS}_{m,GDP}C^m_{SCoA}C^m_{Pi}C^m_{CoASH}C^m_{suc}C^m_{GTP}}{K^{SCoAS}_{i,GDP}K^{SCoAS}_{i,SCoA}K^{SCoAS}_{i,Pi}}$$

$V_{f,SCoAS} = 362\ mMh^{-1}$ $\quad$ $K^{SCoAS}_{m,GTP} = 11.1*10^{-3}mM$

$K_{eq,SCOAS} = 7.43$ $\quad$ $K^{SCoAS}_{i,GDP} = 5.5*10^{-3}mM$

$K^{SCoAS}_{m,GDP} = 16*10^{-3}mM$ $\quad$ $K^{SCoAS}_{i,SCoA} = 100*10^{-3}mM$

$K^{SCoAS}_{m,SCoA} = 55*10^{-3}mM$ $\quad$ $K^{SCoAS}_{i,Pi} = 2000*10^{-3}mM$

$K^{SCoAS}_{m,Pi} = 660.0*10^{-3}mM$ $\quad$ $K^{SCoAS}_{i,CoaSH} = 20*10^{-3}mM$

$K^{SCoAS}_{m,CoaSH} = 20*10^{-3}mM$ $\quad$ $K^{SCoAS}_{i,suc} = 3000*10^{-3}mM$

$K^{SCoAS}_{m,suc} = 880*10^{-3}mM$ $\quad$ $K^{SCoAS}_{i,GTP} = 11.1*10^{-3}mM$

<u>Succinate Dehydrogenase</u> (SDH)

The rate equation for SDH was taken from [246]. The kinetics of SDH was modeled as Theorell-Chance bi bi mechanism. The kinetic constants were adopted from previous literature [249,250,259-261].

Eq. S29:

$$r_{SDH} = \frac{V_{f,SDH}\left(C^m_{suc}C^m_{COQ} - \frac{C^m_{QH_2}C^m_{fum}}{K_{eq,SDH}}\right)}{K^{SDH}_{i,suc}K^{SDH}_{m,COQ}\alpha_{SDH,i1} + K^{SDH}_{m,COQ}C^m_{suc} + K^{SDH}_{m,suc}\alpha_{SDH,i1}C^m_{COQ} + C^m_{suc}C^m_{COQ} + \frac{K^{SDH}_{m,suc}}{K^{SDH}_{i,fum}}C^m_{COQ}C^m_{fum} + \left(\frac{K^{SDH}_{i,suc}K^{SDH}_{m,COQ}}{K^{SDH}_{i,fum}K^{SDH}_{m,QH_2}}\right)\left(K^{SDH}_{m,fum}\alpha_{SDH,i1}C^m_{QH_2} + K^{SDH}_{m,QH_2}C^m_{fum} + \frac{K^{SDH}_{m,fum}}{K^{SDH}_{i,suc}}C^m_{suc}C^m_{QH_2} + C^m_{QH_2}C^m_{fum}\right)}$$

$$\alpha_{SDH,i1} = \frac{\left(1 + \frac{C^m_{OAA}}{K^{SDH}_{i,OAA}} + \frac{C^m_{suc}}{K^{SDH}_{a,suc}} + \frac{C^m_{fum}}{K^{SDH}_{a,fum}}\right)}{\left(1 + \frac{C^m_{suc}}{K^{SDH}_{a,suc}} + \frac{C^m_{fum}}{K^{SDH}_{a,fum}}\right)}$$

$V_{f,SDH} = 5.81*10^4\ mMh^{-1}$
$K_{eq,SDH} = 1.21$
$K^{SDH}_{m,suc} = 467*10^{-3}mM$
$K^{SDH}_{m,COQ} = 480*10^{-3}mM$
$K^{SDH}_{m,QH_2} = 2.45*10^{-3}mM$
$K^{SDH}_{m,fum} = 1200*10^{-3}mM$
$K^{SDH}_{i,suc} = 120*10^{-3}mM$
$K^{SDH}_{i,fum} = 1275*10^{-3}mM$
$K^{SDH}_{i,OAA} = 1.5*10^{-3}mM$
$K^{SCoAS}_{a,suc} = 450*10^{-3}mM$
$K^{SCoAS}_{a,fum} = 375*10^{-3}mM$

<u>Fumarase</u> (FUM)

The rate equation for FUM was taken from [246]. The kinetics of FUM was modeled as ordered uni uni mechanism. The kinetic constants were adopted from previous literature [249,250,259,262,263].

Eq. S30:

$$r_{FUM} = \frac{V_{f,FUM}\left(C^m_{fum} - \frac{C^m_{mal}}{K_{eq,FUM}}\right)}{K^{FUM}_{m,fum}\alpha_{FUM,i1} + C^m_{fum} + \frac{K^{FUM}_{m,fum}C^m_{mal}}{K^{FUM}_{m,mal}}}$$

$$\alpha_{FUM,i1} = 1 + \frac{C^m_{cit}}{K^{FUM}_{i,cit}} + \frac{C^m_{ATP}P_{fATP}}{K^{FUM}_{i,ATP}P_{ATP}} + \frac{C^m_{ADP}P_{fADP}}{K^{FUM}_{i,ADP}P_{ADP}} + \frac{C^m_{GTP}P_{fGTP}}{K^{FUM}_{i,GTP}P_{GTP}} + \frac{C^m_{GDP}P_{fGDP}}{K^{FUM}_{i,GDP}P_{GDP}}$$

$V_{f,FUM} = 2.21*10^4\ mMh^{-1}$
$K_{eq,FUM} = 4.56$
$K^{FUM}_{m,fum} = 44.7*10^{-3}mM$
$K^{FUM}_{m,mal} = 197.7*10^{-3}mM$
$K^{FUM}_{i,cit} = 3500*10^{-3}mM$
$K^{FUM}_{i,ATP} = 40*10^{-3}mM$
$K^{SDH}_{i,ADP} = 400*10^{-3}mM$
$K^{SDH}_{i,GTP} = 80*10^{-3}mM$
$K^{SDH}_{i,GDP} = 330*10^{-3}mM$

<u>Malate Dehydrogenase 2</u> (MDH2)

MDH2 is the isoform that is present in the mitochondria. The rate equation for MDH2 was taken from [246]. The kinetics of MDH2 employs the ordered bi bi mechanism. The kinetic constants were adopted from previous literature [249,250,264,265].

Eq. S31:

$$r_{MDH2} = \frac{V_{f,MDH2}\left(C^m_{NAD^+}C^m_{mal} - \frac{C^m_{OAA}C^m_{NADH}}{K_{eq,MDH2}}\right)}{K^{MDH2}_{i,NAD^+}K^{MDH2}_{m,mal}\alpha_{MDH2,i} + K^{MDH2}_{m,mal}C^m_{NAD^+} + K^{MDH2}_{m,NAD^+}\alpha_{MDH2,i}C^m_{mal} + C^m_{NAD^+}C^m_{mal} + \frac{K^{MDH2}_{m,NAD^+}C^m_{mal}C^m_{NADH}}{K^{MDH2}_{i,NADH}} + \frac{C^m_{NAD^+}C^m_{mal}C^m_{OAA}}{K^{MDH2}_{i,OAA}} + \left(\frac{K^{MDH2}_{i,NAD^+}K^{MDH2}_{m,mal}}{K^{MDH2}_{i,NADH}K^{MDH2}_{m,OAA}}\right)\left(K^{MDH2}_{m,NADH}\alpha_{MDH2,i}C^m_{OAA} + K^{MDH2}_{m,OAA}C^m_{NADH} + \frac{K^{MDH2}_{mNADH}}{K^{MDH2}_{i,NAD^+}}C^m_{NAD^+}C^m_{OAA} + C^m_{OAA}C^m_{NADH} + \frac{C^m_{mal}C^m_{OAA}C^m_{NADH}}{K^{MDH2}_{i,mal}}\right)}$$

$$\alpha_{MDH2,i} = \left(1 + \frac{C^m_{ATP}P_{fATP}}{K^{MDH2}_{i,ATP}P_{ATP}} + \frac{C^m_{ADP}P_{fADP}}{K^{MDH2}_{i,ADP}P_{ADP}} + \frac{C^m_{AMP}P_{fAMP}}{K^{MDH2}_{i,AMP}P_{AMP}}\right)$$

$V_{f,MDH2} = 3.53*10^{8}\ mMh^{-1}$
$K_{eq,MDH2} = 4.02*10^{-4}$
$K^{MDH2}_{m,NAD^+} = 90.55*10^{-3}mM$
$K^{MDH2}_{m,mal} = 250*10^{-3}mM$
$K^{MDH2}_{m,OAA} = 6.128*10^{-3}mM$
$K^{MDH2}_{m,NADH} = 2.58*10^{-3}mM$
$K^{MDH2}_{i,NAD^+} = 279*10^{-3}mM$
$K^{MDH2}_{i,mal} = 360*10^{-3}mM$
$K^{MDH2}_{i,OAA} = 5.5*10^{-3}mM$
$K^{MDH2}_{i,NADH} = 3.18*10^{-3}mM$
$K^{MDH2}_{i,ATP} = 183.2*10^{-3}mM$
$K^{MDH2}_{i,ADP} = 394.4*10^{-3}mM$
$K^{MDH2}_{i,AMP} = 420.0*10^{-3}mM$

NAD/NADH Shuttles

Glutamate Oxaloacetate Transaminase 2 (GOT2)

GOT2 is the isoform that is present in the mitochondria. The rate equation for GOT2 was taken from [246]. The kinetics of GOT2 is modeled as ping pong bi bi mechanism. The kinetic constants were adopted from previous literature [266].

Eq. S32:

$$r_{GOT2} = \frac{V_{f,GOT2}\left(C^m_{asp}C^m_{akg} - \frac{C^m_{OAA}C^m_{glu}}{K_{eq,GOT2}}\right)}{K^{GOT2}_{m,akg}C^m_{asp} + K^{GOT2}_{m,asp}\alpha_{GOT2,i}C^m_{akg} + C^m_{asp}C^m_{akg} + \frac{K^{GOT2}_{m,asp}C^m_{akg}C^m_{glu}}{K^{GOT2}_{i,glu}} + \left(\frac{K^{GOT2}_{i,asp}K^{GOT}_{m,akg}}{K^{GOT2}_{m,OAA}K^{GOT2}_{i,glu}}\right)\left(\frac{K^{GOT2}_{m,glu}C^m_{asp}C^m_{OAA}}{K^{GOT2}_{i,asp}} + C^m_{OAA}C^m_{glu} + K^{GOT2}_{m,glu}\alpha_{GOT2,i}C^m_{OAA} + K^{GOT2}_{m,OAA}C^m_{glu}\right)}$$

$$\alpha_{GOT2,i} = \left(1 + \frac{C^m_{akg}}{K^{GOT2}_{i,akg}}\right)$$

$V_{f,GOT} = 3.87 * 10^6\ mMh^{-1}$
$K_{eq,GOT} = 1.56$
$K^{GOT}_{m,asp} = 0.89\ mM$
$K^{GOT}_{m,akg} = 3.22\ mM$
$K^{GOT}_{m,OAA} = 88 * 10^{-3}\ mM$
$K^{GOT}_{m,glu} = 32.5\ mM$
$K^{GOT}_{i,asp} = 3.9\ mM$
$K^{GOT}_{i,akg} = 0.73\ mM$
$K^{GOT}_{i,OAA} = 48 * 10^{-3}\ mM$
$K^{GOT}_{i,glu} = 10.7\ mM$
$K^{GOT}_{i,AKG} = 26.5\ mM$

Malate Dehydrogenase 1 (MDH1)

MDH1 is the isoform that is present in the mitochondria. The rate equation and kinetic constants for MDH1 were taken from [267]. The kinetics of MDH1 was modeled as ordered bi bi mechanism.

Eq. S33:

$$r_{MDH1} = \frac{V_{mf,MDH1}\left(C^c_{OAA}C^c_{NADH} - \frac{C^c_{NAD^+}C^c_{mal}}{K_{eq,MDH1}}\right)}{K^{MDH1}_{i,NADH}K^{MDH1}_{m,OAA} + K^{MDH1}_{m,OAA}C^c_{NADH} + K^{MDH1}_{m,NADH}C^c_{OAA} + C^c_{OAA}C^c_{NADH} + \frac{K^{MDH1}_{m,NADH}C^c_{OAA}C^c_{NAD^+}}{K^{MDH1}_{i,NAD^+}} + \frac{C^c_{OAA}C^c_{NADH}C^c_{mal}}{K^{MDH1}_{i,mal}}}$$
$$+ \frac{K^{MDH1}_{i,NADH}K^{MDH1}_{m,OAA}}{K^{MDH1}_{i,NAD^+}K^{MDH1}_{m,mal}}\left(K^{MDH1}_{m,NAD^+}C^c_{mal} + K^{MDH1}_{m,mal}C^c_{NAD^+} + \frac{K^{MDH1}_{m,NAD^+}C^c_{Mal}C^c_{NADH}}{K^{MDH1}_{i,NADH}} + C^c_{NAD^+}C^c_{Mal} + \frac{C^c_{Mal}C^c_{OAA}C^c_{NAD^+}}{K^{MDH1}_{i,OAA}}\right)$$

$V_{mf,MDH1} = 3.59*10^7\ mM\ h^{-1}$
$K_{eq,MDH1} = 2.67*10^4$
$K^{MDH1}_{m,NAD^+} = 0.114\ mM$
$K^{MDH1}_{m,mal} = 1.1\ mM$
$K^{MDH1}_{m,OAA} = 0.088\ mM$
$K^{MDH1}_{m,NADH} = 0.026\ mM$
$K^{MDH1}_{i,NADH} = 4.9*10^{-3}\ mM$
$K^{MDH1}_{i,OAA} = 63*10^{-3}\ mM$
$K^{MDH1}_{i,mal} = 7.1\ mM$
$K^{MDH1}_{i,NAD^+} = 0.94\ mM$

<u>Glutamate Oxaloacetate Transaminase 1</u> (GOT1)

GOT1 is the isoform that is present in the cytosol. The rate equation for GOT1 was taken from [246]. The kinetics of GOT1 was modeled as ping pong bi bi mechanism. The kinetic constants were adopted from previous literature [266].

Eq. S34:

$$r_{GOT1} = \frac{V_{mf,GOT1}\left(C^c_{asp}C^c_{akg} - \frac{C^c_{OAA}C^c_{glu}}{K_{eq,GOT1}}\right)}{K^{GOT1}_{m,akg}C^c_{asp} + K^{GOT1}_{m,asp}\alpha_{GOT1,i}C^c_{akg} + C^c_{asp}C^c_{akg} + \frac{K^{GOT1}_{m,asp}C^c_{akg}C^c_{glu}}{K^{GOT1}_{i,glu}} +}$$
$$\left(\frac{K^{GOT1}_{i,asp}K^{GO1}_{m,akg}}{K^{GOT1}_{m,OAA}K^{GOT1}_{i,glu}}\right)\left(\frac{K^{GOT1}_{m,glu}C^c_{asp}C^c_{OAA}}{K^{GOT1}_{i,asp}} + C^c_{OAA}C^c_{glu} + K^{GOT1}_{m,glu}\alpha_{GOT1,i}C^c_{OAA} + K^{GOT1}_{m,OAA}C^c_{glu}\right)$$

$$\alpha_{GOT1,i} = \left(1 + \frac{C^c_{akg}}{K^{GOT1}_{i,akg}}\right)$$

$V_{mf,GOT1} = 2.36*10^3\ mMh^{-1}$
$K_{eq,GOT} = 1.56$
$K^{GOT}_{m,asp} = 4.4mM$
$K^{GOT}_{m,akg} = 0.38mM$
$K^{GOT}_{m,OAA} = 95*10^{-3}mM$
$K^{GOT}_{m,glu} = 9.6mM$
$K^{GOT}_{i,asp} = 3.9mM$
$K^{GOT}_{i,akg} = 0.73mM$
$K^{GOT}_{i,OAA} = 48*10^{-3}mM$
$K^{GOT}_{i,glu} = 8.4mM$
$K^{GOT}_{i,akg} = 26.5mM$

α-Ketoglutarate –Malate shuttle (AKGMAL)

The rate equation for AKGMAL was taken from [246]. The kinetics of AKGMAL was modeled as rapid equilibrium random bi bi mechanism. The kinetic constants were adopted from previous literature [268].

Eq. S35:

$$r_{AKGMAL} = \frac{V_{mf,AKGMAL}\left(C^c_{akg}C^m_{mal} - C^m_{akg}C^c_{mal}\right)}{K^{AKGMAL}_{m,akgi}K^{AKGMAL}_{m,malx}\left(2 + \frac{C^c_{mal}}{K^{AKGMAL}_{m,mali}} + \frac{C^m_{mal}}{K^{AKGMAL}_{m,malx}} + \frac{C^c_{akg}}{K^{AKGMAL}_{m,akgi}} + \frac{C^m_{akg}}{K^{AKGMAL}_{m,akgx}} + \frac{C^c_{mal}C^m_{akg}}{K^{AKGMAL}_{m,mali}K^{AKGMAL}_{m,akgx}} + \frac{C^m_{mal}C^c_{akgi}}{K^{AKGMAL}_{m,malx}K^{AKGMAL}_{m,akgi}}\right)}$$

$V_{mf,AKGMAL} = 3.19*10^6\ mM\ h^{-1}$

$K^{AKGMAL}_{m,mali} = 0.4\ mM$

$K^{AKGMAL}_{m,malx} = 10\ mM$

$K^{AKGMAL}_{m,akgi} = 1.3\ mM$

$K^{AKGMAL}_{m,akgx} = 0.17\ mM$

Aspartate –Glutamate shuttle (ASPGLU)

The rate equation for ASPGLU was taken from [246]. The kinetics of ASPGLU was modeled as rapid equilibrium random bi bi with charge translocation mechanism. The kinetic constants were adopted from previous literature [269].

Eq. S36:

$$r_{ASPGLU} = \frac{V_{mf,ASPGLU}\left(K_{eq,ASPGLU}C^c_{asp}C^m_{glu}C^m_{H^+} - C^m_{asp}C^c_{glu}C^c_{H^+}\right)}{K_{eq,ASPGLU}K^{ASPGLU}_{i,aspi}K^{ASPGLU}_{i,glux}K^{ASPGLU}_{H^+}\left(2m + m\frac{C^c_{asp}}{K^{ASPGLU}_{i,aspi}} + \frac{C^c_{asp}C^m_{glu}C^m_{H^+}}{K^{ASPGLU}_{i,aspi}K^{ASPGLU}_{i,glux}K^{ASPGLU}_{H^+}} + m\frac{C^m_{asp}C^c_{H^+}}{K^{ASPGLU}_{i,aspx}K^{ASPGLU}_{H^+}} + m\frac{C^m_{asp}}{K^{ASPGLU}_{i,aspx}} + \frac{C^m_{asp}C^c_{glu}C^c_{H^+}}{K^{ASPGLU}_{i,aspx}K^{ASPGLU}_{i,glui}K^{ASPGLU}_{H^+}} + m\frac{C^c_{asp}C^m_{H^+}}{K^{ASPGLU}_{i,aspi}K^{ASPGLU}_{H^+}} + m\frac{C^m_{H^+}}{K^{ASPGLU}_{H^+}} + m\frac{C^c_{glu}C^c_{H^+}}{K^{ASPGLU}_{i,glui}K^{ASPGLU}_{H^+}} + m\frac{C^c_{H^+}}{K^{ASPGLU}_{H^+}} + m\frac{C^m_{glu}C^m_{H^+}}{K^{ASPGLU}_{i,glux}K^{ASPGLU}_{H^+}}\right)}$$

$V_{mf,ASPGLU} = 2.49*10^{4} mM\ h^{-1}$

$K_{eq,ASPGLU} = 0.6$

$K_{i,aspi}^{ASPGLU} = 0.028\ mM$

$K_{i,aspx}^{ASPGLU} = 2.8\ mM$

$K_{i,glui}^{ASPGLU} = 0.18\ mM$

$K_{i,glux}^{ASPGLU} = 1.6\ mM$

$K_{H^+}^{ASPGLU} = 10^{-6.5} mM$

$m = 1.8$

Transporters

Glucose Transporter (GLUT): Glucose transporters mediate transport of glucose across plasma membranes. Till date, fourteen glucose transporters (isozymes) have been identified which perform the same function but have very different kinetic properties [270]. Kinetics of the GLUT1 isozyme was considered in the model and was modeled as uni uni steady state kinetics.

Eq. S37:

$$r_{GlcTr} = \frac{V_{mf}^{GlcTr}\frac{C_{glc}^{e}}{K_{glc}^{GlcTr}} - V_{mr}^{GlcTr}\frac{C_{glc}^{c}}{K_{glc}^{GlcTr}}}{1 + \frac{C_{glc}^{e}}{K_{glc}^{GlcTr}} + \frac{C_{glc}^{c}}{K_{glc}^{GlcTr}}}$$

$V_{mf}^{GlcTr} = 7.67\ \text{mM}h^{-1}$

$V_{mr}^{GlcTr} = 0.767\ \text{mM}h^{-1}$

$K_{glc}^{GlcTr} = 1.50\ mM$

Pyruvate –Hydrogen shuttle (PYRH)

PYRH was modeled as reversible mass action kinetics. The rate equation was taken from [246].

Eq. S38:

$$r_{PYRH} = V_{m,PYRH}\left(C^{c}_{pyr}C^{c}_{H^+} - C^{m}_{pyr}C^{m}_{H^+}\right) \qquad V_{m,PYRH}=1*10^{13}\ mM\ h^{-1}$$

<u>Citrate –Malate shuttle</u> (CITMAL)

CITMAL was modeled as reversible mass action kinetics. The rate equation was taken from [246].

Eq. S39:

$$r_{CITMAL} = V_{m,CITMAL}\left(C^{c}_{cit}C^{m}_{mal} - C^{m}_{cit}C^{c}_{mal}\right) \qquad V_{m,CITMAL} = 296.6\,mM\ h^{-1}$$

<u>Malate-Phosphate shuttle</u> (MALPi)

MALPi was modeled as reversible mass action kinetics. The rate equation was taken from [246].

Eq. S40:

$$r_{MALPi} = V_{m,MALPi}\left(C^{c}_{mal}C^{m}_{Pi} - C^{m}_{mal}C^{c}_{Pi}\right) \qquad V_{m,MALPi} = 17.3\,mM\ h^{-1}$$

<u>Glutamate-Hydrogen shuttle</u> (GLUH)

GLUH was modeled as reversible mass action kinetics. The rate equation was taken from [246].

Eq. S41:

$$r_{GLUH} = V_{m,GLUH}\left(C^{c}_{glu}C^{c}_{H^+} - C^{m}_{glu}C^{m}_{H^+}\right) \qquad V_{m,GLUH} = 3.87*10^{8}\ mM\ h^{-1}$$

Other Reactions

Glutaminase (GLS)

The kinetics of GLS was modeled as simple Michaelis-Menten kinetics with non-competitive inhibition by glutamate. The kinetic constants for GLS were taken from [271].

Eq. S42:

$$r_{GLS} = \frac{V_{m,GLS}\left(C^{c}_{gln} - \frac{C^{m}_{glu}}{K_{eq,GLS}}\right)}{K^{GLS}_{m,gln}\left(1 + \frac{C^{m}_{glu}}{K^{GLS}_{i,glu}}\right) + C^{c}_{gln}}$$

$$V_{m,GLS} = 38.8\,mM\ h^{-1}$$
$$K_{eq,GLS} = 1$$
$$K^{GLS}_{m,gln} = 12\,mM$$
$$K^{GLS}_{i,glu} = 55\,mM$$

Glutamate Dehydrogenase (GDH)

The kinetic constants for GDH were taken from [272,273]. The kinetics of GDH was modeled as random bi bi mechanism.

Eq. S43:

$$r_{GDH} = \frac{V_{f,GDH}\left(C^{m}_{NAD}C^{m}_{Glu} - \frac{C^{m}_{AKG}C^{m}_{NADH}C^{m}_{NH3}}{K_{eq,GDH}}\right)}{\begin{aligned}
&K^{GDH}_{i,NAD}K^{GDH}_{Glu} + K^{GDH}_{m,Glu}C^{m}_{NAD} + K^{GDH}_{m,NAD}C^{m}_{Glu} + C^{m}_{Glu}C^{m}_{NAD} + \frac{C^{m}_{Glu}C^{m}_{NAD}C^{m}_{NH3}}{K^{GDH}_{i,AKG}} + \frac{K^{GDH}_{i,NAD}K^{GDH}_{m,Glu}C^{m}_{NADH}}{K^{GDH}_{i,NADH}} \\
&+ \frac{K^{GDH}_{m,Glu}C^{m}_{NAD}C^{m}_{NH3}}{K^{GDH}_{i,NH3}} + \frac{K^{GDH}_{i,NAD}K^{GDH}_{m,Glu}K^{GDH}_{m,NADH}C^{m}_{AKG}C^{m}_{NH3}}{K^{GDH}_{m,NH3}K^{GDH}_{i,AKG}K^{GDH}_{i,NADH}} + \frac{K^{GDH}_{m,NAD}C^{m}_{Glu}C^{m}_{NADH}}{K^{GDH}_{i,NADH}} + \frac{C^{m}_{Glu}C^{m}_{AKG}C^{m}_{NAD}C^{m}_{NH3}}{K^{GDH}_{i,NH3}K^{GDH}_{i,AKG}} \\
&+ \frac{K^{GDH}_{i,NAD}K^{GDH}_{m,Glu}K^{GDH}_{m,AKG}C^{m}_{NADH}C^{m}_{NH3}}{K^{GDH}_{m,NH3}K^{GDH}_{i,AKG}K^{GDH}_{i,NADH}} + \frac{K^{GDH}_{i,NAD}K^{GDH}_{m,Glu}K^{GDH}_{m,AKG}C^{m}_{NH3}C^{m}_{AKG}C^{m}_{NADH}}{K^{GDH}_{m,NH3}K^{GDH}_{i,AKG}K^{GDH}_{i,NADH}} + \frac{C^{m}_{Glu}C^{m}_{NAD}C^{m}_{AKG}}{K^{GDH}_{i,AKG}} \\
&+ \frac{K^{GDH}_{i,NAD}K^{GDH}_{m,Glu}K^{GDH}_{m,AKG}C^{m}_{NH3}}{K^{GDH}_{m,NH3}K^{GDH}_{i,AKG}} + \frac{K^{GDH}_{i,NAD}K^{GDH}_{m,Glu}C^{m}_{Glu}C^{m}_{NADH}C^{m}_{AKG}}{K^{GDH}_{i,Glu}K^{GDH}_{i,AKG}K^{GDH}_{i,NADH}} + \frac{K^{GDH}_{i,NAD}K^{GDH}_{m,Glu}C^{m}_{AKG}C^{m}_{NADH}}{K^{GDH}_{i,AKG}K^{GDH}_{i,NADH}} \\
&+ \frac{K^{GDH}_{m,NADH}K^{GDH}_{m,Glu}C^{m}_{NH3}C^{m}_{AKG}C^{m}_{NAD}}{K^{GDH}_{m,NH3}K^{GDH}_{i,AKG}K^{GDH}_{i,NADH}} + \frac{K^{GDH}_{i,NAD}K^{GDH}_{m,Glu}C^{m}_{Glu}C^{m}_{AKG}C^{m}_{NADH}C^{m}_{NH3}}{K^{GDH}_{m,NH3}K^{GDH}_{i,Glu}K^{GDH}_{i,AKG}K^{GDH}_{i,NADH}}
\end{aligned}}$$

$V_{f,GDH} = 5.55*10^{3}\ mM^{-1}h^{-1}$
$K_{m,Glu}^{GDH} = 3.5\ mM$
$K_{m,NADH}^{GDH} = 0.04\ mM$
$K_{m,AKG}^{GDH} = 1.1\ mM$
$K_{m,NH3}^{GDH} = 6\ mM$
$K_{i,AKG}^{GDH} = 0.25\ mM$
$K_{i,NH3}^{GDH} = 6\ mM$
$K_{i,Glu}^{GDH} = 3.5\ mM$
$K_{i,NADH}^{GDH} = 0.004\ mM$
$K_{i,NAD}^{GDH} = 1\ mM$
$K_{eq,GDH} = 0.003$

ATP-Citrate Lyase (CLY)

The kinetics of CLY was modeled as ordered bi bi mechanism. The kinetic constants were adopted from previous literature [274-277].

Eq. S44:

$$r_{CLY} = \frac{V_{m,CLY} C_{cit}^{c} C_{CoASH}^{c}}{K_{i,cit}^{CLY} K_{m,CoASH}^{CLY} + K_{m,cit}^{CLY} C_{CoASH}^{c} + K_{m,AcCoA}^{CLY} C_{cit}^{c} + C_{cit}^{c} C_{CoASH}^{c} + \frac{K_{m,cit}^{CLY} C_{CoASH}^{c} C_{AcCoA}^{c}}{K_{i,AcCoA}^{CLY}} + \frac{C_{cit}^{c} C_{CoASH}^{c} C_{OAA}^{c}}{K_{i,OAA}^{CLY}} + \frac{K_{i,cit}^{CLY} K_{m,CoASH}^{CLY}}{K_{m,OAA}^{CLY} K_{i,AcCoA}^{CLY}} \left(K_{m,AcCoA}^{CLY} C_{OAA}^{c} + K_{m,OAA}^{CLY} C_{AcCoA}^{c} + \frac{K_{m,AcCoA}^{CLY} C_{cit}^{c} C_{OAA}^{c}}{K_{i,cit}^{CLY}} + C_{OAA}^{c} C_{AcCoA}^{c} + \frac{C_{CoASH}^{c} C_{OAA}^{c} C_{AcCoA}^{c}}{K_{i,CoASH}^{CLY}} \right)}$$

$V_{m,CLY} = 17.5\ mM^{-1}h^{-1}$
$K_{m,cit}^{CLY} = 0.0493\ mM$
$K_{i,cit}^{CLY} = 0.0475\ mM$
$K_{m,CoASH}^{CLY} = 4.4*10^{-3}\ mM$
$K_{i,CoASH}^{CLY} = 6.1*10^{-3}\ mM$
$K_{m,OAA}^{CLY} = 0.177\ mM$
$K_{i,OAA}^{CLY} = 0.177\ mM$
$K_{m,AcCoA}^{CLY} = 9.8*10^{-3}\ mM$
$K_{i,AcCoA}^{CLY} = 9.8*10^{-3}\ mM$

Mitochondrial Malic Enzyme (MMALIC)

The rate equation and kinetic constants for CMALIC were adopted from [278]. The kinetics of CMALIC was modeled as ordered bi ter mechanism.

Eq. S45:

$$r_{mmalic} = \frac{V_{mmalic}\left(C^m_{mal}C^m_{NAD^+} - \frac{C^m_{pyr}C^m_{NADH}C^m_{CO_2}}{K_{eq,mmalic}}\right)}{K^{mmalic}_{mal}C^m_{NAD^+}\left(1+\frac{C^m_{ATP}}{K^{mmalic}_{i,ATP}}\right) + K^{mmalic}_{NAD^+}C^m_{mal} + K^{mmalic}_{mal}K^{mmalic}_{NAD^+}}$$

$V_{mmalic} = 46.3\ mM^{-1}h^{-1}$
$K_{eq,mmalic} = 34.4$
$K^{mmalic}_{mal} = 1.7\ mM$
$K^{mmalic}_{NAD} = 0.16\ mM$
$K^{mmalic}_{i,ATP} = 0.5\ mM$

<u>Cytosolic Malic Enzyme</u> (CMALIC)

The rate equation and kinetic constants for CMALIC were taken from [279]. The kinetics of CMALIC was modeled as ordered bi ter mechanism.

Eq. S46:

$$r_{cmalic} = \frac{V_{f,cmalic}\left(C^c_{mal}C^c_{NADP} - \frac{C^c_{CO_2}C^c_{pyr}C^c_{NADPH}}{K_{eq,cmalic}}\right)}{K^{cmalic}_{i,NADP}K^{cmalic}_{m,mal} + K^{cmalic}_{m,mal}C^c_{NADP} + K^{cmalic}_{m,NADP}C^c_{mal} + C^c_{mal}C^c_{NADP} + \frac{K^{cmalic}_{i,NADP}K^{cmalic}_{m,mal}K^{cmalic}_{m,pyr}C^c_{CO_2}}{K^{cmalic}_{m,CO_2}K^{cmalic}_{i,pyr}}}$$
$$+ \frac{K^{cmalic}_{i,NADP}K^{cmalic}_{m,mal}C^c_{NADPH}}{K^{cmalic}_{i,NADPH}} + \frac{K^{cmalic}_{m,mal}K^{cmalic}_{m,NADPH}C^c_{NADP}C^c_{pyr}}{K^{cmalic}_{i,pyr}K^{cmalic}_{i,NADPH}}\left(\frac{C^c_{CO_2}}{K^{cmalic}_{m,CO_2}} + \frac{K^{cmalic}_{i,CO_2}C^c_{mal}}{K^{cmalic}_{i,mal}K^{cmalic}_{m,CO_2}} + \frac{C^c_{mal}C^c_{CO_2}}{K^{cmalic}_{i,mal}K^{cmalic}_{m,CO_2}}\right)$$
$$+ \frac{K^{cmalic}_{m,NADP}C^c_{mal}C^c_{NADPH}}{K^{cmalic}_{i,NADPH}}\left(1+\frac{C^c_{pyr}}{K^{cmalic}_{i,pyr}} + \frac{C^c_{CO_2}C^c_{pyr}}{K^{cmalic}_{i,CO_2}K^{cmalic}_{i,pyr}}\right) + \frac{K^{cmalic}_{m,mal}K^{cmalic}_{i,NADP}K^{cmalic}_{m,pyr}C^c_{NADPH}}{K^{cmalic}_{i,pyr}K^{cmalic}_{i,NADPH}}\left(\frac{C^c_{pyr}}{K^{cmalic}_{m,pyr}} + \frac{C^c_{CO_2}}{K^{cmalic}_{m,CO_2}}\right)$$
$$+ \frac{K^{cmalic}_{m,mal}K^{cmalic}_{i,NADP}K^{cmalic}_{m,NADPH}C^c_{CO_2}C^c_{pyr}}{K^{cmalic}_{m,CO_2}K^{cmalic}_{i,pyr}K^{cmalic}_{i,NADPH}}\left(1+\frac{C^c_{NADPH}}{K^{cmalic}_{m,NADPH}}\right) + \frac{K^{cmalic}_{m,mal}K^{cmalic}_{m,pyr}C^c_{NADP}C^c_{CO_2}}{K^{cmalic}_{m,CO_2}K^{cmalic}_{i,pyr}}\left(1+\frac{C^c_{mal}}{K^{cmalic}_{i,mal}}\right)$$

$V_{f,cmalic} = 174\ mM^{-1}h^{-1}$
$K^{cmalic}_{i,NADP} = 9.6*10^{-4}\ mM$
$K^{cmalic}_{m,mal} = 120*10^{-3}\ mM$
$K^{cmalic}_{i,mal} = 0.22\ mM$
$K^{cmalic}_{m,NADP} = 1.4*10^{-3}\ mM$
$K^{cmalic}_{i,CO_2} = 11.7*10^{-3}\ mM$
$K^{cmalic}_{m,CO_2} = 13*10^{-3}\ mM$
$K^{cmalic}_{i,pyr} = 7.8\ mM$
$K^{cmalic}_{m,pyr} = 6.4*10^{-3}\ mM$
$K^{cmalic}_{i,NADPH} = 2*10^{-3}\ mM$
$K^{cmalic}_{m,NADPH} = 2.1*10^{-3} mM$
$K_{eq,cmalic} = 34.4$

Glutamate Alanine Transaminase (GPT)

The rate equation and kinetic constants for GPT were taken from [280]. The kinetics of GPT was modeled as ping pong bi bi mechanism.

Eq. S47:

$$r_{GPT} = \frac{V_{f,GPT}\left(C^m_{Ala}C^m_{AKG} - \frac{C^m_{Pyr}C^m_{Glu}}{K_{eq,GPT}}\right)}{K^{GPT}_{Ala}C^m_{AKG} + K^{GPT}_{AKG}C^m_{Ala} + C^m_{AKG}C^m_{Ala} + \frac{K^{GPT}_{Ala}C^m_{AKG}C^m_{Glu}}{K^{GPT}_{i,Glu}} + \frac{K^{GPT}_{AKG}C^m_{Ala}C^m_{Ala}}{K^{GPT}_{IA}} + \frac{K^{GPT}_{AKG}C^m_{Ala}C^m_{Glu}}{K^{GPT}_{RG}} + \frac{V_{f,GPT}}{V_{r,GPT}K_{eq,GPT}}\left(K^{GPT}_{Pyr}C^m_{Glu} + K^{GPT}_{Glu}C^m_{Pyr} + C^m_{Pyr}C^m_{Glu} + \frac{K^{GPT}_{AKG}C^m_{Ala}C^m_{Pyr}}{K^{GPT}_{i,Pyr}} + \frac{K^{GPT}_{Pyr}C^m_{Glu}C^m_{Glu}}{K^{GPT}_{IG}}\right)}$$

$V_{f,GPT} = 66.4\ mM^{-1}h^{-1}$
$V_{r,GPT} = 3.97*10^{7}\ mM^{-1}h^{-1}$
$K^{GPT}_{Ala} = 3\ mM$
$K^{GPT}_{AKG} = 0.12\ mM$
$K^{GPT}_{Pyr} = 0.23\ mM$
$K^{GPT}_{Glu} = 8.1\ mM$
$K^{GPT}_{i,Pyr} = 0.23\ mM$
$K^{GPT}_{i,Glu} = 2.8\ mM$
$K^{GPT}_{IA} = 470\ mM$
$K^{GPT}_{IG} = 96\ mM$
$K^{GPT}_{RG} = 79.16\ mM$
$K_{eq,GPT} = 2.2$

Pyruvate Carboxylase (PC)

The kinetics of PC was modeled as bi uni mechanism. The kinetic constants for PC were taken from [281].

Eq. S48:

$$r_{PC} = \frac{V_{PC}\left(C^m_{pyr}C^m_{CO_2} - \frac{C^m_{OAA}}{K_{eq,PC}}\right)}{K^{PC}_{m,pyr}K^{PC}_{m,CO_2} + K^{PC}_{m,pyr}C^m_{CO_2} + K^{PC}_{m,CO_2}C^m_{pyr} + C^m_{pyr}C^m_{CO_2}}$$

$V_{PC} = 718.2\ mM^{-1}h^{-1}$
$K^{PC}_{m,pyr} = 0.22\ mM$
$K^{PC}_{m,CO_2} = 3.2\ mM$
$K_{eq,PC} = 1$

<u>Mono Carboxylate Transporter</u> (MCT)

The kinetics of MCT was modeled as ordered bi bi mechanism. The kinetic constants for MCT were adopted from [282,283].

Eq. S49:

$$r_{MCT} = \frac{V_{m,MCT}\left(C^c_{H^+}C^c_{lac} - C^e_{H^+}C^e_{lac}\right)}{K^{MCT}_{m,laci}K^{MCT}_{i,H^+} + K^{MCT}_{m,H^+}C^c_{lac} + K^{MCT}_{m,laci}C^c_{H^+} + K^{MCT}_{m,H^+}C^e_{lac} + K^{MCT}_{m,laci}C^e_{H^+} + C^c_{H^+}C^c_{lac}}$$
$$C^e_{H^+}C^e_{lac} + \frac{K^{MCT}_{m,H^+}C^c_{lac}C^e_{H^+}}{K^{MCT}_{i,H^+}} + \frac{K^{MCT}_{m,H^+}C^e_{lac}C^c_{H^+}}{K^{MCT}_{i,H^+}} + \frac{C^c_{lac}C^c_{H^+}C^e_{H^+}}{K^{MCT}_{ii,H^+}} + \frac{C^e_{lac}C^c_{H^+}C^e_{H^+}}{K^{MCT}_{ii,H^+}}$$

$V_{MCT} = 2.73*10^{3}\ mM^{-1}h^{-1}$
$K^{MCT}_{m,H^+} = 10^{-4}\ mM$
$K^{MCT}_{m,laci} = 2.5\ mM$
$K^{MCT}_{i,H^+} = 2*10^{-4}\ mM$
$K^{MCT}_{ii,H^+} = 2*10^{-4}\ mM$

$P_{ATP} = 1 + \frac{C^m_{H^+}}{K_{HATP}} + \frac{C^m_{Mg}}{K_{MgATP}} + \frac{C^m_K}{K_{KATP}}$	$K_{HATP} = 2.57*10^{-7}M$ $K_{MgATP} = 1.51*10^{-4}M$ $K_{KATP} = 1.35*10^{-2}M$
$P_{ADP} = 1 + \frac{C^m_{H^+}}{K_{HADP}} + \frac{C^m_{Mg}}{K_{MgADP}} + \frac{C^m_K}{K_{KADP}}$	$K_{HADP} = 3.8*10^{-7}M$ $K_{MgADP} = 1.62*10^{-3}M$ $K_{KADP} = 2.95*10^{-2}M$
$P_{AMP} = 1 + \frac{C^m_{H^+}}{K_{HAMP}} + \frac{C^m_{Mg}}{K_{MgAMP}} + \frac{C^m_K}{K_{KAMP}}$	$K_{HAMP} = 6.03*10^{-7}M$ $K_{MgAMP} = 1.38*10^{-2}M$ $K_{KAMP} = 8.91*10^{-2}M$
$P_{GTP} = P_{ATP}$	
$P_{GDP} = P_{ADP}$	
$P_{CoASH} = 1 + \frac{C^m_{H^+}}{K_{HCoASH}}$	$K_{HCoASH} = 7.41*10^{-9}M$
$P_{cit} = 1 + \frac{C^m_{H^+}}{K_{Hcit}} + \frac{C^m_{Mg}}{K_{Mgcit}} + \frac{C^m_K}{K_{Kcit}}$	$K_{Hcit} = 2.34*10^{-6}M$ $K_{Mgcit} = 4.27*10^{-4}M$ $K_{Kcit} = 4.58*10^{-1}M$

$P_{scoa} = 1 + \frac{C_{H^+}^m}{K_{Hscoa}}$ $P_{fATP} = 1 + \frac{C_{H^+}^m}{K_{HATP}} + \frac{C_{K^+}^m}{K_{KATP}}$ $P_{fADP} = 1 + \frac{C_{H^+}^m}{K_{HADP}} + \frac{C_{K^+}^m}{K_{KADP}}$ $P_{fAMP} = 1 + \frac{C_{H^+}^m}{K_{HAMP}} + \frac{C_{K^+}^m}{K_{KAMP}}$ $P_{fGTP} = P_{fATP}$ $P_{fGDP} = P_{fGDP}$	$K_{Hscoa} = 1.1 * 10^{-4} M$

10.3.2 Differential Equations

Glycolysis

1. Glucose: $\frac{dC_{glc}^c}{dt} = r_{GlcTr} - r_{HK}$
2. Glucose 6-phosphate: $\frac{dC_{g6p}^c}{dt} = r_{HK} - r_{GPI} - r_{G6PD}$
3. Fructose 6-phosphate: $\frac{dC_{f6p}^c}{dt} = r_{PGI} + r_{TA} + r_{TK2} - r_{PFK2} + r_{F2,6BPase} - r_{PFK}$
4. Fructose 1,6-bisphosphate: $\frac{dC_{f16bp}^c}{dt} = r_{PFK} - r_{ALD}$
5. Fructose 2,6-bisphosphate: $\frac{dC_{f26bp}^c}{dt} = r_{PFK2} - r_{F2,6BPase}$
6. Dihydroxyacetone phosphate: $\frac{dC_{dhap}^c}{dt} = r_{ALD} - r_{TPI}$

7. Glyceraldehyde 3-phosphate: $\frac{dC^c_{gap}}{dt} = r_{ALD} + r_{TPI} + r_{TK1} + r_{TK2} - r_{TA} - r_{GAPDH}$

8. 1,3-bisphosphoglycerate: $\frac{dC^c_{1,3bpg}}{dt} = r_{GAPDH} - r_{PGK}$

9. 3-phosphoglycerate: $\frac{dC^c_{3pg}}{dt} = r_{PGK} - r_{PGM}$

10. 2-phosphoglycerate: $\frac{dC^c_{2pg}}{dt} = r_{PGM} - r_{EN}$

11. Phosphoenolpyruvate: $\frac{dC^c_{pep}}{dt} = r_{EN} - r_{PK}$

12. Pyruvate: $\frac{dC^c_{pyr}}{dt} = r_{PK} - r_{LDH} - r_{PYRH} + r_{CMALIC}$

13. Lactate: $\frac{dC^c_{lac}}{dt} = r_{LDH} - r_{MCT}$

Pentose Phosphate Pathway

14. 6-phosphogluconate: $\frac{dC^c_{6pg}}{dt} = r_{G6PD} - r_{6PGD}$

15. Ribulose 5-phosphate: $\frac{dC^c_{ru5p}}{dt} = r_{6PGD} - r_{RPE} - r_{RPI}$

16. Xylulose 5-phosphate: $\frac{dC^c_{xyl5p}}{dt} = r_{RPE} - r_{TK1} - r_{TK2}$

17. Ribose 5-phosphate: $\frac{dC^c_{r5p}}{dt} = r_{RPI} - r_{PRPPS} - r_{TK1}$

18. Erythrose 4-phospahte**:** $\frac{dC^c_{e4p}}{dt} = r_{TA} - r_{TK2}$

19. Sedoheptulose 7-phosphate: $\frac{dC^c_{s7p}}{dt} = r_{TK1} - r_{TA}$

20. Glutathione: $\frac{dC^{c}_{glutathione}}{dt} = r_{GSSGR} - r_{GSHOX}$

TCA Cycle

21. Mitochondrial pyruvate: $\frac{dC^{m}_{pyr}}{dt} = r_{PYRH} * \frac{V_c}{V_m} - r_{PDH} + r_{mmalic} - r_{PC} + r_{GPT1}$

22. Mitochondrial Acetyl-CoA: $\frac{dC^{m}_{AcCoA}}{dt} = r_{PDH} - r_{CS}$

23. Mitochondrial Citrate: $\frac{dC^{m}_{cit}}{dt} = r_{CS} - r_{ACON} + r_{CITMAL}$

24. Mitochondrial Isocitrate: $\frac{dC^{m}_{icit}}{dt} = r_{ACON} - r_{IDH}$

25. Mitochondrial Alpha-ketoglutarate: $\frac{dC^{m}_{akg}}{dt} = r_{IDH} - r_{AKGD} + r_{AKGMAL} - r_{GOT2} + r_{GDH} - r_{GPT1}$

26. Mitochondrial Succinyl-CoA: $\frac{dC^{m}_{SCoA}}{dt} = r_{AKGD} - r_{SCOAS}$

27. Mitochondrial Succinate: $\frac{dC^{m}_{suc}}{dt} = r_{SCOAS} - r_{SDH}$

28. Mitochondrial Fumarate: $\frac{dC^{m}_{fum}}{dt} = r_{SDH} - r_{FUM}$

29. Mitochondrial Malate: $\frac{dC^{m}_{mal}}{dt} = r_{FUM} - r_{mmalic} - r_{MDH2} - r_{AKGMAL} - r_{CITMAL} + r_{MALPi}$

30. Mitochondrial Oxaloacetate: $\frac{dC^{m}_{OAA}}{dt} = -r_{CS} + r_{MDH2} + r_{GOT2} + r_{PC}$

NAD/NADH Shuttles

31. Mitochondrial Aspartate: $\frac{dC^{m}_{asp}}{dt} = r_{ASPGLU} - r_{GOT2}$

32. Mitochondrial Glutamate: $\frac{dC^m_{glu}}{dt} = r_{GOT2} - r_{ASPGLU} - r_{GDH} - r_{GLUH} + r_{GPT1}$

33. Aspartate: $\frac{dC^c_{asp}}{dt} = -r_{GOT1} - r_{ASPGLU} * \frac{V_m}{V_c}$

34. Glutamate: $\frac{dC^c_{glu}}{dt} = r_{GOT1} + r_{ASPGLU} * \frac{V_m}{V_c} - r_{GLUH} * \frac{V_m}{V_c} + r_{GLS}$

35. Oxaloacetate: $\frac{dC^c_{OAA}}{dt} = r_{GOT1} - r_{MDH1} + r_{CLY}$

36. Malate: $\frac{dC^c_{mal}}{dt} = r_{MDH1} + r_{AKGMAL} * \frac{V_m}{V_c} + r_{CITMAL} * \frac{V_m}{V_c} - r_{MALPi} * \frac{V_m}{V_c} - r_{cmalic}$

37. Alpha-ketoglutarate: $\frac{dC^c_{akg}}{dt} = -r_{AKGMAL} * \frac{V_m}{V_c} - r_{GOT1}$

Other Equations

38. Citrate: $\frac{dC^c_{cit}}{dt} = -r_{CITMAL} * \frac{V_m}{V_c} - r_{CLY}$

39. NAD: $\frac{dC^c_{NAD}}{dt} = r_{LDH} - r_{GAPDH} + r_{MDH1}$

40. NADP: $\frac{dC^c_{NADP}}{dt} = r_{GSSGR} - r_{G6PD} - r_{6PGD} - r_{cmalic}$

Macroscopic Balances

41. Extracellular glucose: $\frac{dC_{glc,extracellular}}{dt} = D(C_{glc,feed} - C_{glc,extracellular}) - r_{GlcTr} * x$

42. Extracellular lactate: $\frac{dC_{lac,extracellular}}{dt} = -D * C_{lac,extracellular} + r_{MCT} * x$

43. Cell concentration: $\frac{dx}{dt} = (\mu - D) * x$

44. Growth rate: $\mu = \mu_{\max} * \frac{C_{glc,extracellular}}{K_{m,Glc} + C_{glc,extracellular}} * \frac{K_{I,lac}}{K_{I,lac} + \left(C_{lac,extracellular}\right)^2}$